Mitosis and Protein N^{α}-Terminal Acetylation

Ana Rita Marques

Dissertation presented to obtain the Ph.D degree in Developmental Biology

Instituto de Tecnologia Química e Biológica
Universidade Nova de Lisboa

Research work performed at:

FUNDAÇÃO CALOUSTE GULBENKIAN
Instituto Gulbenkian de Ciência

This dissertation was sponsored by Fundação para a Ciência e Tecnologia.
"Apoio financeiro da FCT e do FSE no âmbito do Quadro Comunitário de apoio, BD nº SFRH/BD/28767/2006 e projecto FCT-POCI-DG/BIA/82013/06"

FCT
Fundação para a Ciência e a Tecnologia
MINISTÉRIO DA CIÊNCIA, INOVAÇÃO E DO ENSINO SUPERIOR

Oeiras,
July, 2011

INSTITUTO DE TECNOLOGIA QUÍMICA E BIOLÓGICA /UNL
Knowledge Creation

List of publications

The work described in this thesis contributed to the following publications.

1. **Pimenta-Marques, A., Tostoes, R., Marty, T., Barbosa, V., Lehmann, R. and Martinho, R. G.** (2008). Differential requirements of a mitotic acetyltransferase in somatic and germ line cells. *Dev Biol* **323**, 197-206.

2. **Van Damme, P.[#], Hole, K.[#], Pimenta-Marques, A.[#], Helsens, K., Vandekerckhove, J., Martinho, R.G., Gevaert, K., and Arnesen, T.** (2011). NatF contributes to an evolutionary shift in protein N-terminal acetylation and is important for normal chromosome segregation. *PLoS Genet* **7,** e1002169.
   # - These authors contributed equally to this work.

3. **Guilgur, L., Prudêncio, P., Ferreira, T., Pimenta-Marques, A., Martinho, R.G.** (2011). Drosophila aPKC is required for mitotic spindle orientation during symmetric division of epithelial cells (submitted).

This thesis is the result of the work I developed between January 2007 and December 2010 under the supervision of Dr. Rui Gonçalo Martinho, at the laboratory of Early Fly Development at Instituto Gulbenkian de Ciência, Oeiras, Portugal.

Collaborations are indicated in the sections Materials and Methods.

The original manuscript 1 corresponds to chapter III, where I performed all experiments descried in the article.

Concerning manuscript 2, I collaborated in the description of *Drosophila* Naa60-depleted cell phenotypes. Therefore, I will incorporate those results in chapter V.

Acknowledgments / Agradecimentos

First I would like to thank my supervisor Rui Martinho for taking me in his lab and giving me the opportunity to grow as a scientist. He made me believing that I was capable of starting and one day finishing a PhD. It was lots of fun and I will remember this learning process with care and laughter.

I must also thank Thomas Arnesen and Petra Van Damme for all the support and enthusiastic discussions we had about my project and NATs.

To the CCR group I must thank all the support regarding both scientific discussions and reagents. Particularly, Zita Santos and Inês Ferreira for introducing me to the cell culture world. Besides being excellent colleagues, I must also thank them, as well as to Inês Bento and Ana Martins for their true friendship during these years.

Ao Tostões e ao André tenho a agradecer o facto de terem tornado as horas infindáveis na sala das moscas em momentos de autêntica diversão e boa disposição. A amizade deles foi indispensável neste percurso.

À Tânia, Pedro e Gaston tenho a agradecer a amizade e forte companheirismo e união que temos entre nós. É de facto um privilégio acordar de manhã e ir trabalhar com um grupo de pessoas de quem genuinamente gostamos e com quem nos identificamos. Além disso ainda nos fartamos de rir juntos.

Ao Paulinho e à Catarina tenho a agradecer por estarem presentes não só como colegas de trabalho em outros laboratórios mas principalmente por serem meus grandes amigos.

Tenho sido de facto uma privilegiada por ao longo do doutoramento ter feito verdadeiros amigos como os que referi. Sem eles estes anos não teriam sido tão alegres como foram.

Aos meus pais tenho a agradecer do fundo do coração o amor e apoio incondicional que sempre me deram. Ter partilhado com eles os melhores e piores momentos fez-me crescer e aprender a valorizar o que é verdadeiramente importante e a relativizar o dispensável. Se de alguma forma tenho sido bem sucedida na vida, o devo a eles. Quanto às minhas irmãs… são as maiores!!! Sou uma sortuda por ter duas manas destas na minha vida.

Ao meu avô Pimenta agradeço por ser o avô único que é! O meu avô tem sido uma presença constante e fundamental no meu processo de crescimento. Desde que sai de Évora que o meu avô me faz o telefonema da praxe todas as semanas. Essas e outras demonstrações de carinho fazem-me sentir uma "netinha" menina, apesar dos 31 anos, e isso é tão bom!

Aos meus tios Chico e São tenho a agradecer o facto de ter sempre podido contar com eles. Foram também uma presença constante nos momentos importantes da minha vida.

À Ju, Avô João, D.Virginia, Tio e Ana Catarina, tenho a agradecer o facto de me terem acolhido como um verdadeiro membro da família e do pelo forte apoio que me deram nestes últimos anos. Os nossos almoços de fim de semana são uma lufada de ar fresco.

Claro, ao meu maridão tenho a agradecer o amor, amizade, companheirismo e paciência que teve comigo nestes últimos cinco anos. É muito bom para mim ter alguém com a personalidade do Gonçalo ao meu lado. O facto de partilhar a minha vida com ele faz com que tudo o que é bom seja "maravilhoso" e tudo o que é mau seja apenas "menos bom". É cá uma peça o meu marido.

À minha feijoca linda estou grata por ela ter tornado estes últimos meses verdadeiramente únicos e maravilhosos. Ela foi sem dúvida uma força de motivação em momentos mais cinzentos. Tem sido tão bom estarmos juntas, que já não consigo imaginar os meus dias sem ela.

Abstract

Protein N^{α}-terminal acetylation is a highly conserved and widespread modification that occurs on approximately 80% of all soluble, cytoplasmic human proteins. Nevertheless, with few exceptions, little is known about the biological function of protein N^{α}-acetylation. Recently, it was suggested to act as a general protein destabilization signal in yeast (Hwang et al., 2010). Yet, other reports suggest it might act as stabilizer, for instance by blocking protein degradation (Ciechanover and Ben-Saadon, 2004). This protein modification is catalyzed by N^{α}-terminal acetyltransferases (NATs), which are highly conserved from yeast to humans both in subunit composition and substrate specificity (Starheim et al., 2009). Since NATs enzymatic activity and function has been mostly studied in yeast and tissue culture cells, our current understanding of the role of these enzymes during development of multicellular organisms is extremely poor, being our main goal to understand the role of this ubiquitous protein modification during development.

In Chapter II of this work, we isolated two genes from a maternal genetic screen designed to identify genes required for blastoderm embryonic development. Both genes were required for syncytial nuclear divisions. One of the isolated genes corresponded to *separation anxiety* (*san*) (Pimenta-Marques et al., 2008). *san* encoded a poorly characterized NAT known by Naa50p, which is conserved from yeast to humans. San/Naa50p was found in a complex with two other NATs, Naa10p and Naa15p, forming the NatE complex. Interestingly, in contrast to the previously studied NATs, we and others showed that dSan/dNaa50-depleted cells showed specific phenotypes during mitosis (Hou et al., 2007; Pimenta-Marques et al., 2008;

Williams et al., 2003). dSan/dNaa50 was originally described as being involved in centromeric sister chromatid cohesion (Williams et al., 2003). This conclusion came from the observation that *san* mutant neuroblasts exhibited premature loss of sister chromatid cohesion during mitosis accompanied by mislocalization of a subunit of the cohesin complex from the centromeric region.

Detailed characterization of *Drosophila san* mutants (chapter III) revealed striking defects during chromosome segregation in the syncytial nuclear divisions (Pimenta-Marques et al., 2008). These included lagging chromosomes and extensive chromosome bridges. Additionally, we observed that during mitosis a subset of nuclei showed a dramatic decrease in the levels of a condensin subunit. Moreover, a subset of chromosome bridges showed reduced levels of Topoisomerase II. Together, these observations suggested dSan/dNaa50 was also important for chromosome condensation/ resolution, implying a more general mitotic function of this NAT. Surprisingly, our work showed that whereas all analyzed somatic tissues required dSan/dNaa50 for correct cell cycle progression, during *Drosophila* oogenesis we failed to detect mitotic defects in the female germ-line stem cells mutant for dSan/dNaa50, suggesting there are differential requirements for N^{α}-acetylation between the female germ-line and the soma. We hypothesized that different NATs are likely to have different tissue-specific functions throughout development. In order to test this hypothesis we focused on: 1) defining the mitotic function of dSan/dNaa50, 2) understanding why is this enzyme not required in the female germ-line.

To understand in which molecular pathway dSan/dNaa50 is regulating mitosis we decided to identify its *in vivo* mitotic substrates (chapter IV). To that end, we took advantage of the N-terminal

COmbined FRActional Diagonal Chromatography (COFRADIC) methodology to identify proteins whose N^{α}-acetylation levels were reduced in *san* mutant embryos. We identified 18 proteins whose N^{α}-acetylation levels were reduced in *san* mutants. From these 18 proteins, we identified the gamma subunit of the cytosolic chaperonin containing T-complex polypeptide 1 (CTT) (Cctγ), which displayed chromosome segregation defects identical to dSan/dNaa50-depleted cells. Cctγ was shown to be required for the metaphase to anaphase transition by activating the anaphase promoting complex/ cyclosome complex (Camasses et al., 2003), making this protein an excellent candidate for a putative mitotic substrate of dSan/dNaa50. Ongoing complementation experiments in tissue culture cells will allow us to test if the chromosome segregation defects of San-depleted cells are Cctγ-mediated.

In chapter V we addressed why dSan/dNaa50 was not required in the female germ-line stem cells. Each NAT complex preferentially acetylates distinct N-termini. However, recent data suggested that different NAT complexes were partially redundant (Arnesen et al., 2009b; Van Damme et al., 2001). We therefore hypothesized that dSan/dNaa50 was not required within the female germ-line because of redundancy with another NAT specifically on this tissue. To test our hypothesis we identified the *Drosophila* NAT paralogues of dSan/Naa50. Phylogenetic analysis revealed that dNaa60 was the closest NAT paralogue to dSan/dNaa50. Interestingly, dNaa60-depleted cultured cells showed chromosome segregation defects remarkably similar to dSan/dNaa50 (Van Damme et al., 2011), suggesting this NAT was also required for chromosome segregation in mitosis. We hypothesize that dNaa60 is redundant with dSan/dNaa50 specifically in the female germ-line. Ongoing analysis of the female

germ-line stem cell divisions within *san/naa60* double mutants will clarify this potential redundancy.

Sumário

A acetilação N^{α}-terminal de proteínas é uma modificação muito comum e conservada que ocorre em cerca de 80% das proteínas solúveis citoplasmáticas em humanos. Com algumas excepções, pouco se sabe acerca da função biológica da acetilação N^{α}-terminal. Foi recentemente sugerido em levedura, que esta modificação pode actuar como um sinal de destabilização de proteínas (Hwang et al., 2010). Outros trabalhos sugerem que ao invés, possa actuar com estabilizador, como por exemplo no bloqueio de degradação proteica (Ciechanover and Ben-Saadon, 2004). Esta modificação é catalisada por acetiltransferases de N^{α}-terminais (NATs). Estas enzimas são altamente conservados desde as leveduras aos humanos, quer na composição das suas subunidades quer na especificidade dos seus substratos (Starheim et al., 2009). Uma vez que a actividade e função destas enzimas tem sido principalmente estudada em levedura e sistemas de cultura de células, o conhecimento sobre a função da acetilação de N^{α}-terminais no contexto de um organismo multicelular é ainda muito limitado. O nosso principal objectivo é o de compreender a função desta modificação de proteínas durante o desenvolvimento.

No Capítulo II deste trabalho, isolamos dois grupos de complementação de um *screen* materno desenvolvido com o objectivo de identificar genes necessários para o desenvolvimento da blastoderme embrionária. Ambos os genes mutados nestes grupos de complementação são necessários para as divisões nucleares do sincício. Um dos genes isolados correspondeu ao "*separation anxiety*" (*san*). A San codifica uma NAT pouco caracterizada, conhecida por Naa50p, conservada de leveduras a humanos. A San/Naa50p foi

identificada como parte de um complexo com mais duas NATs, a Naa10p e a Naa15p designado por NatE. Curiosamente, e ao contrário do que foi observado para as outras NATs, nós e outros grupos de investigação mostrámos que células onde a actividade da dSan/dNaa50 foi eliminada, apresentam fenótipos específicos durante a mitose (Hou et al., 2007; Pimenta-Marques et al., 2008; Williams et al., 2003). A dSan/dNaa50 foi originalmente descrita como uma proteína envolvida na coesão centromérica das cromatidias irmãs (Williams et al., 2003). Esta conclusão veio da observação de que neuroblastos de mutantes para *san* exibem perda prematura de coesão das cromátidias irmãs durante a mitose. Foi igualmente descrita a deslocalização de uma subunidade do complexo da coesina na região centromérica dos cromossomas.

A caracterização detalhada de mutantes de *Drosophila* para o gene *san* (capítulo III) revelou defeitos marcantes durante a segregação dos cromossomas nas divisões nucleares do sincício (Pimenta-Marques et al., 2008). Estes defeitos incluem pontes cromossómicas e/ou perda de cromossomas no meio do fuso mitótico aquando da segregação cromossomática. Observou-se ainda, que uma percentagem de núcleos mitóticos apresentou uma forte diminuição dos níveis de uma subunidade do complexo de condensina. Igualmente, observámos que um subconjunto de pontes cromossómicas apresentou níveis reduzidos de topoisomerase II. Estas observações sugerem que a dSan/dNaa50 é importante para a condensação/resolução cromossómica, o que implica uma função mais geral desta NAT do que a inicialmente proposta. O nosso trabalho mostrou que a dSan/dNaa50 é necessária para a progressão normal do ciclo celular em todos os tecidos somáticos analisados. Surpreendentemente, durante a oogénese, não fomos capazes de detectar defeitos mitóticos nas células estaminais da linha germinal

em mutantes para a dSan/dNaa50. Os nossos dados sugerem que a linha germinal feminina e as células somáticas apresentam requisitos diferentes para a acetilação de N^{α}-terminais. Com base nos nossos resultados, hipotetizamos que diferentes NATs poderão ter diferentes funções reguladoras ao longo do desenvolvimento de diferentes tecidos. Para testar esta hipótese focámo-nos em 1) definir a função mitótica da dSan/dNaa50, 2) compreender porque é que a dSan/dNaa50 não é necessária na linha germinal feminina.

De modo a identificarmos a via molecular em que a dSan/dNaa50 regula a mitose, decidimos identificar os substratos mitóticos desta NAT (capítulo IV). Para esse fim, tirámos partido da cromatografia combinada de fraccionamento de N-terminais, de forma a identificar proteínas cujos níveis de N^{α}-acetilação estão reduzidos em embriões mutantes para dSan/dNaa50, por comparação com embriões de estirpe selvagem. Desta análise resultou a identificação de 18 proteínas cujos níveis de N^{α}-acetilação foram reduzidos em mutantes para dSan/dNaa50. Uma das 18 proteínas identificadas foi a subunidade gama da chaperonina citosólica contendo o complexo T-polipeptídeo (CTT) (Cct_{γ}). A Cct_{γ} apresentou defeitos de segregação cromossómica muito semelhantes aos observados para células onde a dSan/dNaa50 foi eliminada. Esta chaperonina foi descrita como sendo necessária para a transição metáfase-anáfase por activação do complexo promotor da anáfase/complexo ciclosoma (Camasses et al., 2003). As funções associadas à Cct_{γ} tornam-na numa excelente candidata a ser um substrato mitótico da dSan/dNaa50. Futuras experiências de complementação em cultura de células vão permitir-nos testar se de facto os defeitos de segregação cromossómica observados em células depletadas de dSan/dNaa50 são mediados pela Cct_{γ}.

No capítulo V investigámos porque é que a dSan/dNaa50 não é necessária nas células estaminais da linha germinal feminina. Cada complexo NAT acetila preferencialmente distintos N-terminais. Contudo, dados recentes sugerem que diferentes complexos NAT podem ser parcialmente redundantes (Arnesen e tal., 2009b; Van Damme e tal., 2011). Com base nestes estudos hipotetizámos que a dSan/dNaa50 não é necessária na linha germinal feminina devido à redundância com outra NAT especificamente neste tecido. Para testar esta hipótese identificámos os parálogos da dSan/Naa50 em *Drosophila*. A análise filogenética revelou que a dNaa60 é a NAT paráloga mais próxima da dSan/dNaa50. Após a depleção da dNaa60 em células em cultura observámos defeitos de segregação cromossómica muito semelhantes aos associados a células depletadas para dSan/dNaa50 (Van Damme et al., 2011), indicando que esta NAT é necessária para a segregação de cromossomas na mitose. Tendo em conta estes resultados, a nossa hipótese actual é a de que a dNaa60 é a NAT redundante com a dSan/dNaa50 na linha germinal feminina. A análise de duplos mutantes em *Drosophila* para *san*/*naa60* irá clarificar esta possível redundância.

Abbreviations

Acetyl-CoA	Acetyl-coenzyme A
Ala	Alanine
APC/C	Anaphase promoting complex/cyclosome
Arg	Arginine
BDGP	Berkeley Drosophila Genome Project
BDSC	Bloomington Drosophila Stock Center
Bub3	Budding uninhibited by benzimidazole 3
BubR1	Budding uninhibited by benzimidazole 3 related 1
C(2)M	Crossover suppressor on 2 of Manheim
CCT	Chaperonin containing T-complex polypeptide 1
Cctγ	Gamma subunit of CCT
Cdc20	Cell-division-cycle 20 homologue
Cdh1	cdc20-homologue 1
CDIP	cell death involved p53-target
Cdk	Cyclin-dependent kinase
CDS	Coding DNA sequences
Cnn	Centrosomin
Cid	Centromere identifier
CkIIα	Casein kinase II α subunit
COFRADIC	Combined fractional diagonal chromatography
EGAF	Embryonic Growth-Associated factor
EMS	Ethylmethane sulfonate
EST	Expressed sequence tag
FRT	Flipase recombination targets
GEF	Guanine nucleotide exchange factor
GLC	Germ-line clone
GNAT	Gcn5-related N-acetyltransferases
GSK-3	Glycogen synthase kinase 3
HAT	Histone acetyltransferase

HDAC	Histone deacetylase
HIF-1α	Hypoxia-inducible factor 1α
His	Histidine
HMG	high mobility group
HPLC	High performance liquid chromatography
HYPK	Huntingtin (Htt) yeast two-hybrid protein K
hs-FLP	Heat-shock induced flipase
IKKβ	IkB kinase β
iMet	Initiator methionine
INCENP	Inner centromere protein
Lys	Lysine
Mad2	Mitotic arrest-deficient 2
MAP	Methionine aminopeptidases
MT	Microtubules
MTOC	Microtubule organizing center
NAT	N^{α}-terminal acetyltransferases
NARG1	NMDA receptor-regulated gene 1
NEBD	Nuclear envelope break-down
NMDA	N-methyl-d-aspartate
OR	Oregon-R
ORF	Open reading frame
PCR	Polymerase chain reaction
Plk1	Polo-like kinase 1
PolyQ	Polyglutamine
PP2A	Protein phosphatase 2A
PTM	Posttranslational modification
RF-C	Replication factor C
PGC	Primordial Germ Cell
PKA	Protein kinase A
PSCS	Premature sister chromatid separation

RNAi	RNA interference
RT	Room temperature
San	Separation anxiety
SCX	Strong cation exchange
SAC	Spindle assembly checkpoint
Ser	Serine
Sgo	Shugoshin
SMC	Structural maintenance of chromosomes
snRNP	Small ribonucleproteins
Tbdn-1	Tubedown-1
Thr	Threonine
TNBS	2,4,6-trinitrobenzenesulfonic acid
TNFα	Tumor necrosis factor alpha
TopoII	Topoisomerase II
Tpm1	Tropomyosin 1
TPR	Tetratrico-peptide repeat
P53	Tumor protein 53
Tyr	Tyrosine
Ub	Ubiquitin
vnc	*variable nurse cells*
2R	Second chromosome

Table of contents

CHAPTER I

General Introduction

1. Cell cycle

The cell cycle is a series of events that takes place in a eukaryotic cell leading to its division and replication. Numerous proteins regulate the correct progression of the cell cycle, which ensures the accurate transmission of genetic information from a mother cell to its daughter cells. The eukaryotic cell cycle is typically divided on basis of chromosomal events: interphase and M phase (mitosis) (fig. 1). Interphase is comprised by G1 phase followed by S phase and G2 phase. The G1 and G2 phases represent “gaps” in the cell cycle that occur between the two landmark events – DNA synthesis (S phase) and mitosis (M phase). In these stages, the cells grow and pass through regulatory transitions in which progression to the next phase is controlled by a variety of signals. In G1, cells become committed to either continue or exit from the cell cycle into a quiescent state. The M phase is composed by two events: nuclear division (mitosis) and cell division (cytokinesis).

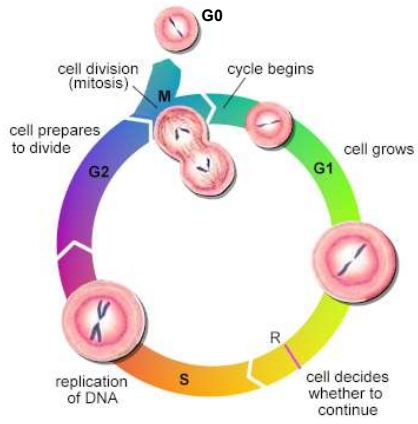

Figure 1: Schematic representation of the cell cycle. The main events of the cell cycle are DNA replication (S phase), chromosome segregation and consequent nuclear division (M phase or mitosis). Between these main events exist the gap phases (G1 and G2). Cells may also enter a G0 phase that is characterized by a more or less prolonged stage of nondividing cells.

1.1. Cell cycle regulation

Cell cycle regulation involves crucial steps such as detection and repair of genetic damage and the provision of various checkpoints that ensure correct segregation of genetic information and prevent uncontrolled cell division. The molecular events that control the cell cycle are ordered and directional. Two key classes of regulatory proteins, cyclins and cyclin-dependent kinases (Cdks) are central players in regulating the cell cycle through its different stages. Cdks are specific serine/threonine protein kinases that are activated at specific points of the cell cycle. Cyclins assure activation of Cdks, as they interact with distinct Cdks providing them with substrate specificity. Cyclins are named from their cyclic expression over the cell cycle, which ensures each Cdk can only be activated at specific stages of the cell cycle. Thus, different cell cycle stages are associated with the presence of specific cyclins and activation of specific Cdks (Revised by Murray A.W., 2004).

1.2. Mitosis

Mitosis results in the production of two daughter cells containing identical genetic information and is subdivided into five successive phases: prophase, prometaphase, metaphase, anaphase and telophase (fig. 2).

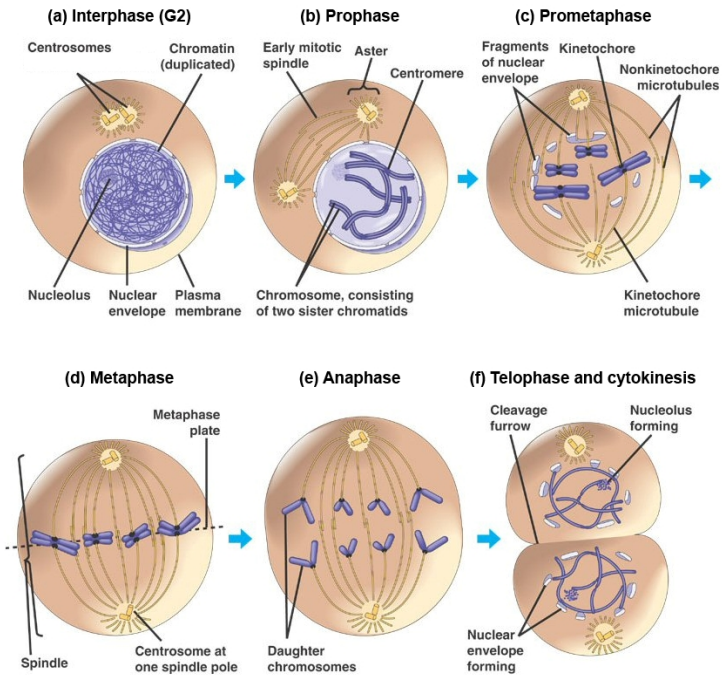

Figure 2: Mitosis in the animal cell. (a) Interphase, where chromosomes are dispersed and not visible as distinct structures. (b) As prophase is initiated centrosomes move towards opposite sides of the cell and chromosome condensation starts to be visible. (c) Prometaphase starts when the nuclear envelope breaks down and chromosome condensation is completed. Each chromosome can be visualized as a structure composed of two sister chromatids held together at the centromeric region. During prometaphase chromosomes are captured by microtubules growing from opposite poles, a process that contributes to chromosome congression and alignment at the metaphase plate (d). (e) At anaphase onset, each chromatid pair separates and segregates to opposite poles of the cell. (f) By the end of mitosis, in telophase, chromosomes decondense and the nuclear membrane re-forms around the daughter nuclei. Cytoplasm division, or cytokinesis, occurs concomitantly as the later stages of mitosis, giving rise to two daughter cells. (Adapted from Lodish, 2003).

During prophase (fig. 2b) two major events can be easily visualized including overall reorganization of the cytoskeleton and condensation of chromatin into compact mitotic chromosomes. Reorganization of cytoskeleton microtubules (MTs) is conducted by

separation and migration to opposite sides of the cell of the two previously duplicated microtubule organizing centers (MTOCs), which in animal cells are called centrosomes. Centrosomal maturation occurs during G2 and plays a major role in promoting the conversion of the highly stable MTs found in interphase to highly dynamic MTs present in mitosis.

Prometaphase (fig. 2c) starts with nuclear envelope break-down (NEBD). This allows MTs, nucleated by centrosomes, to invade the nuclear space and marks the initiation of assembly of the mitotic spindle. MTs are polymers composed of tubulin subunits that exist as heterodimers of α- and β-tubulin. MTs will eventually form the mitotic spindle. Stable interactions between MTs and chromosomes take place at a very specific chromosomal structure called the kinetochore. The kinetochore is a multiprotein complex located at the surface of each sister chromatid at a region called the centromere that corresponds to the primary constriction of condensed chromosomes. As a result of the interaction with the spindle MTs, the chromosomes will eventually move towards the cell center, a process known as chromosome congression.

Metaphase (fig. 2d) occurs when all chromosomes are aligned at the equatorial plane of the mitotic spindle so that each sister chromatid of each chromosome is attached to MTs emanating from opposite poles of the spindle. Chromosome segregation can only occur when all chromosomes are correctly aligned at the spindle equator and are under tension as a result of their attachments to the MTs. In the next stage, which is known by anaphase (fig. 2e), sister chromatids migrate to opposite sides of the spindle. Finally during telophase (fig. 2f), the nuclear envelope reassembles and surrounds each group of segregated chromatids, which then decondense giving rise to two daughter nuclei. At the same time, the cell cytoplasm divides by cytokinesis. This is initiated with the ingression of the

cleavage furrow normally at the center of the cell perpendicular to the long axis of the mitotic spindle and terminates when the two daughter cells finally separate (reviewed by Lodish 2003, Morgan 2007).

1.3. The spindle assembly checkpoint and the metaphase to anaphase transition

The spindle assembly checkpoint (SAC) is a molecular system that ensures the accurate segregation of mitotic chromosomes by delaying anaphase onset until each kinetochore is properly attached to the mitotic spindle (Kops et al., 2005; Rieder et al., 1995; Rieder et al., 1994). The SAC is activated by kinetochores that are not yet attached to mitotic spindle MTs and chromosome pairs that lack tension across sister chromatids generated by spindle forces (Rieder and Maiato, 2004; Yu, 2002). The established concept is that a group of mitotic checkpoint proteins such as budding uninhibited by benzimidazole 3 (Bub3), budding uninhibited by benzimidazole 3 related 1 (BubR1) and mitotic arrest-deficient 2 (Mad2) bind to kinetochores that lack tension or MT attachment leading to a delay in chromosome segregation (Kops et al., 2005). As each pair of sister kinetochores attaches to MTs, they become under tension leading to their stretching. This allows checkpoint proteins to diffuse from the kinetochore silencing the SAC. Silencing the SAC leads to activation of the Anaphase Promoting Complex/Cyclosome (APC/C).

The APC/C regulates the metaphase to anaphase transition through recognition and destruction of ubiquitinated proteins (fig. 3). Ubiquitination by the APC/C is mainly controlled by activator subunits that bind the core components at different points in the cell cycle and promote ubiquitination of specific substrates. Of these, cell-division-cycle 20 homologue (Cdc20) and cdc20-homologue 1(Cdh1) are the most important. Cdc20 activates the APC/C at the metaphase to

anaphase transition allowing further degradation of securin which is an inhibitor of the protease separase. Once securin is degraded, separase will be active and will cleave cohesin, the complex that keeps sister chromatids together. Also, at this stage the mitotic cyclin B is prompted for degradation leading to the subsequent inactivation of its binding partner Cdk1, the major mitotic cyclin dependent kinase. Cdh1 activates the APC/C at the end of mitosis to maintain cyclin destruction (Li and Zhang, 2009).

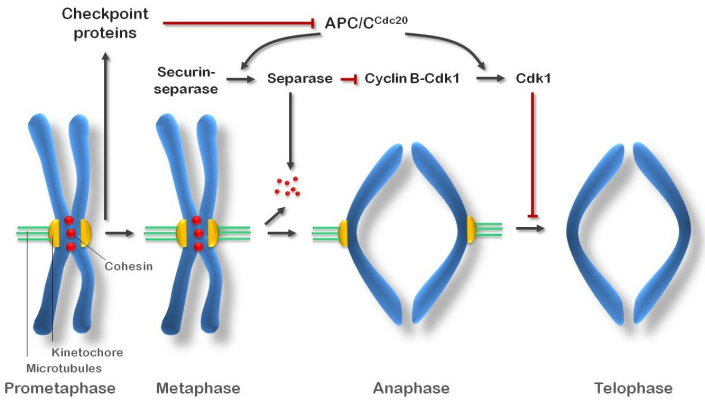

Figure 3: Regulation of anaphase and mitotic exit by APC/C. During prometaphase, SAC proteins such as Mad2 and BubR1 are activated at kinetochores that are not (or not fully) attached with MTs. Activated Mad2 and BubR1 inhibit the capability of the APC/C to ubiquitinate securin and cyclin B and thereby prevent anaphase and mitotic exit. In metaphase, when all kinetochores are attached to MTs, APC/C ubiquitinates securin and cyclin B and thereby activates the protease separase and inactivates Cdk1. Separase then cleaves cohesin complexes which hold sister chromatids together and thereby initiates sister-chromatid separation. Cdk1 inactivation leads to the dephosphorylation of Cdk1 substrates by protein phosphatases, and thereby enables exit from mitosis. (Adapted from Peters, 2006).

1.4. Chromosome cohesion and condensation

Both cohesin and condensin complexes are essential for faithful segregation of chromosomes during the mitotic cell cycle.

Cohesin establishes sister chromatid cohesion between duplicating DNAs in S phase. In prophase, a large structural reorganization of chromosomes is started, with initial release of cohesin and progressive loading of condensins, culminating with the formation of metaphase chromosomes with well-resolved sister chromatids. Sister chromatid resolution, is a prerequisite of the final separation of sister chromatids that is triggered by proteolytic cleavage of cohesin at the onset of anaphase. The dynamic behavior of cohesin and condensins must be tightly regulated under the control of the cell cycle machinery.

1.4.1. Sister chromatid cohesion

To ensure the faithful transmission of chromosomes in mitosis, replicated chromatids remain paired until both sister kinetochores attach to opposite poles of the mitotic spindle, a state known as biorientation. This pairing requires cohesin, a multiprotein complex that ensures proper sister chromatid pairing until anaphase onset.

The cohesin complex contains a pair of structural maintenance of chromosomes (SMC) subunits and ancillary non-SMC subunits. Mitotic cohesion complexes contain a heterodimer of SMC1 and SMC3, the non-SMC subunit Scc3 (also known as SA), and the α-kleisin subunit Mcd1/Scc1/Rad21 (fig. 4). Subunit-subunit interaction assays have shown that cohesin forms a tripartite ring in which the open-V structure of the SMC heterodimer is closed by simultaneous binding of the N- and C-terminal regions of Scc1 to the head domains of SMC3 and SMC1, respectively (fig. 4) (Haering et al., 2002). It has been proposed that the ring-like structure of cohesin holds sister chromatids together by embracing two DNA duplexes within the SMC subunits coiled-coil arms (Haering et al., 2002) (fig 4). In agreement with this model, cohesin dissociates from chromatin upon disruption of the integrity of the ring by cleavage of one of its subunits or, in the

case of circular minichromosomes, upon DNA linearization (Gruber et al., 2003; Ivanov and Nasmyth, 2007; Uhlmann et al., 1999).

In most organisms, meiotic cohesin complexes contain the alternative Rec8 instead of the α-kleisin Drad21. There is no obvious Rec8 orthologue in *D.melanogaster*. Instead, crossover suppressor on 2 of Manheim (C(2)M) encodes a distant α-kleisin member that associates with DmSMC3 and has a role in synaptonemal complex (Heidmann et al., 2004), a regulator the overall process of homologous recombination.

Conserved orthologues of the cohesin proteins are found in metazoans (Darwiche et al., 1999; Losada et al., 1998; Rollins et al., 1999; Sumara et al., 2000), suggesting cohesin is very likely the universal mechanism of sister-chromatid cohesion.

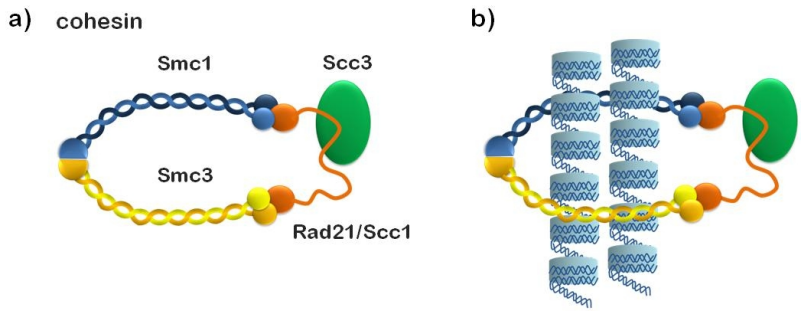

Figure 4: (a) Composition of the cohesin complex. The head domains of cohesin's SMC1/SMC3 dimer are bound by different ends of the Scc1/Rad21 α-kleisin subunit, which also recruits the HEAT repeat-containing Scc3/SA subunit to the complex. **(b) The ring model.** Both sister chromatids (blue cylinders) pass through the same cohesin ring structure, and the major DNA-cohesin interaction is topological.

Loading of cohesin on chromatin requires a heteromeric complex composed of the Scc2 and Scc4 proteins. These proteins are conserved from yeast to humans (Watrin et al., 2006). Scc2 and Scc4 are required to load cohesin onto DNA during the G1 phase of the cell cycle in yeast (Ciosk et al., 2000; Tomonaga et al., 2000), and

telophase in vertebrates, prior to DNA replication (Gillespie and Hirano, 2004; Takahashi et al., 2004). Further establishment of cohesion only occurs during or after DNA replication. Indeed, establishment of sister chromatid cohesion is tightly coupled to replication and some, if not all, cohesion is generated at replication forks (Unal et al., 2007). Cohesion is established by the acetyltransferase Eco1. This protein associates with the DNA polymerase processivity factor PCNA and with components of the clamp loader replication factor C (RF-C) (Kenna and Skibbens, 2003; Moldovan et al., 2006). Deco is the name for the orthologous acetyltransferase needed for centromeric cohesion in flies (Williams et al., 2003). In humans, there are two paralogs of Eco1 known as ESCO1 and ESCO2. Cohesion establishment was shown to be dependent upon Eco1-mediated acetylation of at least two lysine residues of SMC3 at the head region of the protein (Rolef Ben-Shahar et al., 2008; Rowland et al., 2009; Unal et al., 2008; Zhang et al., 2008).

There are at least three proteins which are important for cohesin maintenance following S phase (fig. 5). These proteins include Pds5, Sororin and Wpl1. They interact closely with cohesin and modulate its chromatin association dynamics, although they are not required for cohesion loading. The exact mechanism by which the Pds5 protein modulates cohesion is not well understood. Pds5 is a HEAT-repeat protein conserved from fungi to vertebrates. It interacts with Eco1 and through this interaction is believed to contribute to the dynamic association of cohesion with chromatin (Noble et al., 2006; Tanaka et al., 2001). The phenotypes observed in Pds5 deficient cells are somewhat variable among different organisms. *PDS5* is an essential gene in budding yeast, required during G2/M phase for maintenance of cohesion (Hartman et al., 2000; Panizza et al., 2000).

In *Drosophila*, *pds5* mutants display premature sister chromatid cohesion in brain neuroblasts (Dorsett et al., 2005). Vertebrate cells have two Pds5-like proteins, and mild cohesion defects were observed with decreased levels of these proteins (Losada et al., 2005). Sororin is a vertebrate-specific component of the cohesin network (Rankin et al., 2005; Schmitz et al., 2007). Depletion of Sororin in HeLa cells decreased the fraction of stable chromatin-bound cohesin, causing cohesion defects already in interphase (Schmitz et al., 2007). In contrast to Pds5 and Sororin, Wpl1 promotes dissociation of cohesin from chromosome arms. *Drosophila* mutants of the Wpl1 orthologue (wapl*)* prevented separation of sister chromatids in mitosis (Verni et al., 2000). Consistently, in mammalian cells depleted of Wpl1, cohesin remains associated with chromatids during mitosis, resulting in a mitotic delay (Gandhi et al., 2006; Kueng et al., 2006) (fig. 5).

In metazoans dissolution of most cohesin from chromosome arms is performed during prophase in what has been called the "prophase pathway". Only a small population, enriched at the pericentromeric region remains on chromosomes until metaphase. Cohesin dissociation from chromosome arms requires phosphorylation of the cohesin subunit, SA, by the mitotic kinase Polo-like kinase 1 (Plk1) (Hauf et al., 2005; Sumara et al., 2002). In addition to Plk1, Aurora B may contribute to this process by phosphorylation of other targets. *Xenopus* cell-free extracts depleted of Aurora B approached metaphase with condensed sister chromatids, but the axes failed to resolve (Losada et al., 2002; Sumara et al., 2002). Most of the cohesin dissociated by the prophase pathway is not cleaved at anaphase, but instead relocates to chromatin in telophase to function in the next cell cycle. During the prophase pathway, centromeric cohesin is protected from dissociation by Shugoshin (Sgo/Mei-S332) (Watanabe and Kitajima, 2005). In *Drosophila* or yeast, the contribution of Sgo/Mei-

S332 to mitotic chromosome segregation is modest. In contrast, HeLa cells depleted of Sgo1, one of the two human members of this family, causes premature sister chromatid separation during mitosis (Kitajima et al., 2005; Salic et al., 2004; Tang et al., 2004) Sgo acts in concert with protein phosphatase 2A (PP2A), where it is likely to counteract Plk1-dependent phosphorylation of cohesin and thereby prevent dissociation of cohesion from the centromeres (Kitajima et al., 2006; McGuinness et al., 2005; Riedel et al., 2006; Salic et al., 2004; Tang et al., 2006).

Centromeric cohesin is essential for chromosome segregation in mitosis. For proper chromosome segregation, the sister kinetochores must attach spindle MTs emanating from opposite poles, and centromeric sister chromatid cohesion is essential in antagonizing the pulling force of the spindle microtubules. Centromeric sister chromatid cohesion is dissolved at the metaphase to anaphase transition. Once the SAC is satisfied, the APC/C is activated and promotes the ubiquitin dependent-destruction of the sequestering chaperone securin, which leads to the activation of the protease separase. Cohesin release results from site-specific cleavage of the Scc1 subunit by separase (Uhlmann, 2001). Scc1 phosphorylation by polo is not essential but enhances *in vitro* cleavage by separase (Alexandru et al., 2001; Hauf et al., 2005; Hornig and Uhlmann, 2004).

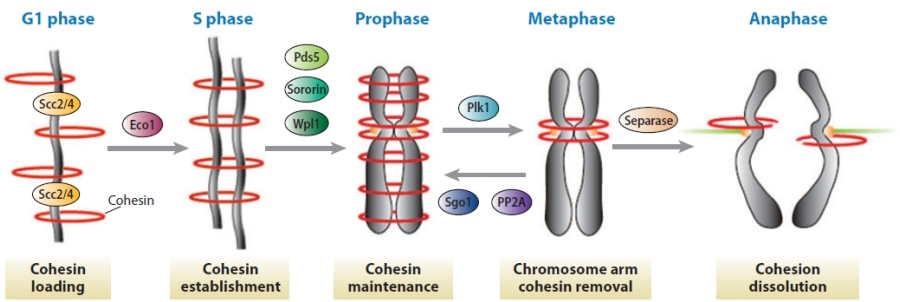

Figure 5: The cohesin network. The Scc2-Scc4 loading complex deposits the cohesin complex onto chromatin in the G1 phase of the cell cycle. Cohesion is established between sister chromatids concomitantly with DNA replication in an Eco1-dependent manner. Upon entry into G2/M phase cohesion is maintained by the proteins Pds5, Sororin and Wpl1. Mammalian cells remove cohesin along chromosome arms during prophase *via* phosphorylation of Scc1/Rad21 by Polo-like kinase. During metaphase centromeric cohesin is protected from removal by Sgo and PP2A. At the onset of anaphase, separase cleaves Scc1/Rad21 leading to the opening of the cohesin ring and the separation of sister chromatids. (Adapted from Xiong and Gerton, 2010).

1.4.2. Chromosome condensation

Chromosome condensation is essential for correct chromosome segregation and therefore faithful transmission of genetic information to daughter cells. One important player of the process of chromosome compaction is the condensin complex. There are two condensin complexes in vertebrate cells: condensin I and II. Both complexes are pentameric composed by two SMC ATPase subunits (SMC2 and SMC4) and three auxiliary subunits (CAP-G/G2, CAP-D2/D3 and CAP-H/H2) (Hirano, 2005; Ono et al., 2003) (fig. 6). *Drosophila* appears to have both complexes but no homologue has been identified for CAP-G2. The condensin complex is highly conserved and is found ubiquitously among eukaryotes, while prokaryotes have a condensin-like complex.

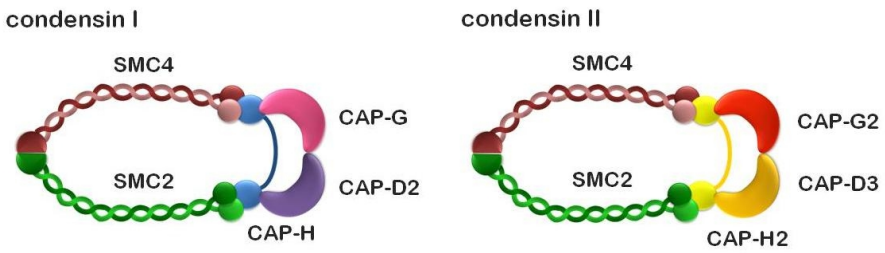

Figure 6: Composition of the condensin complexes. Condensin's SMC2/SMC4 dimer associates with a CAP-H γ-kleisin or with a CAP-H2 β-kleisin in condensin I or II complexes, respectively. Separate pairs of HEAT repeat-containing proteins associate with condensin I (CAP-D2 and CAP-G) or II (CAP-D3 and CAP-G2).

The two condensin complexes have different localization patterns in the cell cycle and on chromosomes. In vertebrates, condensin I is thought to localize to the cytoplasm during interphase and gain access to chromosomes only at the end of prophase after NEBD. It then dissociates again from chromosomes at the end of telophase. Condensin II is nuclear during interphase but only associates with chromatin until prophase, where it remains until the end of telophase (Gerlich et al., 2006; Hirota et al., 2004; Ono et al., 2004). Both complexes are present at centromeres and along chromosome arms. They bind to different places along chromosome axes and are both necessary for mitotic chromosome segregation (Ono et al., 2004).

Recent data in yeast suggests that like cohesin, the condensin complex might be loaded onto chromosomes by the Scc2-Scc4 complex. Budding yeast *scc2* and *scc4* mutants displayed chromosome compaction defects and reduced condensin binding (D'Ambrosio et al., 2008).

Condensin's loading on chromosomes during early mitosis is accompanied by the compaction of sister DNAs into largely separate linear rod-shaped structures. Several studies showed condensin has a role in organizing mitotic chromatids that is essential for their successful segregation during anaphase. However the mechanism of action and its contribution to chromosome condensation is poorly understood. Although *in vitro* studies suggested condensin to be a key player in chromosome condensation (Hagstrom et al., 2002; Hirano, 2005; Hudson et al., 2003; Strunnikov et al., 1995), several studies

showed that chromosomes depleted of condensin do condense. The first defect observed in cells depleted of condensin is associated with a delay in the timing of prophase compaction. Elimination of both condensin complexes in chicken DT40 cells revealed no appreciable chromosome condensation in G2/M cells with intact nuclear envelopes (Hudson et al., 2003). However, after NEBD, chromosomes were able to undergo a nearly normal condensation process (Hudson et al., 2003; Kaitna et al., 2002). Depletion of condensin II-specific subunits, but not in those depleted of condensin I-specific subunits, leads to a delay in chromosome condensation within prophase (Hirota et al., 2004; Ono et al., 2004). By metaphase, depletion of condensin I- or condensin II-specific subunits produces distinct, highly characteristic defects in chromosome architecture, i.e., swollen or curly chromosomes, respectively. These data are consistent with distinct contributions of condensin I and II to mitotic chromosome structure. Depletion of the SMC core subunits causes the severest defects revealing cloud-like chromosomes with a very fuzzy appearance (Ono et al., 2003). Condensin depletion was also shown to lead to the mislocalization of a number of non-histone chromosomal proteins, including topoisomerase II (TopoII), inner centromere protein (INCENP) and KIF4A/chromokinesin (Hudson et al., 2008; Hudson et al., 2003).

TopoII is an evolutionarily conserved protein, and removes catenation between sister chromatids that remains after completion of DNA replication (Wang, 2002). Indeed, it is thought that sister chromatid resolution is achieved by the cooperation between topoisomerase II and condensins (Coelho et al., 2003; Steffensen et al., 2001). DmSMC4-depleted cultured cells failed to localize TopoII to a clearly defined chromatid axial structure and protein extracts from DmSMC4-depleted cells exhibited a significant decrease in TopoII-mediated DNA decatenation activity (Coelho et al., 2003).

In condensin mutants, mitotic chromosomes interact normally with spindle MTs and chromosomes congress to the metaphase plate with rare defects (Gerlich et al., 2006; Hagstrom et al., 2002). Upon anaphase onset, severe defects are observed in condensin mutants and condensin depleted cells. Chromosome segregation at anaphase almost always fails, leading to the formation of prominent chromatin bridges and cytokinesis failure (Hagstrom et al., 2002; Hirota et al., 2004; Hudson et al., 2003; Kaitna et al., 2002; Ono et al., 2003; Saka et al., 1994; Savvidou et al., 2005; Steffensen et al., 2001). Premature loss of chromosome compaction is apparently the cause of these chromosome segregation defects in early anaphase (Gerlich et al., 2006; Vagnarelli et al., 2006), and not due to the failure of TopoII decatenation activity (Vagnarelli et al., 2006). On the other hand, it has also been suggested that condensins have additional and distinct roles during anaphase to achieve proper chromosome segregation (Wignall et al., 2003; Yanagida, 2009). The potential roles of condensins during anaphase remain elusive. Different studies have shown an extent of defects observed in condensin depleted cells. The observed defects seem however to vary among different organisms and different conditions, thereby leaving room for different interpretations (Losada and Hirano, 2005).

2. Posttranslational modifications

One of the most significant conclusions of the Human genome project was the small number of annotated genes, which was approximately twice of the number of genes annotated in *Drosophila melanogaster* (2004; Adams et al., 2000). This suggested that an increase in biological complexity does not necessarily translate in a

proportional increase in gene number. Indeed proteomes may be orders of magnitude more complex than the encoding genomes would predict. The first route of diversification of proteins is at the level of alternative transcriptional start sites and pre-mRNA alternative splicing. The second route of proteome expansion is by covalent posttranslational modification (PTM) of proteins at one or more sites. As the name implies, PTMs are covalent modifications that occur on protein side chains or their backbones by the addition of a chemical group either during or after assembly of the polypeptide chain (Walsh et al., 2005). PTMs can regulate protein function, by causing changes in protein activity, protein cellular locations and dynamic interactions with other proteins (fig.7). Proving the relevance of these modifications in protein processing, about 5% of the genomes of higher eukaryotic can be dedicated to enzymes that carry out PTMs of their proteomes.

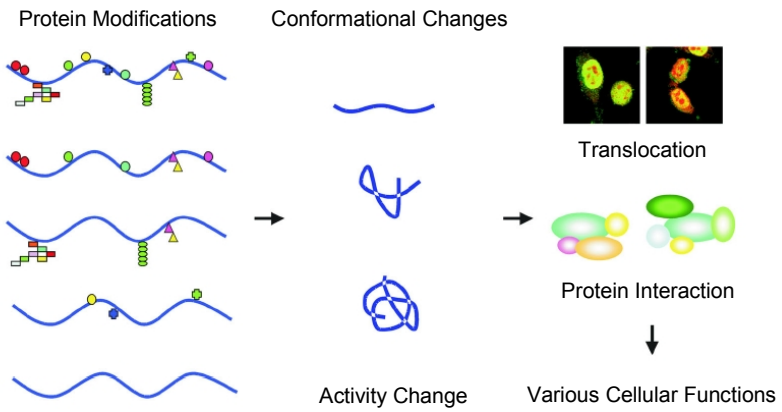

Figure 7: Schematic representation of protein modifications related to the regulation of downstream biological processes. (Adapted from Seo and Lee, 2004).

Most common PTMs include phosphorylation (Burnett and Kennedy, 1954), acetylation (Glozak et al., 2005), methylation (Grewal and Rice, 2004), glycosylation (Spiro, 2002), sumoylation (Gareau and

Lima, 2010), and ubiquitination (Pickart and Eddins, 2004). These modifications regulate a variety of different cellular processes, including cell cycle progression and its regulation.

2.1. Posttranslational modifications and the cell

2.1.1. Phosphorylation

Phosphorylation of Serine (Ser), Threonine (Thr), Tyrosine (Tyr) and Histidine (His) residues is the best known and most ubiquitous PTM. Because the phosphate group ($-O-PO_3^{2-}$) carries a large negative charge at neutral pH, phosphorylation of neutral amino acids induces altered conformations in local protein microenvironments (Johnson and Lewis, 2001). Phosphorylation can therefore modulate protein function by altering protein stability, cellular localization, substrate affinity, complex formation and activity.

The addition of a phosphate group on a substrate protein is catalyzed by protein kinases, while hydrolyses of the phosphate group is achieved by protein phosphatases. Eukaryotes express a large variety of protein kinases (Manning et al., 2002) and phosphatases (Moorhead et al., 2007; Virshup and Shenolikar, 2009), each with a unique substrate specificity and regulation. The expansion of the protein kinase families in higher metazoans accounts for the observed cellular and functional diversity between these organisms. Due to its reversible and transient nature, phosphorylation allows signal transduction pathways to carry out diverse cellular functions. Moreover it also allows essential events such as cell cycle and growth to occur at precise times and locations.

The eukaryotic cell cycle is an example of cellular decision-making based on reversible phosphorylation and dephosphorylation of proteins. One third of the *Drosophila* kinome was shown to affect cell

cycle progression (Bettencourt-Dias et al., 2004). Cdks regulate the G1, S and G2 phases of the cell cycle ensuring DNA duplication and segregation of chromosomes into daughter cells (fig. 8). Cdks are themselves regulated and cooperate with other protein kinases.

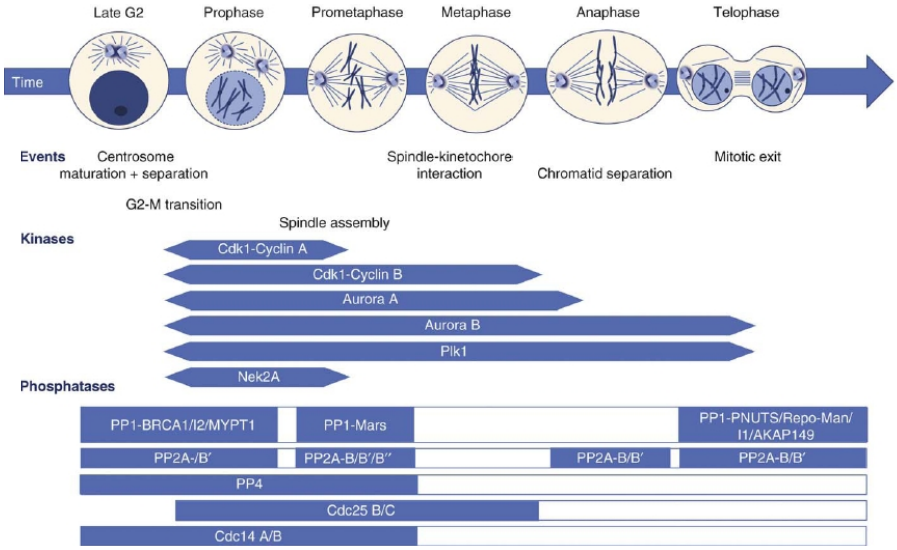

Figure 8: Mitotic phosphoregulation in animal cells. Upper panel shows the different mitotic stages and highlights major events known to be regulated by reversible protein phosphorylation. Middle panel indicates the activity phases of the major mitotic kinases. Lower panel shows known mitotic phosphatases with respect to the depicted mitotic events. Exact timing of activation and inactivation of most mitotic phosphatases is not known as depicted by open bars. (Adapted from Bollen *et al*., 2009).

Among the different kinases, Cdk1 has an essential role in mitotic entry and progression until all chromosomes are properly aligned along the metaphase plate (Morgan, 2007). Entry into anaphase and subsequent mitotic exit requires inactivation of Cdk1 and other mitotic regulators (Sullivan and Morgan, 2007). This inactivation is primarily mediated by proteosome-dependent degradation of proteins by the APC/C and also by controlled removal

of mitotic phosphorylations by different phosphatases. Mitosis relies therefore in a delicate balance between the activities of kinases and their counteracting phosphatases.

2.1.2. Acetylation

The role of acetylation has been suggested to be analogous to that of phosphorylation (Kouzarides, 2000). Many proteins are posttranslationally acetylated, and at least for eukaryotic proteins, acetylation is the most common covalent modification out of over 200 reported types. Protein acetylation is catalyzed by a variety of different acetyltransferases. These enzymes catalyze the transfer of an acetyl group from acetyl-coenzyme A (Acetyl-CoA) to either the α-amino group of amino-terminal residues (N^{α}-terminal acetylation, revised in Chpater I, section 3.) or to the ε-amino group of lysine (Lys) residues at various positions. The α-amino group designates the position of the central carbon atom of amino acids, whereas the ε-amino group of lysine residues designates the position of a carbon atom on the side chain.

The introduction of acetyl groups on Lys side chains potentially converts cationic side chains into neutralized surfaces influencing protein function or its association with other proteins. Acetylation of ε-Lys residues occurs on histones, high mobility group (HMG) proteins, transcription factors, nuclear receptors (Bannister et al., 2000; Imhof et al., 1997; Roth et al., 2001) and α-tubulin (MacRae, 1997).

Most studied acetylated proteins include N^{ε}-acetylation of Lys side chains on the N-terminal tail of histones (Yang, 2004). Two groups of enzymes responsible for regulating the reversible and dynamic state of histone acetylation are histone acetyltransferases (HATs) and histone deacetylases (HDACs). Acetylation of histones, in

general, leads to transcriptional activation by inducing the unpacking of the nucleosomes from the tight 30nm chromatin fibers. This allows manipulating the tightly packed heterochromatin to more relaxed euchromatin state (fig. 9), which in turn allows other transcriptional regulatory proteins to gain access to promoter elements on DNA. The acetylation state of different promoters is maintained by specific combinations of HATs and HDACs. Not surprisingly, histone acetylation appears to influence other processes including cell cycle progression, chromosome dynamics, DNA replication, recombination and repair, silencing and apoptosis (Kouzarides, 1999).

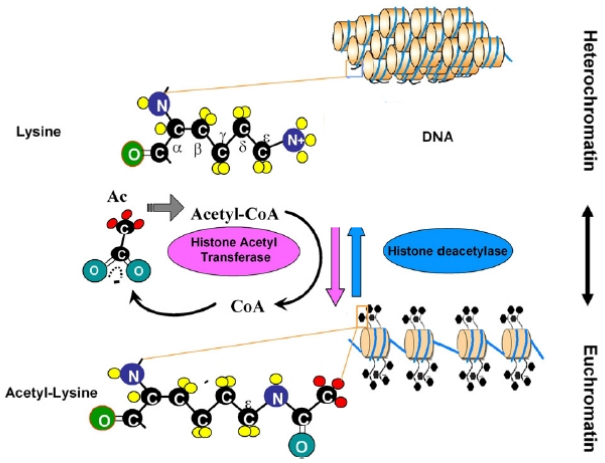

Figure 9: Histone acetylation and transition of heterochromatin to euchromatin. Representation of the molecular structure of acetylated and deacetylated lysine residues and resultant chromatin state. (adapted from Khan and Khan, 2010).

2.1.3. Methylation

Although there are known examples of protein side chain methylation, histone N-terminal tail methylation draws most research attention. Since methyl groups are relatively small, addition of these groups to Lys and Arginine (Arg) residues does not neutralize their charges, having little effect on histone conformation. Instead, methylation has been associated with the creation of binding sites for

specific regulatory proteins (Bannister and Kouzarides, 2005). Therefore, unlike acetylation, which generally correlates with transcriptional activation, histone lysine methylation can signal either activation or repression, depending on the sites of methylation (Cuthbert et al., 2004). The ε-amino group of Lys can accept up to three methyl groups and hence can be mono-, di- or trimethylated (Martin and Zhang, 2005). For certain processes, methylation on the same site can lead to different outcomes depending on the number of methyl groups added.

2.1.4. Ubiquitination

Ubiquitination is likely to affect all proteins at some point in their life cycle. Ubiquitin (Ub) a highly conserved 8.5 kDa protein that becomes covalently attached to Lys residues of target proteins in an inducible and reversible manner. This attachment occurs through a 3 step process involving 3 different types of enzymes, E1, E2 and E3 ligases (Pickart and Eddins, 2004). According to the number of Ubs added, substrate proteins can be monoubiquitinated or polyubiquitinated. Monoubiquitination is believed to serve as a regulatory modification of a target protein in much the same way phosphorylation regulates protein activity (Weissman, 2001). However, the most common role associated to ubiquitination is the tagging of proteins for degradation. The vast majority of proteins (80-90%) tagged by Ub polypeptides are then degraded via the 26 S proteasome (Craiu et al., 1997; Rock et al., 1994). This degradation signal usually involves protein polyubiquitination. One example where ubiquitination plays a central role is in cell cycle progression. The characteristic temporal control of proteins destroyed during the cell cycle, such as the cyclin subunits of cdks, is performed by the E1-E2-E3 ubiquitin ligase machinery of the APC/C (Nakayama and Nakayama, 2006).

3. N^{α}-terminal acetylation

Besides ε-amino acetylation of side chain residues, acetylation can also occur at the α-amino group of protein N-terminals. This modification is an enzyme catalyzed reaction in which the protein α-amino group accepts an acetyl group from Acetyl-CoA. N^{α}-acetylation neutralizes positive charges that can influence protein function, stability, interaction with other molecules, or other subsequent modifications, such as phosphorylation.

N^{α}-acetylation is one of the most common protein modifications in eukaryotes. Indeed, different studies revealed N^{α}-acetylation of approximately 85% of soluble cytosolic human proteins (Arnesen et al., 2009b; Jornvall, 1975; Persson et al., 1985) and approximately 50% in yeast (Arnesen et al., 2009b; Lee et al., 1989).

N^{α}-acetylation often occurs in two consecutive events (Bradshaw et al., 1998; Polevoda and Sherman, 2002). In the first step, the initiator methionine (iMet; fig. 10), is removed from the nascent polypeptide by methionine aminopeptidases (MAP). This event is not obligatory in protein biosynthesis and has been shown to only take place if the second amino acid is small and uncharged (Boissel et al., 1988; Sherman et al., 1985). Larger amino acids at this position prevent removal of iMet by sterical hindrance (Lowther and Matthews, 2000). In the second step, the acetylation of the amino-terminus is catalyzed by N^{α}-terminal acetyltransferases (NATs; fig.10).

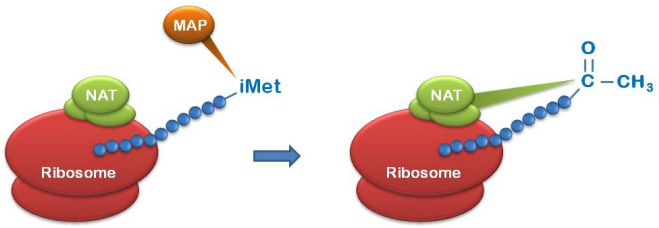

Figure 10: Schematic representation of initial methionine removal followed by N^{α}-terminal acetylation. During translation of a protein, when the iMet is followed by a small and uncharged amino acid residue, it will be removed by a methionine aminopeptidase (MAP, orange). Following iMet removal, the processed amino-terminus will be acetylated at the α-amine of the following amino acid residue by a NAT (green).

NATs form a subfamily within the Gcn5-related N-acetyltransferases (GNAT) superfamily (Polevoda et al., 1999). GNATs are one of the largest known protein superfamilies, with more than 10 000 members in all kingdoms of life (Vetting et al., 2005). Accordingly, NATs have been found in all kingdoms: prokaryotes, archaeal, and eukaryotes (Polevoda and Sherman, 2000; Polevoda and Sherman, 2003b). In humans, as in yeast, three NAT complexes are believed to perform most N^{α}-acetylation events, namely the human NatA, NatB and NatC complexes (Arnesen et al., 2005a; Asaumi et al., 2005; Starheim et al., 2008; Starheim et al., 2009a). Each NAT acts on different groups of amino acid sequences, whose specificity is determined by two or more residues at the amino-terminal positions (table 1). However, for some proteins, acetylation does not occur even if the appropriate amino acid sequences are present, suggesting that additional unknown amino acid sequence patterns or other determinants like secondary structure of the protein N-terminus may play a role (Polevoda and Sherman, 2003b).

All eukaryotic NATs so far identified were shown to interact with ribosomes and N^{α}-acetylation is believed to take place during protein synthesis (Gautschi et al., 2003; Polevoda et al., 2008; Starheim et al., 2008; Starheim et al., 2009a). *In vitro* studies demonstrated that cotranslational N^{α}-acetylation takes place when the nascent polypeptide extrudes 20 to 50 amino acids from the ribosome (Driessen et al., 1985; Kendall et al., 1990).

Type	NatA	NatB	NatC	NatD	NatE
Catalytic subunit	Naa10p (Ard1p) Naa11p (Ard2p)	Naa20p (Nat3p)	Naa30p (Mak3p)	Naa40p (Nat4p)	Naa50p
Auxiliary subunit	Naa15p (Nat1p) Naa16p (Nat2p) HYPK*	Naa25p (Mdm20p)	Naa35p (Mak10p) Naa38p (Mak31p)	-	Naa15p? (Nat1p) Naa10p? (Ard1p)
Substrates	Ser- Ala- Thr- Val- Gly- Cys-	Met-Glu- Met-Asp- Met-Asn-	Met-Leu- Met-Ile- Met-Trp- Met-Phe-	Ser-Gly- (H2A/H4)	Met-Leu-

Table 1: Eukaryotic N-terminal acetyltransferases and there substrates. N-termini of which the iMet is followed by one of the small amino acids, Ser-, Ala-, Thr-, Val-, Gly-, Cys-, and Pro- undergo iMet cleavage performed by a methionine aminopeptidase (MAP). These N-termini, with the exception of Pro-, are often further acetylated by NatA (Arnesen et al., 2009b; Polevoda et al., 1999), or in the case of Histone H2A and H4, by NatD (Song et al., 2003). Met-Asp-, Met-Glu-, Met-Asn- and Met-Gln- are acetylated by NatB (Polevoda et al., 1999; Polevoda and Sherman, 2003b). Hydrophobic Met-Leu-, Met-Ile-, Met-Phe- and Met-Tyr- are acetylated by NatC (Kimura et al., 2000; Polevoda et al., 1999; Tercero et al., 1993). Met-Leu- N-termini have been demonstrated to be acetylated by Naa50p *in vitro* (Evjenth et al., 2009) *HYPK is an interactor partner of NatA in humans and may modulate NAT-activity (Arnesen et al. 2010).

In contrast to other PTMs, very little is known about the biological relevance of N^{α}-acetylation in the context of a developing multicellular organism. Nevertheless, multiple evidences suggest it is essential for development and is likely to play an important role during carcinogenesis (Starheim et al., 2009b). Work in yeast and mammalian cell culture described NATs *in vivo* substrate specificities (table 1) and knockdown phenotypes, yet the N^{α}-acetylated substrates associated to the observed phenotypes are mostly unknown.

3.1. The NatA acetyltransferase complex

Among the three major NAT complexes, NatA acetyltransferase complex is the most studied one. This complex is conserved from yeast to humans in respect to subunit composition (Arnesen et al., 2005a) and substrate specificity (Arnesen et al., 2009b). Functional complementation studies demonstrated that expression of the human NatA complex (hNAA10-hNAA15) rescued the phenotypes observed in a yeast NatA-deletion strain. Furthermore, when expressed in yeast the hNatA complex could N^{α}-acetylate the same set of substrates as the yeast NatA complex *in vivo* (Arnesen et al., 2009b).

The NatA complex acetylates N-termini in which the initial iMet was removed by MAPs. It also seems to be the most degenerate NAT complex, including a wide range of sequences, although N-terminal residues of Ser and alanine (Ala) are the most common ones (Arnesen et al., 2009b; Polevoda et al., 1999) (table 1).

NatA is believed to be the major NAT complex both in yeast and humans having a higher amount of potential substrates in comparison to the NatB and NatC complexes (Arnesen et al., 2009b; Polevoda and Sherman, 2003b). Based on the substrate specificity of this complex and the N-terminal sequences of all known human proteins, it was estimated that more than 8.000 (from a total of 20.000) unique human proteins are hNatA substrates. Indeed, a large number of NatA substrates were identified *in vivo* by analysis of the N^{α}-terminal acetylation levels of protein extracts from control and downregulated NatA subunits in HeLa cells (Arnesen et al., 2009b). Surprisingly, downregulation of the hNatA complex only led to a significant change in the acetylation status of 6% of the identified hNatA substrates. The authors attributed this to a residual presence of the hNatA complex being able to acetylate most of its substrates (Arnesen et al., 2009b).

Another possibility is a partial redundancy of other NATs with the NatA complex.

The NatA complex is composed by the catalytic subunit Naa10p (Ard1p) and the auxiliary subunit Naa15p (Nat1p; Table 1) (Arnesen et al., 2005a; Mullen et al., 1989). Both human subunits were found to be associated with ribosomes, suggesting Naa10p performs cotranslational acetylation of nascent polypeptides (Arnesen et al., 2005a). However, a significant proportion of these subunits were also found to be non-ribosomal (Arnesen et al., 2005a), suggesting these proteins might have other functions independent of the NatA complex. Naa10p protein levels are dependent on Naa15p; depletion of Naa15p significantly diminished Naa10p protein levels on ribossomes, suggesting Naa15p is likely to anchor Naa10p to the ribosome (Hou et al., 2007; Polevoda et al., 2008).

Interestingly, humans contain paralogues of the hNaa10p and hNaa15p proteins, hNaa11p and hNaa16p, respectively (Arnesen et al., 2006b; Arnesen et al., 2009a). These were suggested to form less abundant functional NatA complexes, allowing for four possible combinations of the different NatA subunits (Arnesen et al., 2006b; Arnesen et al., 2009a).

The hNatA complex was recently described to interact with the Huntingtin (Htt) yeast two-hybrid protein K (HYPK). HYPK has chaperone-like properties preventing Htt polyglutamine (polyQ) aggregation. The NatA complex was essential for the proper expression of the HYPK protein and for the modulation of Htt polyQ aggregation. Moreover, the interaction of HYPK with the NatA complex was shown to be required for normal *in vivo* and *in vitro* acetylation of a known NatA substrate (Arnesen et al. 2010). It is not clear in human cells however, if HYPK influences NatA acetylation activity in general or the acetylation of specific substrates. If further studies confirm the

latter hypothesis, it opens a window to hypothesize that the NatA activity might be modulated by different cofactor proteins to modulate different substrate acetylation events.

Another subunit, San/Naa50p (Nat5p), was shown to physically associate with the NatA complex (Gautschi et al., 2003) and form a complex known by NatE. Since San/Naa50p is central for this dissertation, I will further focus on this NAT in more detail on section 3.5. of this chapter.

3.1.1. Naa10/ Ard1 acetyltransferase

Naa10p is the catalytic subunit of the NatA acetyltransferase complex. Different mammalian Naa10p isoforms have been identified. These include mouse variants mNaa10p^{198}, mNaap10^{225} and mNaa10p^{235}, and the human variants hNaa10p^{131} and hNaa10p^{235}. Mouse and human Naa10p^{235} are orthologs and are considered the wild-type protein (Chun et al., 2007; Jeong et al., 2002). hNaa10p^{235} localizes at the nucleus and cytoplasm (Arnesen et al., 2005a), while mNaa10p^{225} and mNaa10p^{235} are present at the cytoplasm and the nucleus, respectively (Chun et al., 2007), suggesting Naa10p may have different functions according to its localization. These Naa10p isoforms share a conserved N-acetyltrasferase domain but contain different sequences and lengths at their C-terminal region (Bilton et al., 2006). The C-terminal region is unstructured and flexible (Sanchez-Puig and Fersht, 2006), and was shown to be phosphorylated at several sites (Beausoleil et al., 2006; Olsen et al., 2006), suggesting a possible regulation of this NAT by different phosphorylation states. Indeed hNaa10p was shown to be phosphorilated at Ser209 by IkB kinase β (IKKβ), leading to the destabilization and induction of proteasome-mediated degradation (Kuo et al., 2009). Some of the

phosphorylation events were also shown to be mediated by Glycogen synthase kinase 3 (GSK-3) kinase (Malen et al., 2009).

Interestingly, mammalian Naa10p was suggested to have ε-amino acetyltransferase activity. mNaa10p^{225} was shown to N$^{\varepsilon}$-acetylate the transcription factor hypoxia-inducible factor 1α (HIF-1α), at Lys532, enhancing its ubiquitination and further proteasomal mediated destruction (Jeong et al., 2002). However mNaa10p^{235} and hNaa10p did not destabilize HIF-1α (Kim et al., 2006), reinforcing the idea that different Naa10p isoforms might have distinct biological functions. Furthermore, a recent study showed hNaa10p is autoacetylated *in vivo* at the internal lysine, K136. Autoacetylation of hNaa10p was required for binding and activation of β-catenin, which is a transcription factor for cyclin D1 expression in human lung cancer cells (Seo et al.). These results suggested that autoacetylation of hNaa10 is required for its enzymatic activity and reinforced the ε-amino acetyltransferase activity of mammalian Naa10p.

hNAA10 seems to be ubiquitously expressed in most human tissues and several human cancer cells lines (Arnesen et al., 2005b; Bilton et al., 2005; Jeong et al., 2002; Starheim et al., 2009b). *hNAA10* was shown to be expressed at higher levels in the brain, heart, liver and skeletal muscle (Jeong et al., 2002).

A mammalian specific gene duplication event of *hNAA10* gave rise to a paralogue known by h*NAA11*. Like hNaa10p, hNaa11p localizes both at the nucleus and the cytoplasm and was shown to be expressed in several human cell lines. In contrast with *hNAA10* which is broadly expressed, expressed sequence tag (EST) data shows that *hNAA11* expression is confined to certain tissues (liver, placenta, skin, testis) (Starheim et al., 2009b). Similar to Naa10p, mouse and human Naa11p interacts with Naa15p and exhibits N$^{\alpha}$-acetyltransferase

activity (Arnesen et al., 2006b; Pang et al., 2009), suggesting this complex may be responsible for protein N^{α}-acetylation in mammalian cells. Interestingly, in NB4 cells undergoing retinoic acid-mediated differentiation, the levels of endogenous hNaa10p and hNaa15p proteins decreased while the level of hNaa11p was maintained stable, suggesting differences in the function of these proteins (Arnesen et al., 2006b).

mNAA11 was shown to be upregulated in testis during male spermatogenesis. No *mNAA11* expression was found in somatic tissues, except for a trace amount in the ovary (Pang et al., 2009). Since *mNAA10* is located on the X chromosome it is not expressed during expermatogenesis, which was confirmed by RT-PCR. The authors proposed that the upregulation of *mNAA11* in the testis was to complement the function of mNaa10p during male meiosis (Pang et al., 2009).

3.1.2. Naa15 /NatH acetyltransferase

hNaa15p is the auxiliary subunit of the NatA complex. It was described to be localized to the cytoplasm (Arnesen et al., 2005a). Protein sequence analysis revealed yeast Naa15p contains 4 or 5 tetratrico-peptide repeat (TPR) motifs (Polevoda and Sherman, 2003a). TPR motifs are usually associated with protein-protein interactions. The authors suggested these domains could be involved in the interaction of yNaa15p with nascent polypeptides or with other NatA subunits (Polevoda and Sherman, 2003a).

Naa15p expression seems to correlate with cell proliferation. *hNAA15* is normally expressed at low levels in most adult tissues, with the exception of parts of the human brain, heart, testis, ovaries, spleen, colon and stomach (Line et al., 2002). High levels of expression were also detected in Burkitt lymphoma cell lines,

colorectal carcinoma SW480 cell lines, and in papillary thyroid carcinomas (Fluge et al., 2002; Line et al., 2002). Expression of this NAT seems to correlate with especially aggressive and undifferentiated tumors (Fluge et al., 2002). These data suggest that Naa15p is involved in cell proliferation, however its exogenous expression in embryonic kidney and papillary thyroid carcinoma cell lines did not significantly alter the cellular proliferation rate (Fluge et al., 2002).

The mouse Naa15p, also known as the NMDA receptor-regulated gene 1 (*NARG1*) was significantly expressed in the developing brain. *mNAA15/NARG1* was shown to be regulated *in vivo* by physiological levels of NMDA receptor function in developing neurons (Sugiura et al., 2001). NMDA receptors are highly expressed in the neonatal brain in regions of neuronal proliferation and migration, but downregulated during early postnatal development.

A mouse splice variant of mNaa15p, also designated by *tubedown-1* (*tbdn-1*) was shown to be expressed in different tissues during development. *Tbdn-1* was shown to be highly expressed in the developing embryo and placenta, and in unstimulated mouse embryonic cell lines during blood vessel development. The protein was also downregulated in myeloid leukemia cells after differentiation induction (Gendron et al., 2000). In adult tissues *Tbdn-1* expression was generally low or undetected with the exception of the arterial endocardium, endothelium of retinal vessels, bone marrow tissue, and ovaries (Gendron et al., 2000).

hNaa15p (Tbdn100) was also proposed to mediate the stable assembly of the Ku-transcriptional complex at the Osteocalcin promoter of in human osteosarcoma cells. Chromatin immunoprecipitation experiments indeed revealed that both Ku and hNaa15 were associated with the Osteocalcin promoter (Willis et al., 2002). Indeed, both the knockdown of Naa15p in animal models and

the suppression of Naa15p expression in human retinal-disease specimens have been associated with increased angiogenesis and pathological neovascular retinopathies (Gendron et al., 2001; Gendron et al., 2006; Paradis et al., 2008; Paradis et al., 2002; Wall et al., 2004).

An orthologue of hNaa15p, hNaa16p, was recently identified. This NAT resulted from an early vertebrate duplication event from the common ancestor of *hNAA15* and *hNAA16*. Immunoprecepitation assays confirmed the presence of the endogenous hNaa10-hNaa16 complex. *hNAA16* was shown to be expressed in a variety of human cell lines. This NAT was shown to be ribosome and non-ribossome associated and to exhibited acetyltransferase activity *in vitro*. Knockdown of hNaa16p lead to cell death suggesting an essential function of this NAT (Arnesen et al., 2009a). In contrast to hNaa15p, *hNAA16* expression does not seem to correlate with cell proliferation. *hNAA15* was shown to be the dominant variant in most tissues, with few exceptions (Arnesen et al., 2009a).

3.1.3. Knockout studies demonstrate that the NatA complex is involved in several biological processes

According to knockout studies, NatA seems to play an important role in cell cycle and cell growth. Yeast mutants of both subunits of the NatA complex are viable but exhibit a wide range of defects including slower growth, temperature sensitivity, salt sensitivity, defects in sporulation, derepression of the silent mating type gene HMLα and failure to enter G0 (Mullen et al., 1989; Park and Szostak, 1992). Both yNaa10p and yNaa15p were shown to influence transcriptional silencing at telomeres (Longtine et al., 1993; Stone et al., 1991). Indeed, overexpression of SIR1, which is known to be

involved in silencing transcription of the silent mating-type genes, suppressed the yNatA mutant defects in mating due to derepression of the silent loci. yNaa15/yNat1 was also identified in a yeast genome-wide search to affect chromosome stability. Both deletion and overexpression of yNaa15p led to chromosome loss (Ouspenski et al., 1999).

In contrast to yeast, orthologues of yNaa10p/yArd1p in higher eukaryotes such as *Trypanosoma brucei* and *Drosophila melanogaster* are essential genes (Ingram et al., 2000; Wang et al. 2010). Knockdown of both Naa10p and Naa15p in *Caenorhabditis elegans* are embryonically lethal (Sonnichsen et al., 2005). Loss-of-function mutations of the *gene variable nurse cells* (*vnc*), which encodes the *Drosophila* Naa10p led to several defects during oogenesis. These defects included abnormal cyst encapsulation, desynchronized cystocyte division, disrupted nurse cell chromosome dispersion and abnormal chorion patterning (Wang et al. 2010). These pleiotropic defects are consistent with the wide range of predicted NatA substrates.

Depletion of *hNAA10-hNAA15* in human cell lines resulted in reduced cell viability by induction of apoptosis and cell cycle arrest (Arnesen et al., 2009a; Arnesen et al., 2006c). Consistently, knockdown of *hNAA10* in HepG2 cells influenced genes involved in cell proliferation and energy metabolism. Genes involved in cell growth, survival and metabolism were down regulated, while antiproliferative genes were upregulated (Fisher et al., 2005). Moreover, over-expression of *hNAA10* led to upregulation of genes involved in cell cycle, growth and survival such as *CDC2* (cell division cycle 2), *CCNA2* (Cyclin A2) and *BIRC5* (apoptosis inhibitor surviving) (Fisher et al., 2005). Indeed, another study suggested hNaa10 could participate in cell proliferation as an activator of the β-catenin pathway (Lim et al., 2006). The authors attributed inhibition of cell proliferation

and induction of G1 arrest in lung cancer cell lines depleted of hNaa10 to the transcriptional repression of the *cyclin D1* gene (Lim et al., 2006). hNaa10p knockdown inhibited the activity of the β-catenin/TCF, which is a transcription factor for cyclin D1. The same study showed hNaa10p associated and acetylated β-catenin, which in turn induced the binding of TCF4 to *cyclin D1* promoter (Lim et al., 2006).

The NatA complex was also implicated in neuronal dentritic development. Both *mNAA15* and *mNAA10* were found to be expressed postnatally in the cerebellum during Purkinje neuron development. Purkinje cells exhibit highly complicated dentritic branching patterns. mNaa10p activity was shown to regulate the fraction of acetylated tubulin and overexpression of a mutant mNaa10p form limited dentritic development.

3.1.4. The NatA complex is associated with tumor development

An increasing amount of data has associated tumor development to the expression of NatA subunits. *hNAA10* was shown to be highly expressed in hepatocellular carcinoma. Its expression was associated with the dedifferentiation step in liver cancer progression (Midorikawa et al., 2002). hNaa10p was also found to be overexpressed in colorectal cancer tissues and breast cancers (Ren et al., 2008; Yu et al., 2009).

hNAA15 was shown to be overexpressed in papillary thyroid carcinoma especially in clinically aggressive and undifferentiated tumors (Fluge et al., 2002). Furthermore, hNaa15p levels were shown to be overexpressed in human thyroid papillary neoplastic versus non-neoplastic tissues (Arnesen et al., 2005b). *hNAA15* was also upregulated in gastric cancer (Line et al., 2002). Consistently, *in vitro*, retinoic acid-induced neuronal differentiation responses of

neuroblastoma cells were associated with a significant decrease in hNaa15p expression (Martin et al., 2007).

Altogether these data strongly suggests a strong correlation between NatA complex and carcinogenesis, the specific molecular mechanisms underlying the role of this complex in cancer development remains mostly unknown.

3.2. The NatB complex

The NatB complex is composed of two subunits, the catalytic subunit Naa20p (Nat3p) and the auxiliary subunit Naa25p (Mdmp) as has been observed in yeast and human cells (Polevoda et al., 2003; Singer and Shaw, 2003; Starheim et al., 2008). Depletion of hNaa25p significantly diminished hNaa20p levels, indicating hNaa25p is required for hNaa20p stability (Starheim et al., 2008). Both hNaa20p and hNaa25p were found at the cytoplasm and present in both ribosome and non-ribosome bond forms. However these proteins were shown to be generally higher in the non-polyribosomal fraction (Starheim et al., 2008), suggesting additional functions than the ones related with the ribosomal-bound ones. The hNaa20p subunit but not hNaa25p, was also found at the nucleus, suggesting hNaa20p might have other functions independent of the NatB complex (Starheim et al., 2008).

The yeast NatB complex was shown to potentially acetylate the N-terminal methionine residue of substrates with the N-terminal sequence Met-Glu-, Met-Asp- and Met-Asn- (table 1) in a highly sequence-specific manner (Polevoda et al., 1999; Polevoda and Sherman, 2003b). Recent studies have shown that the predicted NatB substrates are completely acetylated in yeast and are almost completely acetylated in *Drosophila* and humans (Arnesen et al., 2009b; Goetze et al., 2009). Supporting the conservation of NatB

substrate specificity, hNatB was shown to acetylate a peptide with a Met-Asp- N-terminus *in vitro* (Starheim et al., 2008). This N-terminus corresponds to the NF-kB subunit p65, which is known to be acetylated *in vivo* (Arnesen et al., 2009b).

3.2.1. NatB known substrates and knockdown studies

Deletion of either yNaa20p or yNaa25p genes resulted in the reduction of cell growth and mating, and increased sensitivity to DNA-damaging agents. yNaa20 mutants were defective in actin cable formation (Hermann et al., 1997; Polevoda et al., 2003). This phenotype was linked to the loss of acetylation of actin and tropomyosin 1 (Tpm1), which are known NatB substrates. NatB-dependent N^{α}-terminal acetylation of Tpm1 was shown to be required for its normal interaction with actin (Singer and Shaw, 2003).

Another substrate of the NatB complex is the conserved inhibitor of protease carboxypeptidase Y, Tfs1p. Inhibitor activity of Tfs1p was shown to be N^{α}-acetylation dependent. Interestingly, Tfs1p inhibits Ira2p which is a Ras-GTPase-activating protein in the protein kinase A (PKA) pathway. These data suggest that N^{α}-terminal acetylation of Tfs1p is essential in the regulation of the PKA pathway (Caesar and Blomberg, 2004).

Proteins involved in DNA processing and cell cycle progression were shown to be overrepresented among the yeast predicted substrates of NatB, suggesting the yeast NatB complex might have an important function in cellular proliferation (Caesar et al., 2006). Consistently, knockdown of hNatB subunits inhibited cell growth and proliferation, and disturbed cell cycle progression. One study demonstrated that hNaa20p knockdown led to a G_0/G_1 arrest and an increase in the levels of the inhibitor of cyclin-dependent kinases p21 (Starheim et al., 2008). Another study found that hNaa20p knockdown

led to a reduction of cells in G_0/G_1 but an increase of cells in S phase and an accumulation of cells in G2/M phase. Furthermore, this later study showed a strong increase of the tumor suppressor protein 53 (p53) as well as p21 in hNaa20p-inhibited cells (Ametzazurra et al., 2008). On the other hand, hNaa20p knockdown led to downregulation of genes that promote cell proliferation (Ametzazurra et al., 2008). Upregulation of p53 is associated with induction of growth arrest. p21 is a known inhibitor of cyclin dependent kinases and thus functions as a regulator of cell cycle progression at G1. The expression of p21 is tightly controlled by tumor suppressor protein p53. These results strongly suggest the observed growth arrest is linked to p53 and p21 upregulation.

Knockdown of hNaa25p leaded to cell death, a decrease in G_0/G_1 cells and a decrease in p21 levels. Since hNaa20p protein levels are dependent on hNaa25p levels, knockdown phenotypes of hNaa25p are most likely a combination of the phenotypes of both NatB subunits. The different effects observed by knockdown of hNaa20p and hNaa25p can be attributed to downstream mechanisms of this complex. On the other hand they might also be a result of individual functions of these subunits from those related to the NatB complex (Starheim et al., 2008).

The NatB complex has also been suggested to play a role in neoplastic growth. hNaa20p was found upregulated in tumor tissues of mouse models of hepatocellular carcinoma. Moreover, hNaa20p was shown to be increased in malignant tissue of patients with hepatocellular carcinoma (Ametzazurra et al., 2008).

3.3. The NatC complex

As with the NatA and NatB complexes, the NatC complex is conserved form yeast to humans. It is composed of the Naa30p

(Makp) catalytic subunit, and the auxiliary subunits Naa35p (Mak10p) and Naa38p (Mak31p). In yeast all tree subunits are required for NatC acetyltransferase activity (Polevoda and Sherman, 2001). hNaa30p and hNaa35p localize almost exclusively at the cytoplasm, while hNaa38p also localizes to the nucleus. hNAA38p (Lsmd1) shares sequence similarity with the Sm-like proteins. The Sm-like proteins are small ribonucleproteins (snRNP), which are involved in RNA processing (Mattaj et al., 1993). Therefore, consistent with its nuclear localization, hNAA38p might have a role in RNA processing independent of the NatC complex.

All subunits of the NatC complex were found to be ribosomal and non-ribosomal bound (Starheim et al., 2009a). This suggests that these proteins might have other functions than the ones related with co-translational acetylation at ribosomes.

yNatC was shown to acetylate the N-terminal of proteins containing large hydrophobic amino acids such as isoleucine, leucine, tryptophan, or phenylanine adjacent to the iMet (Polevoda et al., 1999; Polevoda and Sherman, 2003a). *In vitro* assays with hNaa30p revealed similar substrate specificity supporting conservation of the NatC complex in eukaryotes (Starheim et al., 2009a).

3.3.1. NatC known substrates and knockdown studies

Mutant yeast strains of all subunits of the NatC complex display similar phenotypes: diminished growth at 37ºC in medium without fermentable sources (Polevoda and Sherman, 2001), defective L-A virus propagation (Wickner and Toh-e, 1982) and loss of telomere elongation (Askree et al., 2004). A screen for conserved genetic interactions in yeast identified Naa30p as part of a core genetic interaction network, suggesting that NatC activity is required for DNA replication in eukaryotes (Dixon et al., 2008).

NatC is an essential NAT in higher eukaryotes. Deficient Zebrafish for *Embryonic Growth-Associated factor* (*EGAF*), which is a homologue of hNaa30p, fail to develop due to decreased cell proliferation, increased apoptosis and poor blood vessel development contributing to embryonic lethality. Interestingly, TOR expression and signaling is significantly reduced in EGAP/zNaa30p morphans (Wenzlau et al., 2006). mTOR complex is involved in regulation of cell growth, proliferation and survival (Corradetti and Guan, 2006; Foster and Fingar, 2010; Wullschleger et al., 2006) Inhibition of zTOR phenocopied zNaa30 morpholino defects and overexpression of active TOR rescued zNaa30 morphans, suggesting TOR is a direct substrate of the NatC complex (Wenzlau et al., 2006).

Consistent with the zebrafish data, hNatC is required for cell proliferation. NatC knockdown studies in human cells resulted in diminished DNA synthesis, reduced cell viability with an increase in the G1/G0 fraction and p53 induction of apoptosis. hNaa30 knockdown led to an increase in p53 serine 37 phosphorylation, and an increase of the pro-apoptotic p53 downstream genes *KILLER*, *NOXA* and *FAS* (Starheim et al., 2009a).

A known substrate of the NatC complex *in vivo*, is the yeast small Arf-like GTPase Arl3p, which is important for membrane trafficking and organelle structure in eukaryotic cells. Crosslinking experiments demonstrated that Sysp and Arl3p (Setty et al., 2004) in yeast, and the respective homologues hSys1 and ARFRP1 in mammalian cells (Behnia et al., 2004), interact physically, an interaction which requires N^{α}-acetylation of Arl3p, showing this process is conserved. Another potential substrate of the NatC complex is the hArl8b Arf-like GTPase. hArl8b needs to be N^{α}-acetylated for proper lysosomal association (Hofmann and Munro, 2006). Indeed hNaa30 was shown *in vitro* to acetylate an MLAL- N-terminus which correspond to the N-terminal sequence of hArl8b and matches the

substrate specificity of the NatC complex. Consistently, hNaa30p knockdown leaded to aberrant localization of hArl8b (Starheim et al., 2009a).

3.4. The NatD complex

The NatD complex composed by the Naa40p acetyltransferase is well conserved from yeast to humans. Recombinant yNaa40p was shown *in vitro* to acetylate a Ser- N-terminal peptide corresponding to Histone H4. Moreover, yeast H4 and H2A were shown to be unacetylated in yNaa40p mutants (Song et al., 2003). These histones are known to be N^{α}-terminally acetylated in all species from yeast to mammals, suggesting Naa40p-mediated acetylation is conserved. Surprisingly, yeast Naa40p mutants did not exhibit any observable phenotype under all conditions tested (Song et al., 2003).

3.5. San and the NatE complex

The NatE complex is composed of the previously described Naa10p and Naa15p subunits of the NatA complex and a third subunit known by Naa50p. This complex has been identified in yeast, *Drosophila melanogaster* and human cells, therefore hNaa50 and dNaa50 are believed to be homologues of the yNaa50 (yNat5p) (Arnesen et al., 2006a; Gautschi et al., 2003; Williams et al., 2003). In higher eukaryotes Naa50p was first identified in *Drosophila melanogaster* where it was named Separation Anxiety (San) (Williams et al., 2003).

yNaa50 was found in equimolar concentrations with yNaa10 and yNaa15. Combined with previous data on the size of the yNatA complex (Lee et al., 1988; Park and Szostak, 1992), the authors suggested the complex was trimeric (Gautschi et al., 2003). Gel

exclusion chromatography of *Drosophila* embryo protein extracts failed to identify fractions of dSan/dNaa50 corresponding to its monomeric size (Williams et al., 2003). This suggested dSan/dNaa50 only existed in a complex with dNaa10 and dNaa15 proteins. However, in contrast to dSan/dNaa50, 80% of hSan/hNaa50 was found in fractions excluding the NatA complex, suggesting the majority of human San/hNaa50 was either not associated or weakly associated with the NatA complex (Hou et al., 2007).

San/Naa50p is localized at the cytoplasm (Hou et al., 2007; Williams et al., 2003). Stable association of yNaa50p to the ribosome was shown to be dependent on yNatA subunits (Gautschi et al., 2003). Accordingly, optimal protein levels of hSan were also shown to depend on the NatA complex (Arnesen et al., 2006a; Hou et al., 2007). However, a dependency of the NatA complex on hSan was not observed. In contrast to yNatA mutants, knockouts of yNaa50 did not result in any detectable phenotypes neither affected NatA type acetylations (Gautschi et al., 2003). Also yNaa50 was demonstrated to be dispensable for the acetylation of yNaa10p and yNaa15p substrates (Polevoda and Sherman, 2003b). Moreover, knockdown phenotypes of hSan/hNaa50 were distinct from those of the NatA complex, suggesting hSan/hNaa50 functions separately from the NatA complex (Hou et al., 2007).

As with the previously described acetyltransferases, San/Naa50p contains a GNAT domain. Regarding substrate specificity, hSan/hNaa50 preferentially acetylated *in vitro* peptides started by ML- (Evjenth et al., 2009). hSan/hNaa50 was also shown to have both N^{α}- and N^{ε}-acetyltransferase activity *in vitro* (Chu et al. 2010; Evjenth et al., 2009). *In vitro*, hSan/hNaa50 is autoacetylated by an N^{ε}-acetylation event and this autoacetylation led to an increase in its N^{α}- but not N^{ε}-acetyltransferase activity, suggesting autoacetylation is of physiological relevance (Evjenth et al., 2009).

3.5.1. San is required for centromeric sister chromatid cohesion

San/Naa50p seems to share conserved functions in higher eukaryotes. Attempts in yeast failed to detect yNaa50 substrates by two-dimensional gel electrophoresis. The authors (Polevoda and Sherman, 2003b) suggested this could be a reflection of yNaa50 acetylating a small subset of proteins. Consistent with this, depletion of San/Naa50p in higher eukaryotic cells leads to specific phenotypes regarding mitosis.

dSan/dNaa50 was identified in a genetic screen for mitotic mutants causing late larval and pupal lethality. Indeed mitotic progression was severely disrupted in *san* homozygous mutants. *san* mutant neuroblasts exhibited a strong mitotic arrest dependent on the SAC. Moreover, cells which progressed into anaphase revealed chromosome segregation defects which included lagging chromosomes and chromosome bridges. In a wild type cell, sister chromatids do not separate from each other until anaphase onset. Instead, *dsan* mutant centromeric connections were already abolished by prometaphase resulting in premature sister chromatid separation (PSCS) (Williams et al., 2003). Also, the cohesin subunit, Drad21/Scc1, was shown to be absent from chromosomal centromeric regions, suggesting PSCS in *san* mutants is due to mislocalization of the cohesin complex from the centromeres (Williams et al., 2003). During the metaphase to anaphase transition separase degrades centromeric cohesion to allow disjunction of sister chromatids. dSan/dNaa50 was shown to act upstream of separase in ensuring sister chromatid cohesion (Williams et al., 2003).

Depletion of hSan/hNaa50 in cell culture also led to PSCS with loss of the cohesin subunit, SMC1, at the centromeric region (Hou et al., 2007). Depletion of both Plk1 and hSan/hNaa50 rescued sister chromatid cohesion at chromosome arms, but not at the centromeres,

reinforcing the previous observations that San/Naa50p is specifically required for centromeric cohesion. Moreover, the acetyltransferase activity of hSan/hNaa50 was shown to be required for its function in sister chromatid cohesion. A hSan/hNaa50 Y124F mutant form, which abolished acetyltransferase activity, was not able to rescue the cohesion defects when expressed near the physiological levels (Hou et al., 2007). However, this mutant form does not discriminate between the N^{α}- and N^{ε}-acetyltransferase activities. Depletion of hSan/hNaa50 in HeLa cells also lead to mitotic defects which include multipolar spindles and scattered chromosomes along the mitotic spindle (Hou et al., 2007).

San/Naa50p function in centromeric cohesion is apparently conserved in metazoans. Yet, since there are no known *in vivo* substrates of this NAT, the exact molecular mechanism by which it is involved in centromeric sister chromatid cohesion is not known. Identification of San/Naa50p substrates will ultimately shed light on the mechanism by which San/Naa50p regulates centromeric cohesion.

CHAPTER II

Identification of new genes required for syncytial nuclear divisions

1. Introduction

Upon *Drosophila* egg fertilization, embryogenesis starts with 13 synchronous nuclear divisions without cytokinesis. The first 9 divisions occur in the interior of the embryo. After cycle 9, most nuclei move outward towards the periphery, to form the so-called syncytial blastoderm (Foe and Alberts, 1983). This is followed by 4 nuclei divisions (Foe et al., 2000; Karr and Alberts, 1986; Sullivan and Theurkauf, 1995) leading to the formation of a multicellular syncytial blastoderm. Cycles 9/10 are accompanied by the formation of primordial germ cells (PGCs), also known as pole cells, at the posterior end of the embryo. After the initial 13 divisions, the cell cycle pauses at interphase. During interphase of cell cycle 14 the somatic nuclei of the syncytial blastoderm, that are arranged as a cortical monolayer, are enclosed into cells by invagination of the plasma membrane in a process called blastoderm cellularization (Mazumdar and Mazumdar, 2002) (fig. 1). Blastoderm cellularization is a cytokinesis based process leading to the *de novo* formation of a polarized epithelium. The ingrowth of plasma membrane during cellularization requires a number of proteins and membrane materials, which are recruited by a microtubule-dependent pathway. Although some mechanisms may be specific to cellularization, others may share some features with other cellular processes. Therefore, cellularization is a particularly interesting system to study cell polarization during development.

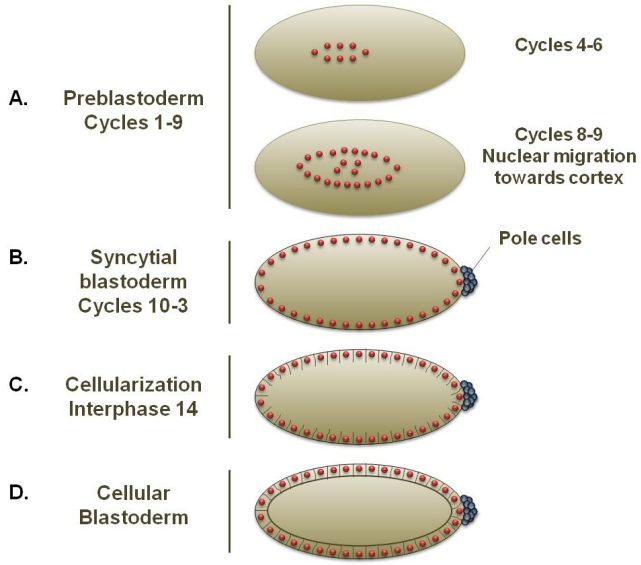

Figure 1: *Drosophila melanogaster* nuclear cycles during early embryogenesis. **A.** In the preblastoderm stage nuclei divide in the interior of the embryo. Nuclear migration towards the cortex occurs during cycles 8 and 9 and nuclei reach the cortex by cycle 10. **B.** Pole cells form at the posterior end of the embryo during cycles 9/10. At the cortex, nuclei divide three times (cycles 10-13) forming the syncytial blastoderm. **C-D.** Cellularization begins during cycle 14 where the plasma membrane invaginates between the nuclei to form ~6000 blastoderm cells (Adapted from Mazumdar and Mazumdar, 2002).

In this chapter we have identified 2 complementation groups defective for syncytial nuclear divisions. One complementation group was allelic to the *separation anxiety* (*san)* gene while the other group was mapped to a genomic region containing two uncharacterized coding genes. Interestingly these alleles do not display egg laying defects, suggesting the mutated genes are not required for germ-line stem cell divisions. Therefore, we hypothesize the activity of these genes is mainly required for cell division in somatic tissues. We speculate that germ-line stem cell mitosis is differentially regulated when compared to the soma.

2. Materials and Methods

2.1. Fly husbandry

Unless otherwise stated, flies were raised at 25ºC under standard procedures (Roberts, 1998). Embryos were collected on apple juice plates with fresh yeast for further analysis.

2.2. 2R maternal screen

In order to identify new genes required for blastoderm cellularization we took advantage of a collection of maternal mutants previously isolated in the laboratory of Dr. Ruth Lehmann (Barbosa et al., 2007). Due to methodological constraints related to the induction of germ-line clones all mutants mapped to the right arm of the second chromosome (2R).

A primary screen isolated 137 independent mutant lines with abnormal blastoderm cellularization and/or germ-band extension defects, but normal formation of PGCs. Mutant lines with egg-laying defects were discarded to avoid mutations in housekeeping genes. A secondary screen isolated 47 lines from the previous 137. These mutant lines showed absence or “scraps” of embryonic cuticle. This phenotype is frequently associated with loss of embryonic ectoderm integrity.

The FLP/FRT *ovo*^{D} system (Chou and Perrimon, 1992) allows the generation of germ-line clones and the isolation of maternal mutant embryos. Mutagenized P[FRT 42B] / CyO virgin females were crossed with P[*hs*-FLP^{22}]/Y; P[FRT42B] P[w^{+} *ovo*^{D}]/ CyO *hs-hid* males. F1 progeny was heat shocked for 1h at 37°C during the second and third larval instar stages. Since induction of *hs-hid* expression in larvae is

lethal, and since *ovo*^{D} is a dominant mutation that inhibits oogenesis, only the germ-line stem cells that induced FRT-mediated mitotic recombination after induction of the flipase (hs-FLP) will produce mature eggs. Mature eggs were necessarily homozygous for isolated maternal mutations.

2.3. Mapping and isolation of complementation groups

Different alleles of the same gene (complementation group) were identified by crossing the mutant lines with each other. We assumed the isolated mutations were recessive and intragenic complementation was unlikely. Lethal and female sterile complementation groups were directly mapped using the Bloomington 2R deficiency kit (Bloomington Drosophila Stock Center). All together these deficiencies (deletions) are known to cover ~80% of the 2R chromosome-arm. To avoid secondary site lethal mutations not related with the isolated phenotypes, deficiency mapping was always performed using at least two different alleles of each complementation group. Any non-complementation result was confirmed with all alleles of each complementation group and with the reciprocal crosses. Once a complementation group was mapped to a given cytological (genetic) interval, a candidate gene approach was taken for all available lethal and sterile mutations known to map to that relevant cytological interval.

2.4. DNA sequencing of candidate genes

To molecularly characterize the isolated mutations on a given complementation group, genomic polymerase chain reaction (PCR) was carried out from mutant males of each isolated allele. An allele from a different complementation group but also isolated on the 2R screen (similar genetic background) was used as a control in order to

identify DNA polymorphisms when compared to the published *Drosophila* genome sequence (Flybase). Two independent genomic PCR fragments from each allele were sequenced and compared with each other and with the control.

2.5. Molecular biology and generation of transgenic lines

2.5.1. *UAS-san* generation

To generate *UAS-san*, *san* open reading frame (ORF) was amplified by PCR with a forward primer containing an *XbaI* restriction site and a reverse primer containing a *KpnI* restriction site. The Amplified PCR product was subcloned into pGEM-T Easy vector (Promega). After verification by digestion and DNA sequencing, *san* cDNA was subcloned into a P[UAST] vector (Brand and Perrimon, 1993). Transgenic san-*UAS* lines were generated by microinjecting the P[UAST-san] construct into *w1118* embryos. UAS-san transgenic lines were created at BestGene Inc. (Chino Hills, CA, USA).

Fly lines with the genotypes w; B16-79/CyO; Actin5C-Gal4/TM6B and w; B50-26/CyO; san-UAST/TM6B were generated to perform rescue experiment. Rescue of complementation group 2 mutation alleles was performed by crossing w; B50-26/CyO; san-UAST/TM6B virgin females with w; B16-79/CyO; Actin5C-Gal4/TM6B males. B50-26 and B16-79 are two mutant alleles of *san* isolated in the maternal screen.

2.5.2. Genomic fragments for complementation group 3

The bacterial artificial chromosome BACR25I01 (Berkeley *Drosophila* Genome Project) containing the entire interval to which the complementation group 3 was mapped, was partially digested with the

restriction endonuclease *XbaI*. The larger DNA fragments (between approximately 8 and 15Kb) were subcloned in bulk into the *XbaI* site of the pCasper 2 vector. Size of the subcloned fragments were identified by digestion and identification was performed by DNA sequencing using the flanking primers pCasperFw 5'-CGCAAAGCTTGGGCTGCAGGTCGA-3' and pCasperRev 5'-TACTAGAATTCGTTAACAGATCT-3'. Six non-overlapping clones were used to generate transgenic flies (table 1, fig. 6). Given the difficulty of cloning the gene affected in complementation group 3 and to facilitate our work, these clones were given names of deserts.

Clone	Clone name	Clone size (bp)	Cloned region of *Drosophila* genome	
			Beginning sequence	End of sequence
1	Kalahari	17 494	CTAGAAGCGCCACCGGGC…	…ATTAGCAAATATGTAGCT
2	Sonora	15 400	CTAGAGAACGAAAGCGAG…	…AATTAAACATAAATATAT
3	Libya	15 555	CTAGATGGAAATTGAAAT…	…TCGCCATTTTCTGCTCAT
4	Sahara	12 922	CTAGAGCGGACCAAGTAA…	…CACGCTTATCGGAGCTGT
5	Atacama	6 671	CTAGATTTATATGTTGAT…	…TCTATAGGAAATTCAACT
6	Mojave	6 528	CTAGAAAAGGTAGTATGT…	…ATCGCGGCATTCTCTGGT

Table 1: Genomic DNA fragments used to map complementation group 3.

2.6. DNA staining of complementation group 3 embryos

For primary phenotypic analysis of complementation group 3 mutants, embryos at 4-5 hours of age were collected and fixed (after dechorionation in 50% bleach for 5 min) by gentle shaking for 1 hour in 4 mL heptane, 0.125 mL 37% formaldehyde and 0.875 mL PBS. Fixation was followed of devitellinization by addition of 4 mL methanol and shaking vigorously during 1 minute. Following rehydration, embryos were three times 5-min washed with phosphate buffered saline (PBS, pH 7.4) containing 0.1% Tween-20. DNA was stained with OliGreen at 1:5000 (Invitrogen) with the addition of 5 µg/mL RNAse A.

Embryos were mounted in Fluorescent Mounting Medium (DakoCytomation, Inc) and immunostainings were visualized using a Leica SP5 confocal microscope. All images are confocal sections.

3. Results

3.1. Right-arm of 2R maternal screen allowed the identification of six complementation groups

The maternal forward genetic screen (Barbosa et al., 2007) allowed the isolation of 47 mutant strains defective for early embryonic development. From our complementation analysis, we identified six complementation groups (table 2), which were zygotically lethal or female sterile (fig. 2). All complementation groups were maternally lethal (e.g., embryos whose maternal contribution was mutant were not viable).

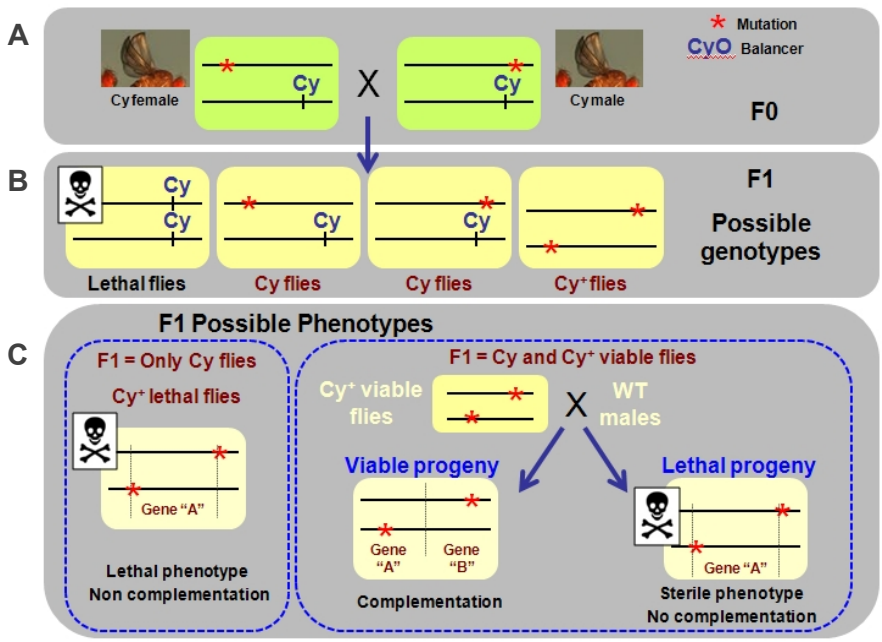

Figure 2: Complementation tests. (A) F0 represents the crosses between all mutant lines obtained from the screen. All lines were in *trans* with the CyO balancer containing the Cy dominant marker (curly wings). (B) Representation of possible F1 genotypes. F1 progeny flies could have two possible phenotypes Cy and Cy^+ (Cy = curly wings; Cy^+ = normal wings). (C) If F1 progeny only contained Cy flies, both mutant lines were likely to be lethal alleles of the same gene. If F1 progeny contained fertile Cy^+ flies (wild-type wings), there was complementation and

most likely they were alleles of different genes. If F1 progeny contained female sterile Cy^+ flies (wild-type wings), both mutant lines were likely to be alleles of the same gene. We assumed the isolated mutations were recessive and intragenic complementation was rare. If Cy males in F0 correspond to a deficiency, then this scheme applies to the cytological mapping of the mutant lines obtained from the screen.

Complementation group 6 was previously shown to be allelic to *scraps*. This gene encodes the Anilin protein, which was previously shown to be essential for syncytial nuclear divisions and blastoderm cellularization (Field et al., 2005).

A primary phenotypic characterization of the six complementation groups allowed us to observe that both complementation groups 2 and 3 revealed syncytial nuclear defects (Chapter II, section 3.4.). Interestingly, we failed to detect any egg laying defects in these mutants, which suggested the mutated genes were not needed for germ-line stem cells mitotic divisions and they were likely to be differentially required between the soma and the female germ-line. We therefore decided to pursue these two complementation groups for further analysis.

Complementation Groups	Alleles	Cuticle	Complementation test
1	A56-12 B12-22 B42-1 B43-36	No cuticle No cuticle No cuticle No cuticle	Lethal Lethal Lethal Lethal
2	B16-79 B50-26	No cuticle No cuticle	Lethal Lethal
3	A10-42 B16-2 B43-36	No cuticle No cuticle No cuticle	Sterile Sterile Sterile
4	B12-43 C2-32 C50-47	Scraps Scraps Scraps	Lethal Lethal Lethal
5	C50-20 C50-61	Scraps Scraps	Sterile Sterile
Scra	B26-35 C82-45	Scraps Scraps	Sterile Sterile

Table 2: 2R screen complementation groups.

3.2. Mapping of complementation group 2

3.2.1. Complementation group 2 is allelic to the gene *separation anxiety* (*san*)

When crossed with each other B16-79 and B50-26 mutant lines failed to complement zygotic lethality, giving rise to complementation group 2 (table 2). To identify the gene mutated in complementation group 2, both alleles were mapped using the Bloomington 2R deficiency kit (see Materials and methods). The following seven deficiencies failed to complement both alleles (B16-79 and B50-26): Df(2R)en-A, Df(2R)en-B, Df(2R)E3363, Df(2R)Exel6060, Df(2R)ix[87i3], Df(2R)ED2219 and Df(2R)ED2155. Whereas, Df(2R)En28 complemented both alleles. Since the breakpoints of each of the deficiencies were cytologically mapped within the 2R chromosome-arm, this allowed mapping group 2 alleles to the cytological interval 47E3 – 47F8, which is comprised of 53 annotated genes (fig. 3). By a candidate gene approach, we concluded that both alleles failed to complement a known lethal mutation (san^2) of the *separation anxiety* (*san*) gene (Williams et al., 2003), which is annotated within the cytological band 47F5.

Sequencing both alleles of complementation group 2 confirmed they are allelic to *san*, as both alleles contained two distinct nonsense mutations within *san* ORF. These two nonsense mutations are predicted to cause severe truncations of the San protein (Chapter III).

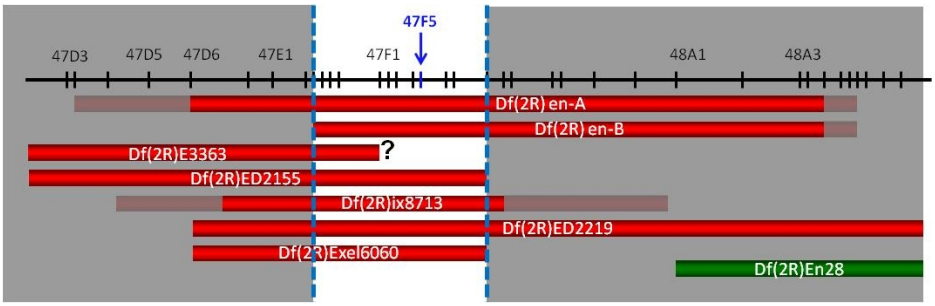

Figure 3: Complementation group 2 cytological interval. Red and green bars represent deleted genomic portions of the corresponding indicated deficiency. Deficiencies that did not complement group 2 are indicated by red. Deficiencies that complemented group 2 are indicated by green. The right limit of deficiency E3363 is not well defined.

3.2.2. *san* cDNA rescues the viability *san* mutants

Both isolated alleles of *san* are recessive lethal. To confirm the lethality was exclusively associated with the *san* locus, rescue experiments were carried out using a *UAS-san* cDNA transgene. The lethality of the transheterozygous flies B16-79/B50-26 was rescued by *UAS-san* driven by a ubiquitous *Gal4* driver (*Act5c*-Gal4). This demonstrated the lethality associated to these alleles was caused by loss of *san* gene activity.

3.3. Mapping of complementation group 3

3.3.1. Cytological mapping of complementation group 3

When crossed with each other A10-42, B16-2 and B43-36 mutant lines failed to complement female sterility, giving rise to complementation group 3 (table 2). As with group 2, all alleles of complementation group 3 (table 2) were mapped using the Bloomington 2R deficiency kit. Deficiencies Df(2R)bw-HB132,Frd^{HB132} and Df(2R)Vir130 did not complement both alleles A10-42 and B43-36

by sterility, nor allele B16-2 by lethality. This suggested that allele B16-2 was a stronger allele than the other two alleles. This allowed mapping of the three mutant alleles to the cytological interval 59D11 - 59E1 (fig. 4).

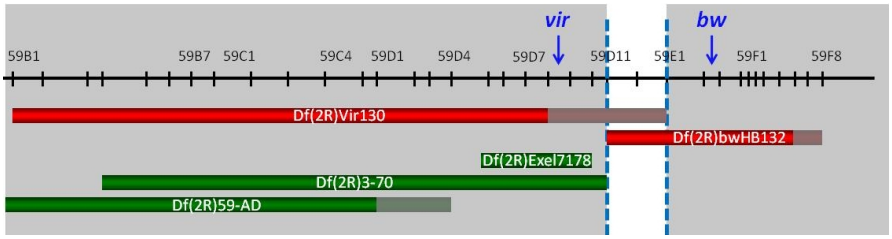

Figure 4: Complementation group 3 cytological interval. Red and green bars represent deleted genomic portions of the corresponding indicated deficiency/ deletion. Deficiencies that did not complement group 3 are indicated in red. Deficiencies that complemented group 3 are indicated in green.

Since there were no additional deficiencies that could narrow this region to a smaller portion of the 2R chromosome, we crossed the deficiencies Df(2R)Vir130 and Df(2R)bw-HB132 to lethal mutations known to map to this interval. Transheterozygous between Df(2R)Vir130 and Df(2R)bw-HB132 were lethal. These deficiencies were crossed with lethal alleles of the *virilizer* (*vir*) and *brown* (*bw*) genes. *vir* was annotated within the cytological bands 59D8-9 and *bw* was annotated within the cytological bands 59E2-3. Df(2R)Vir130 complemented the *bw* mutant, but did not complement the *vir* mutant. Similarly, Df(2R)bw-HB132 did not complement the *bw* mutant, but complemented the *vir* mutant. Complementation group 3 mutations were therefore localized in the interval between the *vir* and the *bw* genes. The genomic region between these two genes corresponded to the annotated base pairs 19247786 to 19426016. This region was 178,23 Kb long and included 25 annotated genes. Since for most genes there were no available mutants, we could not pursue a

candidate gene approach as previously performed for complementation group 2.

3.3.2. A genomic DNA fragment containing 2 genes rescues the sterility of complementation group 3 mutants

Complementation group 3 mutations were likely to be within the transcribed regions of one of the 25 annotated genes within the previously mapped interval. 20 out of the 25 annotated genes were sequenced in alleles A10-42 and B16-2, but we failed to detect any mutation within these genes (fig. 5) (Rui Tostões, unpublished data). The remaining 5 unsequenced genes included yellow-d, yellow-d2, odorant receptor 59A (*or59a*), odorant receptor 59B (*or59b*) and odorant receptor 59C (*or59c*). Both *yellow-d* and *yellow-d2* genes are *yellow* (*y*) related genes (Drapeau, 2001). The *or59a*, *or59b*, *and or59c* genes belong to the larval odor receptor genes. *Or59a* was described to be expressed in larval olfactory receptor neurons (Kreher et al., 2005). Furthermore, according to Affymetrix data (http://www.flyatlas.org/) these 5 genes are not expressed during oogenesis, suggesting they are not maternally provided. Therefore, these genes are unlikely to be associated with the observed cell cycle phenotypes.

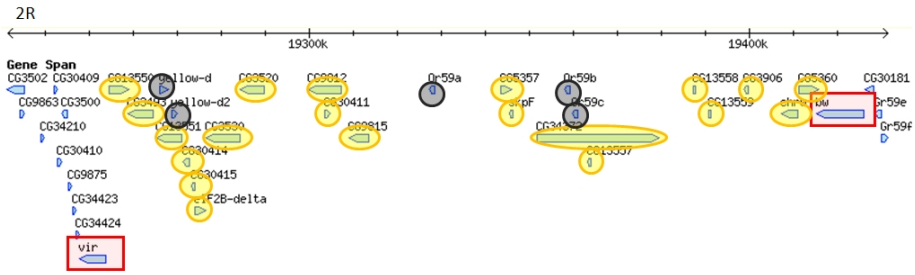

Figure 5: Complementation group 3 alleles did not contain mutations within 20 out of 25 genes annotated between *vir* and *bw*. Representation of the sequenced genes within the genomic region between the *vir* and *bw* genes (red boxes). Sequenced genes are highlighted in yellow. Non sequenced genes are highlighted in gray.

We decided to pursue an alternative experimental approach and use genomic DNA complementation. Transgenic flies carrying non-overlapping genomic DNA fragments mapped to the region between *vir* and *bw* were used to complement female sterility or lethality of complementation group 3 alleles. Six different transgenic lines were generated (see Materials and methods), containing the genomic fragments represented in figure 5. These transgenic lines were called names of different deserts given the difficulty of cloning the affected gene and to facilitate their identification (Table 1; fig. 6).

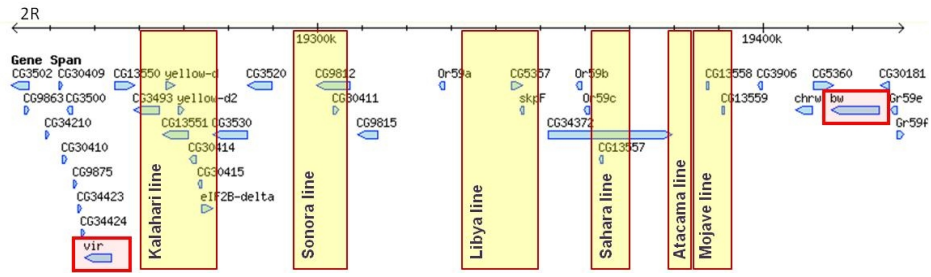

Figure 6: Representation of the genomic regions used for complementation of group 3. Yellow boxes correspond to the regions of DNA that were used to create transgenic flies. Each transgenic line was named after a desert. *vir* and *bw* genes are highlighted in red boxes.

The Mojave transgenic line complemented both the sterility and viability of all complementation group 3 alleles. The Mojave transgenic line contained a genomic region of 6528 bp long. We decided to sequence this region in complementation group 3 mutants and search for possible mutations there. Figure 7 represents the regions corresponding to the Mojave fragment already sequenced in both alleles A10-42 and B43-36 of complementation group 3. Although we have failed to find any mutation, close to 1Kb of genomic DNA still needs to be sequenced. Since both annotated genes within this region lacked 5´and 3´UTRs (Flybase), it was likely the proposed gene structure was incomplete.

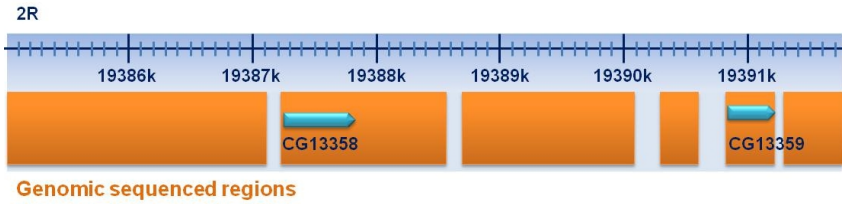

Figure 7: Sequenced genomic regions within the Mojave genomic fragment. Blue area represents the genomic region of the Mojave fragment which complemented complementation group 3 alleles. Orange areas represent the regions already sequenced within this fragment in complementation group 3 mutants.

3.4. *san* and complementation group 3 alleles showed dramatic defects during syncytial nuclei divisions

Although two of the maternal screen criteria were , normal egg laying (a proxy for normal germ-line stem cells mitosis) and normal formation of primordial germ cells (a proxy for posterior migration of syncytial nuclei), complementation groups 2 (Chapter III) and 3 maternal mutant embryos showed clear defects in syncytial nuclear divisions (fig. 8). Although unexpected we decided to pursue analysis of these mutants since they could uncover interesting differences between the soma and the germ-line.

Preliminary phenotypic characterization of complementation group 3 demonstrated that maternal mutant embryos showed defects during syncytial blastoderm divisions. During wild-type syncytial blastoderm development, the nuclei divided synchronously with an even distribution along the embryo (fig. 8A). Maternal mutant embryos for complementation group 3 alleles, however, showed abnormal nuclear divisions with loss of nuclear division synchrony and uneven distribution of nuclei throughout the embryo (fig. 8B).

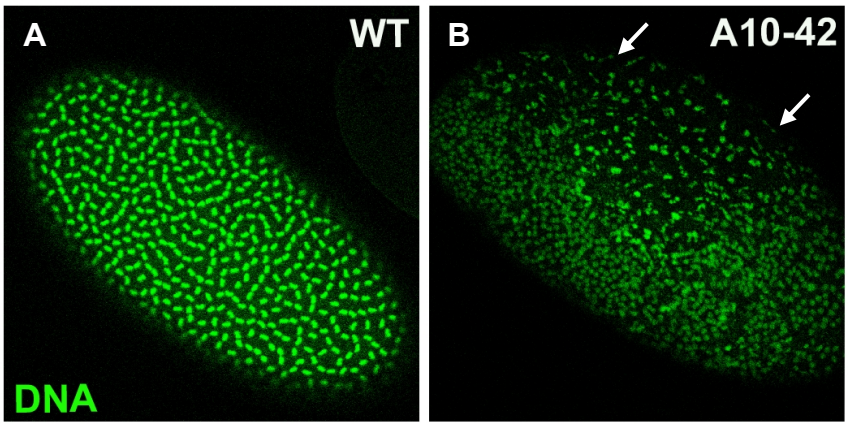

Figure 8: Complementation group 3 mutants showed nuclear division defects during syncytial blastoderm. (A) Wild-type syncytial blastoderm embryo showing synchronous mitosis and evenly spaced nuclei. (B) Maternal mutants of allele A10-42 of group 3 showed abnormal nuclear divisions during syncytial blastoderm. Interestingly, while some nuclei were already decondensed, others were still in telophase (white arrows) connected by a chromosome bridge. All mutant alleles of complementation group 3 showed abnormal nuclear syncytial divisions (data not shown).

4. Discussion

This chapter described the isolation and mapping of two novel complementation groups required for syncytial nuclei divisions. Interestingly, both mutants showed normal egg-laying (data not shown), which suggested the germ-line stem cell mitotic divisions were normal. We hypothesized that the activity of the affected genes was mainly required in somatic tissues, and we speculated that female germ-line stem cells mitosis was differentially regulated when compared to the soma. We isolated two mutant alleles for *separation anxiety* (*san*) (complementation group 2; Chapter III). Since the following chapters of this dissertation will focus on the *san* gene I will focus the discussion of this chapter on complementation group 3 alleles.

Complementation group 3 maternal mutants displayed nuclear division defects during syncytial blastoderm that included uneven nuclear distribution and asynchronous mitosis (fig. 8; Rui Tostões, unpublished data). Complementation group 3 mutants were not further characterized since we failed so far to identify the affected gene. Nevertheless, we mapped this complementation group to a 7Kb genomic interval (Fig. 7).

The 7kb genomic DNA fragment that complemented the group 3 mutants contained two annotated genes, CG13558 and CG13559. According to available DNA arrays and RNAseq expression data (modENCODE project), these genes were the only genomic locus clearly expressed within this region. Nevertheless, we failed to detect any mutation within the transcribed region of these two genes. Yet, since both CG13558 and CG13559 were annotated without 5' and 3'UTRs it was likely the gene structure annotation was incomplete and

suggested the existence of additional unsequenced exons. All mutant alleles isolated in this screen were generated by ethylmethane sulfonate (EMS) treatment. The most common effect of EMS is to generate point mutations by G/C-A/T transitions. Although we cannot exclude the possibility of a point mutation affecting an enhancer or the structure of a non-coding RNA, this is unlikely to occur in three different alleles.

The putative protein encoded by the CG13558 gene is well conserved within insects. BlastP analysis revealed that the putative protein encoded by CG13558 shares some degree of similarity with a putative guanine nucleotide exchange factor (GEF) from the *Pediculus humanus corporis*. GEFs are directly responsible for the activation of Rho-family GTPases by catalyzing the exchange of GDP for GTP. RhoGTPases regulate many aspects of the actin cytoskeleton and membrane organization and thus control cell polarity, behavior, morphology and division (Jaffe and Hall, 2005). Although Rho activation is spatially and temporally regulated, the molecular mechanisms that underlie this tight control are still poorly understood. Rho1 locally regulated activation plays a fundamental role within cytokinesis of animal cells (D'Avino et al., 2005). Separation of the two newly formed daughter cells is achieved by assembly of a contractile ring in the cleavage plane of the mother cell followed by constriction and subsequent abscission. Rho activation is a prerequisite for the assembly of the actomyosin filaments that drive constriction (Bement et al., 2005; Kamijo et al., 2006; Lee et al., 2004; Somers and Saint, 2003; Tatsumoto et al., 1999). Rho1 RNA interference (RNAi) in *Drosophila* cultured cells, results in failure of cytokinesis leading to binucleated cells (Somma et al., 2002).

Inhibition of Rho1 function by drugs or expression of dominant-negative alleles in *Drosophila* embryos leaded to disruption of the actin

cytoskeleton and caused severe defects in membrane invagination during blastoderm cellularization (Crawford et al., 1998). RhoGEF2 was shown to be required for activation of Rho1 during cellularization (Padash Barmchi et al., 2005). Accordingly, *Drosophila RhoGEF2* mutants showed dramatic defects during blastoderm cellularization, with furrow canals often incorrectly formed and sometimes missing (Afshar et al., 2000; Grosshans et al., 2005; Padash Barmchi et al., 2005).

Despite the absence of cell boundaries, the first 13 nuclear divisions within *Drosophila* embryos require an intact F-actin network (Mavrakis et al., 2009). In cycles 10–13, metaphase furrows, which are invaginations of the plasma membrane, form during metaphase to create mitotic domains and prevent adjacent mitotic figures from interacting or “colliding” with one another. Inhibition of Rho1 at mitotic stages 10-13 lead to disruption of metaphase furrows and failure to proceed into cellularization (Crawford et al., 1998). In contrast to Rho1 inhibition, RhoGEF2 loss of function mutants did not show defects in the syncytial blastoderm (Grosshans et al., 2005), which suggests another GEF is regulating the activity of Rho1 in these earlier nuclear divisions. If CG13588 is the affected gene in group 3 mutants we hypothesize it might encode a new GEF required for activation of Rho1 in the syncytial blastoderm.

CG13559 encodes a protein closely related with the human LITAF-like protein, named cell death involved p53-target (CDIP) (Brown et al., 2007). CDIP was shown to be a transcriptional target of p53, capable of upregulating the tumor necrosis factor alpha (TNFα) (Brown et al., 2007). Work done in human cells suggested that under genotoxic stress TNFα was up-regulated by p53 in a CDIP dependent manner to induce apoptosis. Many factors that induce apoptosis are conserved between mammals and *Drosophila* (Igaki et al., 2002;

Moreno et al., 2002; Song, 2005). *Drosophila Eiger* was shown to be the sole member of the TNF superfamily (Igaki et al., 2002; Moreno et al., 2002). If CG13559 was the gene affected in group 3 mutants, we could expect CG13559 would be playing a role in the activation of the Eiger. It has been suggested that Eiger is a ligand for the *Drosophila* JNK pathway, and its overexpression induces JNK-dependent cell death in imaginal epithelia (Igaki et al., 2002; Moreno et al., 2002). However, *eiger* loss-of-function mutants show no morphological or cell death defects during normal development (Igaki et al., 2002). In contrast to complementation group 3 alleles, where mutant females were sterile due to the syncytial nuclei division defects, *eiger* loss-of-function mutants were viable and fertile (Brodsky et al., 2004; Igaki et al., 2002). However, we cannot exclude the possibility of CG13559 being involved in a pathway other then TNF activation that would justify the observed mitotic phenotypes.

In summary, complementation group 3 is most likely bearing mutant alleles of the either the CG13558 or the CG13559 gene. Identification of the mutated gene will allow a better understanding of the molecular mechanisms regulating syncytial nuclear divisions and possibly will uncover interesting differences between the soma and the germ-line.

CHAPTER III

Differential requirements of a mitotic acetyltransferase in somatic and germ line cells

Developmental Biology 323 (2008) 197–206

Contents lists available at ScienceDirect

Developmental Biology

journal homepage: www.elsevier.com/developmentalbiology

Differential requirements of a mitotic acetyltransferase in somatic and germ line cells

Ana Pimenta-Marques [a], Rui Tostões [a], Thomas Marty [b], Vítor Barbosa [b], Ruth Lehmann [b], Rui Gonçalo Martinho [a,*]

[a] Instituto Gulbenkian de Ciência, Rua da Quinta Grande, n 6, 2781-901 Oeiras, Portugal
[b] The Skirball Institute and Howard Hughes Medical Institute, New York University School of Medicine, New York, New York 10016, USA

ARTICLE INFO

Article history:
Received for publication 29 March 2008
Revised 18 August 2008
Accepted 18 August 2008
Available online 29 August 2008

Keywords:
Drosophila
Germ line
Oogenesis
Mitosis
Sister chromatid cohesion
Separation anxiety

ABSTRACT

During mitosis different types of cells can have differential requirements for chromosome segregation. We isolated two new alleles of the *separation anxiety* gene (*san*). *san* was previously described in both *Drosophila* and in humans to be required for centromeric sister chromatid cohesion (Hou et al., 2007; Williams et al., 2003). Our work confirms and expands the observation that *san* is required *in vivo* for normal mitosis of different types of somatic cells. In addition, we suggest that *san* is also important for the correct resolution of chromosomes, implying a more general function of this acetyltransferase. Surprisingly, during oogenesis we cannot detect mitotic defects in germ line cells mutant for *san*. We hypothesize the female germ line stem cells have differential requirements for mitotic sister chromatid cohesion.

Introduction

Drosophila embryonic development starts with thirteen nuclear divisions without cytokinesis (Foe et al., 1993). The nuclei migrate outward to the egg periphery during nuclear division 8 and 9, with most nuclei arriving at the surface of the embryo during interphase 10. After four additional nuclear divisions, the cortical nuclei arrest mitosis during interphase 14. Once arrested, the nuclei become synchronously encased by polarized invaginations of the plasma membrane and a monolayer of epithelial cells is formed *de novo*.

Sister chromatid cohesion is crucial for chromosome alignment during metaphase (Losada, 2007; Nasmyth and Haering, 2005). The evolutionarily conserved multisubunit cohesin complex is required for sister chromatid cohesion. This complex contains four core subunits: Smc1, Smc3, Scc3, and Scc1/Mcd1/Rad21 (Losada, 2007). In vertebrates, Scc3 has two isoforms: SA1 and SA2 (Losada et al., 2000; Sumara et al., 2000). Another protein, Pds5, is weakly associated with the cohesin complex and may regulate the dynamic interaction of cohesin with chromatin (Hartman et al., 2000; Panizza et al., 2000).

In yeast cohesion is established in multiple steps: before S-phase the Scc2 and Scc4 proteins regulate the chromosomal loading of cohesin at centromeres and at regularly spaced intergenic regions along chromosome arms (Ciosk et al., 2000; Glynn et al., 2004; Tomonaga et al., 2000). During ensuing DNA replication, sister chromatid cohesion is established (Uhlmann and Nasmyth, 1998). The Eco1/Ctf7 protein is the main regulator of this event (Skibbens et al., 1999; Toth et al., 1999). Yeast mutants lacking the acetyltransferase Eco1/Ctf7 (or Eso1 in fission yeast) exhibit defective cohesion despite cohesins continuing to localize to the chromosomes (Skibbens et al., 1999; Tanaka et al., 2000; Toth et al., 1999). Recent studies support the idea that this protein makes a direct connection with the replication fork when establishing cohesion (Lengronne et al., 2006; Moldovan et al., 2006). The cohesin links will then remain until anaphase when they are removed through proteolytic cleavage of Scc1 (Uhlmann et al., 1999).

Meiotic and mitotic sister chromatid cohesion are distinct. Meiotic cells contain specific cohesin subunits, including the α-kleisin Rec8 (Nasmyth and Haering, 2005). Rec8 is crucial for meiotic cohesion and for synaptonemal complex (SC) formation in all organisms studied (Klein et al., 1999; Molnar et al., 1995; Pasierbek et al., 2001). In *Drosophila*, meiotic cohesion depends on the protein Orientation Disruptor (Ord) (Bickel et al., 1996, 1997; Miyazaki and Orr-Weaver, 1992). In *ord* mutants, sister chromatids segregate randomly through both meiotic divisions (Bickel et al., 1997; Webber et al., 2004). Ord is enriched at the centromeres of meiotic chromosomes in both males and females (Bickel et al., 1997; Webber et al., 2004). Smc1 and Smc3 subunits colocalize with Ord at centromeres of ovarian germ line cells and in flies lacking Ord activity, cohesin SMCs fail to accumulate at oocyte centromeres (Khetani and Bickel, 2007).

In *Drosophila*, the *separation anxiety* (*san*) gene encodes an acetyltransferase known to be required for mitotic sister chromatid cohesion in neuroblasts and S2 cells (Williams et al., 2003). *san* function was associated with sister chromatid cohesion since mutant cells showed loss of the cohesin Scc1 specifically at the centromeres.

* Corresponding author. Instituto Gulbenkian de Ciência, Rua da Quinta Grande 6, Oeiras, 2780-156, Portugal.
E-mail address: rmartinho@igc.gulbenkian.pt (R.G. Martinho).

0012-1606/$ – see front matter © 2008 Elsevier Inc. All rights reserved.
doi:10.1016/j.ydbio.2008.08.021

Recently, *san* was shown to have a homologue in humans (Arnesen et al., 2006). RNAi experiments depleting *SAN* in HeLa cells caused defects in sister chromatid cohesion and cohesin SMC1 was no longer detected at the centromeres (Hou et al., 2007).

In this study we isolated two new loss-of-function alleles of *san* in a forward genetic screen for maternal mutants defective in blastoderm cellularization. We confirm and expand the observation that during mitosis *san* is required *in vivo* and in different types of somatic cells for chromosome segregation. In addition, our work suggests that *san* is also important for chromosome resolution. This implies a more general function of this acetyltransferase and a possible interplay between cohesion and chromosome condensation/resolution. Surprisingly, during oogenesis we cannot detect mitotic defects in germ line cells mutant for *san*. We hypothesize the female germ line stem cells have differential requirements for mitotic sister chromatid cohesion.

Results

atado is required maternally for the correct segregation of chromosomes during syncytial blastoderm

To identify new genes involved in *Drosophila* blastoderm cellularization and germ-band extension, we took advantage of a previously reported maternal screen (Barbosa et al., 2007). This screen used the FLP-FRT/*ovo*^{D} system (Chou and Perrimon, 1992) to generate germ line mutant clones. The screen was carried out in the right-arm of the second chromosome (2R) and 137 independent mutant lines within the "germ cells only" class of mutants were isolated on the basis of an extremely abnormal soma but where the germ cells were formed normally at the posterior pole of the embryo. The secondary screen involved isolation of mutants defective in cuticle production. Absence of cuticle is a good marker for defects in apicobasal polarization of epithelial cells. Secondary screening allowed the isolation of 47 of the initial 137 lines. Complementation studies of these mutants identified 9 complementation groups by zygotic lethality or sterility. Complementation group 2 contained two alleles, which we will initially refer to as *atado*^{1} and *atado*^{2}. These two alleles will later be renamed *san*^{3} and *san*^{4}, respectively.

To characterize the role of the *atado* gene during *Drosophila* early embryonic development, we examined germ line clone embryos of both alleles of *atado*. Both mutant alleles had similar maternal phenotypes, with 87% (n=39) of *atado*^{2} embryos exhibiting nuclear division abnormalities during syncytial blastoderm (2.5%, n=40, in wild-type embryos) (Supplementary Fig. 1). During syncytial blastoderm development wild-type nuclei divide synchronously and are evenly distributed throughout the embryo (Figs. 1A, D, G). We observed that the *atado* embryos frequently showed nuclei division

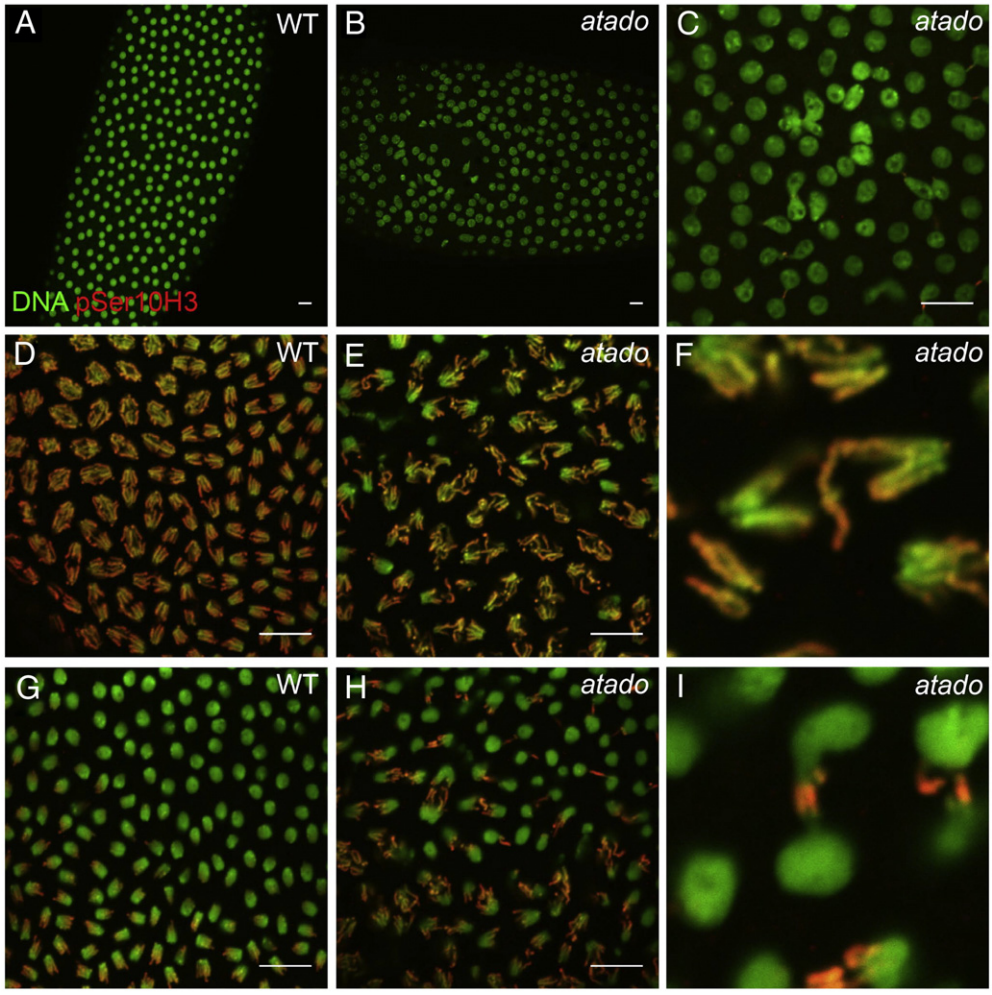

Fig. 1. *atado* is required maternally for chromosome segregation during syncytial blastoderm. Embryos mutant for *atado*^{2} show abnormal anaphases (D, E), with a high frequency of chromosome bridges (A–C, G–I) and chromosome lagging (F). All panels show syncytial blastoderm embryos. *atado*^{2} mutant embryos were obtained after the induction of germ line clones (maternal mutants). All embryos were stained for DNA (green) and pSer10 Histone H3 (red). Low magnification of a wild type (A) and *atado*^{2} (B) embryo during interphase. (C) Shows a detail of the *atado*^{2} embryo shown in panel B. High magnification of a wild type (D) and *atado*^{2} (E) embryo during anaphase. (F) Shows a detail of the *atado*^{2} embryo shown in panel E. High magnification of a wild type (G) and *atado*^{2} (H) embryo during late anaphase/telophase. (I) Shows a detail of the *atado*^{2} embryo shown in panel H. pSer10 histone H3 staining marks condensed chromosomes. For quantitative data on the observed chromosome bridges, refer to Figure S1. Scale bars equals 10 μm.

asynchrony (data not shown) and irregular distribution of the nuclei (Fig. 1B). Yet, the most striking phenotype in *atado* embryos was chromosome segregation defects during mitosis (Fig. 1). Anaphase, whilst being mainly bipolar in *atado* embryos, appeared significantly more disorganized in *atado* than in wild-type embryos (Figs. 1D, E). *atado* embryos showed a high frequency of chromosome lagging (Fig. 1F) and formation of chromosome bridges (Figs. 1H, I). We also observed interphase nuclei fused together or attached by chromosome bridges (Fig. 1C, Supplementary Fig. 1). Due to these chromatin bridges we refer to our mutant as *atado*, "tied-up" in Portuguese.

Chromosome lagging in *atado* embryos may be explained by kinetochore abnormalities, but we failed to detect any obvious defects in the localization of Centromere identifier (Cid) during metaphase or anaphase (Supplementary Figs. 2A, B). Chromosome lagging could also be explained by centrosome/mitotic spindle defects. Yet, we did not detect any obvious defects in the localization of Centrosomin (Cnn) (Supplementary Figs. 2C–F), and the mitotic spindle was bipolar and correctly attached to chromosomes and centrosomes (Supplementary Figs. 2E, F).

atado is necessary zygotically for neuroblasts mitosis and imaginal discs development

atado mutations were zygotically lethal. To better characterize the zygotic lethality of *atado* alleles, we followed the development of transheterozygote $atado^1/atado^2$ mutants. All isolated transheterozygote *atado* larvae reached the third instar larval stage, pupated and died at the pupa stage ($n=14$). All isolated heterozygous larvae (*atado*/+) were viable ($n=16$). Therefore, the maternal contribution of *atado* was sufficient for development to larval stage, but not for pupa and metamorphosis to the adult.

We expected the lethality to be associated with mitotic defects, and hence we analyzed the brains and imaginal discs of transheterozygote third instar larvae. We observed that *atado* mutant larvae had smaller brains and extremely small imaginal discs (Supplementary Fig. 3, data not shown). This is the typical zygotic phenotype of several cell cycle mutants (Gatti and Baker, 1989; Krause et al., 2001). *atado* neuroblasts showed chromosome congression defects during metaphase (Figs. 2A, B) and abnormal segregation of chromosomes during anaphase (Figs. 2D, E). To further confirm that *atado* is important for cell proliferation, we induced *atado* mutant clones in imaginal discs of an otherwise heterozygote larva (one copy GFP). Imaginal disc clones mutant for $atado^2$ (marked by the absence of GFP) were absent or significantly smaller than the twin-spot wild-type clones (marked by two copies of GFP) (Figs. 2G, H). In contrast, control clones also marked by absence of GFP had a similar size to the twin-spot clones (Fig. 2I). This suggested that *atado* is required for normal development of larvae imaginal discs.

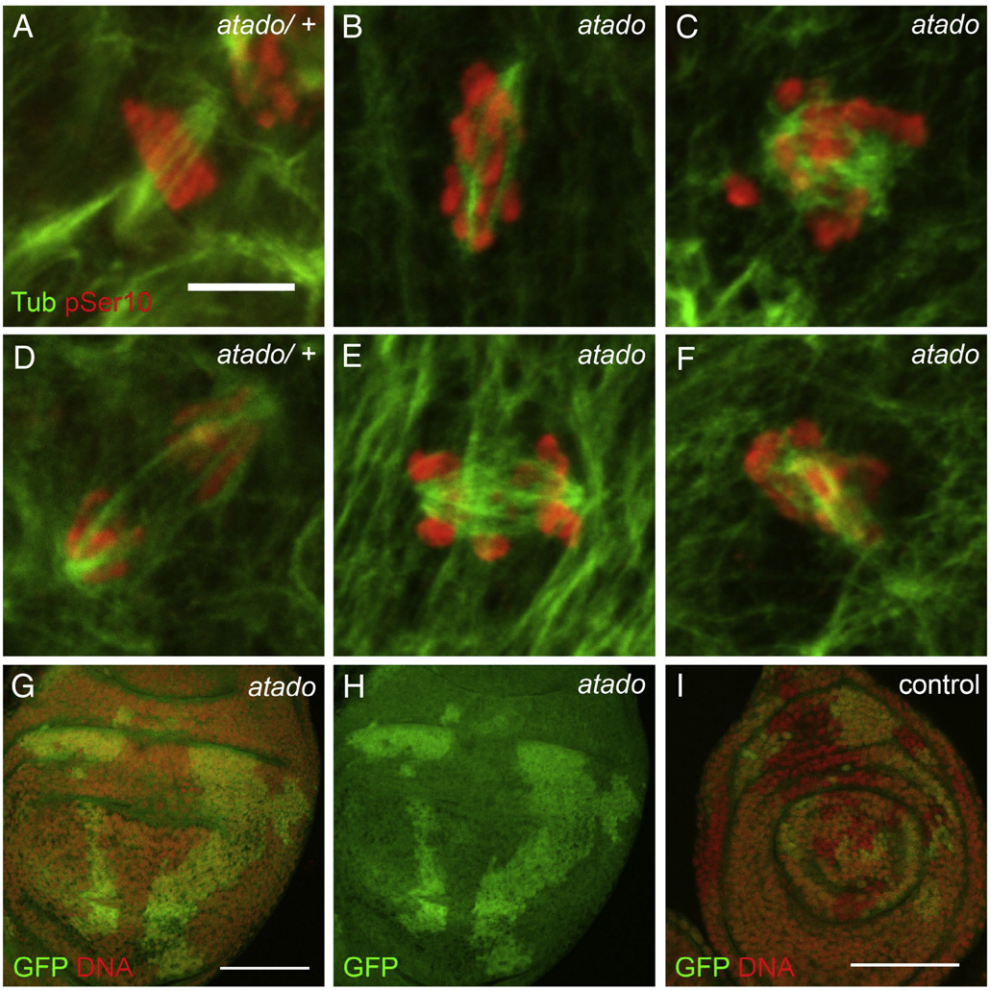

Fig. 2. *atado* is required zygotically for normal mitosis of larvae neuroblasts and imaginal discs development. Larvae zygotically mutant for $atado^2$ contain smaller brains (refer to Figure S3) and the neuroblasts show mitotic defects (A–F). Neuroblasts mutant for $atado^2$ show chromosome congression defects during metaphase (A, B) and chromosome lagging during anaphase (D, E). In larvae imaginal discs, clones with two copies of GFP (control clones) are significantly bigger than the twin-clones without GFP (clones mutant for $atado^2$) (G–H). In control imaginal discs both types of clones have equivalent sizes (I). (A–F) Neuroblasts were stained for α-Tubulin (green) and pSer10 Histone H3 (red). (G–I) Imaginal discs were stained for DNA (red). Scale bars equals (A–F) 5 μm, (G–H) 50 μm, and (I) 30 μm.

atado is allelic to separation anxiety (san), a gene required for mitotic sister chromatid cohesion

To identify the gene responsible for the *atado* mutant phenotypes, we mapped both *atado* alleles using the Bloomington 2R deficiency kit (see Materials and methods), defining a cytological interval comprising 47 genes. By a candidate gene approach we concluded that *atado* was most likely allelic to the gene *separation anxiety* (*san*) since both *atado* alleles failed to complement san^2 (Fig. 3A), a lethal P-element of the *san* gene (Williams et al., 2003). Furthermore, san^2 germ line clones produced mutant embryos phenotypically indistinguishable from $atado^1$ and $atado^2$ (Supplementary Fig. 4). The *san* gene was previously predicted to encode an acetyltransferase, which transfers acetyl groups to the N-terminus of other proteins (Williams et al., 2003). San protein contains 184 amino acids and analysis of San primary sequence revealed an acetyltransferase domain composed by two acetyltransferase subdomains from amino acids 74–94 and 117–129, respectively (Fig. 3B) (Williams et al., 2003). Sequencing both alleles of *atado* confirmed that *atado* was allelic to *san*, as both alleles contained distinct nonsense mutations within *san* open reading frame (ORF). These two nonsense mutations were predicted to cause severe truncations of the San protein (Fig. 3B). We failed to detect San from embryonic total protein extracts (Fig. 3C). The San antibody is polyclonal and it was raised against most of San protein (Williams et al., 2003). It was nevertheless possible that it did not recognize the truncate proteins encoded by the *atado* alleles. We expressed in bacteria the smallest truncated protein, which was predicted to be encoded by $atado^2/san^4$. The San antibody used in this work was able to recognize the recombinant protein in total extracts from bacteria (Supplementary Fig. 5). We concluded that the isolated *atado* alleles are loss-of-function alleles of *san*. We therefore renamed $atado^1$ and $atado^2$, respectively to san^3 and san^4 alleles.

san is required for chromosome resolution

Syncytial blastoderm embryos mutant for *san* showed dramatic chromosome segregation defects during anaphase (Fig. 1). We observed that during metaphase the defects in chromosome congression and alignment were comparatively mild (Figs. 4A–C and Supplementary Fig. 4). This is in contrast to the dramatic defects in chromosome congression and alignment recently reported in Scc1-depleted embryos (Pauli et al., 2008). Additionally, we only detected a minor separation of the sister chromatid kinetochores (due to the loss of centromeric cohesion) in *san* mutant embryos arrested in metaphase (Figs. 4D, E). Given this evidence we decided to investigate if San had additional functions that could explain the observed phenotypes.

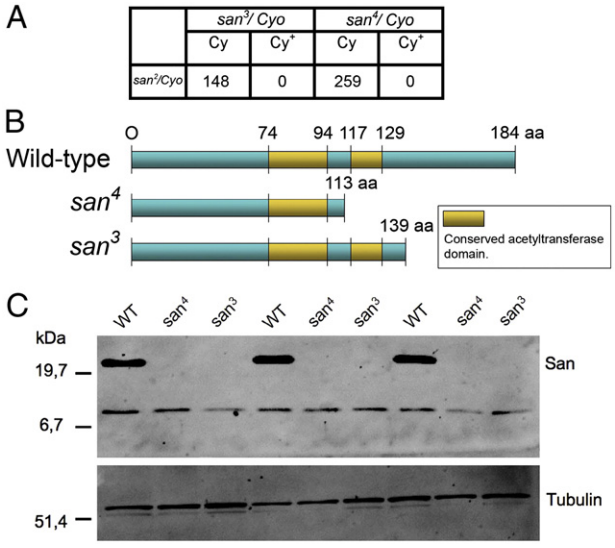

Fig. 3. *atado* is allelic to *separation anxiety* (*san*). Both alleles of *atado* contain nonsense mutations within *san* open-reading frame and are protein null for San. The mutations of both alleles of *atado* were mapped to a small cytological interval using the 2R deficiency kit. Using a candidate gene approach it was observed that both alleles of *atado* failed to complement a loss-of-function allele of the gene *separation anxiety* (san^2) (A). The *atado* alleles ($atado^1$ and $atado^2$) were therefore respectively renamed as san^3 and san^4. Both isolated alleles of *san* contain nonsense mutations within *san* open-reading frame, which will putatively lead to the truncation of San protein (B). Total protein extracts from embryos mutant for both alleles of *san* show absence or undetectable levels of San protein (C).

Cohesion defects can explain the lagging chromosomes and the high frequency of chromosome bridges observed in *san* mutant embryos, but we noticed that a large proportion of these bridges did not involve centromeric regions of the chromosome (negative for Cid staining). Of the scored bridges between nuclei in late-mitosis/interphase, 55.6%±18.2 were negative for Cid staining, 32%±11.5 were positive for Cid staining, and in 12.4%±10 of the cases the result was inconclusive ($n=104$ bridges) (Supplementary Fig. 6). Bridges involving distal chromosome regions were previously described in mutants defective in chromosome condensation and/or resolution (Bhat et al., 1996; Steffensen et al., 2001). Consistent with the hypothesis that *san* could be involved in chromosome resolution/condensation; we observed that during mitosis a subset of nuclei showed a dramatic decrease in the levels of Barren (Figs. 4F–J) (number of cortical nuclei with a detectable reduction of Barren localization, wild-type: 0±0 nuclei, $n=780$, 11 embryos, san^4: 19.7%±12.9 nuclei, $n=980$, 11 embryos; Student's t test, 95% confidence interval, $p<3\times10^{-5}$). Embryos mutant for *barren* are defective in chromosome segregation with the formation of chromosome bridges (Bhat et al., 1996). Although the reduction of Barren localization suggests defects in chromosome resolution and/or condensation, we did not detect reduced levels of this condensin specifically at chromosome bridges (data not shown). Consistent with chromosome resolution defects, during interphase we observed a subset of chromosome bridges showing reduced levels of Topoisomerase II (Figs. 4K, L). TopoII is important for DNA decatenation and chromosome resolution (Holm et al., 1989; Uemura et al., 1987). Chromosomal localization of TopoII is condensin-dependent (Coelho et al., 2003). We did not detect any change in the levels of TopoII in embryo total extracts (data not shown).

During oogenesis san is not required for germ line mitosis

Our data implied *san* as being important for mitosis of distinct types of somatic cells. This is consistent with previous published work that showed that *san* is required *in vivo* in neuroblasts, *ex vivo* in S2 cells and human HeLa cells, for mitotic sister chromatid cohesion (Hou et al., 2007; Williams et al., 2003). At this point it is important to emphasize that the maternal screen from which we isolated both san^3 and san^4 alleles was designed to exclude mutants with mitotic defects during oogenesis as egg laying had to be normal. To investigate if egg laying from females with a germ line mutant for *san* was normal, we induced germ line clones using the FLP-FRT/ovo^D system (Chou and Perrimon, 1992). We compared the number of eggs laid by *san* and control females (with an identical FRT chromosome), and concluded that egg laying between these females was identical for more than 15 days after pupa eclosion (Supplementary Fig. 7) (see Materials and methods). Since clones were induced at larvae stages by heat-shock, this suggested that *san* and control germ line stem cells divided continuously and at similar rates for almost 20 days after clone induction.

To test the hypothesis that *san* mitotic function is not required during oogenesis, we generated females with genetically mosaic ovaries using the FLP-FRT-mediated mitotic recombination and a nuclear GFP clone marker. Absence of GFP (green) indicates that the cells are homozygous for *san* mutations. After the induction of clones

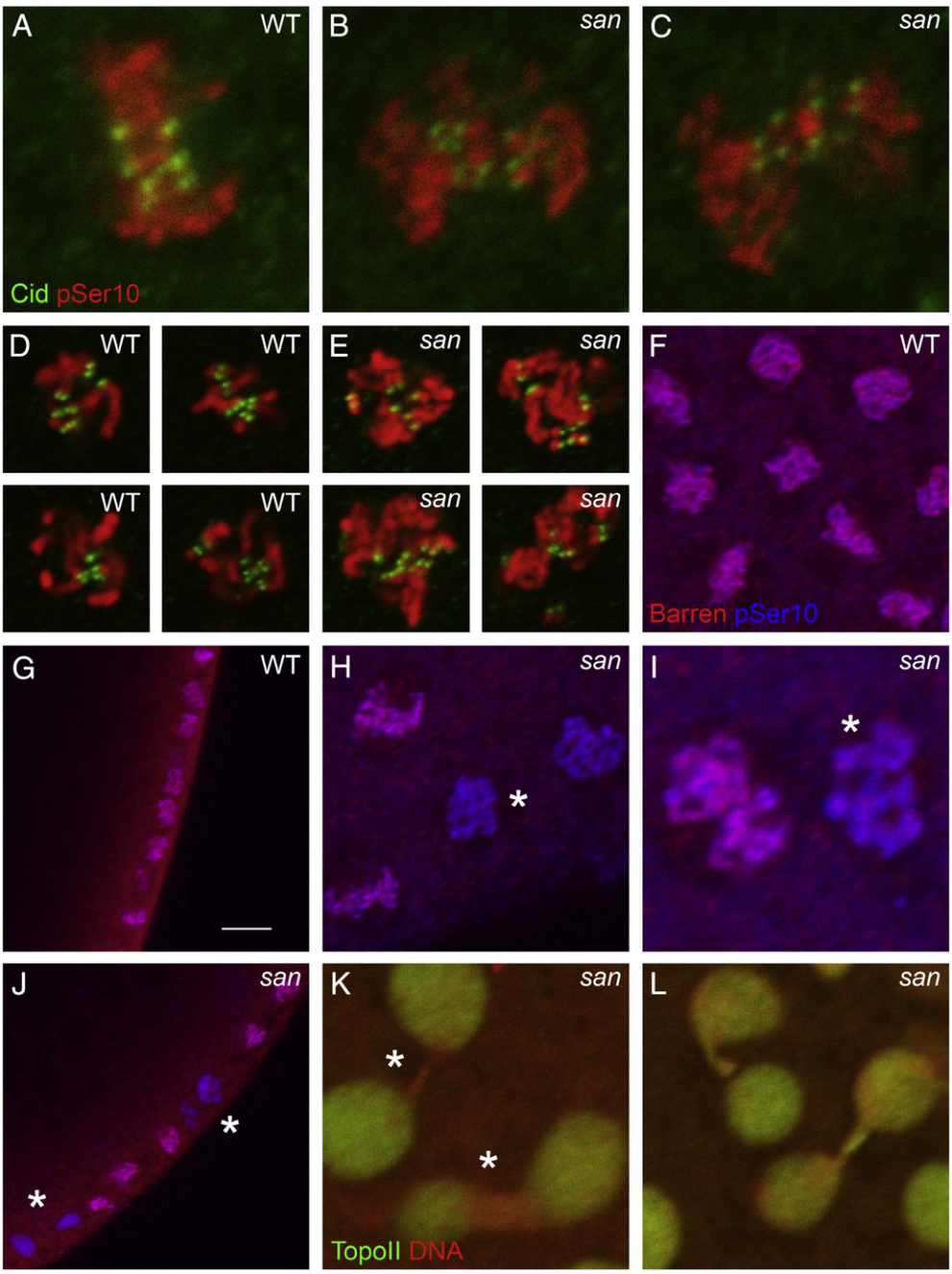

Fig. 4. A subset of nuclei from syncytial blastoderm embryos mutant for *san* show reduced levels of Barren and Topoisomerase II. Embryos mutant for san^4 show mild defects in chromosome congression and alignment during metaphase (A–C). san^4 embryos incubated with colchicine arrest the cell cycle with condensed chromosomes and show a minor separation of the sister chromatid kinetochores (D, E). Subsets of mitotic nuclei in san^4 embryos show a dramatic reduction in Barren localization (F–J; asterisks indicates reduction in Barren localization; see text for quantification). Subsets of interphasic nuclei in san^4 embryos show reduced levels of TopoII localization specifically in the chromosome bridges (K, L; asterisk indicates reduction of TopoII). All panels show syncytial blastoderm embryos. (A–E) Embryos were stained for Cid (green) and pSer10 Histone H3 (red). (F–J) Embryos were stained for Barren (red) and pSer10 Histone H3 (blue). (K, L) Embryos were stained for Topoisomerase II (green) and DNA (red). (D, E) Embryos were incubated with colchicine for 15 min at room temperature. Scale bar equals 10 μm.

at larvae stages, we observed a consistently high frequency of *san* clones in the adult ovaries (data not shown). This suggested that the proliferating larvae primordial germ cells mutant for *san* could efficiently compete for the adult germ line stem cell niche. Confirming that *san* is not required during oogenesis for germ line mitosis, egg chambers mutant for *san* from females with 7/8 or 15 days old after pupa eclosion showed a normal determination of the oocyte (Figs. 5B–D), a normal condensed karyosome (Fig. 5E—asterisks indicates a condensed karyosome), a normal number of nurse cells (15 nurse cells, $n=16$), a normal fusome (Fig. 5F), and a normal eggshell without fused dorsal appendages (*spindle* phenotype) (data not shown). Similar results were obtained with a previously isolated loss-of-function allele of *san* (san^2) (Supplementary Figs. 8A–E).

Since germ line clones mutant for *san* did not show mitotic defects during oogenesis, we investigated if San is required within the somatic follicle cells. Each *Drosophila* egg chamber contains 16 germ line cells surrounded by a follicle cell epithelium of somatic origin. Follicle cell clones were induced by heat-shock at larvae stages (as described for germ line clones— See Materials and methods). Whereas we were able to isolate large clones (negative for GFP) using a control chromosome (Supplementary Figs. 8G–L), in the case of *san* mutants (FRT san^2 and

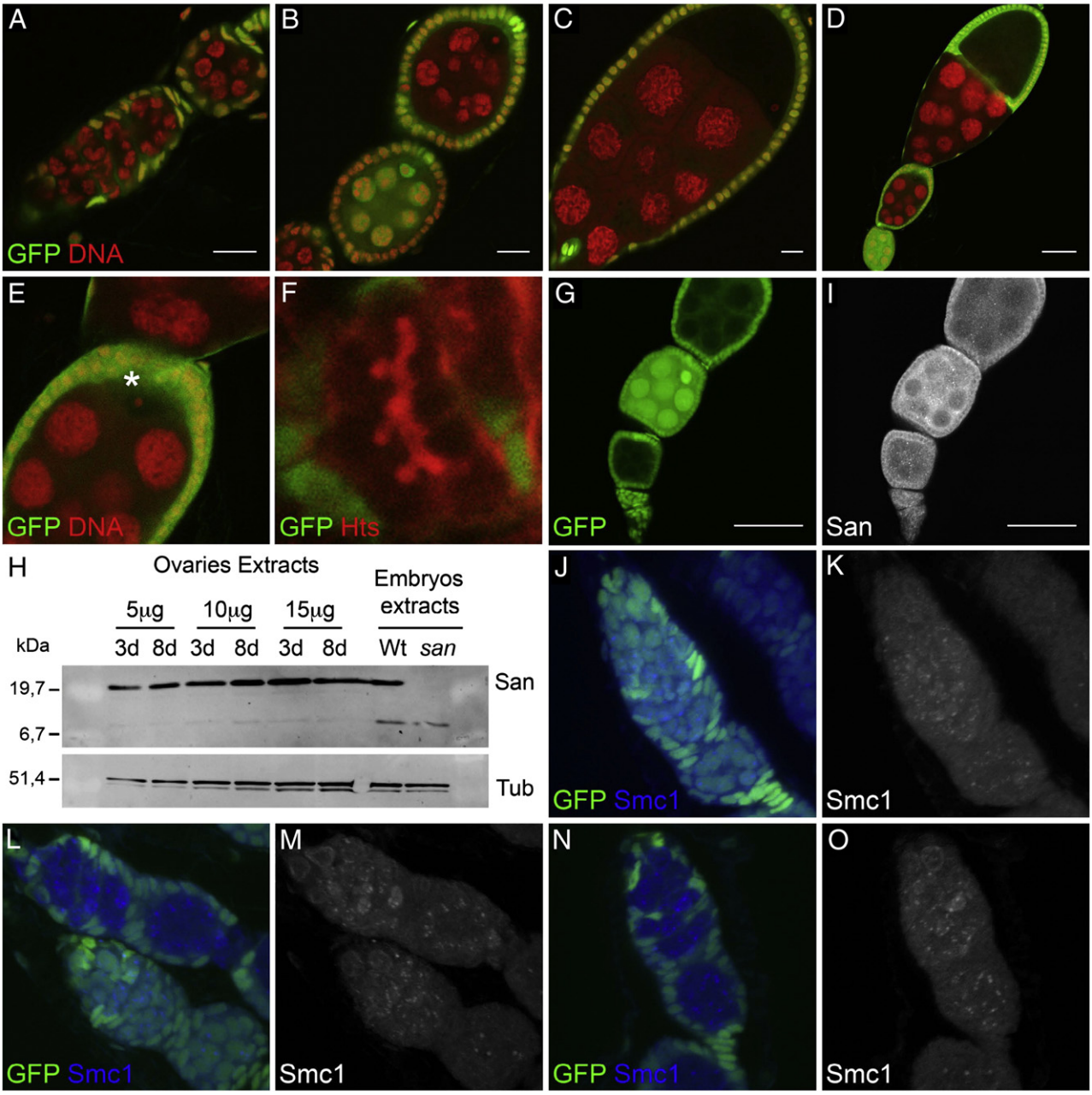

Fig. 5. During oogenesis *san* is not required for germ line mitosis. Absence of endogenous GFP (green) indicates that the cells are homozygous for *san* mutations. Germ line mutant clones of san^4 were induced at larvae stages using heat-shock-controlled flipase. Ovaries were dissected from adult females that were 7/8 (A–C, F, G, I–O) or 15 days (D, E) old after hatching (pupal eclosion). *Drosophila* germarium whose germ line is mutant for san^4 develops normally (A). Germ line stem cells mutant for san^4 divide normally since egg-laying is identical to the one observed in control females (refer to Figure S7) and egg-chambers mutant for san^4 develop normally (A–D), with a normal condensed karyosome (E; asterisk indicates karyosome) and a normal fusome (F). San is expressed in the ovaries (H) and no obvious difference in the expression levels of San could be detected between young (3 days) and older females (8 days). San is expressed within the ovaries germ line (G, I). Germarium whose germ line is mutant for san^4 (L–O) show Smc1 expression identical to the one observed in wild-type germarium (J, K). Absence of GFP indicates that the germ-line is mutant for san^4. (A–E) Ovaries were stained for DNA (red). (F) Ovary was stained for fusome marker Hts (red). (G, I) Ovary was stained for San (gray). (J–O) Ovaries were stained for Smc1 (blue or gray). (H) Total ovaries and embryonic protein extracts were analyzed by SDS-PAGE and western blot using an anti-San polyclonal antibody. An anti-α-tubulin antibody was used as a loading control. Scale bars equals (A–C) 10 µm, (D, G, I) 50 µm. (E) Is a detailed view of the image shown in panel D.

FRT san^4), the isolated clones were both significantly smaller and less frequent (Supplementary Figs. 8A–F); suggesting a requirement of *san* function within follicle cells.

We were able to recover *san* clones within the follicle cells if they were induced in adult flies and if the ovaries were dissected two/three days after induction (data not shown). This was most likely due to San protein perdurance within the follicle cells.

We also tested whether San was expressed in wild-type ovaries. Western blots of total protein extracts showed that San was expressed in the ovaries (Fig. 5H), with no obvious differences in the expression levels detected between younger (3 days) and older females (8 days). Additionally, San immunostaining of mosaic ovaries confirmed San expression within the ovaries germ line, as we detected a specific cytoplasmic staining between the control (presence of GFP) and mutant egg chambers (absence of GFP) (Figs. 5G, I).

Previous studies with *san* homologue in HeLa cells showed that the inactivation of *san* expression by RNAi induced an abnormal expression of cohesin SMC1 (Hou et al., 2007). To check if integrity of the cohesin complex during oogenesis was affected in *san* mutants, mosaic ovaries were stained for Smc1. Consistent with the absence of

defects during oogenesis, we could not detect any change in Smc1 localization in germaria whose germ-line was mutant for *san* (Figs. 5J–O), with bright foci and a diffuse staining present as was previously described for wild-type germarium (Khetani and Bickel, 2007). We failed to detect specific immunostaining for Scc1 in wild-type germarium (data not shown). We also did not detect specific immunostaining for Scc1 and Smc1 in the syncytial blastoderm embryo (data not shown).

Discussion

We isolated two new alleles of the *san* gene: san^3 and san^4. *san* was previously described to be required for centromeric sister chromatid cohesion in *Drosophila* (neuroblasts and *ex vivo* in S2 cells) and in humans (*ex vivo* in HeLa cells) (Hou et al., 2007; Williams et al., 2003).

Our work confirms and extends the observation that *san* is required *in vivo* for mitosis of different types of somatic cells. It also suggests that in addition to the previously described role in sister chromatid cohesion, *san* is also important for chromosome resolution. We also propose that female germ line stem cells have differential requirements for sister chromatid cohesion, since we could not detect mitotic defects when they were mutant for *san*.

san is required in vivo for mitosis of different types of somatic cells

Since the mitotic function of *san* had only been studied *in vivo* in *Drosophila* neuroblasts (Williams et al., 2003), we decided to characterize its function during different stages of *Drosophila* development. Our analysis shows that *san* is important for chromosome segregation during syncytial blastoderm nuclei division (maternal phenotype) and, as previously shown, in larvae neuroblast mitosis (zygotic phenotype). We also observe that imaginal discs from larvae mutant for *san* are extremely small. Clonal analysis confirms *san* function is required within larvae imaginal discs and adult ovary follicle cells.

san is required for chromosome resolution

Defects in mitotic sister chromatid cohesion in yeast and higher eukaryotes have similar defects in chromosome alignment during metaphase and chromosome lagging during anaphase (Dorsett et al., 2005; Sonoda et al., 2001; Toyoda and Yanagida, 2006; Vass et al., 2003). *Drosophila* embryos depleted for Scc1 have dramatic defects in chromosome congression and alignment during metaphase (Pauli et al., 2008). In contrast, *san* mutant embryos have clear defects in chromosome segregation, but only show remarkably mild abnormalities during metaphase. These phenotypic discrepancies suggest that loss of *san* function causes other problems beyond sister chromatid cohesion defects.

Embryos mutant for *san* show a high frequency of chromosome bridges during anaphase. Sister chromatid cohesion defects can cause a high frequency of anaphase bridging (Pauli et al., 2008; Vass et al., 2003). Yet a large proportion of chromosome bridges in *san* embryos are negative for Cid staining. Bridges involving distal regions of the chromosomes were previously described in mutants with chromosome condensation and/or resolution defects (Bhat et al., 1996; Cobbe et al., 2006; Dej et al., 2004; Steffensen et al., 2001).

Chromosome condensation during mitosis relies on the condensin multisubunit protein complex (Hirano, 2005). Together with topoisomerase II, this complex has an important role in organizing the individual axes of sister chromatids prior to their segregation during anaphase (Hirano, 2006). Mutants for the condensin complex *SMC4* or *gluon* and *Barren* show chromosome segregation defects with the formation of chromosome bridges during anaphase. After depletion of SMC4, TopoII fails to localize to a clearly defined chromatid axial structure and there is a significant decrease in TopoII DNA decatenation activity (Coelho et al., 2003). TopoII is important for chromosome resolution, and inactivation of *topoII* in *Drosophila* embryos and S2 cells results in chromosome bridges (Buchenau et al., 1993; Chang et al., 2003).

Given the phenotypic similarities between *san*, *topoII*, and *barren* mutant embryos we investigated if Barren and TopoII expression was abnormal in *san* mutant embryos. In *san* mutant embryos a subset of mitotic nuclei show a dramatic decrease in Barren levels, suggesting defects in chromosome condensation. Interestingly, we also observe a subset of the chromosome bridges connecting the interphase nuclei showing reduced levels of TopoII. We hypothesize that *san* is important not only for sister chromatid cohesion but also for chromosome resolution, which implies a more general function of this acetyltransferase.

Several lines of evidence argue against a cross talk between the cohesin and condensin complexes: 1) cohesins and condensins were isolated as separate complexes in solution (Losada et al., 1998). 2) Condensin DmSMC4 depletion did not alter the localization or removal of cohesins from mitotic chromatin in *Drosophila* S2 cells (Coelho et al., 2003). 3) In yeast has been shown that although sister chromatid separation did not occur normally in condensin *Ycs4* mutants (Cap-D2 in *Drosophila*), cohesin MCD1/SCC1 was released normally from chromosomes at the metaphase–anaphase transition (Bhalla et al., 2002). 4) In higher eukaryotes cohesion depletion did not appear to affect chromosome condensation (Losada et al., 1998; Sonoda et al., 2001; Vass et al., 2003).

Nevertheless, previous reports in budding yeast have suggested mechanistic interactions between cohesins and condensins (Castano et al., 1996; Lavoie et al., 2002). We show that *san* is genetically upstream of both sister chromatid cohesion and chromosome resolution/condensation. Our current interpretation is that San acetyltransferase activity is necessary for sister chromatid cohesion and chromosome resolution/condensation without being a core component of these processes. To what extent we are uncovering a cross talk is still unclear, but this is a plausible possibility.

During oogenesis san is not required for germ line mitosis

The female ovary is composed of 16–20 ovarioles (Gilboa and Lehmann, 2004; Spradling, 1993). The germarium is at the anterior tip of each ovariole and is responsible for egg chamber formation. Two to three germ line stem cells are positioned at the anterior tip of each germarium. These cells divide asymmetrically: the most anterior daughter cell keeps a germ line stem cell fate whereas the most posterior daughter cell (the cystoblast) starts a differentiation program that ultimately produces an egg. The cystoblast divides mitotically four times in order to form a cyst of 16 cells connected by ring-canals and a highly branched cytoskeletal structure called fusome. One of these cells becomes the oocyte, the other 15 nurse cells.

In accordance with previously published work (Williams et al., 2003), we clearly demonstrate that *san* is necessary *in vivo* for normal mitosis in *Drosophila melanogaster*. It was therefore surprising that analysis of germ line clones mutant for *san* did not detect any obvious mitotic defects during oogenesis. 1) The mitotic divisions of the germ line stem cells and cysts mutant for *san* are normal based on morphological analysis of the DNA, number of nurse cells, and fusome organization. 2) Egg-laying from females whose germ line is mutant for *san* is equivalent to the control females, even two weeks after pupa eclosion (hatching). This suggests that loss of *san* function does not reduce the mitotic rate or impair the viability of the germ line stem cells. 3) Egg chambers mutant for *san* show a normal determination and positioning of the oocyte, and a normal condensed karyosome. 4) *Drosophila* eggs mutant for *san* have a normal size and a normal dorsal ventral (DV) patterning (absence of *spindle* phenotype). If *san* activity were necessary within the germ line for chromosome segregation we

would expect defects in the subsequent stages of oogenesis. Consistent with this expectation, defects in the repair of DNA double strand breaks (DSB) during meiosis activates the DNA damage checkpoint (Ghabrial and Schupbach, 1999), delaying meiosis, inhibiting karyosome condensation, and mutant females lay eggs with DV patterning defects.

A possible explanation for the lack of mitotic abnormalities in females whose germ line is mutant for *san* is that San protein is extremely stable. We do not favor this hypothesis for four separate reasons: 1) we induce germ line clones for *san* during larvae development (2nd and 3rd instar larvae) and analyze their effect at least 12 days later in adult females that were 7/8 and 15 days old (after pupa eclosion). 2) We consistently detect mitotic defects in embryos laid by females whose germ line is mutant for *san*. 3) *san* zygotic mutants reaching larvae stage is a typical phenotype associated with several previously characterized cell cycle mutants (Gatti and Baker, 1989; Krause et al., 2001). 4) *san* mutant clones in larvae imaginal discs show defects only three days after clone induction.

The isolated alleles of *san* contain nonsense mutations within the open reading frame (ORF) and since they are protein-null alleles, the lack of oogenesis defects is not the result of a putative hypomorphic nature of the isolated alleles. Similar results were also obtained with san^2, a previously isolated loss-of-function allele of *san* (Williams et al., 2003). We conclude that during oogenesis *san* is not required for germ line mitosis.

san is possibly not required during oogenesis due to a functional redundancy with *deco* acetyltransferase. This is improbable since these two proteins are thought to have different substrates: San was predicted to be an *N*-acetyltransferase (Williams et al., 2003), and Deco was predicted to acetylate internal lysines (Ivanov et al., 2002). Additionally, San was shown to localize to the cytoplasm during the interphase of *Drosophila* Kc cells and human HeLa cells (Hou et al., 2007; Williams et al., 2003), whereas members Eco1/Ctf7 family (that includes *Drosophila* Deco) localize to the nucleus (Hou and Zou, 2005; Skibbens et al., 1999; Toth et al., 1999). Nevertheless, even if the observed results are a consequence of a redundancy between *san* and *deco* specifically within the germ line, this is consistent with the hypothesis that during oogenesis female germ line cells have differential requirements for mitotic sister chromatid cohesion (see bellow).

Female germ line cells have differential requirements for mitotic sister chromatid cohesion

Here we have shown that during mitosis different types of cells can have differential requirements for chromosome segregation. We cannot discard the possibility that some somatic cells might not require the mitotic function of *san*, but our data suggest that female germ line cells have differential requirements for mitotic sister chromatid cohesion. Consistent with this hypothesis a previous analysis of Smc1 germ line clones (focused primarily on prophase I cysts) has not reported mitotic defects during oogenesis (Khetani and Bickel, 2007). Identification of the *in vivo* substrates of *san* acetyltransferase should help a better understanding of the molecular nature of these differences.

Materials and methods

Fly work and genetics

atado/*san* alleles were isolated from a maternal screen previously done in the laboratory of Ruth Lehmann (Barbosa et al., 2007). From this screen we identified 9 complementation groups on the right arm of the second chromosome. These mutants fail to form embryonic cuticle or have scraps of cuticle, however the primordial germ cells are formed properly at the posterior pole of the embryo. Complementation Group 2 contained two alleles that initially were named $atado^1$ and $atado^2$. Later on these alleles were respectively renamed to san^3 and san^4. All flies were raised at 25 °C unless otherwise indicated, using standard techniques.

Germ line clones were induced using the FLP/FRT ovo^D system (Chou and Perrimon, 1992). Germ line clones of san^3 and san^4 were made by crossing FRT42B *san*/CyO virgins to *hs flp*; FRT42B ovo^D/Cyohshid males and heat shocking the progeny once at 37 °C for 1 h during second and third larval instar.

Mosaic ovaries with the nuclear GFP clone marker were generated by FLP-FRT-mediated mitotic recombination as described (Caceres and Nilson, 2005; Chou and Perrimon, 1992). FRT42B san^4/CyO virgins were crossed with *yw* P[w^+, hsFLP]^1; P[mini-w^+, FRT42B] P[w^+; ubi-nls-GFP]/CyOhshid males. The P[w^+; ubi-nls-GFP] FRT chromosomes bear a polyubiquitin promoter that drives ubiquitous nuclear green fluorescent protein (GFP) expression. Recombination was induced by a 1 h heat shock at 37 °C during the second and third instar stage. Adult ovaries were harvested from females with 7–8 days and 15 days old, and were subsequently processed for immunofluorescence. Germ line and follicle cell clones were identified by the absence of nuclear endogenous GFP.

To generate clones marked by the absence of GFP in imaginal discs, FRT42B san^4/CyOhshid males were crossed with *yw* P[w^+, hsFLP]^1; P[mini-w^+, FRT42B] P[w^+; ubi-nls-GFP]/CyOhshid virgins. The offspring were heat-shocked for 2 h at 37 °C at both 24 and 48 h after a 24 h egg collection, corresponding to the first and second larval instar.

To test the egg laying, 1 to 3 days old females from both *hs flp;* FRT 42B san^4/FRT42B ovo^D germ line clones and control *hs flp;* FRT42B/ovo^D FRT 42B, where germ line clones had been induced by heat-shock during the second and third larval instar, were mated in parallel to 30 wild-type (Oregon R) males. Egg laying was counted every 24 h during 15 days.

Both san^3 and san^4 alleles were balanced over a CyO Actin-GFP to enable isolation of transheterozygous mutant larvae. Mutant larvae were harvested on the basis of lack of GFP and transferred to fresh tubes. Development was followed until pupae stage where *san* mutant larvae died.

In order to compare *san* mutant phenotypes with a known lethal P-element insertion on the *separation anxiety gene* (*san*) (Williams et al., 2003), we recombined san^2 allele with a FRT42B chromosome. This allowed us to generate san^2 germ line clones and confirm that they are phenotypically indistinguishable from san^3 *and* san^4 germ line clones.

Cloning atado

Both alleles of *atado*/*san* gene were mapped using the Bloomington 2R deficiency kit. Deficiencies were crossed with both *atado*/*san* alleles and F1 progeny scored for zygotic lethality. The following seven deficiencies failed to complement *atado* alleles: Df(2R)en-A, Df(2R) en-B, Df(2R)E3363, Df(2R)Exel6060, Df(2R)ix[87i3], Df(2R)ED2219 and Df(2R)ED2155. This allowed us to map *atado*/*san* mutation to the cytological interval 47E3–47F5, comprising 47 genes. By a candidate gene approach we concluded that both alleles of *atado*/*san* failed to complement a known lethal P-element of the *san* gene, san^2 (Williams et al., 2003).

To molecularly characterize the isolated *san* mutations, genomic PCR was carried out from heterozygous mutants of *san* gene (*san*/Cyo). As a control, and in order to detect DNA polymorphisms, we used a mutant from a different complementation group isolated in the same screen. Two independent genomic PCR fragments from each allele were sequenced and compared with each other, and with the control. Both *san* alleles have distinct nonsense mutations within *san* open reading frame that are predicted to cause a truncation of the San protein.

Immunohistochemistry

For phenotypic analysis of *san* embryos, at 2–3 h of age, embryos were collected and fixed (after dechorionation in 50% bleach for 5 min) by gentle shaking for 1 h in 4 mL heptane, 0.125 mL 37% formaldehyde and 0.875 mL PEMS. Fixation was followed of devitellinization by addition of 4 mL methanol and shaking vigorously during 1 min. Following rehydration, embryos were blocked in phosphate buffered saline (PBS, pH 7.4) containing 0.1% Tween-20, 0.1% bovine serum albumin and 5% serum (BBS), at 4 °C overnight. To analyze nuclei arrested in metaphase, *san* embryos were incubated 15 min with 250 μM colchicine, PBS and heptane, prior to fixation.

Primary antibody incubations were carried in BBS at 4 °C overnight. Antibodies used were anti-Cid at 1:500 kindly provided by David Glover's laboratory, anti-Neurotactin at 1:133 (BP106 Hybridoma Bank), anti-pSer10-Histone H3 at 1:1000 (Upstate Biotechnology), anti-Topoisomerase II at 1:400 (Buchenau et al., 1993), anti-Barren at (1:2000) (Bhat et al., 1996), anti-Cnn at 1:1000 kindly provided by Jordan Raff, Anti-αTubulin clone YL1/2 at 1:50 (Serotec UK). The embryos were washed extensively in PBS containing 0.1% Tween-20 (PBT), reblocked in BBS and incubated with the appropriate secondary antibody for 2 h at room temperature (RT). Secondary antibodies were Cy3- and Cy5-conjugated at 1:1000 (Jackson ImmunoResearch Laboratories, West Grove, PA). After extensively washed in PBT, DNA was stained with OliGreen (Molecular Probes, Eugene, OR) at 1:5000 with the addition of 5 μg/mL RNAse A. For scoring the number of cortical nuclei with reduced levels of Barren we focused in embryos where the remaining nuclei (positive for Barren) were at metaphase or early anaphase stages. These are the stages when Barren localization in the chromosomes is the highest.

Ovaries were processed for immunofluorescence as described (Navarro et al., 2004), with exception of DNA staining. Primary antibody was rabbit polyclonal anti-San (Williams et al., 2003) at 1:1000 and secondary antibody was Cy5-conjugated at 1:1000. For DNA staining, ovaries were incubated with 100 μg of RNAse/mL for 30 min following incubation with 0.17 μg/mL propidium iodide. Ovaries were 2 times 5-min washed in PBT and 2 rinses in PBS, following mounting. Endogenous GFP was used to distinguish mutant clone egg chambers from chambers that did not have clones.

For ovary staining with anti-Smc1 antibody, ovaries were processed as described (Song et al., 2002). Primary antibody was anti-Smc1 at 1:2000 (Khetani and Bickel, 2007) and anti-Hts at 1:50 (1B1 Hybridoma Bank). Secondary detection was done using rodamin red at 1:1000 (Jackson ImmunoResearch Laboratories) and Cy5-conjugated at 1:1000.

Imaginal discs were dissected in PBS from crawling late third instar larvae. Discs were fixed in 4% formaldehyde with PEMS during 30 min on ice, following a 15 min wash in PBS with 0,2% Triton X-100. DNA was stained with propidium iodide as previously described.

Whole brains from transheterozygous mutants of *san* (san^3/san^4) were dissected from third instar larvae in PBS and fixed for 20 min in 3.7% formaldehyde, 2 mM EGTA in PBS. Briefly, brains were three times 5-min washed with PBS, permeabilized for 10 min in PBS+0,3% Triton X-100 and blocked in PBS containing 0.1% Triton X-100 and 1% BSA for 1 h at RT. Anti-αTubulin at 1:50 and anti-pSer10 Histone H3 at 1:300 were incubated with PBS+0.1% Triton X-100 and 1% BSA overnight at 4 °C. After three 5-min washes, Cy3- and Cy5-conjugated secondary antibodies were incubated for 4 h at RT. Brains were rinsed with PBS and DNA was stained with propidium iodide as previously described.

Embryos and all tissues were mounted in Fluorescent Mounting Medium (DakoCytomation, Inc) and immunostainings were visualized using a Leica SP5 confocal microscope. All images are confocal sections, with the exception of Figs. 5J–O, Sup. Fig. 4, and Sup. Fig. 6, which are Z-stacks. The Z-stacks projections were obtained using Image J program (Grouped ZProjector, maximum pixel intensity).

Western blotting

Embryos were collected on apple juice agar after 3 h egg laying. Each protein sample was collected by lysing 10 embryos in SDS-PAGE sample buffer. Samples were boiled for 5 min and loaded on 5×8 cm 12.5% polyacrylamide gels.

Ovaries were dissected from 3-to 8-day-old Oregon females. Ovaries were homogenized in buffer containing 50 mM Tris–HCl (pH 7.5), 150 mM NaCl, 2 mM EDTA, 0,1% NP-40, 2 mM DTT, 10 mM NaF and protease inhibitor (Roche). A Bio-Rad™ Bradford protein microassay ensured loading of 5, 10 and 15 μg of protein onto 12% SDS polyacrylamide gels. As for embryo extracts, samples were boiled for 5 min in SDS-PAGE sample buffer before loading.

Proteins were then transferred onto Hybond-ECL membranes (Amersham) and western blotting was performed with standard procedure. Briefly, the membrane was blocked in 5% non-fat milk/PBT (0,1% Tween-20, 1× PBS) overnight at 4 °C. Primary antibodies were incubated with the membrane overnight at 4 °C. Following washes with PBT secondary antibodies were incubated for 4 h at RT. After washes with PBT, the membranes were detected with an ECL Plus western blotting detection system (GE Healthcare). Primary antibodies used were anti-Cid (1:2000), rabbit polyclonal anti-San (1:1000), rabbit anti-Smc4 (1:1000) (Steffensen et al., 2001), rat anti-Tubulin (1:250). Secondary detection was performed with rabbit and rat HRP-conjugated antibodies used at a final concentration of 1:5000.

Recombinant San^4 protein expression and detection

We expressed in bacteria a recombinant C-terminal polyhistidine (6xHis)-tagged fragment of San corresponding to residues 1–113 by cloning a cDNA EcoRI–XhoI fragment into the pET22b vector (Novagene) and expressing it in *E. coli* BL21. This is the truncated protein predicted to be encoded by $atado^2/san^4$. Since the San antibody was generated against a GST-San fusion protein, we cloned san^4 cDNA in a His-tag expression vector to avoid cross-reactivity with GST. The San^4-6xHis protein was induced with 10 mM IPTG in *E. coli* BL21. Bacterial samples were collected at 90, 120 and 180 min from both induced and non-induced cultures. The bacterial pellets from each time point were ressuspended in SDS-sample buffer, boiled for 5 min and loaded on two 15% polyacrylamide gels. One gel was stained with brilliant coomassie and the other gel was used for western blotting using the San antibody.

Acknowledgments

We thank Monica Bettencourt-Dias, Alvaro Tavares, Miguel Godinho, Raquel Oliveira, Richard Hampson, Nicolas Malmanche, and Claudio Sunkel for suggestions that greatly improved the manuscript; the Martinho lab, Monica Bettencourt-Dias, Alvaro Tavares, Gonçalo Costa, and IGC fly community for discussions. We thank A. Arkov, Y. Arkova, N. Kimm, P. Kunwar, A. Renault, H. Sano and H. Zinszner for help in performing the mutagenesis screen from which the two *atado* alleles were originally isolated. This work was supported by a Marie Curie International Reintegration Grant (029165) and grants from Fundação para a Ciência e Tecnologia [Grants PPCDT/DG/BIA/82013/2006 and PTDC/BIA-BCM/69256/2006]. A.R.M. has a fellowship from Fundação para a Ciência e Tecnologia [SFRH/BD/28767/2006].

Appendix A. Supplementary data

Supplementary data associated with this article can be found, in the online version, at doi:10.1016/j.ydbio.2008.08.021.

References

Arnesen, T., Anderson, D., Torsvik, J., Halseth, H.B., Varhaug, J.E., Lillehaug, J.R., 2006. Cloning and characterization of hNAT5/hSAN: an evolutionarily conserved component of the NatA protein *N*-alpha-acetyltransferase complex. Gene 371, 291–295.

Barbosa, V., Kimm, N., Lehmann, R., 2007. A maternal screen for genes regulating *Drosophila* oocyte polarity uncovers new steps in meiotic progression. Genetics 176, 1967–1977.

Bhalla, N., Biggins, S., Murray, A.W., 2002. Mutation of YCS4, a budding yeast condensin subunit, affects mitotic and nonmitotic chromosome behavior. Mol. Biol. Cell. 13, 632–645.

Bhat, M.A., Philp, A.V., Glover, D.M., Bellen, H.J., 1996. Chromatid segregation at anaphase requires the barren product, a novel chromosome-associated protein that interacts with Topoisomerase II. Cell 87, 1103–1114.

Bickel, S.E., Wyman, D.W., Miyazaki, W.Y., Moore, D.P., Orr-Weaver, T.L., 1996. Identification of ORD, a *Drosophila* protein essential for sister chromatid cohesion. Embo J. 15, 1451–1459.

Bickel, S.E., Wyman, D.W., Orr-Weaver, T.L., 1997. Mutational analysis of the *Drosophila* sister-chromatid cohesion protein ORD and its role in the maintenance of centromeric cohesion. Genetics 146, 1319–1331.

Buchenau, P., Saumweber, H., Arndt-Jovin, D.J., 1993. Consequences of topoisomerase II inhibition in early embryogenesis of *Drosophila* revealed by in vivo confocal laser scanning microscopy. J. Cell Sci. 104 (Pt 4), 1175–1185.

Caceres, L., Nilson, L.A., 2005. Production of gurken in the nurse cells is sufficient for axis determination in the *Drosophila* oocyte. Development 132, 2345–2353.

Castano, I.B., Brzoska, P.M., Sadoff, B.U., Chen, H., Christman, M.F., 1996. Mitotic chromosome condensation in the rDNA requires TRF4 and DNA topoisomerase I in Saccharomyces cerevisiae. Genes Dev. 10, 2564–2576.

Chang, C.J., Goulding, S., Earnshaw, W.C., Carmena, M., 2003. RNAi analysis reveals an unexpected role for topoisomerase II in chromosome arm congression to a metaphase plate. J. Cell Sci. 116, 4715–4726.

Chou, T.B., Perrimon, N., 1992. Use of a yeast site-specific recombinase to produce female germline chimeras in *Drosophila*. Genetics 131, 643–653.

Ciosk, R., Shirayama, M., Shevchenko, A., Tanaka, T., Toth, A., Shevchenko, A., Nasmyth, K., 2000. Cohesin's binding to chromosomes depends on a separate complex consisting of Scc2 and Scc4 proteins. Mol. Cell 5, 243–254.

Cobbe, N., Savvidou, E., Heck, M.M., 2006. Diverse mitotic and interphase functions of condensins in *Drosophila*. Genetics 172, 991–1008.

Coelho, P.A., Queiroz-Machado, J., Sunkel, C.E., 2003. Condensin-dependent localisation of topoisomerase II to an axial chromosomal structure is required for sister chromatid resolution during mitosis. J. Cell Sci. 116, 4763–4776.

Dej, K.J., Ahn, C., Orr-Weaver, T.L., 2004. Mutations in the *Drosophila* condensin subunit dCAP-G: defining the role of condensin for chromosome condensation in mitosis and gene expression in interphase. Genetics 168, 895–906.

Dorsett, D., Eissenberg, J.C., Misulovin, Z., Martens, A., Redding, B., McKim, K., 2005. Effects of sister chromatid cohesion proteins on cut gene expression during wing development in *Drosophila*. Development 132, 4743–4753.

Foe, V.E., Odell, G.M., Edgar, B.A., 1993. Mitosis and Morphogenesis in the *Drosophila* embryo: point and counterpoint. In: Press, C.S.H.L. (Ed.), In The development of *Drosophila melanogaster*, vol. 1, p. 149.

Gatti, M., Baker, B.S., 1989. Genes controlling essential cell-cycle functions in *Drosophila melanogaster*. Genes Dev. 3, 438–453.

Ghabrial, A., Schupbach, T., 1999. Activation of a meiotic checkpoint regulates translation of Gurken during *Drosophila* oogenesis. Nat. Cell. Biol. 1, 354–357.

Gilboa, L., Lehmann, R., 2004. How different is Venus from Mars? The genetics of germline stem cells in *Drosophila* females and males. Development 131, 4895–4905.

Glynn, E.F., Megee, P.C., Yu, H.G., Mistrot, C., Unal, E., Koshland, D.E., DeRisi, J.L., Gerton, J.L., 2004. Genome-wide mapping of the cohesin complex in the yeast Saccharomyces cerevisiae. PLoS Biol. 2, E259.

Hartman, T., Stead, K., Koshland, D., Guacci, V., 2000. Pds5p is an essential chromosomal protein required for both sister chromatid cohesion and condensation in Saccharomyces cerevisiae. J. Cell Biol. 151, 613–626.

Hirano, T., 2005. Condensins: organizing and segregating the genome. Curr. Biol. 15, R265–275.

Hirano, T., 2006. At the heart of the chromosome: SMC proteins in action. Nat. Rev. Mol. Cell. Biol. 7, 311–322.

Holm, C., Stearns, T., Botstein, D., 1989. DNA topoisomerase II must act at mitosis to prevent nondisjunction and chromosome breakage. Mol. Cell Biol. 9, 159–168.

Hou, F., Zou, H., 2005. Two human orthologues of Eco1/Ctf7 acetyltransferases are both required for proper sister-chromatid cohesion. Mol. Biol. Cell. 16, 3908–3918.

Hou, F., Chu, C.W., Kong, X., Yokomori, K., Zou, H., 2007. The acetyltransferase activity of San stabilizes the mitotic cohesin at the centromeres in a shugoshin-independent manner. J. Cell Biol. 177, 587–597.

Ivanov, D., Schleiffer, A., Eisenhaber, F., Mechtler, K., Haering, C.H., Nasmyth, K., 2002. Eco1 is a novel acetyltransferase that can acetylate proteins involved in cohesion. Curr. Biol. 12, 323–328.

Khetani, R.S., Bickel, S.E., 2007. Regulation of meiotic cohesion and chromosome core morphogenesis during pachytene in *Drosophila* oocytes. J. Cell Sci. 120, 3123–3137.

Klein, F., Mahr, P., Galova, M., Buonomo, S.B., Michaelis, C., Nairz, K., Nasmyth, K., 1999. A central role for cohesins in sister chromatid cohesion, formation of axial elements, and recombination during yeast meiosis. Cell 98, 91–103.

Krause, S.A., Loupart, M.L., Vass, S., Schoenfelder, S., Harrison, S., Heck, M.M., 2001. Loss of cell cycle checkpoint control in *Drosophila* Rfc4 mutants. Mol. Cell. Biol. 21, 5156–5168.

Lavoie, B.D., Hogan, E., Koshland, D., 2002. In vivo dissection of the chromosome condensation machinery: reversibility of condensation distinguishes contributions of condensin and cohesin. J. Cell Biol. 156, 805–815.

Lengronne, A., McIntyre, J., Katou, Y., Kanoh, Y., Hopfner, K.P., Shirahige, K., Uhlmann, F., 2006. Establishment of sister chromatid cohesion at the S. cerevisiae replication fork. Mol. Cell 23, 787–799.

Losada, A., 2007. Cohesin regulation: fashionable ways to wear a ring. Chromosoma 116, 321–329.

Losada, A., Hirano, M., Hirano, T., 1998. Identification of Xenopus SMC protein complexes required for sister chromatid cohesion. Genes Dev. 12, 1986–1997.

Losada, A., Yokochi, T., Kobayashi, R., Hirano, T., 2000. Identification and characterization of SA/Scc3p subunits in the Xenopus and human cohesin complexes. J. Cell Biol. 150, 405–416.

Miyazaki, W.Y., Orr-Weaver, T.L., 1992. Sister-chromatid misbehavior in *Drosophila* ord mutants. Genetics 132, 1047–1061.

Moldovan, G.L., Pfander, B., Jentsch, S., 2006. PCNA controls establishment of sister chromatid cohesion during S phase. Mol. Cell 23, 723–732.

Molnar, M., Bahler, J., Sipiczki, M., Kohli, J., 1995. The rec8 gene of Schizosaccharomyces pombe is involved in linear element formation, chromosome pairing and sister-chromatid cohesion during meiosis. Genetics 141, 61–73.

Nasmyth, K., Haering, C.H., 2005. The structure and function of SMC and kleisin complexes. Annu. Rev. Biochem. 74, 595–648.

Navarro, C., Puthalakath, H., Adams, J.M., Strasser, A., Lehmann, R., 2004. Egalitarian binds dynein light chain to establish oocyte polarity and maintain oocyte fate. Nat. Cell. Biol. 6, 427–435.

Panizza, S., Tanaka, T., Hochwagen, A., Eisenhaber, F., Nasmyth, K., 2000. Pds5 cooperates with cohesin in maintaining sister chromatid cohesion. Curr. Biol. 10, 1557–1564.

Pasierbek, P., Jantsch, M., Melcher, M., Schleiffer, A., Schweizer, D., Loidl, J., 2001. A Caenorhabditis elegans cohesion protein with functions in meiotic chromosome pairing and disjunction. Genes Dev. 15, 1349–1360.

Pauli, A., Althoff, F., Oliveira, R.A., Heidmann, S., Schuldiner, O., Lehner, C.F., Dickson, B.J., Nasmyth, K., 2008. Cell-Type-Specific TEV Protease Cleavage Reveals Cohesin Functions in *Drosophila* Neurons. Dev. Cell 14, 239–251.

Skibbens, R.V., Corson, L.B., Koshland, D., Hieter, P., 1999. Ctf7p is essential for sister chromatid cohesion and links mitotic chromosome structure to the DNA replication machinery. Genes Dev. 13, 307–319.

Song, X., Zhu, C.H., Doan, C., Xie, T., 2002. Germline stem cells anchored by adherens junctions in the *Drosophila* ovary niches. Science 296, 1855–1857.

Sonoda, E., Matsusaka, T., Morrison, C., Vagnarelli, P., Hoshi, O., Ushiki, T., Nojima, K., Fukagawa, T., Waizenegger, I.C., Peters, J.M., Earnshaw, W.C., Takeda, S., 2001. Scc1/Rad21/Mcd1 is required for sister chromatid cohesion and kinetochore function in vertebrate cells. Dev. Cell 1, 759–770.

Spradling, A.C., 1993. Development genetics of oogenesis. In: Press, C.S.H.L. (Ed.), The development of *Drosophila melanogaster*, vol. 1, p. 1.

Steffensen, S., Coelho, P.A., Cobbe, N., Vass, S., Costa, M., Hassan, B., Prokopenko, S.N., Bellen, H., Heck, M.M., Sunkel, C.E., 2001. A role for *Drosophila* SMC4 in the resolution of sister chromatids in mitosis. Curr. Biol. 11, 295–307.

Sumara, I., Vorlaufer, E., Gieffers, C., Peters, B.H., Peters, J.M., 2000. Characterization of vertebrate cohesin complexes and their regulation in prophase. J. Cell Biol. 151, 749–762.

Tanaka, K., Yonekawa, T., Kawasaki, Y., Kai, M., Furuya, K., Iwasaki, M., Murakami, H., Yanagida, M., Okayama, H., 2000. Fission yeast Eso1p is required for establishing sister chromatid cohesion during S phase. Mol. Cell Biol. 20, 3459–3469.

Tomonaga, T., Nagao, K., Kawasaki, Y., Furuya, K., Murakami, A., Morishita, J., Yuasa, T., Sutani, T., Kearsey, S.E., Uhlmann, F., Nasmyth, K., Yanagida, M., 2000. Characterization of fission yeast cohesin: essential anaphase proteolysis of Rad21 phosphorylated in the S phase. Genes Dev. 14, 2757–2770.

Toth, A., Ciosk, R., Uhlmann, F., Galova, M., Schleiffer, A., Nasmyth, K., 1999. Yeast cohesin complex requires a conserved protein, Eco1p(Ctf7), to establish cohesion between sister chromatids during DNA replication. Genes Dev. 13, 320–333.

Toyoda, Y., Yanagida, M., 2006. Coordinated requirements of human topo II and cohesin for metaphase centromere alignment under Mad2-dependent spindle checkpoint surveillance. Mol. Biol. Cell. 17, 2287–2302.

Uemura, T., Ohkura, H., Adachi, Y., Morino, K., Shiozaki, K., Yanagida, M., 1987. DNA topoisomerase II is required for condensation and separation of mitotic chromosomes in S. pombe. Cell 50, 917–925.

Uhlmann, F., Nasmyth, K., 1998. Cohesion between sister chromatids must be established during DNA replication. Curr. Biol. 8, 1095–1101.

Uhlmann, F., Lottspeich, F., Nasmyth, K., 1999. Sister-chromatid separation at anaphase onset is promoted by cleavage of the cohesin subunit Scc1. Nature 400, 37–42.

Vass, S., Cotterill, S., Valdeolmillos, A.M., Barbero, J.L., Lin, E., Warren, W.D., Heck, M.M., 2003. Depletion of Drad21/Scc1 in *Drosophila* cells leads to instability of the cohesin complex and disruption of mitotic progression. Curr. Biol. 13, 208–218.

Webber, H.A., Howard, L., Bickel, S.E., 2004. The cohesion protein ORD is required for homologue bias during meiotic recombination. J. Cell Biol. 164, 819–829.

Williams, B.C., Garrett-Engele, C.M., Li, Z., Williams, E.V., Rosenman, E.D., Goldberg, M.L., 2003. Two putative acetyltransferases, san and deco, are required for establishing sister chromatid cohesion in *Drosophila*. Curr. Biol. 13, 2025–2036.

Supplementary figure 1

Embryos mutant for *atado*^{2} show high frequency of chromosome bridges during syncytial blastoderm. (A) Syncytial blastoderm is abnormal in 87% of the embryos mutant for *atado*^{2} and 2.5% of the control embryos. (B) Chromosome bridges during late-mitosis and interphase can be observed in 12.3% ± 20.5 of the nuclei mutant for *atado*^{2} (n= 1033 nuclei, 12 embryos) and only 0.7%±1.8 of the control nuclei (n=2081 nuclei, 12 embryos) (Student's t test, 95% confidence interval, $p<0.03$). Nuclei were only scored when pSer10 histone H3 staining was absent (or almost absent) from the syncytial nuclei. This allows the exclusion of most nuclei going through mitosis.

Supplementary figure 2

Embryos mutant for *atado*^{2} apparently have normal kinetochores, centrosomes, and mitotic spindles. Embryos mutant for *atado*^{2} show normal localization of Cid (A, B), Cnn (C, D), and α-Tubulin (E, F). All panels show syncytial blastoderm embryos. (A, B) Embryos were stained for Cid (green), DNA (red), and pSer10 H3 (blue). (C, D) Embryos were stained for DNA (green) and Cnn (red). (E, F) Embryos were stained for α-Tubulin (green), DNA (red), Cnn (blue). Scale bars equals (A, B) 10μm and (C, D) 5μm.

Supplementary figure 3

Larvae mutant for *atado* (zygotic mutants) show smaller and morphological abnormal brains. Transheterozygotic *atado*^{1}/*atado*^{2} third-instar larvae show smaller and morphologically abnormal brains (br) when compared to the ones from control larvae (*atado*/Cyo Actin-GFP). Control larvae were identified using an Actin-GFP transgene. Central ganglia (gl) from *atado* and control larvae have similar sizes.

Supplementary figure 4

Embryos mutant for *san*^{2} (germ-line clones) are phenotypically indistinguishable from *atado* mutant embryos. Embryos mutant for **san**^{2} show abnormal anaphases (C, D), with a high frequency of chromosome bridges (E). Chromosome congression during metaphase occurs normally, yet a subset of chromosomes although positive for pSer10 H3 (B) appear to have chromosome condensation problems (A). All panels show syncytial blastoderm embryos. The same embryo was stained for DNA (A) and pSer10 H3 (B). Embryos (C–F) were stained for DNA (green) and pSer10 Histone H3 (red). (D, E) show details of the embryo shown in C. Embryo shown in (F) is wild type. Embryos shown in (A–E) are mutant for *san*^{2} (germ-line clones crossed with wild type males). Images shown are Z-stacks obtained using Image J program (Grouped ZProjector, maximum pixel intensity).

Supplementary figure 5

San antibody is able to recognize a truncated protein predicted to be encoded by *atado*^{2}*/san*^{4}. Western blot from bacteria protein extracts from induced (with IPTG) and mock induced (no IPTG) bacteria show that San antibody is able to recognize a truncated protein predicted to be encoded by *atado*^{2}*/san*^{4}. An embryonic extract from wild type embryos is used as a positive control. Since the San antibody was raised against a GST-San recombinant protein, the truncate protein was tagged with a 6xHis-tag in order to avoid GST cross-reactivity.

Supplementary figure 6

In *san*^{2} embryos, a large proportion of the bridges between interphase nuclei are negative for Cid staining. All panels show interphase nuclei from syncytial blastoderm embryos mutant for *san*^{2}. A large proportion of bridges were negative for Cid staining (C–F). Yet

some were positive for Cid (G, H). Of the scored bridges between nuclei in late-mitosis/interphase: 55.6% ± 18.2 were negative for Cid staining, 32% ± 11.5 were positive for Cid staining, and in 12.4% ± 10 of the cases the result was inconclusive (n= 104 bridges). All embryos were stained for DNA (green) and Cid (red). Panels (C–I) show details of the embryos shown in (A, B). Images shown are Z-stacks obtained using Image J program (Grouped ZProjector, maximum pixel intensity).

Supplementary figure 7

***san* is not required within the germ line for normal egg laying.** The egg-laying of *san*^{4} and control females (with an identical FRT chromosome) is identical. Germ line clones using the FRT-*ovo*^{D} system were induced by heat-shock at larvae stages. For more experimental information please see MATERIALS AND METHODS.

Supplementary figure 8

During oogenesis san **is required within somatic follicle cells but is not required within the germ line for normal mitosis.** *san*^{2} is a previously characterized loss-of-function allele of **san**. Absence of endogenous GFP (green) indicates that the cells are homozygous for *san*^{2} (A–F) or control FRT chromosome (G-L). Germ line and follicle cell clones of *san*^{2} (A–F) or control FRT chromosome (G–L) were induced at larvae stages using heat-shock-controlled flipase and the ovaries were dissected from adult females that were 7/8 old after hatching (pupal eclosion). *Drosophila* germarium whose germ line is mutant for *san*^{2} developed normally (A–F). Follicle cell clones mutant for *san*^{2} were rare and small (B, D, E, F). Follicle cell clones from control FRT chromosome were more frequent and significantly larger than the ones observed for *san*^{2} (G–L). Ovaries are stained for DNA (red). Scale bars equal (A, C) 25μm, (E) 50μm, (G) 40μm, and (J)

50µm. The images shown in (A, B), (C, D), (E, F), (G–I), and (J, K) correspond to the same egg chambers.

CHAPTER IV

dSan/dNaa50 *in vivo* N^{α}-acetylates multiple targets and shares partial redundancy with other N^{α}-terminal acetyltransferases

1. Introduction

N^{α}-terminal acetylation is a highly conserved and widespread modification occurring on approximately 80% of all soluble, cytoplasmic human proteins (Arnesen et al., 2009). With few exceptions, little is known about the biological function of protein N^{α}-terminal acetylation. Recently, it was suggested to act as a general destabilization signal for some yeast proteins (Hwang et al., 2010). Other reports suggest it might act as stabilizer, for instance by blocking protein degradation (Ciechanover and Ben-Saadon, 2004). Since it's such a conserved and widespread modification, protein N^{α}-acetylation can be envisioned as a housekeeping modification. Consistent with this idea, knockdown phenotypes of the main studied N^{α}-terminal acetyltransferase (NAT) complexes are generally associated with cell cycle arrest or apoptosis (Ametzazurra et al., 2008; Arnesen et al., 2006b; Fisher et al., 2005; Lim et al., 2006; Starheim et al., 2008; Starheim et al., 2009). In contrast to the NatA, NatB and NatC complexes, knockdown of the NatE complex leads to more specific phenotypes.

The NatE complex is composed by the NAT Naa50p associated to Naa10p and Naa15p (Arnesen et al., 2006a; Gautschi et al., 2003; Williams et al., 2003). dSan/dNaa50p was first identified in a large-scale genetic screen for mitotic mutations in *Drosophila* (Williams et al., 2003). dSan/dNaa50 mutant neuroblasts exhibited premature sister chromatid separation. Moreover, in dSan/dNaa50-depleted cultured cells, the cohesin subunit Drad21/Scc1 was delocalized from the centromeres of the detached chromatids. This work, therefore, associated dSan/dNaa50 function to centromeric sister chromatid cohesion (Williams et al., 2003). However we further observed dSan/dNaa50 was also required for chromosome resolution/ condensation implying a more general mitotic function of this

acetyltransferase (Pimenta-Marques et al., 2008). Recent *in vitro* studies showed hSan/hNaa50 preferentially acetylates N-termini with the consensus MLGP- and MLDP- (Evjenth et al., 2009), however there are no known *in vivo* substrates of San/Naa50p. Identifying the *in vivo* substrates of dSan/dNaa50 would shed light on the molecular pathway in which this NAT is involved and how protein N^{α}-acetylation regulates mitosis.

With the goal of identifying *in vivo* substrates of dSan/dNaa50, we took advantage of the N-terminal COmbined FRActional Diagonal Chromatography (COFRADIC) methodology to identify proteins whose N^{α}-acetylation levels were reduced in *san* mutant embryos. In this chapter we describe the identification of 18 proteins whose N^{α}-acetylation levels are indeed reduced in *san* mutants. From these 18 proteins we looked for candidate proteins as being associated to the mitotic phenotypes observed in dSan/dNaa50 depleted cells. From these, we identified the gamma subunit of the cytosolic chaperonin containing T-complex polypeptide 1 (CTT) (Cctγ) which displayed chromosome segregation defects very similar to dSan/dNaa50 depleted cells. Interestingly Cctγ is required for the metaphase to anaphase transition by activating the APC/C complex, making this protein an excellent candidate for a mitotic substrate of dSan/dNaa50. Additionally, we describe the identification of candidate mitotic targets of dSan/dNaa50 by analysis of protein N-terminus. Since both *Drosophila* and human San/Naa50p depleted cells share similar mitotic phenotypes (Hou et al., 2007; Williams et al., 2003) we expect mitotic substrates of this NAT to also share a conserved N-terminus. Interestingly, we found the cohesin Drad21/Scc1 protein contains a conserved N-terminus within higher eukaryotes. Additionally, this N-terminus falls into the category of an N-terminus acetylated by

hSan/hNaa50, making Drad21/Scc1 a candidate to further explore as a mitotic substrate of dSan/dNaa50.

2. Materials and methods

2.1. Embryonic protein extracts

Germ line clones of *san*^{4} were made using standard techniques (Chou and Perrimon, 1992) as described in chapter II. Females with mutant germ-line (Cy^{+} females) were crossed with wild-type (Oregon R) males. Maternal mutant embryos for *san*^{4} and wild-type (control) embryos were independently collected every two hours in apple juice plates, dechorionated in 50% bleach for 5 min, rinsed 3x in ddH_20, 2x rinsed in PBT and 1x PBS. Embryos were frozen in liquid nitrogen and kept at -80ºC. Embryos were homogenized in lysis buffer containing 50 mM Tris, 12 mM EDTA, 250 mM NaCl, 140 mM Na_2HPO_4 (pH 7,6), and protease inhibitor (Roche). Samples were centrifuged 3x at 14000g for 5 min at 4ºC, between each centrifugation the middle layer was collected avoiding the upper-lipid layer as much as possible. A Bio-Rad™ Bradford protein microassay was preformed to quantify the total amount of protein in *san* mutant and wild-type (control) protein extracts. Extracts were kept at -80ºC.

2.2. Identification of dSan/dNaa50 NAT substrates by COFRADIC

Work developed by Petra Van Damme in Kris Gavert's laboratory (VIB Department of Medical Protein Research, Ghent University) and in collaboration with Thomas Arnesen (University of Bergen).

To identify *in vivo* targets of dSan/dNaa50, we used COFRADIC proteomics. Briefly, proteins were denaturated to their

primary structure (fig. 1). All free primary amines (α-amines of the N-terminals and ε-amines from internal amino acids) were further blocked by a forced *in vitro* AcD3C13-acetylation (5Da heavier form of NHS-acetate which introduced a $^{13}C_2$ and D3 labeled acetyl moiety on all free amines). Extracts were further digested with trypsin. Digestion resulted in a mixture of N-terminal peptides which were *in vivo* or *in vitro* acetylated and internal peptides which now had a free α-amine group. By performing a strong cation exchange (SCX) step at pH 3.0, acetylated peptides which carried one positive charge less than the internal peptides were retained significantly less with SCX resins. This step allowed discarding the majority of internal peptides. SCX treatment was followed by a primary high performance liquid chromatography (HPLC) fractionation of the different samples. After the first HPLC run all fractions were treated with 2,4,6-trinitrobenzenesulfonic acid (TNBS). This allowed blockage of internal peptides that were not eliminated by the SCX treatment. Since TNBS treatment conferred a high hydrophobicity to the remaining internal peptides, they were efficiently discarded by a second HPLC run. This step increases the purity of the final analysed samples to 95% of true N-terminal peptides. The different fractions were analyzed by liquid chromatography-tandem mass spectrometry (LC-MS/MS), which allowed the identification and quantification of the *in vivo* N-terminal acetylated peptides (fig. 1) (Gevaert et al., 2003; Van Damme et al., 2009).

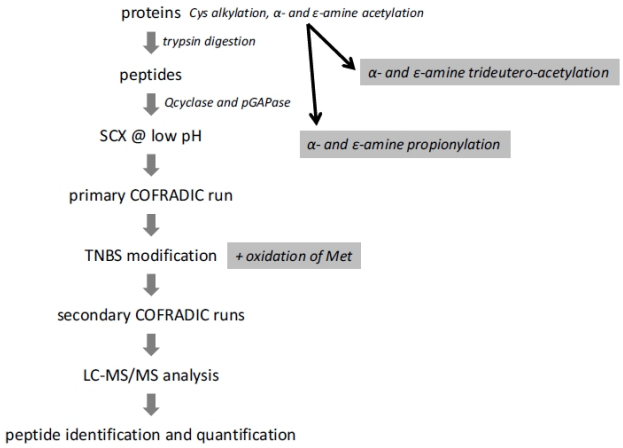

Figure 1: General work-flow of the N-terminal COFRADIC Procedure. (Adapted from Van Damme et al., 2009).

N^{α}-acetylation states of N-termini identified in both setups were comparatively analyzed by inspection of their respective MS-spectra. We distinguished between *in vivo* N^{α}-acetylation and free N-termini by making use of *in vitro* AcD3C13-acetylation. Each N-terminus was defined as a peptide that was N^{α}-acetylated *in vivo* or AcD3C13-acetylated *in vitro* (*in vivo* free N-terminus) starting at position 1 or 2 of the annotated protein sequence or at positions beyond position 2 of the annotated protein sequence according to the SwissProt database.

The ratios of all Arg-C type N-terminal peptides were quantified by MASCOT Distiller (http://www.matrixscience.com/distiller.html) and the extent of N^{α}-acetylation was calculated after extracting the peak-intensities. Therefore, the modified peptide sequences were used to calculate the theoretical isotope peak distribution using the MS-isotope pattern calculator (http://prospector.ucsf.edu). For all two possible variants (*in vivo* N-acetylated (peak at m/Z) and *in vitro* $^{13}C_2D3$-N-acetylated (peak at m/z +5Da) the predicted intensity of the 5^{th} contributing isotope (isotopic pattern of contributing -5Da peak) was

subtracted from the measured intensity of all corresponding monoisotopic peaks of the other isotopic clusters in order to correct for the overlapping isotopic envelopes.

For all unique N-termini identified, the average of all ratios were calculated per peptide and the corresponding highest scoring MS-spectra were visually inspected in order to evaluate the extent of the N^{α}-acetylation calculated and to assure a high quality catalogue of the global N^{α}-acetylation status in control and *san* mutant proteomes.

2.3. RNA interference and drug treatment of cultured *Drosophila* Dmel2 cells

Cells were always cultured at 25ºC. *Drosophila* Dmel2 cells were grown in SFM Medium (GIBCO) supplemented with 1x glutamine and 1x PenStrep. Cells were counted and diluted to $2x10^6$ cells/mL in SFM medium, supplemented with glutamine but without Penstrep. RNA interference (RNAi) was performed according to Clemens *et al.* (Clemens et al., 2000) in *Drosophila* Dmel2 cells. Table 1 contains the primers used for the construction of different amplicons and their corresponding size. Each result was always confirmed using two different dsRNAs against the same mRNA to minimize off-target effects. GFP RNAi was used as control. Each primer incorporated a T7 RNA polymerase binding site. All PCR products were used as templates to synthesize dsRNA by utilizing the T7 RiboMAX™ Express kit (Promega). Cells were incubated during 1h with 40µg of dsRNA at a concentration of 1µg/µL for each RNAi experiment performed. After 1h incubation with dsRNA, 3mL of SFM media supplemented with glutamine and PenStrep were added back.

To arrest cells in mitosis, colchicine (Sigma) was added to culture medium to a final concentration of 25 µM and then incubated

for 11 or 16 hours. 11h colchicine treatment corresponded to 88h incubation with dsRNAs and 16h colchicine treatment corresponded to 93h dsRNA treatment. At each desired time point, cells were harvested for immunofluorescence and/or immunoblotting.

Protein to deplete	Amplicon	Primers	Amplicon size (bp)
dSan	dSan Amp1	5'- AGCAGCATCGAACTGGGC -3' 5'-CGCTTATAGTATTGCTCCTTGGT-3'	413
	dSan Amp2	5'-CAACACTGAGAACCAGCGGC-3' 5'-CGTAGTAAAGCACGACAGTTCAC-3'	354
PPP4R24	PPP4R2r Amp1	5'-AAGACAGGCGGAGTTACAGC-3' 5'-AGGTCGTCGAGTCTGATAAACC-3'	613
	PPP4R2r Amp2	5'-CACAATCGATCCTGGACGCAAGC-3' 5'-GCCTCGTCATCGGCAGATGATGGG-3'	489
CG1785	CG1785 Amp1	5'-TATTGATCAGGTGGTGGAACG-3' 5'-CCTCTTGAGCTCTGTTTGACG-3'	450
	CG1785 Amp2	5'-CGTTCGCGGATAAACAGGATG-3' 5'-CAGACGCTGTTCCAGTTTTACG-3'	299
CkIIα	CkIIα Amp 1	5'-TAATGCATCGTGATGTAAAGCC-3' 5'-TGGCTTCTATCCCAAACTCG-3'	615
	CkIIα Amp 2	5'-CGGCTCGCGTGTACACAGATG-3' 5'-GGCTTTACATCACGATGCATTATTCC-3'	454
Cctγ	Cctγ Amp1	5'-AGGAGTCGTGTGTTCTTAAGGG-3' 5'-GTATGATCTCTAGGGCGTGGG-3'	696
	Cctγ Amp2	5'-CCAAGGCCTGCACCATCCTGC-3' 5'-GATGTTCTTCACGTTCATGTCCACG-3'	454
RpL19	RpL19 Amp1	5'-GAAAGCGTAAGGGTACTGCG-3' 5'-ATCATTTCGGCCAAACTAAAGG-3'	464
	RpL19 Amp 2	5'-CTTTCCTAGCCACGACGAGG-3' 5'-CACGGTAACGGGAGTGGAC-3'	215
GFP	GFP Amp	5'-ACCATGCCGCTACTGTGAATC-3' 5'-GTGCGCCAATGGAAGAATC-3'	420

Table 1: Primers used to produce different dsRNAs for RNAi experiments.

2.4. Immunofluorescence of Dmel2 Cells

After 93 hours of dsRNA treatment with or without colchicine induced mitotic arrest, $2x10^6$ cells were added to coverslips by 1h incubation at 25ºC. Cells were fixed with 4% formaldehyde, 0.03M PIPES, 0.11M HEPES, 0.01M EGTA and 4mM $MgSO_4$ for 10 min, followed by two washes in 1x PBS. Permeabilization and blocking was performed for 1h with PBSTB (PBS, 0.1% Triton X-100, 1% fetal bovine serum). Primary antibody incubations were done in PBSTB for

2h at room temperature or overnight at 4°C, followed by three 5 min washes in PBSTB. Secondary antibody incubations were performed as described for the primary antibodies, including the three 5 min washes. Primary antibodies used were mouse anti-α-tubulin DM1A (1:500; Sigma) and rabbit anti-pSer10-Histone H3 (1:500; Upstate Biotechnology). Rabbit anti-pSer10-Histone H3 was used to mark and count mitotic cells. DNA was stained with DAPI at 1:1000 (stock concentration 1 mg/ml).

2.5. Microscopy

Visualization of fixed cells was performed using a Delta Vision Core System (Applied Precision) using a 100× UplanSApo objective and a cascade2 EMCCD camera (Photometrics). Images were acquired as a series of z-sections separated by 0.2-μm intervals. Deconvolution was performed using the conservative ratio method in softWoRx software. Phenotypic quantification was performed using a regular Epifluorescent microscope, DMRA2 (Leica).

3. Results

3.1. dSan/dNaa50 N^{α}-terminal acetyltransferase acetylates multiple different substrates *in vivo*

NATs can have a large number of *in vivo* substrates (Arnesen et al., 2009). In order to define the *in vivo* consensus of dSan/dNaa50 substrates we took advantage of COFRADIC to analyze *in vivo* the N-terminal acetylation profiles of wild-type (control) and *san* mutant embryos proteomes. This work was done in collaboration with Thomas Arnesen (University of Bergen, Norway) and Kris Gavert (Department of Medical Protein Research, VIB, B-9000 Ghent, Belgium).

The COFRADIC method allowed the identification of 432 unique N-termini derived from 399 unique SwissProt *Drosophila* protein accessions. Of the 432 unique N-termini identified, 364 acquired a start position at amino acid 1 or 2 (84%), while 68 had a start position after the amino acid 2 (16%). 292 unique N-termini were identified in control and *san* mutant protein extracts, while 100 and 40 were uniquely identified in the control or mutant protein extracts, respectively. The N^{α}-acetylation profile of 265 out of 292 unique N-termini were identified in both control and *san* mutant embryos (Van Damme and Kris Gevaert; unpublished data).

The COFRADIC analysis allowed the identification of 18 proteins whose *in vivo* N^{α}-acetylation was reduced in *san* mutant embryos (fig. 2). Significant variations in N^{α}-acetylation between control and *san* mutant embryos were arbitrarily set at 10% difference. Nevertheless some of the N-termini affected to a lesser extent (between >5% and 10% difference in the extent of N^{α}-acetylation)

were also considered as possible targets of dSan/dNaa50 due to known mitotic functions. Such targets were included in the substrate list (table 2).

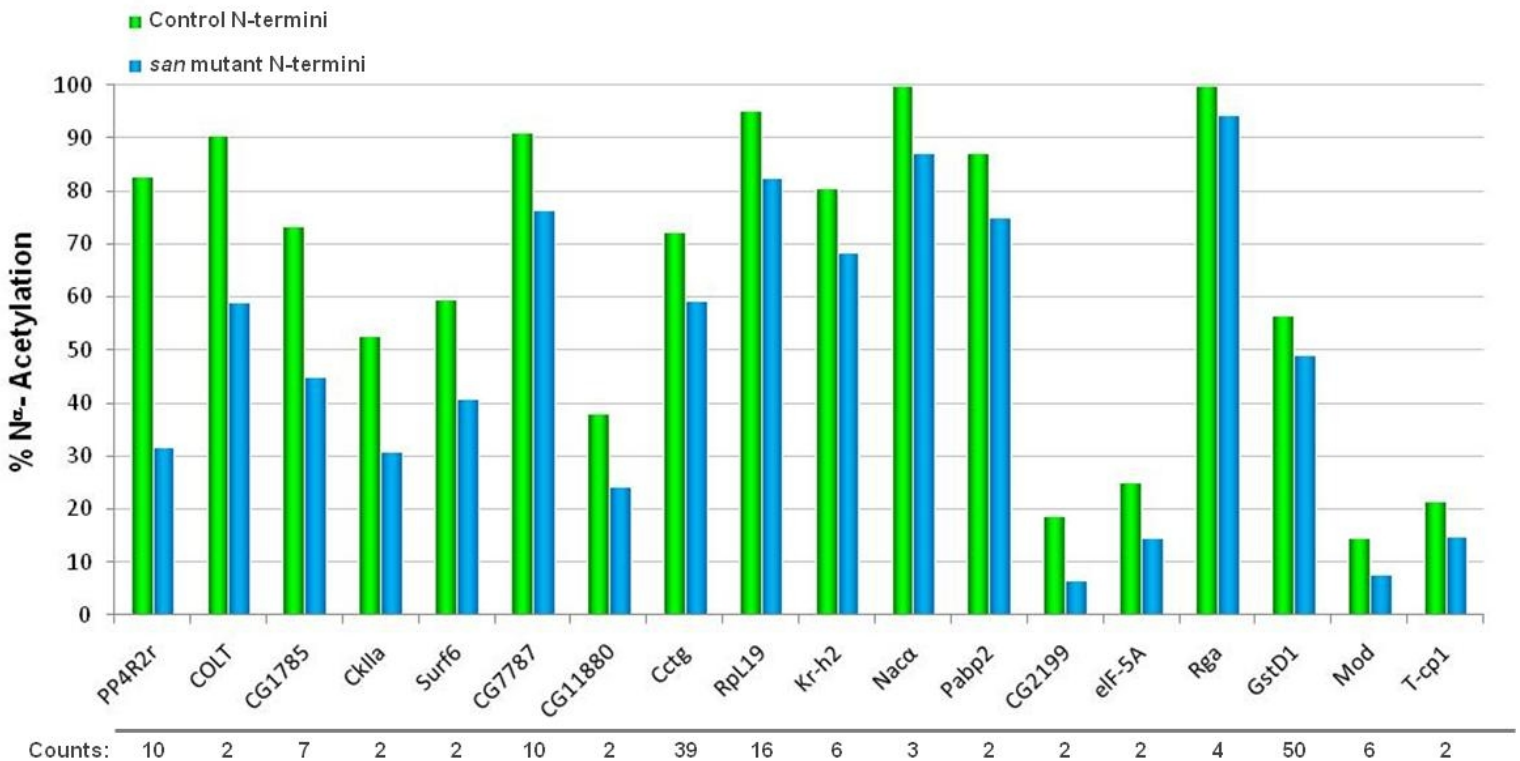

Figure 2: Plot representing proportion of N^{α}-acetylation in control and *san* mutant embryos. Green and blue bars represent control and *san* mutant embryos, respectively. Numbers below the plot correspond to the number of counts done for each peptide.

Identified N-termini	Ac aa	Coding gene	Fly base symbol	%Ac wild-type	%Ac *san* mutant	% ΔAc
VTMENSDEIMQILER	VT	CG2890	PPP4R2r	82,8	31,8	**51,0**
TTTENVSTER	TT	CG3057	COLT	90,6	59,0	**31,6**
TAVEPATKKKR	TA	CG1785	-	73,4	45,1	**28,3**
TLPSAAR	TL	CG17520	CKIIα	52,7	31,0	**21,7**
TQAEIVKCLR	TQ	CG4510	Surf6	59,6	40,9	**18,7**
TEEADFSEQITDGKNKSNVR	TE	CG7787	-	91,0	76,4	**14,60**
TESVELMNKYGEPLR	TE	CG11880	-	38,0	24,4	**13,6**
MFGGQQPILVLSQNTKR	MF	CG8977	Cctγ	72,2	59,4	**12,90**
SSLKLQKR	SS	CG2746	RpL19	95,1	82,5	**12,6**
SAPTDQPPR	SA	CG9159	Kr-h2	80,6	68,4	**12,2**
TEIKSEAAPSTSAEAKPEDVR	TE	CG8759	Nacα	100,0	87,2	**12,8**
MQIDPELEAIKAR	MQ	CG2163	Pabp2	87,3	75,0	**12,4**
TKVQKEVR	TK	CG2199	-	18,8	6,5	**12,3**
SGASTTYPMQCSALR	SG	CG3186	eIF-5ª	25,2	14,6	**10,5**
ANLNFQQPPR	AN	CG2161	Rga	100,0	94,5	**5,5**
VDFYYLPGSSPCR	VD	CG10045	GstD1	56,5	49,1	**7,5**
AQKKAVTVKGKKATNGEEKPLAKR	AQ	CG2050	Mod	14,6	7,6	**7,0**
TLASPLSIAGTR	TL	CG5374	T-cp1	21,4	15,0	**6,4**

Table 2: Summary of N$^{\alpha}$-acetylation in control and *san* mutant embryos. Reduction of *in vivo* protein N$^{\alpha}$-acetylation in control and *san* mutant embryos. Yellow cells show N$^{\alpha}$-acetylated peptides at position 1 or 2 of the annotated protein sequence at SwissProt database, whereas pink cells show peptides N$^{\alpha}$-acetylated at positions beyond position two of the annotated protein sequence. (AC aa) Column displaying two residues of each peptide in which the first residue was detected as being acetylated one.

3.2. Tissue culture cells depleted for dSan/dNaa50 showed chromosome segregation defects

We used RNAi in Dmel2 cells to analyze the consequence of dSan/dNaa50-depletion in tissue culture. Cells treated during 93h with dsRNA for dSan/dNaa50 demonstrated a clear decrease in dSan/dNaa50 protein levels (fig. 3).

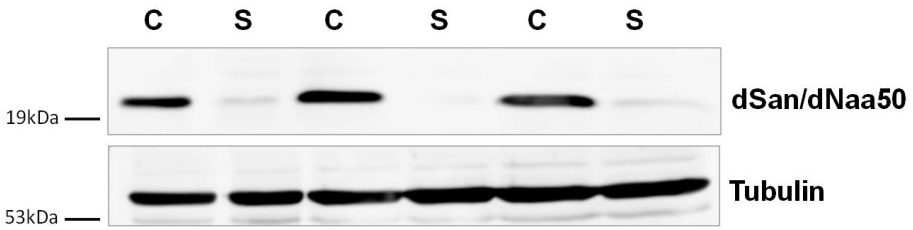

Figure 3: Decrease of dSan/dNaa50 protein levels after RNAi treatment. Dmel2 cells showed a decrease of dSan/dNaa50 protein. Tubulin was used as loading control. C, control RNAi; S, dSan/dNaa50 RNAi.

While the control exhibited mostly normal metaphase and anaphase cells (fig. 4 A,B,C), dSan/dNaa50-depleted cells showed a moderate increase in chromosome congression defects during metaphase (fig. 4 D,G). 28% of dSan/dNaa50-depleted cells in metaphase displayed a visible metaphase plate, but still with DNA out of the equator (vs. 5% in control cells) (fig. 5 A). 10,9% of dSan/dNaa50-depleted cells in metaphase were highly abnormal with DNA scattered along the mitotic spindle (vs. 1,7% in control cells) (fig. 5 A). Also, dSan/dNaa50-depleted cells, showed a mitotic index increase (fig. 5 B). There was a 2-fold increase in dSan/dNaa50-RNAi cells positive for histone H3 phosphorilated on serine 10 (PH3) (a marker for mitosis) (fig. 5 B), suggesting a cell cycle arrest during metaphase.

During the metaphase to anaphase transition, sister chromatids lose cohesion and segregate equally from the metaphase plate to both poles of the mitotic spindle (fig. 4 B, C). dSan/dNaa50-depleted cells did not segregate sister chromatids equally to the spindle poles, showing segregation defects that included lagging chromosomes and chromosome bridges (fig. 4 E, F, H and I). dSan/dNaa50-depleted cells showed segregation defects in 67,8% of cells undergoing anaphase A (early anaphase)(vs. 13,3% in control cells) and 49,7% of cells undergoing anaphases B (late anaphase)(vs. 6% in control cells) (fig. 5 A). Both control and dSan/dNaa50-depleted cells arrested mitosis in response to incubation with the microtubule (MT) depolymerization agent colchicine (fig. 5 C). This suggested dSan/dNaa50 depleted cells had an active spindle assembly checkpoint (SAC). Depleting dSan/dNaa50 in *Drosophila* cultured cells caused chromosome segregation defects identical to the ones observed *in vivo* in *san* mutant embryos (Pimenta-Marques et al., 2008). Similar to what was observed *in vivo*, dSan/dNaa50-depleted cells transiently arrested in mitosis, most likely in a SAC-dependent manner.

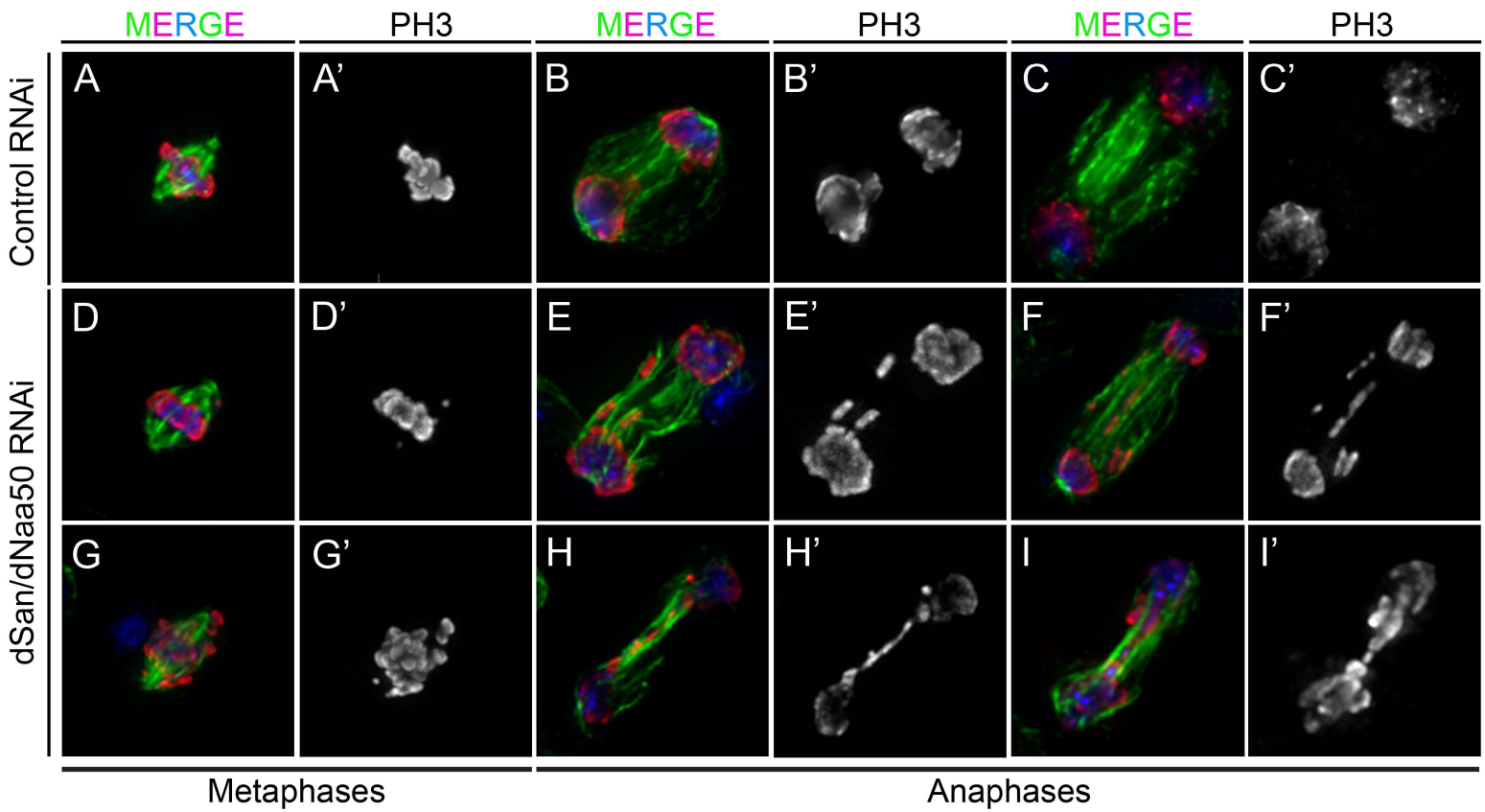
MERGE
PH3
MERGE
PH3
MERGE
PH3
Control RNAi
dSan/dNaa50 RNAi
A
A'
B
B'
C
C'
D
D'
E
E'
F
F'
G
G'
H
H'
I
I'
Metaphases
Anaphases

Figure 4

Figure 4: dSan/dNaa50 is required for proper metaphase chromosome alignment and chromosome segregation during anaphase. dSan/dNaa50-depleted cells displayed chromosome congression defects during metaphase. Metaphase congression defects were either classified into mildly or highly abnormal. (A) Control metaphase. (D) Cell representative of a mildly abnormal metaphase, with congression of the majority of chromosomes but where some chromosomes are still not aligned at the metaphase equator. (G) Cell representative of a highly abnormal metaphase showing chromosomes scattered along the mitotic spindle instead of being aligned at the spindle equator. dSan/dNaa50-depleted cells showed chromosome segregation defects which included lagging chromosomes and chromosome bridges. (B, C) Control cells undergoing anaphase B. (E, F) dSan/dNaa50-depleted cells undergoing anaphase B with lagging chromosomes. (H, I) dSan/dNaa50-depleted cells undergoing anaphase B displaying extensive chromosome bridges. Histone 3 phosphorylated on Serine 10 (red), α-tubulin (green) and DNA (blue). Gray pictures illustrate Histone 3 phosphorylated on Serine 10.

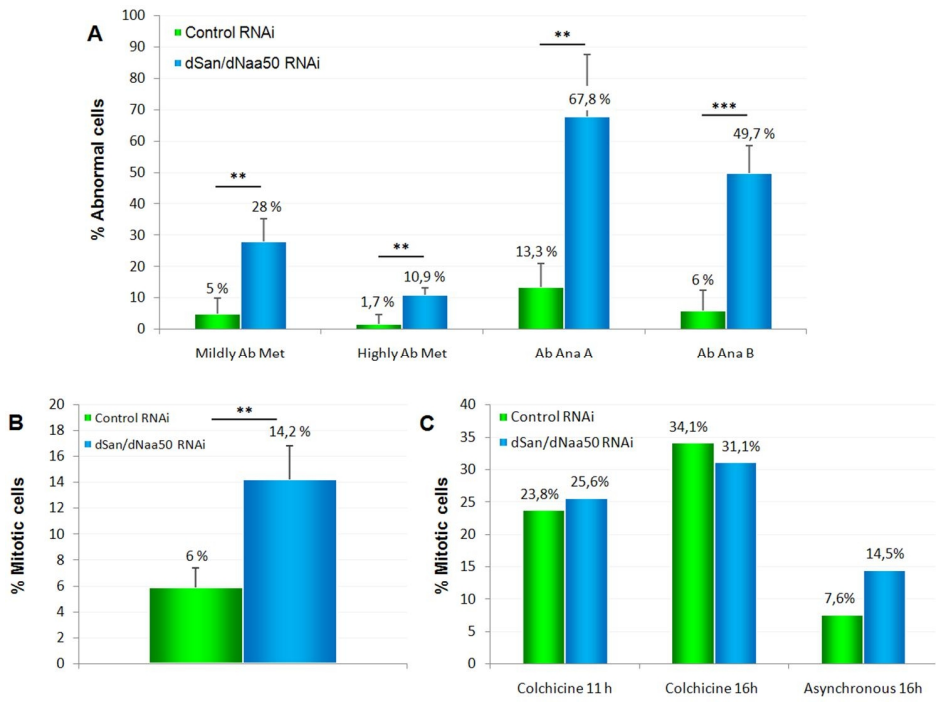

Figure 5: dSan/dNaa50 is required for proper chromosome alignment in metaphase and chromosome segregation during anaphase. (A) Quantification of mitotic defects. Percentage of cells undergoing metaphase with mildly and highly

abnormal chromosome congression defects (M Ab Met and H Ab Met) and anaphases A and B with lagging chromosomes or chromosome bridges (Ab Ana A and Ab Ana B) in control and dSan/dNaa50 dsRNA-treated cells. Quantification: Mildly abnormal metaphases in 28% ± 7,2 in dSan/dNaa50-depleted cells versus 5% ± 5 in control cells. 10,9% ± 2,4 of dSan/dNaa50-depleted cells exhibited highly abnormal metaphases versus 1,7% ± 2,9 in control cells. dSan/dNaa50-depleted cells, n=64 metaphases; control cells, n=61 metaphases. dSan/dNaa50-depleted cells exhibited 67,8% ± 19,7 abnormal anaphases A (n=60) versus 13,3% ± 7,6 in control cells (n=60). dSan/dNaa50 depleted cells exhibited 49,7% ± 9 abnormal anaphases B (n=65) versus 6% ± 6,6 in control cells (n=63) (**p<0,01; ***p<0,001 Student's test). **(B)** Mitotic index in dSan/dNaa50-depleted cells and control cells. dSan/dNaa50-depleted cells showed a mitotic index of 14,2% ± 2,6 (n=1326) against 6% ± 1,5 in control cells (n=1086) (**p<0,01 Student's test). **(C)** Control and dSan/dNaa50-depleted cells were incubated with 25μM colchicine, and the mitotic index was recorded after 11 and 16 h colchicine treatment. (Colchicine 11h: Control RNAi n=501, dSan/dNaa50 RNAi n=523; Colchicine 16h: Control RNAi n=504, dSan/dNaa50 RNAi n=582; Asynchronous cells: Control RNAi n=525, dSan/dNaa50 RNAi n=565).

3.3. Cctγ and dSan/dNaa50-depleted cells have similar chromosome segregation defects

In vivo analysis of dSan/dNaa50 targets allowed the identification of 18 putative substrates of dSan/dNaa50. From these, 5 proteins (table 3) were chosen to be tested as mitotic targets of dSan/dNaa50. These proteins were selected from the initial 18 taking into account two main criteria: a) proteins with an already described mitotic function and/or positive hits in a previous published screen for mitotic spindle morphology (Goshima et al., 2007); b) proteins for which the COFRADIC analysis displayed a large reduction in N^{α}-acetylation.

PPP4R2r showed the highest decrease in N^{α}-acetylation in dSan/dNaa50 mutants. Importantly, PPP4R2r is required for neuroblast asymmetric divisions by mediating the correct localization of the Miranda protein complex (Sousa-Nunes et al., 2009). The

protein encoded by the gene CG1785 also showed a large reduction in N^{α}-acetylation in *san* mutants (fig. 2 and table 2). CG1785 shared a high degree of similarity with the human protein Glioma tumor-suppressor candidate region gene 2 (GLTSCR2) and several results suggested it might be a tumor suppressor (Kim et al., 2008; Okahara et al., 2006; Smith et al., 2000). Casein kinase II α subunit (CkIIα) is the catalytic subunit of the casein kinase II (CKII) tetrameric complex which was shown to *in vitro* modulate topoisomerase II (TopoII) activity by phosphorilation (Ackerman et al., 1985). Cctγ is a subunit of the conserved chaperonin containing TCP-1 (CCT) complex that functioned as a molecular chaperone in the eukaryotic cytosol. The chaperone activity of this complex has been shown to be associated with tubulin, actin and activators of the APC/C, cdc20 and cdh1 (Camasses et al., 2003). Interestingly Cctγ was a positive hit in a screen performed to identify regulators of the mitotic spindle assembly (Goshima et al., 2007). RpL19 is a 60S ribosomal protein L19, involved in translational elongation. This protein was recently suggested to be involved in centrosome duplication (Muller et al., 2010), and was previously associated with mitotic spindle morphology (Goshima et al., 2007).

Candidate proteins	*Dmel.* N-terminus	Human N-terminus	Known mitotic function
PPP4R2r	M**VT**MENSDEIMQILER	MDVERLQEALKDFEK	**Yes**
CG1785	M**TA**VEPATKKKR	MAAGGSGVGGKRSSK	**Yes**
CkIIα	M**TL**PSAAR	MSGPVPSRARVYTDV	**Yes**
Cctγ	**MF**GGQQPILVLSQNTKR	MMGHRPVLVLSQNTK	**Yes**
RpL19	M**SS**LKLQKR	MSMLRLQKRLASSVL	**Yes**

Table 3: Putative substrates of dSan/dNaa50 selected for further analysis. Column 1 contains the corresponding proteins to the N-termini identified by the COFRADIC procedure in column 2. In all targets with exception of Cctγ the initial methionine was cleaved by aminopeptidases prior to N^{α}-acetylation. Blue residues highlight amino acids at the initial start position 1 and 2 in the N-termini identified by

MS in COFRADIC analysis. Column 3 contains the N-termini of the corresponding homologous proteins in humans.

Substrates of dSan/dNaa50 selected for further analysis were initially tested in *Drosophila* cell cultures by RNAi. RpL19-depleted cells revealed pleiotropic defects. After 72 h RNAi treatment there were very few cells suggesting a strong cell cycle arrest and further cell death (data not shown). Depletion of PPP4R2r and CG1785 had no effect on mitosis and these cells presented a mitotic index comparable with control cells (fig. 6B) without major defects on chromosome alignment during metaphase and chromosome segregation during anaphase (fig. 7A and table 4). 35% of CkIIα-depleted cells showed chromosome segregation defects during anaphase A (vs. 13,3% in control cells) and 16,3% during anaphase B (vs. 6% in control cells) (fig. 7A and table 4). CkIIα depletion had however no effect on the mitotic index (fig. 7B).

Cctγ-depleted cells showed striking chromosome segregation defects with 36% of cells in anaphase A and 59% in anaphase B displaying lagging chromosomes and/or chromosome bridges (table 4, fig. 6A and fig 7B, C and E). Moreover, Cctγ-depleted cells showed a major increase in the mitotic index (fig. 6B). Interestingly, the chromosome segregation defects observed in Cctγ and dSan/dNaa50-depleted cells were very similar (fig. 6 E, F). These data suggest that Cctγ is the best candidate as being a mitotic target of dSan/dNaa50, and therefore being involved in the mitotic phenotypes observed in dSan/dNaa50-depleted cells.

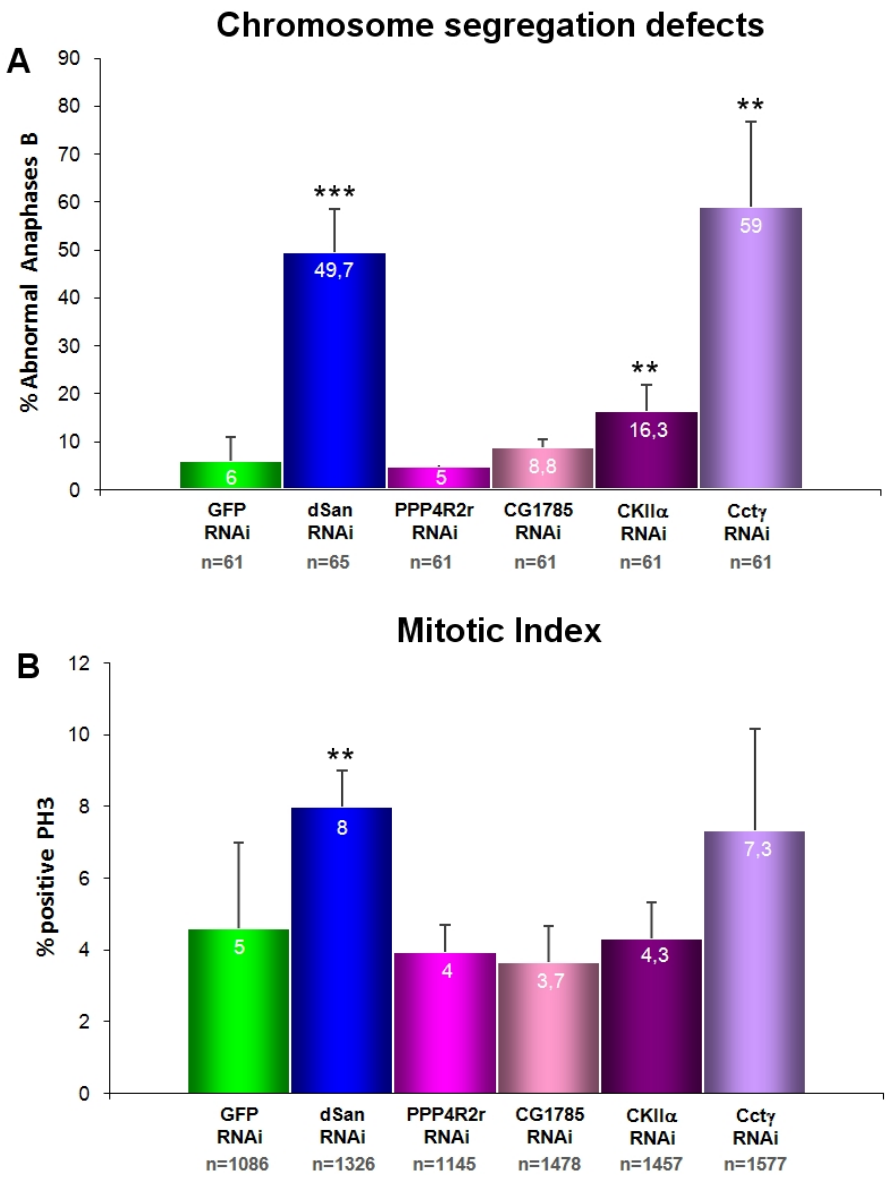

Figure 6: Cctγ is required for chromosome segregation during anaphase and Cctγ-depleted cells arrest transiently in mitosis. (A) Percentage of abnormal anaphases B for mitotic targets of dSan/dNaa50. **(B)** Percentage of cells positive for histone 3 phosphorylated on Serine 10 (PH3).

RNAi	Mildly abnormal Metaphases (%)	Highly abnormal Metaphases (%)	Abnormal Anaphases A (%)	Abnormal Anaphases B (%)
GFP	4,92 ± 5	1,7 ± 2,9	13,3 ± 7,6	6 ± 6,6
dSan	28 ± 7,2	10,9 ± 2,4	67,8 ± 19,7	49,7 ± 9
PPP4R2r	8,3 ± 5,8	0	21,2 ± 9,9	5 ± 0,1
CG1785	0	0	7,7 ± 2,5	8,84 ± 1,6
CKIIα	15,7 ± 8,1	5,7 ± 6	35 ± 5	16,3 ± 5,5
Cctγ	11,4 ± 5,6	1,6 ± 2,7	36,7 ± 14,4	59 ± 17,7

Table 4: Percentage of mitotic defects in cells depleted for candidate substrates of dSan/dNaa50. For each RNAi experiment, between 60-64 cells in metaphase, 60-63 in anaphase A and 61-65 in anaphase B were counted.

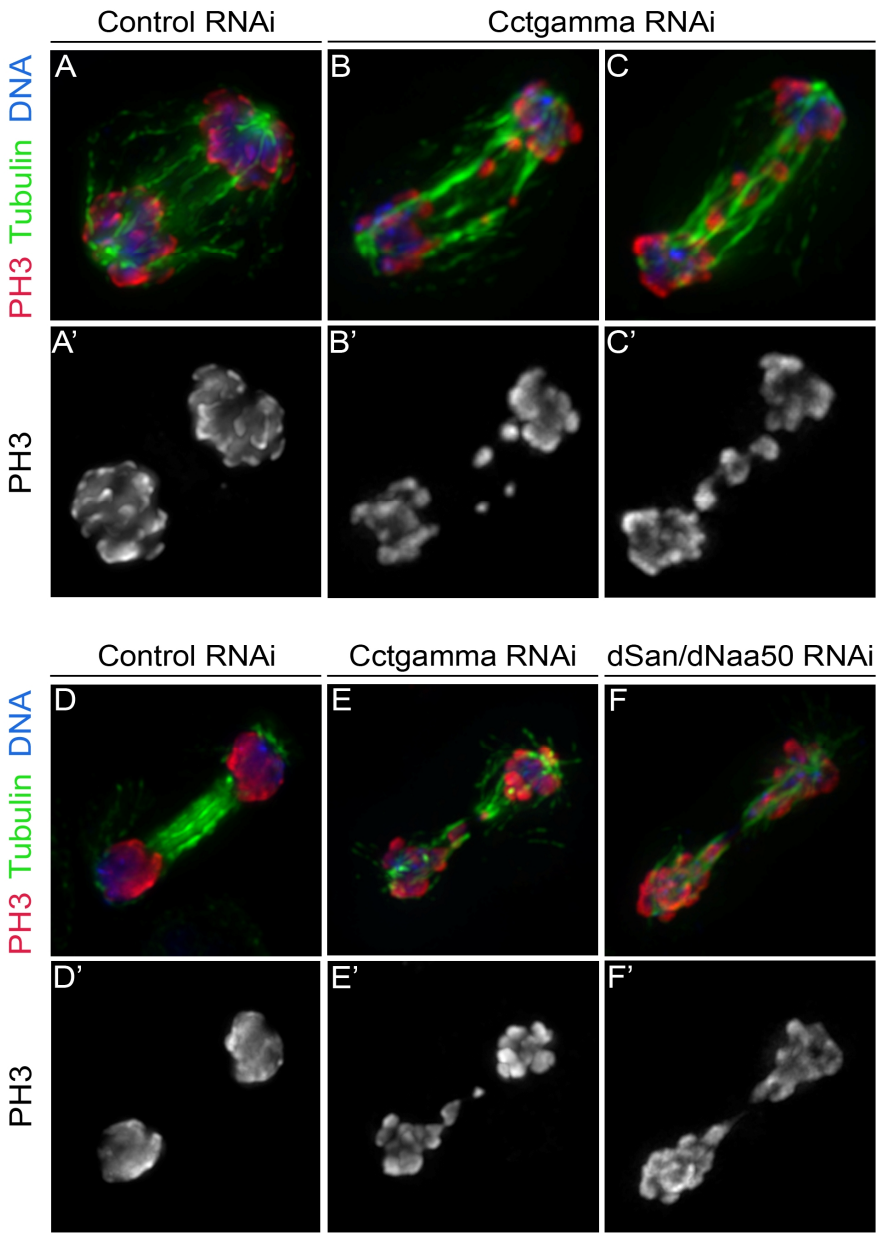

Figure 7: Cctγ and dSan/dNaa50 depleted cells show identical chromosome segregation defects (A-C) Anaphase B. (D-F) Telophase. (A) Anaphase B in control cells with equal distribution of DNA to both poles of the mitotic spindle. (B, C) Cctγ-depleted cells undergoing anaphase B with lagging chromosomes and unequal distribution of DNA content to mitotic spindle poles. (D) Control late anaphase/ telophase. (E) Cctγ-depleted cells showed late anaphases/telophases with stretched

DNA at the spindle equator region, similarly to dSan/dNaa50-depleted cells (F). (PH3) Histone 3 phosphorylated on Serine 10. (Tubulin) α-tubulin immunostaining. (DNA) DAPI staining.

3.4. Looking for mitotic substrates of dSan/dNaa50 using a N-terminal substrate consensus

Recent *in vitro* studies showed hSan/hNaa50 preferentially acetylates N-termini with the consensus MLGP- and MLDP- (Evjenth et al., 2009). Similar to *Drosophila* San/Naa50p, hSan/hNaa50 associated with hNaa10 (hARD1) and hNaa15 (hNATH). hSan/hNaa50-depleted HeLa cells showed loss of the cohesin SMC1 at the centromere (Hou et al., 2007), similar to what was previously observed in *Drosophila* neuroblasts (Williams et al., 2003). We expected the mitotic substrates of San/Naa50p in *Drosophila* and humans to be conserved, which implied a conserved N-terminus. Taking this into account, hSan/hNaa50 N-terminus substrate consensus was used to search in *Drosophila* for candidate substrates of San/Naa50p. Such analysis was performed using the 4 amino acids of the consensus MLGP- and MLDP-. Analysis of proteins with such consensus was done using the available database from ExPasy: ScanProsite (http://expasy.org/tools/ scanprosite/). This analysis failed to retrieve any potentially interesting candidate mitotic proteins.

3.5. Cohesin Drad1/Scc1 shares a well conserved N-terminus within higher eukaryotes

Drosophila cultured cells depleted for the cohesin Drad21/Scc1 showed loss of sister chromatid cohesion (Vass et al., 2003). Inhibition of Drad21/Scc1 in *Drosophila* embryos caused chromosome segregation defects, which included chromosome bridges similar to

san mutant embryos (Oliveira et al.; Pimenta-Marques et al., 2008; Vass et al., 2003). *Drosophila* mutants for subunits of the condensing complex such as *barren* and *gluon* showed defects in chromosome segregation, which also included extensive chromosome bridges (Bhat et al., 1996; Steffensen et al., 2001). Moreover, inhibition of TopoII, an interactor of the condensing complex, also lead to chromosome bridges during *Drosophila* syncytial blastoderm (Buchenau et al., 1993).

Both *Drosophila san* mutants and hSan/hNaa50-depleted cells showed chromosome segregation defects and mislocalization of cohesin subunits at the centromeric region (Hou et al., 2007; Pimenta-Marques et al., 2008; Williams et al., 2003).

Since mutants or inhibition of the cohesin and condensing complexes shared phenotypic similarities with *san* mutants, the N-termini of these proteins were analyzed from yeast to humans and compared to the *in vitro* substrate consensus of hSan/hNaa50 (fig. 8). Drad21/Scc1 displayed conservation in the first 3 amino acids off all organisms analyzed and the N-terminus shared hydrophobic properties compatible with the *in vitro* substrate consensus reported for hSan/hNaa50 (Evjenth et al., 2009). Nevertheless we failed to detect any change in total protein levels of Drad21/Scc1 in *san* mutant embryos by western blot analysis (fig. 9).

Cohesin Complex	SMC1	SMC3	Rad21/Scc1	Scc3/SA1	SA2
D.mel		MATA			
	MTEE	MHIK	MFYE	MMAR	MSDI
H.sap	MGFL	MYIK	MFYA	MITS	MIAA
M.mus	MGFL	MYIK	MFYA	MITS	MIAA
D.rer	MGYL	MYIK	MFYA	MITS	MIAA
S.p	MGRL	MYIT	MFYS	MTAV	MTAV
S.c	MGRL	MYIK	MVTE	MSES	MSES
	*	*	*.	*	*

Condensin Complex I	SMC2	SMC4	CAP-H	CAP-G	CAP-D2
D.mel	MYVK	MQKA	MTLP	MAKP	MEES
H.sap	MHIK	MPRK	MGPP	MGAE	MAPQ
M.mus	MYVK	MRRK	MNSS	MAAQ	MSPH
D.rer	MYIK	MPVK	MSAF	MPGD	MSWD
S.p	MKIE	MSDK	MKRA	MSCI	MSLD
S.c	MKVE	MSDS	MKRA	MQDP	MSGF
	* ::	*	*	*	*

Condensin Complex II	CAP-D3	CAP-H2
D.mel	MSDF	MSDD
	MRQT	MERI
H.sap	MVAL	MEDV
M.mus	MALQ	MEDV
D.rer	-	MWRC
		MDSV
S.p	-	-
S.c	-	-

Candidate proteins	Topo II
D.mel	MENG
H.sap	MAKS
M.mus	MAKS
D.rer	MSNG
S.p	MSID
S.c	MSTE
	*

Figure 8: N-terminus alignments of subunits of the cohesin and condensing complexes. Both condensin complex I and II were analyzed. Topoisomerase II is known to interact with the condensin complex and promote chromosome condensation (Bhat et al., 1996; Uemura et al., 1987). (*) residues or nucleotides in that column are identical in all sequences in the alignment. (:) Conserved substitutions have been observed, according to the color table above. (.) Semi-conserved substitutions were observed. Red corresponds to small aa (small+ hydrophobic (incl.aromatic -Y)). Blue correspond to acidic aa. Magenta corresponds to basic residues. Green corresponds to Hydroxyl + Amine + Basic – Q residues. Gray shaded N-termini correspond to additional isoforms which contain different N-terminus.

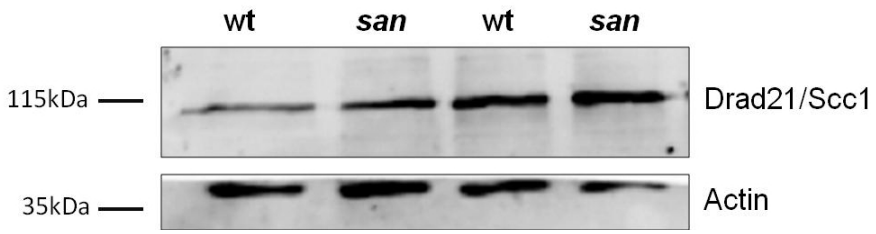

Figure 9: Drad21/Scc1 protein levels were not affected in *san* mutant embryos. Actin was used as loading control. Protein extracts from wild-type (wt) and *(san)* san^4 mutant GLC embryos.

4. Discussion

4.1. Is Cctγ a mitotic substrate of dSan/dNaa50?

dSan/dNaa50 N^{α}-terminal acetyltransferase is required for chromosome segregation during anaphase (Hou et al., 2007; Pimenta-Marques et al., 2008; Williams et al., 2003). In contrast to other NATs whose mutants showed pleiotropic phenotypes (e.g., mutants of the gene coding for dNaa10 (dArd1) (Wang et al., 2010) *san* mutant phenotypes were comparatively more specific. Given this we hypothesized that only a small subset of proteins should have their function impaired in *san* mutants. In order to define the substrate consensus of *Drosophila* San/Naa50p and identify mitotic substrates of this NAT, we took advantage of COFRADIC and liquid chromatography-tandem mass spectrometry LC-MS/MS for *in vivo* identification of proteins whose N^{α}-acetylation was reduced in *san* mutant embryos.

From the 399 unique *Drosophila* proteins identified in our analysis, 292 were present in both control and *san* mutant embryo samples. The annotated *Drosophila* proteome is over 13000 proteins (Adams et al., 2000) and recently nearly 2000 new transcribed regions were identified in the *Drosophila* transcriptome (Graveley et al., 2010). The fact that more than 70% of the identified proteins were present in both samples suggested a strong experimental bias, possibly to highly abundant and soluble proteins. Although this bias was potentially problematic, as highly abundant proteins were likely to be involved in housekeeping functions, we rationalized our dataset would nevertheless be useful to identify proteins whose N^{α}-acetylation was impaired in *san* mutant embryos and define an *in vivo* N-terminal substrate consensus for dSan/dNaa50.

From this work we identified 18 proteins (table 2) whose N^{α}-acetylation was significantly reduced in *san* mutant embryos. Interestingly we failed to identify any protein that had completely lost acetylation in *san* mutant embryos, which suggested dSan/dNaa50 was likely to be partially redundant with one or more NATs *in vivo*. The majority of the identified 18 proteins showed initial methionine (iMet) cleavage and acetylation of Thr-, Val-, Ser-, or Ala- residues. Since the NatA complex was already known to acetylate these residues after iMet cleavage (Arnesen et al., 2005; Arnesen et al., 2009; Mullen et al., 1989; Polevoda et al., 1999) and *Drosophila* and human San/Naa50p was known to be partially associated with this complex (Hou et al., 2007; Williams et al., 2003), we concluded the NatA activity was being partially impaired in *san* mutant embryos. Nevertheless, the effect on NatA activity had to be only partial as the phenotypes associated after depletion of NatA subunits were significantly more pleotropic than the ones observed after dSan/dNaa50-depletion. For example, *Drosophila* mutants for the NatA catalytic subunit dNaa10 showed severe oogenesis defects (Wang et al., 2010), whereas loss of function alleles of *san* showed no detectable defects during oogenesis and displayed normal egg-laying (Pimenta-Marques et al., 2008) (Chapter III). Moreover, cohesion defects were observed in HeLa cells depleted for hSan/hNaa50, but not in cells depleted for either hNaa10 or hNaa15, suggesting the NatA complex is not involved in sister chromatid cohesion (Hou et al., 2007). Although it was possible *san* mutant mitotic phenotypes were mediated by a partial reduction of NatA activity, we did not favor this hypothesis, as the observed phenotypes were significantly distinct.

hNaa10 was proposed to be involved in cell division through facilitating reformation of the midbody in the late phase of cell mitosis, and stabilization of MTs. Human cells showed specific localization of hNaa10 at the midbody region, and hNaa10-depleted cells showed

reduced levels of acetylated α-tubulin at this region (Shen et al., 2009). One possibility could be *san* mutants affecting the proposed mitotic function of dNaa10. However, in contrast to hNaa10-depleted cells, we were not able to detect any significant difference in acetylated α-tubulin at midbody region between WT and dSan/dNaa10-depleted cells (data not shown).

hSan/hNaa50 was shown to preferentially acetylate *in vitro* and *in vivo* N-termini without iMet cleavage (Evjenth et al., 2009) (Van Damme and Kris Gevaert; unpublished data). Of the identified proteins whose N^{α}-acetylation was reduced in *san* mutant embryos, Cctγ and Pabp2 were the only ones to be acetylated at the iMet (table 2).

Analysis of the best candidates by RNAi in Dmel2 cells revealed that cells depleted for Cctγ showed chromosome segregation defects identical to the ones observed in dSan/dNaa50-depleted cells, including lagging chromosomes and chromosome bridges. This suggested Cctγ was a good candidate as a mitotic substrate of dSan/dNaa50. Interestingly, Cctγ N-terminus was, among all 18 candidates, the one that fulfilled the requirements of a previously published *in vitro* substrate consensus for hSan/hNaa50 (Evjenth et al., 2009). This work showed that small and hydrophobic N-termini such as ML**G**P- or negatively charged ML**D**P-, are good *in vitro* substrates of hSan/hNaa50. Cctγ N-terminal sequence (MFGG-) included the highly hydrophobic phenylanine amino acid at position 2 and two small glycin residues.

Cctγ is a subunit of the conserved CCT complex that acts as a molecular chaperone within the eukaryotic cytosol (Brackley and Grantham, 2009). Work done in budding yeast showed that Cctγ promotes the activation of the APC/C complex through the generation of active Cdc20 and Cdh1 (Camasses et al., 2003). Activation of the

APC/C by Ccd20 at the metaphase to anaphase transition is essential for sister chromatid separation and to initiate inactivation of cyclin-dependent kinases (Cdks), namely cyclin-dependent kinase 1 (Cdk1) (Sullivan and Morgan, 2007). During late anaphase, Cdc20 is replaced by Cdh1, which sustains APC/C activity during mitotic exit (Fang et al., 1998; Jaspersen et al., 1999; Kramer et al., 2000; Visintin et al., 1998; Zachariae et al., 1998). We expected reduced levels of Cctγ activity would be associated with a reduced activation of the APC/C complex. As a result, Cdk1 would not be properly inhibited for effective mitotic exit.

Recent data has associated high levels of Cdk1 in *Drosophila* embryos with abnormal syncytial nuclear divisions (Li et al., 2010; Oliveira et al., 2010). Xeroderma pigmentosum group D (Xpd) is known to negatively regulate the cell cycle function of Cyclin-dependent kinase 7 (Cdk7). Cdk7 regulates cell cycle progression as the major Cdk-activating kinase (CAK) activity. *Drosophila xpd* mutant embryos showed an abnormal anaphase inactivation of Cdk1 (Li et al., 2010). Interestingly, *xpd* and *san* mutant embryos showed similar chromosome segregation defects (Li et al.; Pimenta-Marques et al., 2008). Furthermore, recent data showed that the correct segregation of chromosomes required not only degradation of cohesin, but also effective degradation of Cdk1 (Oliveira et al., 2010). If we further observe Cctγ activity is dSan/dNaa50-acetylation dependent, we hypothesize that cells depleted for dSan/dNaa50 function did not have the required amount of functional Cctγ to correctly induce the APC/C activation through Cdc20 and Cdh1. Since *san* mutant neuroblasts showed mislocalisation of Drad21/Scc1 at the centromeric region (Williams et al., 2003), we speculated there was sufficient activation of the APC/C to induce cohesin degradation, but not enough to induce complete degradation of Cdk1.

To test if Cctγ dSan/dNaa50-dependent acetylation is required for proper metaphase to anaphase transition, future work will focus on addressing the following questions:

1) Can high levels of Cctγ suppress dSan/dNaa50-depleted cells?

N^{α}-acetylation has been associated to protein stability (Jornvall, 1975; Rubenstein and Deuchler, 1979). One possibility is the mitotic phenotypes observed in dSan/dNaa50-depleted cells being mediated by destabilization of total levels of Cctγ due to reduced levels of N^{α}-acetylation. If that is the case, we would expect to suppress the mitotic defects observed in dSan/dNaa50-depleted cells by expressing high levels of Cctγ. If indeed we observe a suppression of the phenotype we will proceed with the following set of experiments described below.

2) Is Cctγ function dependent on N^{α}-terminus acetylation?

We will first investigate if indeed Cctγ N^{α}-acetylation is required for its role in mitosis. To do that we will take advantage of the (X)PX role which states that a protein with the sequence X_1-Pro-X_3 or Pro-X_2 at its very amino-terminus remains unacetylated under all circumstances (X being Met or any small amino acid that allows iMet removal by aminopeptidases) (Goetze et al., 2009). Previous studies in *Drosophila* indeed demonstrated that proteins with a proline residue at the N-terminus position 1 or 2 had an *in vitro* and *in vivo* acetylation inhibitory effect (Goetze et al., 2009). We will therefore modify the M**F**GG- wild-type Cctγ N-terminus to a mutated M**P**GG- form and test its relevance for the proteins function. If our hypothesis is correct we expect to rescue Cctγ-depleted cells and homozygous mutants with a wild-type N-terminus Cctγ form, but not with a M**P**GG- mutated form. These experiments will be performed *in vitro* and *in vivo* as described in the study mentioned above.

3) Is Cctγ N^{α}-acetylation dependant on dSan/dNaa50?

If N^{α}-acetylation of Cctγ turns out to be required for its mitotic function, we will further investigate if this acetylation event is dSan/dNaa50-dependent. If that is the case we expect to rescue dSan/dNaa50-depleted cells and homozygous *san* mutants with a M**A**GG-, M**E**GG- or M**I**GG- N-terminus Cctγ form amenable of being acetylated by the *Drosophila* NatA, NatB and NatC complexes, respectively.

If our hypothesis is correct, we expect Cdk1 to not be effectively inhibited in dSan/dNaa50-depleted cells during the metaphase to anaphase transition. Cdk1 is inhibited through degredation of cyclin B by the APC/C. We will therefore perform immunostainings for these mitotic players to further check if they are still active during anaphase.

4) Live imaging analysis of dSan/dNaa50-depleted cells

Additional studies will involve a detailed live-cell imaging analysis of the mitotic phenotypes observed after dSan/dNaa50 depletion. These experiments will allow us to have better insights into the mitotic phenotypes of dSan/dNaa50 and narrow the molecular pathways in which dSan/dNaa50 might be involved.

4.2. Is Drad21/Scc1 a mitotic substrate of dSan/dNaa50?

In vitro human San/Naa50p preferentially acetylated the Met residue from N-terminus that contained hydrophobic amino acids (Evjenth et al., 2009). *Drosophila* mutants or embryos inhibited for cohesin and condensing subunits showed chromosome segregation defects similar to *san* mutant embryos (Bhat et al., 1996; Dej et al., 2004; Oliveira et al., 2010; Vass et al., 2003). Therefore, these proteins were good candidates to be acetylated by dSan/dNaa50. Since the mitotic function of San/Naa50p was apparently conserved from *Drosophila* to humans, we expected the mitotic targets of

dSan/dNaa50 to show some degree of conservation within their N-terminal sequence. Consistent with this possibility, Drad21/dScc1 presented a high degree of conservation and the N-terminus shared hydrophobic properties compatible with the *in vitro* consensus of hSan/hNaa50. Nevertheless, since we failed to detect any change of total Drad21/Scc1 levels in *san* mutant embryos, it is possible dSan/dNaa50-dependent acetylation of the cohesin subunit is important for its correct localization at the centromeric region.

Most of metazoan cells oscillate their chromosomes at the metaphase plate for many minutes until anaphase initiates. As a result of bipolar spindle-pulling forces, these movements are accompanied by changes in the distance between sister kinetochores (Mellone and Allshire, 2003), commonly referred to as “centromere breathing”. Studies done in yeast suggested there are two pools of cohesin, cohesin loaded before DNA replication and cohesin loaded after DNA replication (Lengronne et al., 2006). The first pool which establishes sister chromatid cohesion disappears during “breathing”, while the second pool is partially retained (Ocampo-Hafalla et al., 2007). Interestingly as sisters re-associate after transient separation, cohesin is reloaded at the centromere in a manner independent of the canonical cohesin loader Scc2/Scc4. Additionally, this work suggested sister chromatid cohesion is likely to be re-established in a manner dependent, to some extent, on Eco1 (Ocampo-Hafalla et al., 2007). Interestingly, Deco acetyltransferase, the *Drosophila* homologue of yeast Eco1, was identified in the same genetic screen as dSan/dNaa50. Both *san* and *deco* mutant neuroblasts exhibited mislocalization of the cohesin subunit Drad21/Scc1 at the centromeric region (Williams et al., 2003). We hypothesize N^{α}-terminal acetylation dRad21/Scc1 by dSan/dNaa50 is potentially required for either reloading of cohesin or reestablishment of cohesion at the centromere after breathing movements.

To test this hypothesis, we will create a stable cell line expressing Drad21/Scc1 C-terminal hemagglutinin (HA) tagged. In order to only deplete the endogenous Drad21/Scc1, these cells will be subjected to RNAi by targeting the 5'UTR region of the *drad21/scc1* mRNA. We will further purify and analyze Drad21/Scc1-HA by using LC-MS/MS. Since these cells will be simultaneously induced to transiently arrest in mitosis we expect to have an enrichment of centromeric Drad21/Scc1-HA. If our hypothesis is correct we expect a substantial pool of the centromeric cohesin subunit Drad21/Scc1-HA to be N^{α}-acetylated. If we observe Drad21/Scc1 is indeed N^{α}-acetylated we will further address if the acetylation is relevant for its function and if it is dSan/dNaa50-dependent. These experiments will be performed as described above for Cctγ.

4.3. Are dSan/dNaa50 knockout phenotypes mediated by internal acetylation of β-tubulin?

Recently, hSan/Naa50 was proposed to negatively regulate MT polymerization by acetylation of β-tubulin at K252 (Chu et al., 2010). hSan/hNaa50-depleted showed a normal MT cytoskeleton in interphase cells. However, cold-induced MT depolymerization and regrowth assays showed that MT regrowth from the centrosome was much faster in hSan/hNaa50-depleted cells. Interestingly, hSan/hNaa50 acetylated Lys252 of β-tubulin *in vitro*, which was shown to be acetylated *in vivo* at the same residue. To establish a relationship between MT polymerization and acetylation of β-tubulin at K252, the authors investigated tubulin polymerization rates of K252A/Q and K252R mutants, which they considered to mimic acetylated and unacetylated forms of β-tubulin, respectively. Although the K252 mutants formed less stable heterodymers *in vitro*, they were

incorporated into MTs *in vivo*. Yet, Cold-induced MT depolymerization and regrowth assays showed that the acetylation-mimicking forms of β-tubulin (K252A/Q) were incorporated into MTs at much slower rates than the wild-type protein. Based on this work it was proposed that hSan/hNaa50 catalyzes β-tubulin K252 internal acetylation, which inhibits tubulin incorporation into MTs (Chu et al., 2010).

In our opinion there are significant problems with the above results and conclusions:

1) The authors did not show that hSan/hNaa50-depleted cells displayed reduced levels of acetylation of β-tubulin at Lys252. Therefore it is still unclear if hSan/hNaa50 acetylates K252 *in vivo*.

2) The authors considered that K252A and K252Q are acetylation mimicking forms of β-tubulin at Lys252. This assumption came from previous functional studies performed with acetylation mimicking forms of Hsp90 at K294 (K194A/Q) (Scroggins et al., 2007). Nevertheless, we cannot exclude the possibility that in the case of β-tubulin these two point mutations are simply inducing conformational changes that affect the function of β-tubulin independently of its "acetylation mimicking properties". Consistent with this possibility, both acetylation (K252A and K252Q) and unacetylation (K252R) mimicking mutations affected protein stability.

3) The authors observed that the acetylation mimicking mutant forms (K252A/Q) were incorporated at slower rates than the wild-type protein, which is consistent with the faster MT regrowth observed in hSan/hNaa50-depleted cells. However, the authors also observe a

decrease in MT incorporation in the unacetylated mimicking mutation (K252R), which is consistent with the hypothesis that these mutations are behaving as simple point mutations, independently of any “acetylation mimicking effect”. Furthermore, the mutant forms are also expressed at lower levels, which is likely to introduce a bias in the MT incorporation assays.

If indeed hSan/hNaa50 regulates MT polymerization by β-tubulin acetylation, one obvious question to this project, is if the mitotic chromosome segregation defects observed in San/Naa50p-depleted cells and loss of function mutants are mediated by β-tubulin acetylation? If that was the case, we would expect that expression of an unacetylated form of β-tubulin at K252 in β-tubulin-depleted cells, would lead to mitotic phenotypes similar to the ones observed in San/Naa50p depleted cells. Expression of a supposedly unacetylated mimicking form (K252R) of β-tubulin lead to a disorganized and/or disintegrated MT cytoskeleton in both interphase and mitotic cells, which is a phenotype dramatically different from the one observed in San/Naa50p depleted-cells. This is consistent with the hypothesis that these β-tubulin mutations are simply affecting the normal folding and stability of this protein.

Furthermore, if the mitotic defects observed in San/Naa50p-depleted cells were mediated by lack of acetylation of β-tubulin K252, we predict that expression of the acetylation-mimicking forms of β-tubulin (K252A/Q) in San/Naa50p-depleted cells, would lead to a suppression of the chromosome segregation defects. The authors did not address these questions, failing to integrate the suggested function of San/Naa50p in modulating MT polymerization with the mitotic phenotypes observed in San/Naa50p-depleted cells.

CHAPTER V

dNaa60 is required for chromosome segregation during anaphase

1. Introduction

N^{α}-terminal acetyltransferases (NATs) are conserved from yeast to humans both in subunit composition and substrate specificity (Starheim et al., 2009b). There is a higher number of NAT paralogues in higher eukaryotes (Arnesen et al., 2006; Arnesen et al., 2009a), which suggests these new paralogues have evolved to accommodate new tissue-specific functions. Consistent with this hypothesis, our previous data suggests there are tissue-specific requirements for N^{α}-acetylation. dSan/dNaa50 NAT, is required for chromosome segregation in somatic tissues but not in the female germ-line (Pimenta-Marques et al., 2008). Understanding why dSan/dNaa50 is not rate-limiting in the female germ-line might shed light on how N^{α}-acetylation is possibly regulating tissue-specific functions during the development of a multicellular organism.

Each NAT complex preferentially acetylates distinct N-termini (Arnesen et al., 2009b; Evjenth et al., 2009; Kimura et al., 2000; Polevoda et al., 1999; Polevoda and Sherman, 2003; Tercero et al., 1993). However, recent data suggests that NATs are partially redundant (Arnesen et al., 2009b; Van Damme et al., 2011). We therefore hypothesized that dSan/dNaa50 is not required within the female germ-line due to another redundant NAT specifically in this tissue.

In this chapter, we describe the identification of the putative *Drosophila* paralogues of dSan/Naa50. Phylogenetic analysis revealed dNaa60 is the closest paralogue to dSan/dNaa50. Interestingly, dNaa60-depleted cultured cells showed chromosome segregation defects remarkably similar to dSan/dNaa50, suggesting this NAT is also required for chromosome segregation in mitosis. Our data suggests that dNaa60 is likely to be redundant to dSan/dNaa50 specifically in the female germ-line.

2. Materials and methods

2.1. Bioinformatic analysis of *Drosophila* paralogues of dSan/dNaa50

In order to identify the closest NATs related to dSan/dNaa50 within the *Drosophila* proteome, we performed a BLAST (Basic Local Alignment Search Tool) followed by a PSI-BLAST (http://blast.ncbi.nlm. nih.gov/Blast.cgi) analysis with a cut-off E-value of 1.0e-10. PSI-BLAST allowed us to build a PSSM (position-specific scoring matrix) using the results of the first BlastP run and search new sequences (Altschul et al., 1997). This analysis retrieved eight dSan/dNaa50-related NATs (table 2). Homologues of the dSan/dNaa50-related NATs from *Homo sapiens, Mus musculus, Danio rerio, Saccharomyces cerevisiae* and *Schizosaccharomyces pombe* were obtained by BlastP analysis of species-specific protein databases. All NATs were confirmed to contain a GNAT5 domain by a PROSITE database search (Sigrist et al., 2009).

All sequences were aligned using CLUSTALW. A phylogenetic tree was constructed using distance neighbor-joining (NJ). The tree was based on pair-wise distances between amino acids using MEGA4 program (Tamura et al., 2007).

2.2. RNA interference on cultured *Drosophila* Dmel2 cells

Cells were cultured at 25ºC. RNAi was performed according to Clemens and colleagues (Clemens et al., 2000) in *Drosophila* Dmel2 cells. Table 1 contains the primers used for the construction of the different amplicons, and the corresponding size of each amplicon used for RNAi. GFP RNAi was used as a control. Each primer incorporated a T7 RNA polymerase binding site. All PCR products were used as

templates to synthesize dsRNA by utilizing the T7 RiboMAX™ Express kit (Promega). *Drosophila* Dmel2 cells were grown in SFM Medium (GIBCO) supplemented with 1x glutamine and 1x PenStrep. Cells were counted, diluted to $2x10^6$ cells/mL, and incubated for 1h with 40µg of each dsRNA at a concentration of 1µg/µL. After 1h incubation with dsRNA, 3mL of SFM media supplemented with glutamine and PenStrep was added back. After 93h of dsRNA treatment, cells were harvested and prepared for immunofluorescence.

Protein to deplete	Amplicon	Primers	Amplicon size (bp)
dSan	San Amp1	5'-AGCAGCATCGAACTGGGC-3' 5'-CGCTTATAGTATTGCTCCTTGGT-3'	413
CG18177	CG18177 Amp1	5'-CAACAAACACAGTGCGCC-3' 5'-CACATTTCGATAGGGTTTGATTTC-3'	274
	CG18177 Amp2	5'-GACTCGATGGGTCGTTCCGC-3' 5'-GTGGATGGCCGCCGTTAAT-3'	300
CG11412	CG11412 Amp1	5'-GATCGGATTCGAACTCCCTC-3' 5'-CATTTGGTGTTCAGCCTCG-3'	305
Ard1	Ard1 Amp 1	5'-ACACCACCACGGCAGAGC-3' 5'-AGGGCGTTGGTGTAGAGGTTC-3'	447
CG10414	CG10414 Amp1	5'-ACCATGCCGCTACTGTGAATC-3' 5'-GTGCGCCAATGGAAGAATC-3'	321
CG14222	CG14222 Amp1	5'-TCACCTGCGACGACCTCTT-3' 5'-GTATGACCGACTTTTTGTTGACG-3'	465
CG31730	CG31730 Amp1	5'-ATGCGTTTCGATGATTTGTTC-3' 5'-TTCTCAATTCGTAGGCACTTTCTG-3'	439
CG32319	CG32319 Amp1	5'-GCCGTTCTTATTCAAAAGGAAC-3' 5'-GTAGAGCGCCAATGCAGGT-3'	495
CG31851	CG31851 Amp1	5'-GTGATGGATCCCTTGGCG-3' 5'-TCGTATCCATGGTCGTCGG-3'	404
GFP	GFP Amp	5'-ACCATGCCGCTACTGTGAATC-3' 5'-GTGCGCCAATGGAAGAATC-3'	420

Table 1: Primers used to produce different dsRNA's for RNAi experiments

2.3. Transfection of constructs with tagged proteins

cDNA clones of CG18177 isoform A and B (LD46538 and LD27619, DGRC) were cloned into a plasmid with a C-terminal Myc tag, using the Gateway system (Invitrogen).

Drosophila Dmel2 cells were maintained in SFM Medium (GIBCO) supplemented with 1x glutamine and 1x PenStrep, according

to standard tissue culture techniques. To transiently transfect cells, we used the following protocol: $4x10^6$ cells were plated per well (6-well plate); the following day, 3 µg of the plasmid construct were mixed in ddH_20 (sterile and free of nucleases) to a final volume of 100 µL. To this mixture, 15 µL of FuGENE transfection agent (Roche) were added. This solution was incubated at room temperature (RT) for 30 min and added to the cells. Cells were left to express the tagged proteins for 48 hours. Both proteins were tagged with a Myc protein. Control cells were transfected with a construct expressing Myc tag alone.

2.4. Immunofluorescence of Dmel2 Cells

After 93 hours of dsRNA treatment or transient transfection experiments, $2x10^6$ cells were added to coverslips by 1h incubation at 25ºC. Cells were fixed with 4% formaldehyde, 0.03M PIPES, 0.11M HEPES, 0.01M EGTA and 4mM $MgSO_4$ for 10 min, followed by two washes in 1x PBS. Permeabilization and blocking was performed for 1h with PBSTB (PBS, 0.1% Triton X-100, 1% fetal bovine serum). Primary antibody incubations were done in blocking solution for 2h at room temperature or overnight at 4°C, followed by three 5 min washes in PBSTB. Secondary antibody incubations were performed as described for the primary antibodies, including the three 5 min washes. Primary antibodies included mouse anti-α-tubulin DM1A (1:500; Sigma), rabbit anti-pSer10-Histone H3 (1:500; Upstate Biotechnology), chicken anti-Cid (1:500; kindly provided by David Glover), rat anti-Cnn (1:500; kindly provided by Jordan Raff), rabbit cis-Golgi marker anti-Gm130 (1:500; Abcam, ab30637) and mouse anti-Myc (1:250; Hybridoma bank, clone 9E 10). F-actin was stained with rhodamine-conjugated phalloidin (Sigma) and DNA was stained with DAPI at 1:1000 (stock concentration 1 mg/ml).

2.5. Microscopy

Visualization of fixed cells was performed using a Delta Vision Core System (Applied Precision) using a 100× UplanSApo objective and a cascade2 EMCCD camera (Photometrics). Images were acquired as a series of z-sections separated by 0.2-µm intervals. Deconvolution was performed using the conservative ratio method in softWoRx software. Phenotypic quantification was performed using a regular Epifluorescent microscope Leica DMRA2.

2.6. Creation of CG18177/*dnaa60* mutants

The fly stock, w;;PCG18177^{EP3301}/TM3,Sb, with a P-element insertion (EP3301) near the beginning of the 5'UTR of the CG18177 gene, was obtained from the Bloomington Drosophila Stock Center. Excision of PCG18177^{EP3301} was generated by crossing the P-element line to a transposase-expressing line (w;;Δ(2:3)99B,Sb/TM6B). Male progeny with the genotype w;; PCG18177^{EP3301}/ Δ(2:3)99B,Sb and patchy colored eyes, were then crossed with virgin females of w;;MKRS/TM6B. From each cross, potential excision events were identified by the loss of the *w*+ marker, and white-eyed males with the genotype w; ΔCG18177*/TM6B were collected to establish a balanced P-element stock. Twenty excision lines were crossed with the deficiency Df(3L)AC1 which deletes the CG18177 gene. The progeny obtained from each different cross with the genotype ΔCG18177*/Df(3L)AC1, was tested by genomic PCR reaction with primers that covered the CG18177 gene locus. We identified a line where approximately 1305bp were deleted. This deletion mutant line was called dNaa60Δ^{20}. This deletion abrogates the 5'UTR and first and second exons of the predicted isoforms, B and C. For predicted

isoform A, the deletion abrogates the 5'UTR as well as the first exon and half of the second exon (fig. 1).

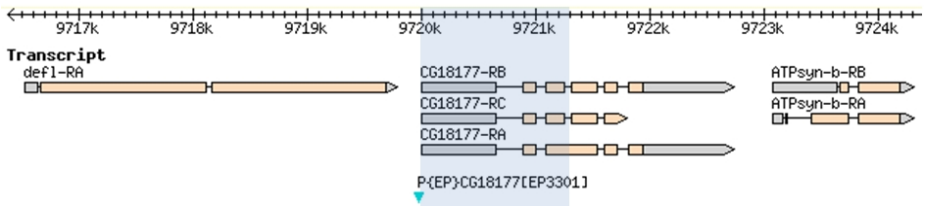

Figure 1: Deletion mutant line of CG18177 abrogates the first 3 exons of this gene. Gray boxes represent the 5' and 3' UTR of the genes represented in the figure. Pink boxes represent the exons of the represented genes. Blue triangle represents the P-element used to create the mutant deletion lines. The blue shaded box represents the genome region deleted in the dNaa60Δ^{20} line. The created deletion line does not affect any of the neighboring genes of CG18177, *deflated* (*def1*) and *ATP synthase, subunit b* (*ATPsun-b*).

3. Results

3.1. Identification of *Drosophila* paralogues of dSan/dNaa50

dSan/dNaa50 was shown to be essential for chromosome congression and segregation during mitosis in different somatic tissues, but was dispensable within germ-line stem cells (Pimenta-Marques et al., 2008). COFRADIC analysis on *san* mutant embryonic protein extracts suggested a partial redundancy between dSan/dNaa50 and other NATs (Chapter IV). We hypothesized there was another NAT redundant with dSan/dNaa50 within the germ-line. If that was to be the case we expected the NATs most closely related to dSan/dNaa50 to be the best candidates for this redundancy.

BLAST analysis retrieved eight dSan/dNaa50-related NATs (table 2). Phylogenetic analysis of the NATs most similar to dSan/dNaa50 allowed the identification of the putative homologues of the NatA, NatB and NatC complexes (fig. 2). The gene coding for the NatA catalytic subunit, Naa10p, suffered a duplication event giving rise to a new NAT, Naa11p, which is present in both humans and mouse (Arnesen et al., 2006). We did not identify a gene coding for Naa11p within *Drosophila* and Zebrafish (fig. 2). The *Drosophila* CG14222 gene encodes a putative NAT which is likely to be the closest homologue of hNaa20. Additionally, within the NatB complex group we identified two putative paralogs of *Drosophila* Naa20p. These proteins were not found in the genomes of other analyzed organisms (fig. 2). Within the NatC complex, *Drosophila* has two putative paralogues of hNaa30. Both CG11412 and CG32319 encode proteins which are closely related to hNaa30 (fig.2). The CG10414 gene encodes a new putative NAT which is only present in higher eukaryotes (fig. 2). According to our phylogenetic analysis, the protein encoded by CG18177 is the closest NAT related to dSan/dNaa50. dSan/dNaa50

and CG18177 seem to have originated from a common ancestor (fig. 2).

The NAT encoded by CG18177 is the putative homologue of the human Naa60 protein, which was recently shown to display *in vivo* NAT activity (Van Damme et al., 2011).

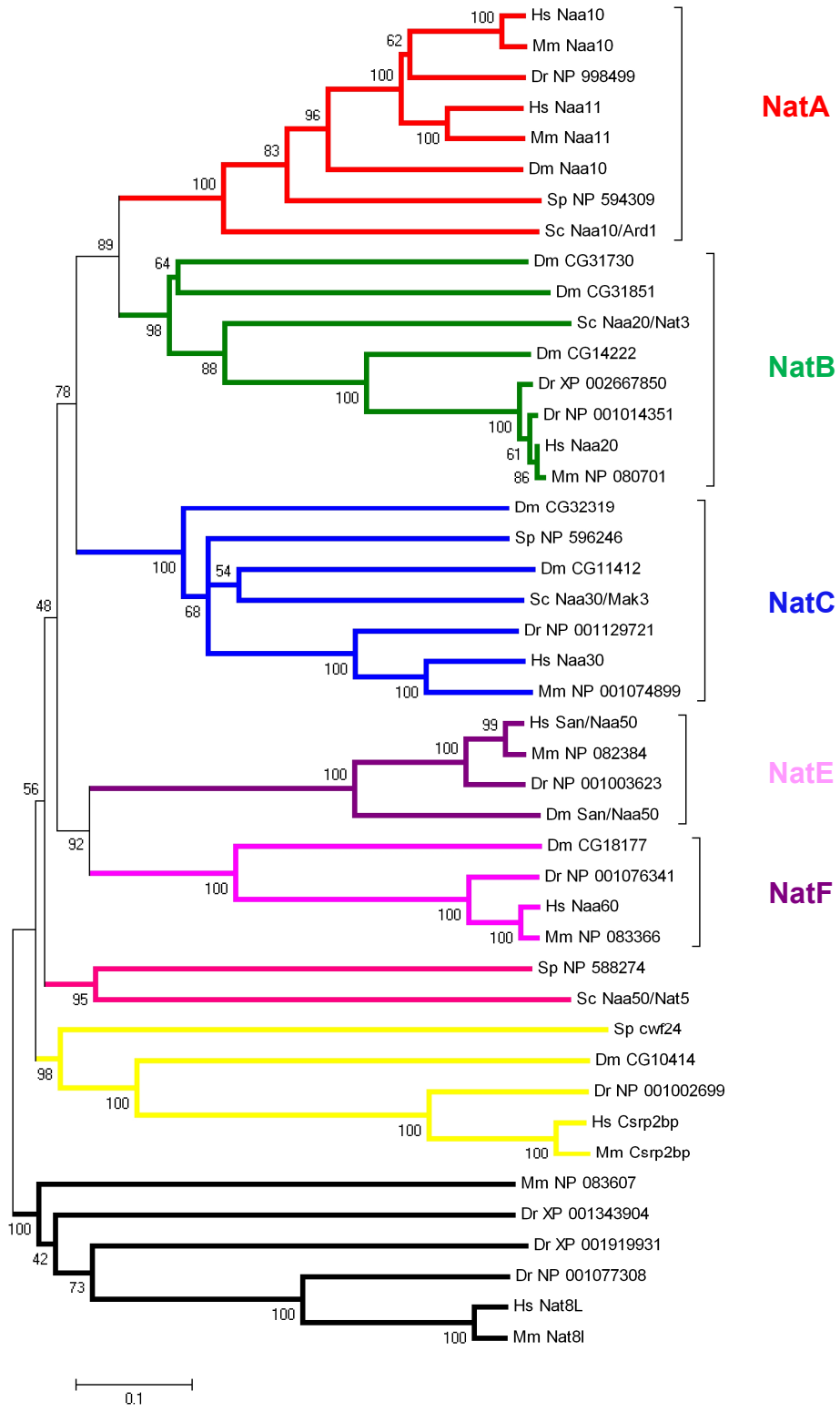
Hs Naa10
Mm Naa10
Dr NP 998499
Hs Naa11
Mm Naa11
Dm Naa10
Sp NP 594309
Sc Naa10/Ard1
NatA
Dm CG31730
Dm CG31851
Sc Naa20/Nat3
Dm CG14222
Dr XP 002667850
Dr NP 001014351
Hs Naa20
Mm NP 080701
NatB
Dm CG32319
Sp NP 596246
Dm CG11412
Sc Naa30/Mak3
Dr NP 001129721
Hs Naa30
Mm NP 001074899
NatC
Hs San/Naa50
Mm NP 082384
Dr NP 001003623
Dm San/Naa50
NatE
Dm CG18177
Dr NP 001076341
Hs Naa60
Mm NP 083366
NatF
Sp NP 588274
Sc Naa50/Nat5
Sp cwf24
Dm CG10414
Dr NP 001002699
Hs Csrp2bp
Mm Csrp2bp
Mm NP 083607
Dr XP 001343904
Dr XP 001919931
Dr NP 001077308
Hs Nat8L
Mm Nat8l
0.1

Figure 2: Phylogenetic tree of dSan/dNaa50 NAT paralogues. dSan/dNaa50 paralogues include *Drosophila* homologues of the NatA, NatB and NatC catalytic subunits. CG18177 is the closest NAT related to dSan/dNaa50. Both dSan/dNaa50 and CG18177 originated from a common ancestor protein. Tree was drawn to scale, with branch lengths in the same units as those of the evolutionary distances used to infer the phylogenetic tree. Scale bar corresponds to 0.1 millions of years ago. Hs, *Homo sapiens* (Hs Naa10, NP_003482; Hs Naa10, NP_116082; Hs Naa20, NP_057184; Hs Naa30, NP_001011713; Hs San/Naa50, NP_079422; Hs Naa60, NP_079121; Hs Csrp2bp, NP_065397; Nat8L, NP_848652); Mm, *Mus musculus* (Mm Naa10, NP_001171436; Mm Naa11, NP_001028363; Mm Csrp2bp, NP_852082; Mm Nat8l, NP_001001985); Dr, *Danio rerio*; Dm, *Drosophila melanogaster* (Dm Naa10, NP_648378; Dm CG31730, NP_723799; CG31851, NP_723798; CG14222, NP_608331; CG32319, NP_728606; CG11412, NP_569903; Dm San/Naa50, NP_524779; Dm CG18177, NP_996032; Dm CG10414, NP_609889); Sc, *Saccharomyces cerevisiae* (Sc Naa10/Ard1, NP_011877; Sc Naa20/Nat3, NP_015456; Sc Naa30/Mak3, NP_015376; Sc Naa50/Nat5, NP_014896); Sp, *Schizosaccharomyces pombe* (Sp cwf24, NP_596257).

Gene ontology number	Gene Symbol	Closest human Homologue	NAT Complex
CG18177	-	Naa60	NatF
CG11412	-	Naa30	NatC
CG11989	Ard1	Naa10	NatA
CG10414	-	Csrp2bp	-
CG14222	-	Naa20	NatB
CG31730	-	Naa20	NatB
CG32319	-	Naa30	NatC
CG31851	-	Naa20	NatB

Table 2: *Drosophila* NATs most closely related to dSan/dNaa50.

3.2. Identification of a new NAT required for chromosome segregation

Both dSan/dNaa50 and dNaa60 seemed to have originated from a common ancestor (fig. 2). To test if dNaa60 also had mitotic functions, we depleted this NAT in Dmel2 cells and analyzed mitotic cells. Chromosome congression at the metaphase plate was indistinguishable between control and dNaa60-depleted cells (fig. 3 A compare with B). dNaa60-depleted cells displayed a mitotic index comparable to control cells (5,7% in dNaa60-depleted cells and 6,0% in control cells), suggesting they did not arrest in mitosis. However, dNaa60-depleted cells displayed a moderate but consistent increase in the percentage of cells undergoing anaphase with chromosome segregation defects (22,9% ± 3,9 of dNaa60-depleted cells had abnormal anaphases versus 7,0% ± 3,1 in control cells). Interestingly the observed lagging chromosomes and chromosome bridges in dNaa60-depleted cells were identical to the ones observed in dSan/dNaa50 depleted cells (fig. 3 D, F and G).

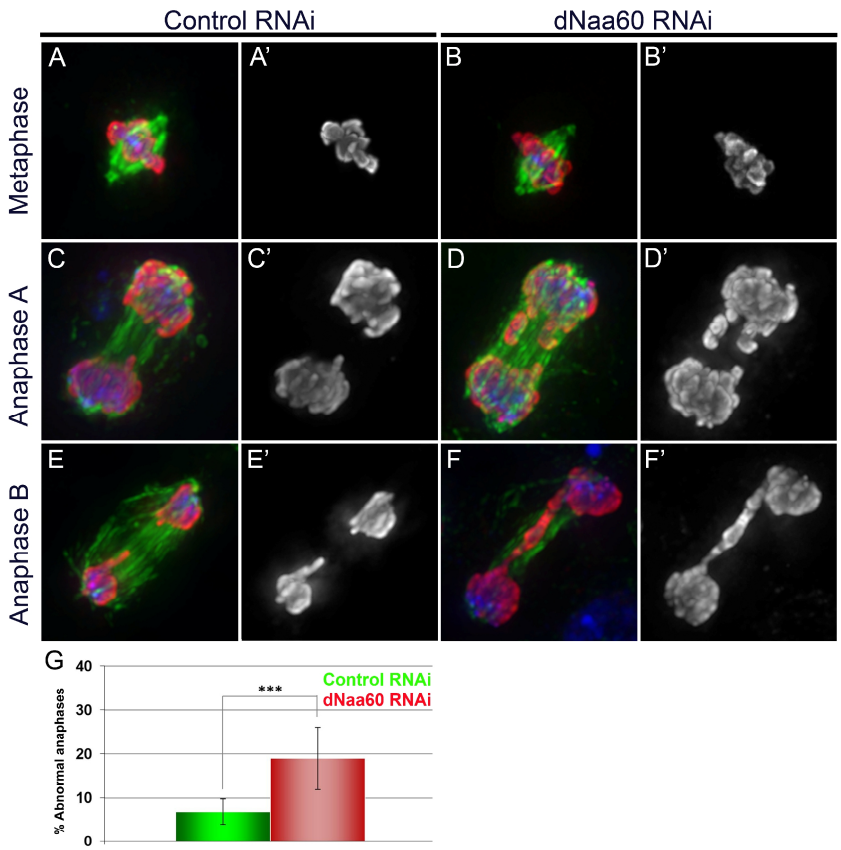

Figure 3: dNaa60 is required for chromosome segregation during anaphase. (A and B) dNaa60-depleted Dmel2 cells did not exhibit detectable chromosome congression defects during metaphase. (C-F) dNaa60-depleted cells displayed lagging chromosomes and chromosome bridges during anaphase. Histone 3 phosphorylated at Serine 10 (PH3) (red), α-tubulin (green) and DNA (blue). (A', B', C' D' E' and F') Black and white images display cells with PH3 staining alone. (G) Quantification of chromosome segregation defects in dNaa60-depleted cells (n=278) and control cells (n=179) (***P<0,001 Student's test).

Chromosome lagging and bridging in dNaa60-depleted cells may be explained by kinetochore abnormalities, but we failed to detect any obvious defects in the localization of the Centromere identifier (Cid) protein during metaphase or anaphase (fig. 4 A-D). We also failed to detect any obvious cohesion defects since the distance between kinetochores during metaphase was apparently normal

according to Cid localization (fig. 4 A, B). Chromosome lagging could also be explained by centrosome/mitotic spindle defects. Yet, we did not detect any obvious defects in the localization of Centrosomin (Cnn), and the mitotic spindle was bipolar and correctly attached to chromosomes and centrosomes (fig. 8 A-D). dNaa60-depleted cells showed no obvious defects in the actin and microtubule cytoskeleton in both mitotic and interphase cells (fig. 8 E-J). Additionally, dNaa60-depleted cells undergoing chromosome segregation defects also showed an apparently normal actin cytoskeleton (Figure 8 H).

These data suggested dNaa60 was required for normal chromosome segregation during mitosis.

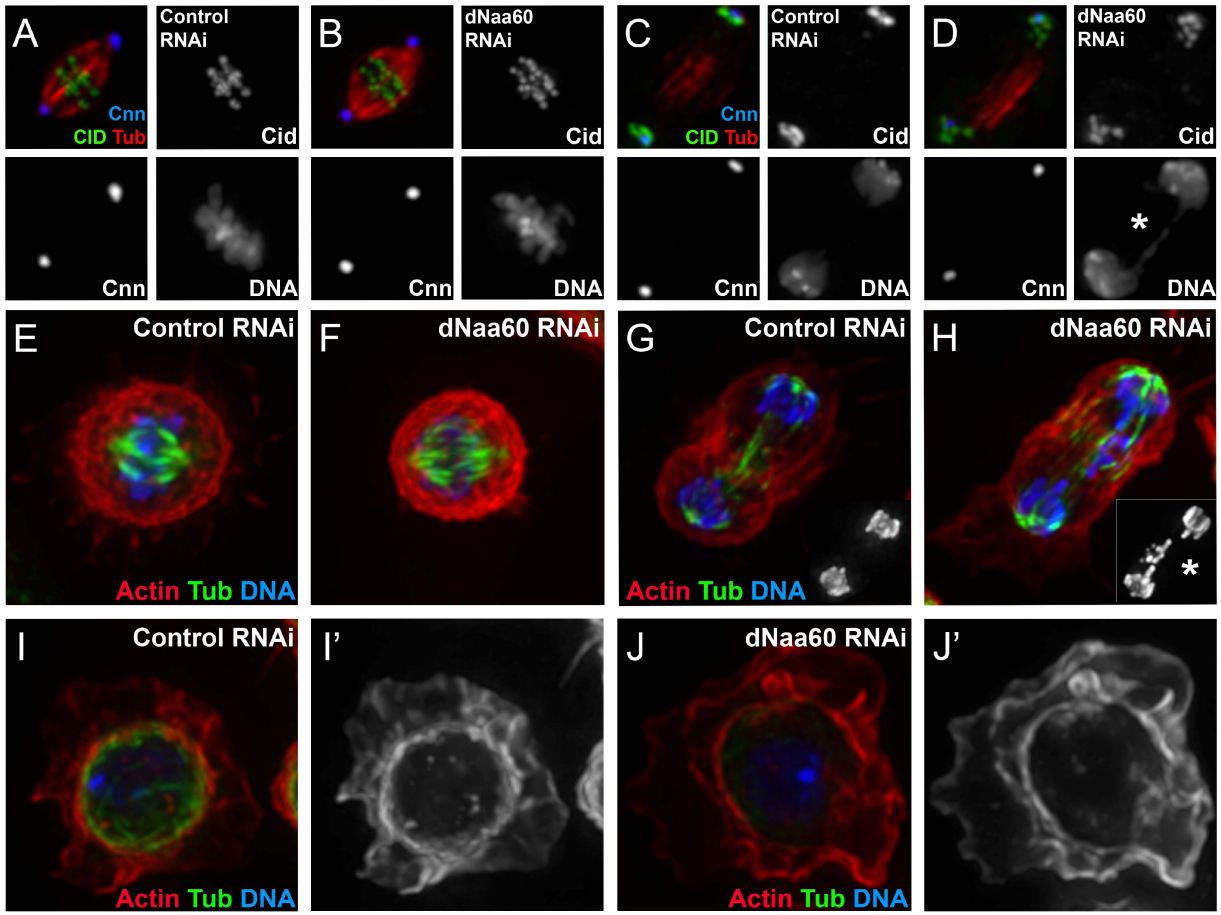
A
Cnn
CID Tub
Control RNAi
Cid
B
dNaa60 RNAi
Cid
C
Cnn
CID Tub
Control RNAi
Cid
D
dNaa60 RNAi
Cid
Cnn
DNA
Cnn
DNA
Cnn
DNA
Cnn
DNA
*
E
Control RNAi
Actin Tub DNA
F
dNaa60 RNAi
G
Control RNAi
Actin Tub DNA
H
dNaa60 RNAi
*
I
Control RNAi
Actin Tub DNA
I'
J
dNaa60 RNAi
Actin Tub DNA
J'

Figure 4

Figure 4: dNaa60-depleted cells show apparently normal mitotic spindles and normal actin cytoskeleton. Control dsRNA treated cells (A,C,E,G, and I). dNaa60 dsRNA treated cells (B,D,F,H and J). dNaa60-depleted cells showed no significant defects in the localization of both Cnn and Cid proteins (A-D). Both control and dNaa60-depleted cells exhibited bypolar spindles with correct alignment of chromosomes at the metaphase plate (A,B). Anaphase cells with chromosome segregation defects in dNaa60-depleted cells showed no obvious defects in Cnn and CID localization (C,D). α-tubulin (red), CID (green) and Cnn (blue). dNaa60-depleted cells undergoing anaphase with chromosome segregation defects also showed a normal actin and microtubule cytoskeleton (G,H; detail with Histone 3 phosphorylated on Serine 10 staining). Control and dNaa60-deplted cells exhibit proper chromosome alignment during metaphase with no detectable defects in the actin and microtubule cytoskeleton (E,F). dNaa60-depleted cells in interphase show no detectable defects regarding the actin and microtuble cytoskeleton (I-J). Actin (red), α-tubulin (green) and Histone 3 phosphorylated on Serine 10 (blue).

3.3. *dnaa60* is not an essential gene

Since dNaa60 is required for mitosis in *Drosophila* cultured cells, it is therefore a good candidate for the putative NAT redundant with dSan/dNaa50 in the germ-line. In order to test this hypothesis we created a deletion mutant of dNaa60 (see Materials and methods) that deleted the 5'UTR along with the first and second exons of the predicted isoforms of this NAT. The generated deletion was likely to be a loss of function allele of dNaa60 as it generated a severely truncated protein. The deletion mutant was zygotic lethal with occasional escaper homozygous adult flies. To investigate if dNaa60 was an essential gene, the created dNaa60 deletion mutants were crossed with a deficiency that completely abrogated the CG18177 gene locus. Virgin females of w;;dNaa60Δ^{20}/TM6B were crossed with males of the deficiency Df(3L)AC1/TM3,Sb. This cross gave rise to viable dNaa60 mutant progeny with the genotype w;;dNaa60 Δ^{20}/Df(3L)AC1 (table 3), which suggested dNaa60Δ^{20} deletion contained a second lethal

mutation not associated with dNaa60. To test the maternal requirement of dNaa60, virgin females of the genotype w;;dNaa60 Δ^{20}/Df(3L)AC1 were crossed with males of the same genotype. These flies laid normal eggs that gave rise to normal progeny. We concluded that in contrast to dSan/dNaa50, dNaa60 is not an essential gene.

F0	w;; dNaa60Δ^{20}/TM6B x Df(3L)AC1/TM3, SB	
F1	TM6B and/or TM3,Sb	TM6B^{+} or TM3,Sb^{+}
Counted flies	63	22

Table 3: *dnaa60* is not an essential gene. Crossing *dnaa60* deletion mutant with a deficiency for the CG18177 gene resulted in F1 progeny containing transheterozygous flies for the *dnaa60* deletion at the expected Mendelian proportion.

3.4. dNaa60 is not required for female oogenesis

Oogenesis in maternal mutant *dnaa60* flies was indistinguishable from control flies. According to DNA staining, nuclei within the germarium had a normal morphology comparable to control germariums (fig. 5 A, B compared with E, F). *dnaa60* mutant egg chambers contained 15 nurse cells and a posteriorly-localized oocyte, and they were surrounded by a layer of somatically derived follicular cells (fig.5 D, H). This suggested the germ-line stem cells were dividing normally, giving rise to cytoblasts that would undergo 4 rounds of mitosis resulting in a normal egg chamber. The germ-line-specific Vasa protein immunostaining confirmed that the female germ-line was correctly determined in *dnaa60* mutants.

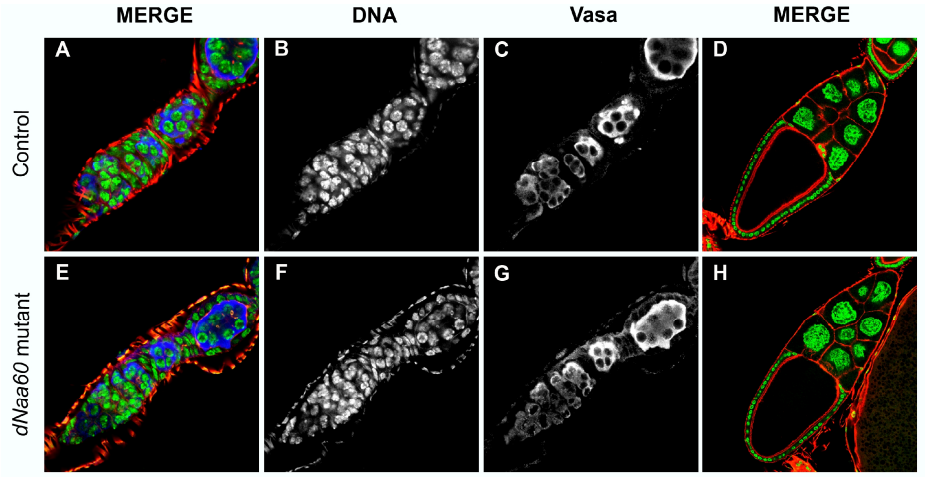

Figure 5: dNaa60 is not required for female oogenesis. Control (A-C) and mutant (E-G) *dnaa60* ovariole showing a germarium and a stage 1 egg chamber. (D) Control stage 10 egg chamber. (H) *dnaa60* mutant stage 10 egg chamber. Ovaries were stained for the germ-line specific RNA binding protein Vasa, actin and DNA.

3.5. dNaa60 localizes to cellular membranous compartments

Expression of a tagged version of hNaa60, showed colocalization between this NAT and membranous compartments, such as Golgi, lysosomes and late endosomes (Arnesen T., unpublished data). This data suggested hNaa60 was potentially the first identified NAT that could be involved in post-translational N^{α}-acetylation (Arnesen T., unpublished data). To have better insights into a possible functional conservation between human and *Drosophila* Naa60p, both isoforms A and B of dNaa60 were expressed in *Drosophila* cultured cells. Both isoforms displayed localization patterns suggestive of the membranous compartments (fig 6). Myc–tagged dNaa60 isoforms showed a strong localization around the nucleus and partial colocalization with a cis-Golgi marker (Gm130). This suggests that hNaa60 and dNaa60 are likely to be functionally conserved from *Drosophila* to humans.

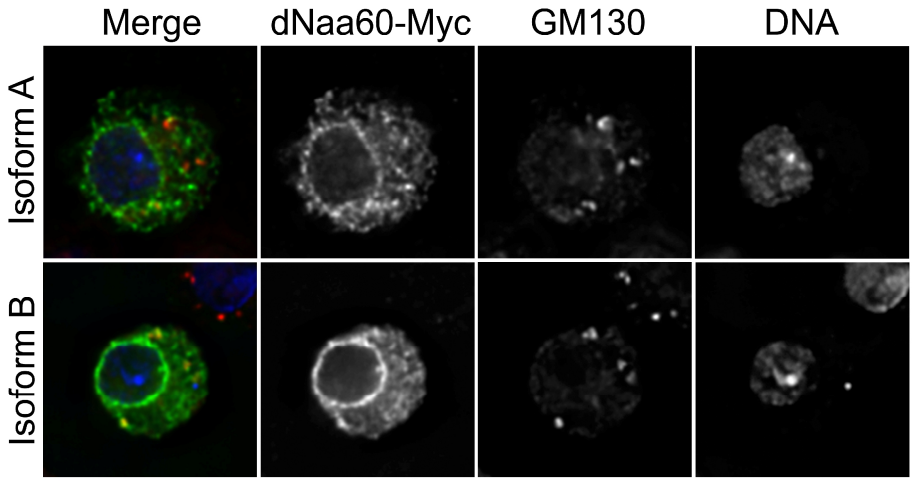

Figure 6: dNaa60 potentially localized to the membranous compartments of Dmel2 cells. dNaa60 expression partially colocalized with a cis-Golgi marker. These results were confirmed using a GFP tagged version of dNaa60 Isoform A and B (data not shown). (Green) dNaa60-Myc, (red) Cis-Golgi marker - Gm130, (blue) DNA.

4. Discussion

4.1. Higher complexity in the regulation of protein N^{α}-terminal acetylation in *Drosophila melanogaster*

N^{α}-terminal acetylation is a highly conserved and widespread protein modification. This modification is performed by NATs, which are highly conserved from yeast to humans. Higher eukaryotes seem not only to have a higher number of NATs, but alternative splicing of some of the coding genes is associated to the expression of additional NAT isoforms. We performed a phylogenetic analysis of most *Drosophila* NATs and consistent with other higher eukaryotes, *Drosophila* has a higher number of NATs when compared to yeast. Yet, surprisingly, *Drosophila* contained additional paralogues not found in humans. *Drosophila*-putative homologues of the genes coding Naa20p and Naa30p suffered duplication events. dNaa20 (encoded by CG14222) suffered two rounds of gene duplication into two new putative NATs encoded by the genes CG31730 and CG31851. These new paralogues are adjacent to each other within the 2L chromosome. We also detected two *Drosophila* paralogues within the Naa30p NAT group.

These duplication events seem to correlate with the localization of one of the paralogues on the X chromosome. *Drosophila*-putative Naa20p (encoded by CG14222) is located on the X chromosome and its putative paralogues encoded by the genes CG31730 and CG31851 are located on the 2L chromosome. Among the two *Drosophila* paralogues of Naa30p, CG11412 is located on the X chromosome, while CG32319 is located on the 3L chromosome. In mouse and humans the genes encoding Naa20p and Naa30p are located on autosomal chromosomes and they are not associated with gene duplication events. In contrast, both human and mouse Naa10p are

located on the X chromosome and both contain paralogues (Naa11p) on autosomal chromosomes. Both *Drosophila* and Zebrafish Naa10p are located on autosomal chromosomes and we failed to detect any gene duplication event of Naa10p in these two organisms.

Since mouse Naa11p was shown to be highly expressed in testis during male meiosis (Pang et al., 2009), it was proposed Naa11p expression would compensate for the loss of the X-chromosome linked gene *mNAA10* during male meiosis (Pang et al., 2009). Likewise, a requirement for dNaa20p and dNaa30p in male meiosis would explain why these NATs are duplicated in *Drosophila* but not in other organisms. Indeed, according to Affymetrix data available at FlyAtlas, both CG31730 and CG31851 mRNAs were only detected in male testis. Affymetrix data also detected an upregulation of CG32319 mRNA in testis and none or low levels of transcript in other tissues. As for the other eukaryotic organisms, dSan/dNaa50, dNaa60 and the putative NAT encoded by CG10414, which are located on autosomal chromosomes, did not duplicate into new genes.

4.2. Potential redundancy between dSan/dNaa50 and dNaa60 within the female germ-line

dSan/dNaa50 is required for normal mitosis in the soma but not in the germ-line. We hypothesize that this is likely due to a redundancy of another mitotic NAT within the female germ-line. According to phylogenetic analysis, dNaa60 and dSan/dNaa50 originated from a common ancestral gene, making dNaa60 the closest dSan/dNaa50 paralogue. Consistent with the phylogenetic proximity between both these NATs, we found that dNaa60-depleted Dmel2 cells show chromosome segregation defects identical to dSan/dNaa50-depleted cells. These defects included lagging chromatids and chromosome bridges during anaphase. COFRADIC analysis of yeast cells

expressing human San/Naa50p and human Naa60p suggested these NATs have similar substrate specificity *in vivo* (Van Damme et al., 2011; Van Damme and Kris Gevaert; unpublished data). Moreover, *in vitro* peptide library screening assays confirmed these NATs share an identical substrate-repertoire with rather subtle differences (Van Damme et al., 2011; Van Damme and Kris Gevaert; unpublished data). We hypothesize that dNaa60 is a good candidate NAT to be redundant with dSan/dNaa50 within the female germ-line. However, in contrast to dSan/dNaa50, *dnaa60* deletion mutants are viable, showing *dnaa60* is not an essential gene. Embryos mutant for *dnaa60* show normal syncytial nuclei divisions (data not shown) and we failed to detect any defects within female oogenesis. If our hypothesis is correct this suggests that although these two NATs are partially redundancy, dSan/dNaa50 is most likely the main mitotic NAT. Since *dnaa60* is highly expressed in the ovaries (Chintapalli et al., 2007), this raises the hypothesis that dSan/dNaa50 activity is not rate-limiting in the female germ-line due to high levels of dNaa60 activity. To test this hypothesis we will generate a *san/dnaa60* double mutant and check if we can detect mitotic defects in the female germ-line.

If complementation of dSan/dNaa50 mitotic functions in the female germ-line was due to high levels of dNaa60 this would imply that zygotic mutants of *san* would only show mitotic phenotypes on somatic tissues with low levels of *dnaa60* expression. However, we detected chromosome segregation defects in *san* mutant larvae neuroblasts (zygotic mutants) where dNaa60 mRNA was apparently detected at high levels (Chintapalli et al., 2007). This suggests that if dSan/dNaa50 and dNaa60 are redundant in the female germ-line, then dNaa60 activity in the female germ-line must be significantly higher or distinct (maybe due to different cofactors) from its activity in the soma.

Another issue associated with the dSan/dNaa50 and dNaa60 redundancy hypothesis relates with the fact that most genes highly

expressed in the female germ-line show a strong maternal contribution in the embryo. Since *dnaa60* is highly expressed in the ovaries, it is likely to be present at high levels in the syncytial embryo. Yet, maternal mutant embryos of *san* show chromosome segregation defects during syncytial blastoderm (early embryonic development). We hypothesize dNaa60 complements dSan/dNaa50 function in the female germ-line but not during early embryogenesis, due to the extremely fast blastoderm syncytial nuclear divisions. If this hypothesis is correct, then we would predict that up-regulation of dNaa60 will suppress the chromosome segregation defects observed in embryos mutant for dSan/dNaa50.

If we failed to detect any mitotic defect in the *san/dnaa60* double mutant female germ-line, it is still possible that another NAT is partially redundant with dSan/dNaa50 and maybe dNaa60. The NatC complex N^{α}-acetylates Met-Leu- N-termini (Polevoda et al., 1999; Starheim et al., 2009a), which were also shown to be N^{α}-acetylated by hNaa50 *in vitro* (Evjenth et al., 2009), hNaa60 *in vivo* and both human and *Drosophila* Naa60p *in vitro* (Van Damme et al., 2011). Although unlikely, these three NATs could all together be redundant in N^{α}-acetylating a substrate containing a Met-Leu- N-terminus. An alternative explanation is that our hypothesis is wrong and these two NATs are not redundant in the female germ-line. If this is the case, the absence of mitotic defects in female germ-line mutant for *san* could be associated with the fact that the dSan/dNaa50-dependent N^{α}-acetylation and/ or the mitotic substrates of dSan/dNaa50 are not rate-limiting for female germ-line development. If this is the case, it is crucial to identify the mitotic substrates of dSan/dNaa50 and test their functional requirements in the soma and in the germ-line.

4.3. dNaa60 is possibly involved in posttranslational N^{α}-acetylation

Phylogenetic analysis of dSan/dNaa50, allowed the identification of a closely related NAT named dNaa60. Naa60p is a highly conserved NAT within higher eukaryotes. *In vitro* peptide library assays revealed hNaa60 and dNaa60 share almost indistinguishable substrate specificity (Van Damme et al., 2011). Human Naa60p was recently identified in human cells and was shown to have N^{α}-acetylation activity (Van Damme et al., 2011). hNaa60 was shown to be enriched at membranous fractions, and expression-tagged studies found that this NAT colocalized with Golgi, lyzosomes and late endosomes (Arnesen T., unpublished data). Consistently, we also observed that myc-tagged dNaa60 was localized to cellular membranous compartments of Dmel2 cells, which suggested both NATs were functionally conserved.

Association of NAT complexes with ribosomes suggests a model where these enzymes perform co-translational acetylation of nascent polypeptides during protein synthesis (Arnesen et al., 2005). The localization of hNaa60 to the Golgi, lysosomes and possibly late endosomes suggests Naa60p might be the first known NAT to be involved in posttranslational N^{α}-acetylation. Interestingly, COFRADIC analysis on human cells revealed the majority of the identified hNaa60 protein substrates contain membrane-spanning /transmembrane regions (Van Damme and Kris Gevaert; unpublished data). We hypothesize Naa60p function is important to the posttranslation N^{α}-acetylation of integral membrane proteins. Future studies will elucidate the impact of Naa60p-mediated N^{α}-acetylation on these proteins.

CHAPTER V

General Discussion

1. Tissue specific functions of N$^{\alpha}$-terminal acetylation?

Protein N$^{\alpha}$-terminal acetylation is a highly conserved and widespread modification that occurs on approximately 80% of all soluble, cytoplasmic human proteins (Arnesen et al., 2009b). However, with some few examples, little is known about the biological function of this modification. N$^{\alpha}$-acetylation acetylation was shown to be important for the localization and function of specific proteins (Behnia et al., 2004; Caesar and Blomberg, 2004; Coulton et al., 2009). Some reports suggested N$^{\alpha}$-acetylation could act as a stabilizer, for instance by blocking N-terminal ubiquitination mediated degradation (Ciechanover and Ben-Saadon, 2004), while recent work in yeast suggested it could act as a general destabilization signal (Hwang et al., 2010). In higher eukaryotes knockdowns of NatA, NatB and NatC subunits by RNAi produce pleiotropic phenotypes generally associated with cell cycle arrest or apoptosis (Ametzazurra et al., 2008; Arnesen et al., 2006b; Fisher et al., 2005; Lim et al., 2006; Starheim et al., 2008; Starheim et al., 2009).

Higher eukaryotes contain an increased number of N$^{\alpha}$-terminal acetyltransferases (NATs) when compared to lower eukaryotes due to gene duplication events. Maintenance of these duplicated genes suggest either neo-functionalization, where one gene copy acquired a new beneficial function while the other retained the original function (Nowak et al., 1997; Ohta, 1988; Walsh, 1995) or subfunctionalization, where the two gene copies specialize to perform complementary functions (Force et al., 1999; Lynch and Force, 2000). For example, during retinoic acid-induced differentiation in NB4 cells, human *NAA10* expression levels show a significant decrease, while the paralog (*hNAA11*) expression remained unchanged (Arnesen et al., 2006a).

We hypothesize that the higher number of NATs observed in *Drosophila* and humans increased the complexity of N^{α}-acetylation regulation and allowed a higher prevalence of tissue-specific regulatory functions. For example, dSan/dNaa50 is required for normal chromosome segregation during mitosis in somatic but not in the female germ-line stem cells (Pimenta-Marques et al., 2008). Furthermore, female oogenesis develops normally in the absence of dSan/dNaa50. This suggests that dSan/dNaa50 is either redundant with another NAT specifically in the female germ-line or that San/dNaa50-dependent N^{α}-terminal acetylation is not rate limiting during *Drosophila* oogenesis. Since tissue culture cells depleted for dNaa60 (Chapter V), the closest paralogue of dSan/dNaa50, show chromosome segregation defects identical to cells depleted for dSan/dNaa50, and since these two NATs show similar substrate specificities *in vitro* and *in vivo* (Van Damme et al., 2011; Van Damme and Kris Gevaert; unpublished data), we favor the hypothesis that dNaa60 complements the mitotic functions of dSan/dNaa50 in the female germ-line but not in the soma.

The germ line is a highly specialized and differentiated cell-lineage whose function is to give rise to the male and female gametes. The ability of giving rise to totipotent cells is associated to unique regulatory processes that avoid somatic differentiation and maintain totipotent potential (Gilboa and Lehmann, 2004). To what extend the redundancy between dSan/dNaa50 and dNaa60 is important for germ line development is still unclear. We propose that dSan/dNaa50 is not rate-limiting in the female germ-line due to either a selective pressure for redundancy with dNaa60 to ensure N^{α}-acetylation robustness or that dSan/dNaa50 function is differentially required in the soma and in the germ-line. We speculate that similar to dSan/dNaa50, other NATs

and/ or other NAT isoforms are likely to have such tissue-specific functions in higher eukaryotes.

2. Regulatory functions of N^{α}-terminal acetylation?

If higher eukaryotes show tissue-specific regulation of N-terminal acetylation (as shown for dSan/dNaa50), and if depletion of some NATs produces tissue-specific phenotypes, it is unlikely these enzymes are just performing strictly cellular housekeeping functions important for cell viability. We hypothesize that a subset of NATs has regulatory functions important for proliferation and development of different cell-lineages.

If a subset of NATs has tissue-specific functions, we expect these NATs to have a small number of substrates and reduced redundancy with other NATs, as this would facilitate tissue-specific modulation of N^{α}-acetylation. Nevertheless, the available experimental data suggests otherwise. Recent *in vivo* and *in vitro* data showed NATs can have a high number of substrates and many show significant substrate redundancy (Arnesen et al., 2009b; Van Damme et al., 2011). Consistently, although cells deleted for dSan/dNaa50 show tissue-specific mitotic phenotypes, COFRADIC analysis of protein extracts from *Drosophila* mutant embryos for *san* identified at least two different putative substrates of dSan/dNaa50 out of 292 proteins analyzed (which is less than 2% of the *Drosophila* proteome; Chapter IV). Assuming this proportion is representative of the entire proteome, this suggests dSan/dNaa50 is likely to have at least 100 substrates. Furthermore, since these two substrates of dSan/dNaa50 (Cctγ and Pabp2) are not completely unacetylated in loss of function alleles of *san* (Chapter IV), this suggests that another partially

redundant NAT (most likely dNaa60) is capable of acetylating these two proteins *in vivo*.

In order to resolve the apparent paradox between the increased regulatory complexity of NAT activity in higher eukaryotes and the tissue-specific phenotypes on the one hand, and the partial redundancy and high number of NAT substrates on the other hand, we propose a regulatory "Net-model" for N^{α}-acetylation.

2.1. "Net model" for N^{α}-terminal acetylation

We propose that in the cases where N^{α}-acetylation has tissue-specific regulatory functions, the associated substrates will be mostly acetylated by one or two NATs (fig. 1). In contrast, in the cases where N^{α}-acetylation has housekeeping functions, the associated substrates will be acetylated by multiple NATs (fig. 1). If correct, this hypothesis would allow the modulation of N^{α}-acetylation for tissue specific functions even if most NATs were partially redundant and were likely to have a large number of substrates. Furthermore, this model suggests that although most NATs have a high number of substrates, the described knockdown phenotypes are mostly due to the loss/reduction of N^{α}-acetylation in a small subset of substrates. Consistently, whereas *san* mutant embryos show highly specific mitotic phenotypes (Pimenta-Marques et al., 2008), our COFRADIC analysis suggests this enzyme has a large number of substrates.

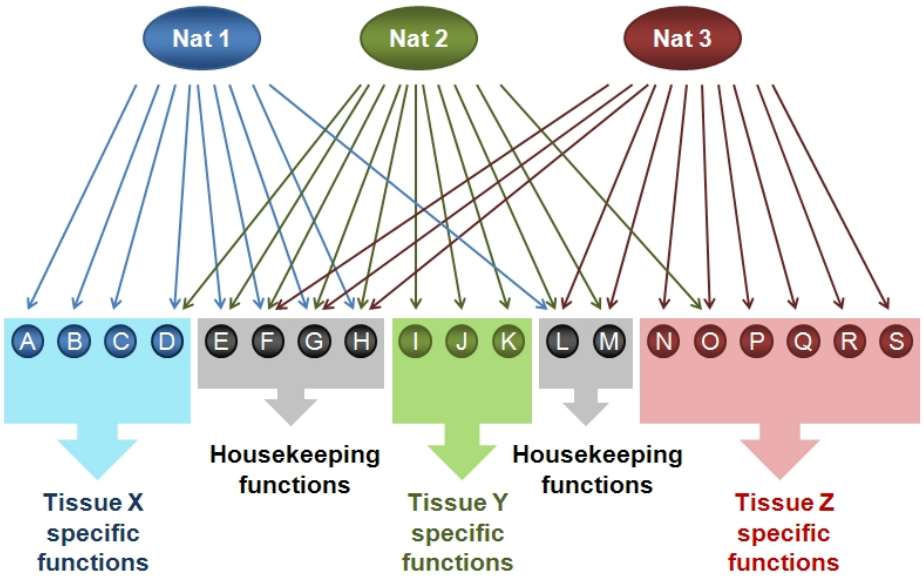

Figure 1: "Net model" hypothesis for N$^{\alpha}$-terminal acetylation. Hypothetical Nat1, Nat2 and Nat3, N$^{\alpha}$-acetylate different proteins from "A" to "S". Substrates whose acetylation has housekeeping functions are mostly acetylated by several NATs. Substrates whose acetylation has tissue-specific regulatory functions are mostly acetylated by one or two NATs.

2.2. Can different substrates require different levels of N$^{\alpha}$-terminal acetylation?

Analysis of protein N$^{\alpha}$-acetylation levels in humans, estimated that from the approximately 76% of N$^{\alpha}$-acetylated proteins, 8% were only partially N$^{\alpha}$-acetylated (Arnesen et al., 2009b). Our COFRADIC analysis suggested that wild-type *Drosophila* embryos contain a significant fraction of partially N$^{\alpha}$-acetylated proteins (Chapter IV). This suggests the total levels of N$^{\alpha}$-acetylation are differentially important for the function of different substrates. If this hypothesis is correct then the down-regulation of a given NAT activity will differentially affect the activity of its substrates as they have distinct N$^{\alpha}$-acetylation cutoffs.

Likewise, tissue-specific expression of different NATs (even if partially redundant) can differentially modulate the activity of their substrates, as they will be associated to different kinetics of N^{α}-acetylation (fig.2).

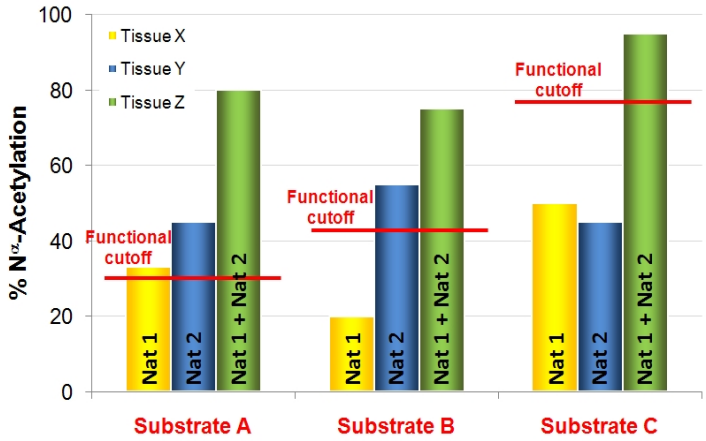

Figure 2: Different substrates require different levels of N^{α}-terminal acetylation. Tissue X expresses Nat1, tissue Y expresses Nat2 and tissue Z expresses both NATs. Red bar represents the % of N^{α}-acetylation that a given substrate requires to effectively perform its function. In tissue X, only substrate A is functional as Nat1 is not able to efficiently N^{α}-acetylate the other two substrates above the functional cutoff. In tissue Y, substrates A and B are functional as Nat2 is capable of N^{α}-acetylating these two proteins (but not substrate C) above their functional cutoff. Tissue Z expresses both NATs and all substrates are efficiently N^{α}-acetylated above their functional cutoff.

2.3. Is NATs activity modulated by cofactor proteins?

Distinct NAT activities can potentially arise from the combination of different catalytic subunits with different auxiliary subunits. For example, the paralogue catalytic subunits hNaa10 and hNaa11 and the paralogue auxiliary subunits hNaa15 and hNaa16 differentially participate in functional hNatA complexes (Arnesen et al., 2006a; Arnesen et al., 2009a). Moreover, these paralogues seem to be differentially expressed in different tissues and cell lines (Arnesen et

al., 2006a; Arnesen et al., 2009a; Pang et al., 2009; Sugiura et al., 2003). One might think that expression of different NAT complex subunits or alternative splicing of these subunits could modulate the activity of different NAT complexes. In *Drosophila*, *dnaa60* gene locus encodes two different protein isoforms due to alternative splicing (Chapter V). One possibility is that these isoforms display different NAT activities and are therefore expressed in different tissues which show differential requirements for protein N^{α}-acetylation.

3. Conclusion

Our work confirms that during *Drosophila melanogaster* development, the regulation of protein N^{α}-acetylation is unexpectedly complex and some of its functions are tissue-specific. We propose that similar to other post-translational modifications, N^{α}-acetylation has tissue-specific regulatory functions important for development and maintenance of tissue homeostasis.

4. Future work

Our goal is to better understand the function of protein N^{α}-acetylation during multicellular organism development. From our work we hypothesize that similarly to dSan/dNAA50, other NATs are likely have tissue-specific functions in higher eukaryotes (Chapter VI 1.1.).

1) To test if NATs tissue-specific functions can be obtained at transcriptional level by differential expression of these enzymes we propose to perform a systematic expression screen of the main NAT complexes subunits during *Drosophila* development. We will perform in *situ* hybridization and immunostaining experiments to detect the mRNA

and protein levels of the different NAT subunits during development, such as ovaries, testis, embryos and larval wing discs and brain neuroblasts. We expect NATs that have predominantly housekeeping functions to be ubiquitously expressed, whereas NATs with predominantly regulatory functions to have more narrowed expression profiles. If we manage to identify a NAT whose expression is highly enriched in a given tissue (or developmental stage) we will investigate the function of this enzyme during *Drosophila* development.

2) Alternatively the tissue specific functions of N^{α}-acetylation can be simply due to different combinations of partially redundant NATs that are broadly (but not ubiquitously) expressed in different tissues. Based on this hypothesis we propose a “net model”, where most tissue-specific N^{α}-acetylation events are mostly (but not exclusively) performed by one or two NATs. Since this model hypothesizes most housekeeping N^{α}-acetylation events are usually performed by multiple partially redundant NATs, than we predict most phenotypes observed in cells depleted for different NATs subunits would be only due to the loss/reduction of N^{α}-acetylation of a small subset of substrates (Chapter V 1.2.1.).

To test this we propose to analyze the N^{α}-acetylation profiles of wild-type and mutants for different subunits of the NAT complexes during *Drosophila* development. If the "net model" is correct and there is a tissue-specific combinatory code of NATs expression, than we expect some proteins will be differentially acetylated during *Drosophila* development even if most NATs show broadly expression profiles. By performing a similar analysis with different NAT mutants we should be able to identify some of the functionally relevant NATs.

3) It is also possible that the distinct NAT activities can potentially arise from the differential combination of catalytic and regulatory NAT subunits (section 2.3). To test this hypothesis we will immunopurify, using fusion-tagged proteins expressed at endogenous levels, all known NAT complexes from different tissues and identify interacting proteins by LC-MS/MS. If our hypothesis is correct we expect to identify different NAT complexes in different tissues.

If our expectations are fulfilled, the experiments previously described will provide strong evidence suggesting N^{α}-acetylation has tissue-specific functions and has evolved to accommodate regulatory functions in a developing multicellular organism.

References

(2004). Finishing the euchromatic sequence of the human genome. *Nature* **431**, 931-45.

Ackerman, P., Glover, C. V. and Osheroff, N. (1985). Phosphorylation of DNA topoisomerase II by casein kinase II: modulation of eukaryotic topoisomerase II activity in vitro. *Proc Natl Acad Sci U S A* **82**, 3164-8.

Adams, M. D. Celniker, S. E. Holt, R. A. Evans, C. A. Gocayne, J. D. Amanatides, P. G. Scherer, S. E. Li, P. W. Hoskins, R. A. Galle, R. F. et al. (2000). The genome sequence of Drosophila melanogaster. *Science* **287**, 2185-95.

Afshar, K., Stuart, B. and Wasserman, S. A. (2000). Functional analysis of the Drosophila diaphanous FH protein in early embryonic development. *Development* **127**, 1887-97.

Alexandru, G., Uhlmann, F., Mechtler, K., Poupart, M. A. and Nasmyth, K. (2001). Phosphorylation of the cohesin subunit Scc1 by Polo/Cdc5 kinase regulates sister chromatid separation in yeast. *Cell* **105**, 459-72.

Altschul, S. F., Madden, T. L., Schaffer, A. A., Zhang, J., Zhang, Z., Miller, W. and Lipman, D. J. (1997). Gapped BLAST and PSI-BLAST: a new generation of protein database search programs. *Nucleic Acids Res* **25**, 3389-402.

Ametzazurra, A., Larrea, E., Civeira, M. P., Prieto, J. and Aldabe, R. (2008). Implication of human N-alpha-acetyltransferase 5 in cellular proliferation and carcinogenesis. *Oncogene* **27**, 7296-306.

Arnesen, T., Anderson, D., Baldersheim, C., Lanotte, M., Varhaug, J. E. and Lillehaug, J. R. (2005a). Identification and characterization of the human ARD1-NATH protein acetyltransferase complex. *Biochem J* **386**, 433-43.

Arnesen, T., Anderson, D., Torsvik, J., Halseth, H. B., Varhaug, J. E. and Lillehaug, J. R. (2006a). Cloning and characterization of hNAT5/hSAN: an evolutionarily conserved component of the NatA protein N-alpha-acetyltransferase complex. *Gene* **371**, 291-5.

Arnesen, T., Betts, M. J., Pendino, F., Liberles, D. A., Anderson, D., Caro, J., Kong, X., Varhaug, J. E. and Lillehaug, J. R. (2006b). Characterization of hARD2, a processed hARD1 gene duplicate, encoding a human protein N-alpha-acetyltransferase. *BMC Biochem* **7**, 13.

Arnesen, T., Gromyko, D., Horvli, O., Fluge, O., Lillehaug, J. and Varhaug, J. E. (2005b). Expression of N-acetyl transferase human and human Arrest defective 1 proteins in thyroid neoplasms. *Thyroid* **15**, 1131-6.

Arnesen, T., Gromyko, D., Kagabo, D., Betts, M. J., Starheim, K. K., Varhaug, J. E., Anderson, D. and Lillehaug, J. R. (2009a). A novel human NatA Nalpha-terminal acetyltransferase complex: hNaa16p-hNaa10p (hNat2-hArd1). *BMC Biochem* **10**, 15.

Arnesen, T., Gromyko, D., Pendino, F., Ryningen, A., Varhaug, J. E. and Lillehaug, J. R. (2006c). Induction of apoptosis in human cells by RNAi-mediated knockdown of hARD1 and NATH, components of the protein N-alpha-acetyltransferase complex. *Oncogene* **25**, 4350-60.

Arnesen, T., Starheim, K. K., Van Damme, P., Evjenth, R., Dinh, H., Betts, M. J., Ryningen, A., Vandekerckhove, J., Gevaert, K. and Anderson, D. The chaperone-like protein HYPK acts together with NatA in cotranslational N-terminal acetylation and prevention of Huntingtin aggregation. *Mol Cell Biol* **30**, 1898-909.

Arnesen, T., Van Damme, P., Polevoda, B., Helsens, K., Evjenth, R., Colaert, N., Varhaug, J. E., Vandekerckhove, J., Lillehaug, J. R., Sherman, F. et al. (2009b). Proteomics analyses reveal the evolutionary conservation and divergence of N-terminal acetyltransferases from yeast and humans. *Proc Natl Acad Sci U S A* **106**, 8157-62.

Asaumi, M., Iijima, K., Sumioka, A., Iijima-Ando, K., Kirino, Y., Nakaya, T. and Suzuki, T. (2005). Interaction of N-terminal acetyltransferase with the cytoplasmic domain of beta-amyloid precursor protein and its effect on A beta secretion. *J Biochem* **137**, 147-55.

Askree, S. H., Yehuda, T., Smolikov, S., Gurevich, R., Hawk, J., Coker, C., Krauskopf, A., Kupiec, M. and McEachern, M. J. (2004). A genome-wide screen for Saccharomyces cerevisiae deletion mutants that affect telomere length. *Proc Natl Acad Sci U S A* **101**, 8658-63.

Bannister, A. J. and Kouzarides, T. (2005). Reversing histone methylation. *Nature* **436**, 1103-6.

Bannister, A. J., Miska, E. A., Gorlich, D. and Kouzarides, T. (2000). Acetylation of importin-alpha nuclear import factors by CBP/p300. *Curr Biol* **10**, 467-70.

Barbosa, V., Kimm, N. and Lehmann, R. (2007). A maternal screen for genes regulating Drosophila oocyte polarity uncovers new steps in meiotic progression. *Genetics* **176**, 1967-77.

Beausoleil, S. A., Villen, J., Gerber, S. A., Rush, J. and Gygi, S. P. (2006). A probability-based approach for high-throughput protein phosphorylation analysis and site localization. *Nat Biotechnol* **24**, 1285-92.

Behnia, R., Panic, B., Whyte, J. R. and Munro, S. (2004). Targeting of the Arf-like GTPase Arl3p to the Golgi requires N-terminal acetylation and the membrane protein Sys1p. *Nat Cell Biol* **6**, 405-13.

Bement, W. M., Benink, H. A. and von Dassow, G. (2005). A microtubule-dependent zone of active RhoA during cleavage plane specification. *J Cell Biol* **170**, 91-101.

Bettencourt-Dias, M., Giet, R., Sinka, R., Mazumdar, A., Lock, W. G., Balloux, F., Zafiropoulos, P. J., Yamaguchi, S., Winter, S.,

Carthew, R. W. et al. (2004). Genome-wide survey of protein kinases required for cell cycle progression. *Nature* **432**, 980-7.
Bhat, M. A., Philp, A. V., Glover, D. M. and Bellen, H. J. (1996). Chromatid segregation at anaphase requires the barren product, a novel chromosome-associated protein that interacts with Topoisomerase II. *Cell* **87**, 1103-14.
Bilton, R., Mazure, N., Trottier, E., Hattab, M., Dery, M. A., Richard, D. E., Pouyssegur, J. and Brahimi-Horn, M. C. (2005). Arrest-defective-1 protein, an acetyltransferase, does not alter stability of hypoxia-inducible factor (HIF)-1alpha and is not induced by hypoxia or HIF. *J Biol Chem* **280**, 31132-40.
Bilton, R., Trottier, E., Pouyssegur, J. and Brahimi-Horn, M. C. (2006). ARDent about acetylation and deacetylation in hypoxia signalling. *Trends Cell Biol* **16**, 616-21.
Boissel, J. P., Kasper, T. J. and Bunn, H. F. (1988). Cotranslational amino-terminal processing of cytosolic proteins. Cell-free expression of site-directed mutants of human hemoglobin. *J Biol Chem* **263**, 8443-9.
Bollen, M., Gerlich, D. W. and Lesage, B. (2009). Mitotic phosphatases: from entry guards to exit guides. *Trends Cell Biol* **19**, 531-41.
Brackley, K. I. and Grantham, J. (2009). Activities of the chaperonin containing TCP-1 (CCT): implications for cell cycle progression and cytoskeletal organisation. *Cell Stress Chaperones* **14**, 23-31.
Bradshaw, R. A., Brickey, W. W. and Walker, K. W. (1998). N-terminal processing: the methionine aminopeptidase and N alpha-acetyl transferase families. *Trends Biochem Sci* **23**, 263-7.
Brand, A. H. and Perrimon, N. (1993). Targeted gene expression as a means of altering cell fates and generating dominant phenotypes. *Development* **118**, 401-15.
Brodsky, M. H., Weinert, B. T., Tsang, G., Rong, Y. S., McGinnis, N. M., Golic, K. G., Rio, D. C. and Rubin, G. M. (2004). Drosophila melanogaster MNK/Chk2 and p53 regulate multiple DNA repair and apoptotic pathways following DNA damage. *Mol Cell Biol* **24**, 1219-31.
Brown, L., Ongusaha, P. P., Kim, H. G., Nuti, S., Mandinova, A., Lee, J. W., Khosravi-Far, R., Aaronson, S. A. and Lee, S. W. (2007). CDIP, a novel pro-apoptotic gene, regulates TNFalpha-mediated apoptosis in a p53-dependent manner. *EMBO J* **26**, 3410-22.
Buchenau, P., Saumweber, H. and Arndt-Jovin, D. J. (1993). Consequences of topoisomerase II inhibition in early embryogenesis of Drosophila revealed by in vivo confocal laser scanning microscopy. *J Cell Sci* **104 (Pt 4)**, 1175-85.
Burnett, G. and Kennedy, E. P. (1954). The enzymatic phosphorylation of proteins. *J Biol Chem* **211**, 969-80.
Caesar, R. and Blomberg, A. (2004). The stress-induced Tfs1p requires NatB-mediated acetylation to inhibit carboxypeptidase Y and to regulate the protein kinase A pathway. *J Biol Chem* **279**, 38532-43.

Caesar, R., Warringer, J. and Blomberg, A. (2006). Physiological importance and identification of novel targets for the N-terminal acetyltransferase NatB. *Eukaryot Cell* **5**, 368-78.
Camasses, A., Bogdanova, A., Shevchenko, A. and Zachariae, W. (2003). The CCT chaperonin promotes activation of the anaphase-promoting complex through the generation of functional Cdc20. *Mol Cell* **12**, 87-100.
Chintapalli, V. R., Wang, J. and Dow, J. A. (2007). Using FlyAtlas to identify better Drosophila melanogaster models of human disease. *Nat Genet* **39**, 715-20.
Chou, T. B. and Perrimon, N. (1992). Use of a yeast site-specific recombinase to produce female germline chimeras in Drosophila. *Genetics* **131**, 643-53.
Chu, C. W., Hou, F., Zhang, J., Phu, L., Loktev, A. V., Kirkpatrick, D. S., Jackson, P. K., Zhao, Y. and Zou, H. A novel acetylation of {beta}-tubulin by San modulates microtubule polymerization via down-regulating tubulin incorporation. *Mol Biol Cell*.
Chun, K. H., Cho, S. J., Choi, J. S., Kim, S. H., Kim, K. W. and Lee, S. K. (2007). Differential regulation of splicing, localization and stability of mammalian ARD1235 and ARD1225 isoforms. *Biochem Biophys Res Commun* **353**, 18-25.
Ciechanover, A. and Ben-Saadon, R. (2004). N-terminal ubiquitination: more protein substrates join in. *Trends Cell Biol* **14**, 103-6.
Ciosk, R., Shirayama, M., Shevchenko, A., Tanaka, T., Toth, A. and Nasmyth, K. (2000). Cohesin's binding to chromosomes depends on a separate complex consisting of Scc2 and Scc4 proteins. *Mol Cell* **5**, 243-54.
Clemens, J. C., Worby, C. A., Simonson-Leff, N., Muda, M., Maehama, T., Hemmings, B. A. and Dixon, J. E. (2000). Use of double-stranded RNA interference in Drosophila cell lines to dissect signal transduction pathways. *Proc Natl Acad Sci U S A* **97**, 6499-503.
Coelho, P. A., Queiroz-Machado, J. and Sunkel, C. E. (2003). Condensin-dependent localisation of topoisomerase II to an axial chromosomal structure is required for sister chromatid resolution during mitosis. *J Cell Sci* **116**, 4763-76.
Corradetti, M. N. and Guan, K. L. (2006). Upstream of the mammalian target of rapamycin: do all roads pass through mTOR? *Oncogene* **25**, 6347-60.
Coulton, A. T., East, D. A., Galinska-Rakoczy, A., Lehman, W. and Mulvihill, D. P. The recruitment of acetylated and unacetylated tropomyosin to distinct actin polymers permits the discrete regulation of specific myosins in fission yeast. *J Cell Sci* **123**, 3235-43.
Craiu, A., Gaczynska, M., Akopian, T., Gramm, C. F., Fenteany, G., Goldberg, A. L. and Rock, K. L. (1997). Lactacystin and clasto-lactacystin beta-lactone modify multiple proteasome beta-subunits and

inhibit intracellular protein degradation and major histocompatibility complex class I antigen presentation. *J Biol Chem* **272**, 13437-45.
Crawford, J. M., Harden, N., Leung, T., Lim, L. and Kiehart, D. P. (1998). Cellularization in Drosophila melanogaster is disrupted by the inhibition of rho activity and the activation of Cdc42 function. *Dev Biol* **204**, 151-64.
Cuthbert, G. L., Daujat, S., Snowden, A. W., Erdjument-Bromage, H., Hagiwara, T., Yamada, M., Schneider, R., Gregory, P. D., Tempst, P., Bannister, A. J. et al. (2004). Histone deimination antagonizes arginine methylation. *Cell* **118**, 545-53.
D'Ambrosio, C., Schmidt, C. K., Katou, Y., Kelly, G., Itoh, T., Shirahige, K. and Uhlmann, F. (2008). Identification of cis-acting sites for condensin loading onto budding yeast chromosomes. *Genes Dev* **22**, 2215-27.
D'Avino, P. P., Savoian, M. S. and Glover, D. M. (2005). Cleavage furrow formation and ingression during animal cytokinesis: a microtubule legacy. *J Cell Sci* **118**, 1549-58.
Darwiche, N., Freeman, L. A. and Strunnikov, A. (1999). Characterization of the components of the putative mammalian sister chromatid cohesion complex. *Gene* **233**, 39-47.
Dej, K. J., Ahn, C. and Orr-Weaver, T. L. (2004). Mutations in the Drosophila condensin subunit dCAP-G: defining the role of condensin for chromosome condensation in mitosis and gene expression in interphase. *Genetics* **168**, 895-906.
Dixon, S. J., Fedyshyn, Y., Koh, J. L., Prasad, T. S., Chahwan, C., Chua, G., Toufighi, K., Baryshnikova, A., Hayles, J., Hoe, K. L. et al. (2008). Significant conservation of synthetic lethal genetic interaction networks between distantly related eukaryotes. *Proc Natl Acad Sci U S A* **105**, 16653-8.
Dorsett, D., Eissenberg, J. C., Misulovin, Z., Martens, A., Redding, B. and McKim, K. (2005). Effects of sister chromatid cohesion proteins on cut gene expression during wing development in Drosophila. *Development* **132**, 4743-53.
Drapeau, M. D. (2001). The Family of Yellow-Related Drosophila melanogaster Proteins. *Biochem Biophys Res Commun* **281**, 611-3.
Driessen, H. P., de Jong, W. W., Tesser, G. I. and Bloemendal, H. (1985). The mechanism of N-terminal acetylation of proteins. *CRC Crit Rev Biochem* **18**, 281-325.
Evjenth, R., Hole, K., Karlsen, O. A., Ziegler, M., Arnesen, T. and Lillehaug, J. R. (2009). Human Naa50p (Nat5/San) displays both protein N alpha- and N epsilon-acetyltransferase activity. *J Biol Chem* **284**, 31122-9.
Fang, G., Yu, H. and Kirschner, M. W. (1998). Direct binding of CDC20 protein family members activates the anaphase-promoting complex in mitosis and G1. *Mol Cell* **2**, 163-71.

Field, C. M., Coughlin, M., Doberstein, S., Marty, T. and Sullivan, W. (2005). Characterization of anillin mutants reveals essential roles in septin localization and plasma membrane integrity. *Development* **132**, 2849-60.

Fisher, T. S., Etages, S. D., Hayes, L., Crimin, K. and Li, B. (2005). Analysis of ARD1 function in hypoxia response using retroviral RNA interference. *J Biol Chem* **280**, 17749-57.

Fluge, O., Bruland, O., Akslen, L. A., Varhaug, J. E. and Lillehaug, J. R. (2002). NATH, a novel gene overexpressed in papillary thyroid carcinomas. *Oncogene* **21**, 5056-68.

Foe, V. E. and Alberts, B. M. (1983). Studies of nuclear and cytoplasmic behaviour during the five mitotic cycles that precede gastrulation in Drosophila embryogenesis. *J Cell Sci* **61**, 31-70.

Foe, V. E., Field, C. M. and Odell, G. M. (2000). Microtubules and mitotic cycle phase modulate spatiotemporal distributions of F-actin and myosin II in Drosophila syncytial blastoderm embryos. *Development* **127**, 1767-87.

Force, A., Lynch, M., Pickett, F. B., Amores, A., Yan, Y. L. and Postlethwait, J. (1999). Preservation of duplicate genes by complementary, degenerative mutations. *Genetics* **151**, 1531-45.

Foster, K. G. and Fingar, D. C. Mammalian target of rapamycin (mTOR): conducting the cellular signaling symphony. *J Biol Chem* **285**, 14071-7.

Gandhi, R., Gillespie, P. J. and Hirano, T. (2006). Human Wapl is a cohesin-binding protein that promotes sister-chromatid resolution in mitotic prophase. *Curr Biol* **16**, 2406-17.

Gareau, J. R. and Lima, C. D. The SUMO pathway: emerging mechanisms that shape specificity, conjugation and recognition. *Nat Rev Mol Cell Biol* **11**, 861-71.

Gautschi, M., Just, S., Mun, A., Ross, S., Rucknagel, P., Dubaquie, Y., Ehrenhofer-Murray, A. and Rospert, S. (2003). The yeast N(alpha)-acetyltransferase NatA is quantitatively anchored to the ribosome and interacts with nascent polypeptides. *Mol Cell Biol* **23**, 7403-14.

Gendron, R. L., Adams, L. C. and Paradis, H. (2000). Tubedown-1, a novel acetyltransferase associated with blood vessel development. *Dev Dyn* **218**, 300-15.

Gendron, R. L., Good, W. V., Adams, L. C. and Paradis, H. (2001). Suppressed expression of tubedown-1 in retinal neovascularization of proliferative diabetic retinopathy. *Invest Ophthalmol Vis Sci* **42**, 3000-7.

Gendron, R. L., Good, W. V., Miskiewicz, E., Tucker, S., Phelps, D. L. and Paradis, H. (2006). Tubedown-1 (Tbdn-1) suppression in oxygen-induced retinopathy and in retinopathy of prematurity. *Mol Vis* **12**, 108-16.

Gerlich, D., Hirota, T., Koch, B., Peters, J. M. and Ellenberg, J. (2006). Condensin I stabilizes chromosomes mechanically through a dynamic interaction in live cells. *Curr Biol* **16**, 333-44.
Gevaert, K., Goethals, M., Martens, L., Van Damme, J., Staes, A., Thomas, G. R. and Vandekerckhove, J. (2003). Exploring proteomes and analyzing protein processing by mass spectrometric identification of sorted N-terminal peptides. *Nat Biotechnol* **21**, 566-9.
Gilboa, L. and Lehmann, R. (2004). How different is Venus from Mars? The genetics of germ-line stem cells in Drosophila females and males. *Development* **131**, 4895-905.
Gillespie, P. J. and Hirano, T. (2004). Scc2 couples replication licensing to sister chromatid cohesion in Xenopus egg extracts. *Curr Biol* **14**, 1598-603.
Glozak, M. A., Sengupta, N., Zhang, X. and Seto, E. (2005). Acetylation and deacetylation of non-histone proteins. *Gene* **363**, 15-23.
Goetze, S., Qeli, E., Mosimann, C., Staes, A., Gerrits, B., Roschitzki, B., Mohanty, S., Niederer, E. M., Laczko, E., Timmerman, E. et al. (2009). Identification and functional characterization of N-terminally acetylated proteins in Drosophila melanogaster. *PLoS Biol* **7**, e1000236.
Goshima, G., Wollman, R., Goodwin, S. S., Zhang, N., Scholey, J. M., Vale, R. D. and Stuurman, N. (2007). Genes required for mitotic spindle assembly in Drosophila S2 cells. *Science* **316**, 417-21.
Graveley, B. R., Brooks, A. N., Carlson, J. W., Duff, M. O., Landolin, J. M., Yang, L., Artieri, C. G., van Baren, M. J., Boley, N., Booth, B. W. et al. The developmental transcriptome of Drosophila melanogaster. *Nature* **471**, 473-9.
Grewal, S. I. and Rice, J. C. (2004). Regulation of heterochromatin by histone methylation and small RNAs. *Curr Opin Cell Biol* **16**, 230-8.
Grosshans, J., Wenzl, C., Herz, H. M., Bartoszewski, S., Schnorrer, F., Vogt, N., Schwarz, H. and Muller, H. A. (2005). RhoGEF2 and the formin Dia control the formation of the furrow canal by directed actin assembly during Drosophila cellularisation. *Development* **132**, 1009-20.
Gruber, S., Haering, C. H. and Nasmyth, K. (2003). Chromosomal cohesin forms a ring. *Cell* **112**, 765-77.
Haering, C. H., Lowe, J., Hochwagen, A. and Nasmyth, K. (2002). Molecular architecture of SMC proteins and the yeast cohesin complex. *Mol Cell* **9**, 773-88.
Hagstrom, K. A., Holmes, V. F., Cozzarelli, N. R. and Meyer, B. J. (2002). C. elegans condensin promotes mitotic chromosome architecture, centromere organization, and sister chromatid segregation during mitosis and meiosis. *Genes Dev* **16**, 729-42.
Hartman, T., Stead, K., Koshland, D. and Guacci, V. (2000). Pds5p is an essential chromosomal protein required for both sister chromatid

cohesion and condensation in Saccharomyces cerevisiae. *J Cell Biol* **151**, 613-26.
Hauf, S., Roitinger, E., Koch, B., Dittrich, C. M., Mechtler, K. and Peters, J. M. (2005). Dissociation of cohesin from chromosome arms and loss of arm cohesion during early mitosis depends on phosphorylation of SA2. *PLoS Biol* **3**, e69.
Heidmann, D., Horn, S., Heidmann, S., Schleiffer, A., Nasmyth, K. and Lehner, C. F. (2004). The Drosophila meiotic kleisin C(2)M functions before the meiotic divisions. *Chromosoma* **113**, 177-87.
Hermann, G. J., King, E. J. and Shaw, J. M. (1997). The yeast gene, MDM20, is necessary for mitochondrial inheritance and organization of the actin cytoskeleton. *J Cell Biol* **137**, 141-53.
Hirano, T. (2005). Condensins: organizing and segregating the genome. *Curr Biol* **15**, R265-75.
Hirota, T., Gerlich, D., Koch, B., Ellenberg, J. and Peters, J. M. (2004). Distinct functions of condensin I and II in mitotic chromosome assembly. *J Cell Sci* **117**, 6435-45.
Hofmann, I. and Munro, S. (2006). An N-terminally acetylated Arf-like GTPase is localised to lysosomes and affects their motility. *J Cell Sci* **119**, 1494-503.
Hornig, N. C. and Uhlmann, F. (2004). Preferential cleavage of chromatin-bound cohesin after targeted phosphorylation by Polo-like kinase. *EMBO J* **23**, 3144-53.
Hou, F., Chu, C. W., Kong, X., Yokomori, K. and Zou, H. (2007). The acetyltransferase activity of San stabilizes the mitotic cohesin at the centromeres in a shugoshin-independent manner. *J Cell Biol* **177**, 587-97.
Hudson, D. F., Ohta, S., Freisinger, T., Macisaac, F., Sennels, L., Alves, F., Lai, F., Kerr, A., Rappsilber, J. and Earnshaw, W. C. (2008). Molecular and genetic analysis of condensin function in vertebrate cells. *Mol Biol Cell* **19**, 3070-9.
Hudson, D. F., Vagnarelli, P., Gassmann, R. and Earnshaw, W. C. (2003). Condensin is required for nonhistone protein assembly and structural integrity of vertebrate mitotic chromosomes. *Dev Cell* **5**, 323-36.
Hwang, C. S., Shemorry, A. and Varshavsky, A. (2010). N-terminal acetylation of cellular proteins creates specific degradation signals. *Science* **327**, 973-7.
Igaki, T., Kanda, H., Yamamoto-Goto, Y., Kanuka, H., Kuranaga, E., Aigaki, T. and Miura, M. (2002). Eiger, a TNF superfamily ligand that triggers the Drosophila JNK pathway. *EMBO J* **21**, 3009-18.
Imhof, A., Yang, X. J., Ogryzko, V. V., Nakatani, Y., Wolffe, A. P. and Ge, H. (1997). Acetylation of general transcription factors by histone acetyltransferases. *Curr Biol* **7**, 689-92.
Ingram, A. K., Cross, G. A. and Horn, D. (2000). Genetic manipulation indicates that ARD1 is an essential N(infinity)-

acetyltransferase in Trypanosoma brucei. *Mol Biochem Parasitol* **111**, 309-17.
Ivanov, D. and Nasmyth, K. (2007). A physical assay for sister chromatid cohesion in vitro. *Mol Cell* **27**, 300-10.
Jaffe, A. B. and Hall, A. (2005). Rho GTPases: biochemistry and biology. *Annu Rev Cell Dev Biol* **21**, 247-69.
Jaspersen, S. L., Charles, J. F. and Morgan, D. O. (1999). Inhibitory phosphorylation of the APC regulator Hct1 is controlled by the kinase Cdc28 and the phosphatase Cdc14. *Curr Biol* **9**, 227-36.
Jeong, J. W., Bae, M. K., Ahn, M. Y., Kim, S. H., Sohn, T. K., Bae, M. H., Yoo, M. A., Song, E. J., Lee, K. J. and Kim, K. W. (2002). Regulation and destabilization of HIF-1alpha by ARD1-mediated acetylation. *Cell* **111**, 709-20.
Johnson, L. N. and Lewis, R. J. (2001). Structural basis for control by phosphorylation. *Chem Rev* **101**, 2209-42.
Jornvall, H. (1975). Acetylation of Protein N-terminal amino groups structural observations on alpha-amino acetylated proteins. *J Theor Biol* **55**, 1-12.
Kaitna, S., Pasierbek, P., Jantsch, M., Loidl, J. and Glotzer, M. (2002). The aurora B kinase AIR-2 regulates kinetochores during mitosis and is required for separation of homologous Chromosomes during meiosis. *Curr Biol* **12**, 798-812.
Kamijo, K., Ohara, N., Abe, M., Uchimura, T., Hosoya, H., Lee, J. S. and Miki, T. (2006). Dissecting the role of Rho-mediated signaling in contractile ring formation. *Mol Biol Cell* **17**, 43-55.
Karr, T. L. and Alberts, B. M. (1986). Organization of the cytoskeleton in early Drosophila embryos. *J Cell Biol* **102**, 1494-509.
Kenna, M. A. and Skibbens, R. V. (2003). Mechanical link between cohesion establishment and DNA replication: Ctf7p/Eco1p, a cohesion establishment factor, associates with three different replication factor C complexes. *Mol Cell Biol* **23**, 2999-3007.
Khan, S. N. and Khan, A. U. Role of histone acetylation in cell physiology and diseases: An update. *Clin Chim Acta* **411**, 1401-11.
Kim, S. H., Park, J. A., Kim, J. H., Lee, J. W., Seo, J. H., Jung, B. K., Chun, K. H., Jeong, J. W., Bae, M. K. and Kim, K. W. (2006). Characterization of ARD1 variants in mammalian cells. *Biochem Biophys Res Commun* **340**, 422-7.
Kim, Y. J., Cho, Y. E., Kim, Y. W., Kim, J. Y., Lee, S. and Park, J. H. (2008). Suppression of putative tumour suppressor gene GLTSCR2 expression in human glioblastomas. *J Pathol* **216**, 218-24.
Kimura, Y., Takaoka, M., Tanaka, S., Sassa, H., Tanaka, K., Polevoda, B., Sherman, F. and Hirano, H. (2000). N(alpha)-acetylation and proteolytic activity of the yeast 20 S proteasome. *J Biol Chem* **275**, 4635-9.
Kitajima, T. S., Hauf, S., Ohsugi, M., Yamamoto, T. and Watanabe, Y. (2005). Human Bub1 defines the persistent cohesion site along the

mitotic chromosome by affecting Shugoshin localization. *Curr Biol* **15**, 353-9.
Kitajima, T. S., Sakuno, T., Ishiguro, K., Iemura, S., Natsume, T., Kawashima, S. A. and Watanabe, Y. (2006). Shugoshin collaborates with protein phosphatase 2A to protect cohesin. *Nature* **441**, 46-52.
Kops, G. J., Weaver, B. A. and Cleveland, D. W. (2005). On the road to cancer: aneuploidy and the mitotic checkpoint. *Nat Rev Cancer* **5**, 773-85.
Kouzarides, T. (1999). Histone acetylases and deacetylases in cell proliferation. *Curr Opin Genet Dev* **9**, 40-8.
Kouzarides, T. (2000). Acetylation: a regulatory modification to rival phosphorylation? *EMBO J* **19**, 1176-9.
Kramer, E. R., Scheuringer, N., Podtelejnikov, A. V., Mann, M. and Peters, J. M. (2000). Mitotic regulation of the APC activator proteins CDC20 and CDH1. *Mol Biol Cell* **11**, 1555-69.
Kreher, S. A., Kwon, J. Y. and Carlson, J. R. (2005). The molecular basis of odor coding in the Drosophila larva. *Neuron* **46**, 445-56.
Kueng, S., Hegemann, B., Peters, B. H., Lipp, J. J., Schleiffer, A., Mechtler, K. and Peters, J. M. (2006). Wapl controls the dynamic association of cohesin with chromatin. *Cell* **127**, 955-67.
Kuo, H. P., Lee, D. F., Xia, W., Lai, C. C., Li, L. Y. and Hung, M. C. (2009). Phosphorylation of ARD1 by IKKbeta contributes to its destabilization and degradation. *Biochem Biophys Res Commun* **389**, 156-61.
Lee, F. J., Lin, L. W. and Smith, J. A. (1988). Purification and characterization of an N alpha-acetyltransferase from Saccharomyces cerevisiae. *J Biol Chem* **263**, 14948-55.
Lee, F. J., Lin, L. W. and Smith, J. A. (1989). N alpha-acetyltransferase deficiency alters protein synthesis in Saccharomyces cerevisiae. *FEBS Lett* **256**, 139-42.
Lee, J. S., Kamijo, K., Ohara, N., Kitamura, T. and Miki, T. (2004). MgcRacGAP regulates cortical activity through RhoA during cytokinesis. *Exp Cell Res* **293**, 275-82.
Lengronne, A., McIntyre, J., Katou, Y., Kanoh, Y., Hopfner, K. P., Shirahige, K. and Uhlmann, F. (2006). Establishment of sister chromatid cohesion at the S. cerevisiae replication fork. *Mol Cell* **23**, 787-99.
Li, M. and Zhang, P. (2009). The function of APC/CCdh1 in cell cycle and beyond. *Cell Div* **4**, 2.
Li, X., Urwyler, O. and Suter, B. Drosophila Xpd regulates Cdk7 localization, mitotic kinase activity, spindle dynamics, and chromosome segregation. *PLoS Genet* **6**, e1000876.
Lim, J. H., Park, J. W. and Chun, Y. S. (2006). Human arrest defective 1 acetylates and activates beta-catenin, promoting lung cancer cell proliferation. *Cancer Res* **66**, 10677-82.

Line, A., Stengrevics, A., Slucka, Z., Li, G., Jankevics, E. and Rees, R. C. (2002). Serological identification and expression analysis of gastric cancer-associated genes. *Br J Cancer* **86**, 1824-30.
Lodish, H. F. (2003). Molecular Cell Biology, (ed.: New York, W.H. Freeman and Company.
Longtine, M. S., Enomoto, S., Finstad, S. L. and Berman, J. (1993). Telomere-mediated plasmid segregation in Saccharomyces cerevisiae involves gene products required for transcriptional repression at silencers and telomeres. *Genetics* **133**, 171-82.
Losada, A., Hirano, M. and Hirano, T. (1998). Identification of Xenopus SMC protein complexes required for sister chromatid cohesion. *Genes Dev* **12**, 1986-97.
Losada, A., Hirano, M. and Hirano, T. (2002). Cohesin release is required for sister chromatid resolution, but not for condensin-mediated compaction, at the onset of mitosis. *Genes Dev* **16**, 3004-16.
Losada, A. and Hirano, T. (2005). Dynamic molecular linkers of the genome: the first decade of SMC proteins. *Genes Dev* **19**, 1269-87.
Losada, A., Yokochi, T. and Hirano, T. (2005). Functional contribution of Pds5 to cohesin-mediated cohesion in human cells and Xenopus egg extracts. *J Cell Sci* **118**, 2133-41.
Lowther, W. T. and Matthews, B. W. (2000). Structure and function of the methionine aminopeptidases. *Biochim Biophys Acta* **1477**, 157-67.
Lynch, M. and Force, A. (2000). The probability of duplicate gene preservation by subfunctionalization. *Genetics* **154**, 459-73.
MacRae, T. H. (1997). Tubulin post-translational modifications--enzymes and their mechanisms of action. *Eur J Biochem* **244**, 265-78.
Malen, H., Lillehaug, J. R. and Arnesen, T. (2009). The protein Nalpha-terminal acetyltransferase hNaa10p (hArd1) is phosphorylated in HEK293 cells. *BMC Res Notes* **2**, 32.
Manning, G., Whyte, D. B., Martinez, R., Hunter, T. and Sudarsanam, S. (2002). The protein kinase complement of the human genome. *Science* **298**, 1912-34.
Martin, C. and Zhang, Y. (2005). The diverse functions of histone lysine methylation. *Nat Rev Mol Cell Biol* **6**, 838-49.
Martin, D. T., Gendron, R. L., Jarzembowski, J. A., Perry, A., Collins, M. H., Pushpanathan, C., Miskiewicz, E., Castle, V. P. and Paradis, H. (2007). Tubedown expression correlates with the differentiation status and aggressiveness of neuroblastic tumors. *Clin Cancer Res* **13**, 1480-7.
Mattaj, I. W., Tollervey, D. and Seraphin, B. (1993). Small nuclear RNAs in messenger RNA and ribosomal RNA processing. *FASEB J* **7**, 47-53.
Mavrakis, M., Rikhy, R. and Lippincott-Schwartz, J. (2009). Plasma membrane polarity and compartmentalization are established before cellularization in the fly embryo. *Dev Cell* **16**, 93-104.

Mazumdar, A. and Mazumdar, M. (2002). How one becomes many: blastoderm cellularization in Drosophila melanogaster. *Bioessays* **24**, 1012-22.
McGuinness, B. E., Hirota, T., Kudo, N. R., Peters, J. M. and Nasmyth, K. (2005). Shugoshin prevents dissociation of cohesin from centromeres during mitosis in vertebrate cells. *PLoS Biol* **3**, e86.
Mellone, B. G. and Allshire, R. C. (2003). Stretching it: putting the CEN(P-A) in centromere. *Curr Opin Genet Dev* **13**, 191-8.
Midorikawa, Y., Tsutsumi, S., Taniguchi, H., Ishii, M., Kobune, Y., Kodama, T., Makuuchi, M. and Aburatani, H. (2002). Identification of genes associated with dedifferentiation of hepatocellular carcinoma with expression profiling analysis. *Jpn J Cancer Res* **93**, 636-43.
Moldovan, G. L., Pfander, B. and Jentsch, S. (2006). PCNA controls establishment of sister chromatid cohesion during S phase. *Mol Cell* **23**, 723-32.
Moorhead, G. B., Trinkle-Mulcahy, L. and Ulke-Lemee, A. (2007). Emerging roles of nuclear protein phosphatases. *Nat Rev Mol Cell Biol* **8**, 234-44.
Moreno, E., Yan, M. and Basler, K. (2002). Evolution of TNF signaling mechanisms: JNK-dependent apoptosis triggered by Eiger, the Drosophila homolog of the TNF superfamily. *Curr Biol* **12**, 1263-8.
Morgan, D. O. (2007). The Cell Cycle: Principles of Control.
Mullen, J. R., Kayne, P. S., Moerschell, R. P., Tsunasawa, S., Gribskov, M., Colavito-Shepanski, M., Grunstein, M., Sherman, F. and Sternglanz, R. (1989). Identification and characterization of genes and mutants for an N-terminal acetyltransferase from yeast. *EMBO J* **8**, 2067-75.
Muller, H., Schmidt, D., Steinbrink, S., Mirgorodskaya, E., Lehmann, V., Habermann, K., Dreher, F., Gustavsson, N., Kessler, T., Lehrach, H. et al. Proteomic and functional analysis of the mitotic Drosophila centrosome. *EMBO J* **29**, 3344-57.
Murray, A. W. (2004). Recycling the cell cycle: cyclins revisited. *Cell* **116**, 221-34.
Nakayama, K. I. and Nakayama, K. (2006). Ubiquitin ligases: cell-cycle control and cancer. *Nat Rev Cancer* **6**, 369-81.
Noble, D., Kenna, M. A., Dix, M., Skibbens, R. V., Unal, E. and Guacci, V. (2006). Intersection between the regulators of sister chromatid cohesion establishment and maintenance in budding yeast indicates a multi-step mechanism. *Cell Cycle* **5**, 2528-36.
Nowak, M. A., Boerlijst, M. C., Cooke, J. and Smith, J. M. (1997). Evolution of genetic redundancy. *Nature* **388**, 167-71.
Ocampo-Hafalla, M. T., Katou, Y., Shirahige, K. and Uhlmann, F. (2007). Displacement and re-accumulation of centromeric cohesin during transient pre-anaphase centromere splitting. *Chromosoma* **116**, 531-44.

Ohta, T. (1988). Time for acquiring a new gene by duplication. *Proc Natl Acad Sci U S A* **85**, 3509-12.
Okahara, F., Itoh, K., Nakagawara, A., Murakami, M., Kanaho, Y. and Maehama, T. (2006). Critical role of PICT-1, a tumor suppressor candidate, in phosphatidylinositol 3,4,5-trisphosphate signals and tumorigenic transformation. *Mol Biol Cell* **17**, 4888-95.
Oliveira, R. A., Hamilton, R. S., Pauli, A., Davis, I. and Nasmyth, K. Cohesin cleavage and Cdk inhibition trigger formation of daughter nuclei. *Nat Cell Biol* **12**, 185-92.
Olsen, J. V., Blagoev, B., Gnad, F., Macek, B., Kumar, C., Mortensen, P. and Mann, M. (2006). Global, in vivo, and site-specific phosphorylation dynamics in signaling networks. *Cell* **127**, 635-48.
Ono, T., Fang, Y., Spector, D. L. and Hirano, T. (2004). Spatial and temporal regulation of Condensins I and II in mitotic chromosome assembly in human cells. *Mol Biol Cell* **15**, 3296-308.
Ono, T., Losada, A., Hirano, M., Myers, M. P., Neuwald, A. F. and Hirano, T. (2003). Differential contributions of condensin I and condensin II to mitotic chromosome architecture in vertebrate cells. *Cell* **115**, 109-21.
Ouspenski, II, Elledge, S. J. and Brinkley, B. R. (1999). New yeast genes important for chromosome integrity and segregation identified by dosage effects on genome stability. *Nucleic Acids Res* **27**, 3001-8.
Padash Barmchi, M., Rogers, S. and Hacker, U. (2005). DRhoGEF2 regulates actin organization and contractility in the Drosophila blastoderm embryo. *J Cell Biol* **168**, 575-85.
Pang, A. L., Peacock, S., Johnson, W., Bear, D. H., Rennert, O. M. and Chan, W. Y. (2009). Cloning, characterization, and expression analysis of the novel acetyltransferase retrogene Ard1b in the mouse. *Biol Reprod* **81**, 302-9.
Panizza, S., Tanaka, T., Hochwagen, A., Eisenhaber, F. and Nasmyth, K. (2000). Pds5 cooperates with cohesin in maintaining sister chromatid cohesion. *Curr Biol* **10**, 1557-64.
Paradis, H., Islam, T., Tucker, S., Tao, L., Koubi, S. and Gendron, R. L. (2008). Tubedown associates with cortactin and controls permeability of retinal endothelial cells to albumin. *J Cell Sci* **121**, 1965-72.
Paradis, H., Liu, C. Y., Saika, S., Azhar, M., Doetschman, T., Good, W. V., Nayak, R., Laver, N., Kao, C. W., Kao, W. W. et al. (2002). Tubedown-1 in remodeling of the developing vitreal vasculature in vivo and regulation of capillary outgrowth in vitro. *Dev Biol* **249**, 140-55.
Park, E. C. and Szostak, J. W. (1992). ARD1 and NAT1 proteins form a complex that has N-terminal acetyltransferase activity. *EMBO J* **11**, 2087-93.
Persson, B., Flinta, C., von Heijne, G. and Jornvall, H. (1985). Structures of N-terminally acetylated proteins. *Eur J Biochem* **152**, 523-7.

Peters, J. M. (2006). The anaphase promoting complex/cyclosome: a machine designed to destroy. *Nat Rev Mol Cell Biol* **7**, 644-56.
Pickart, C. M. and Eddins, M. J. (2004). Ubiquitin: structures, functions, mechanisms. *Biochim Biophys Acta* **1695**, 55-72.
Pimenta-Marques, A., Tostoes, R., Marty, T., Barbosa, V., Lehmann, R. and Martinho, R. G. (2008). Differential requirements of a mitotic acetyltransferase in somatic and germ line cells. *Dev Biol* **323**, 197-206.
Polevoda, B., Brown, S., Cardillo, T. S., Rigby, S. and Sherman, F. (2008). Yeast N(alpha)-terminal acetyltransferases are associated with ribosomes. *J Cell Biochem* **103**, 492-508.
Polevoda, B., Cardillo, T. S., Doyle, T. C., Bedi, G. S. and Sherman, F. (2003). Nat3p and Mdm20p are required for function of yeast NatB Nalpha-terminal acetyltransferase and of actin and tropomyosin. *J Biol Chem* **278**, 30686-97.
Polevoda, B., Norbeck, J., Takakura, H., Blomberg, A. and Sherman, F. (1999). Identification and specificities of N-terminal acetyltransferases from Saccharomyces cerevisiae. *EMBO J* **18**, 6155-68.
Polevoda, B. and Sherman, F. (2000). Nalpha -terminal acetylation of eukaryotic proteins. *J Biol Chem* **275**, 36479-82.
Polevoda, B. and Sherman, F. (2001). NatC Nalpha-terminal acetyltransferase of yeast contains three subunits, Mak3p, Mak10p, and Mak31p. *J Biol Chem* **276**, 20154-9.
Polevoda, B. and Sherman, F. (2002). The diversity of acetylated proteins. *Genome Biol* **3**, reviews0006.
Polevoda, B. and Sherman, F. (2003a). Composition and function of the eukaryotic N-terminal acetyltransferase subunits. *Biochem Biophys Res Commun* **308**, 1-11.
Polevoda, B. and Sherman, F. (2003b). N-terminal acetyltransferases and sequence requirements for N-terminal acetylation of eukaryotic proteins. *J Mol Biol* **325**, 595-622.
Rankin, S., Ayad, N. G. and Kirschner, M. W. (2005). Sororin, a substrate of the anaphase-promoting complex, is required for sister chromatid cohesion in vertebrates. *Mol Cell* **18**, 185-200.
Ren, T., Jiang, B., Jin, G., Li, J., Dong, B., Zhang, J., Meng, L., Wu, J. and Shou, C. (2008). Generation of novel monoclonal antibodies and their application for detecting ARD1 expression in colorectal cancer. *Cancer Lett* **264**, 83-92.
Riedel, C. G., Katis, V. L., Katou, Y., Mori, S., Itoh, T., Helmhart, W., Galova, M., Petronczki, M., Gregan, J., Cetin, B. et al. (2006). Protein phosphatase 2A protects centromeric sister chromatid cohesion during meiosis I. *Nature* **441**, 53-61.
Rieder, C. L., Cole, R. W., Khodjakov, A. and Sluder, G. (1995). The checkpoint delaying anaphase in response to chromosome

monoorientation is mediated by an inhibitory signal produced by unattached kinetochores. *J Cell Biol* **130**, 941-8.
Rieder, C. L. and Maiato, H. (2004). Stuck in division or passing through: what happens when cells cannot satisfy the spindle assembly checkpoint. *Dev Cell* **7**, 637-51.
Rieder, C. L., Schultz, A., Cole, R. and Sluder, G. (1994). Anaphase onset in vertebrate somatic cells is controlled by a checkpoint that monitors sister kinetochore attachment to the spindle. *J Cell Biol* **127**, 1301-10.
Roberts, D. B. (1998). Drosophila: A Practical Approach, (ed. O. U. Press).
Rock, K. L., Gramm, C., Rothstein, L., Clark, K., Stein, R., Dick, L., Hwang, D. and Goldberg, A. L. (1994). Inhibitors of the proteasome block the degradation of most cell proteins and the generation of peptides presented on MHC class I molecules. *Cell* **78**, 761-71.
Rolef Ben-Shahar, T., Heeger, S., Lehane, C., East, P., Flynn, H., Skehel, M. and Uhlmann, F. (2008). Eco1-dependent cohesin acetylation during establishment of sister chromatid cohesion. *Science* **321**, 563-6.
Rollins, R. A., Morcillo, P. and Dorsett, D. (1999). Nipped-B, a Drosophila homologue of chromosomal adherins, participates in activation by remote enhancers in the cut and Ultrabithorax genes. *Genetics* **152**, 577-93.
Roth, S. Y., Denu, J. M. and Allis, C. D. (2001). Histone acetyltransferases. *Annu Rev Biochem* **70**, 81-120.
Rowland, B. D., Roig, M. B., Nishino, T., Kurze, A., Uluocak, P., Mishra, A., Beckouet, F., Underwood, P., Metson, J., Imre, R. et al. (2009). Building sister chromatid cohesion: smc3 acetylation counteracts an antiestablishment activity. *Mol Cell* **33**, 763-74.
Rubenstein, P. and Deuchler, J. (1979). Acetylated and nonacetylated actins in Dictyostelium discoideum. *J Biol Chem* **254**, 11142-7.
Saka, Y., Sutani, T., Yamashita, Y., Saitoh, S., Takeuchi, M., Nakaseko, Y. and Yanagida, M. (1994). Fission yeast cut3 and cut14, members of a ubiquitous protein family, are required for chromosome condensation and segregation in mitosis. *EMBO J* **13**, 4938-52.
Salic, A., Waters, J. C. and Mitchison, T. J. (2004). Vertebrate shugoshin links sister centromere cohesion and kinetochore microtubule stability in mitosis. *Cell* **118**, 567-78.
Sanchez-Puig, N. and Fersht, A. R. (2006). Characterization of the native and fibrillar conformation of the human Nalpha-acetyltransferase ARD1. *Protein Sci* **15**, 1968-76.
Savvidou, E., Cobbe, N., Steffensen, S., Cotterill, S. and Heck, M. M. (2005). Drosophila CAP-D2 is required for condensin complex stability and resolution of sister chromatids. *J Cell Sci* **118**, 2529-43.

Schmitz, J., Watrin, E., Lenart, P., Mechtler, K. and Peters, J. M. (2007). Sororin is required for stable binding of cohesin to chromatin and for sister chromatid cohesion in interphase. *Curr Biol* **17**, 630-6.
Scroggins, B. T., Robzyk, K., Wang, D., Marcu, M. G., Tsutsumi, S., Beebe, K., Cotter, R. J., Felts, S., Toft, D., Karnitz, L. et al. (2007). An acetylation site in the middle domain of Hsp90 regulates chaperone function. *Mol Cell* **25**, 151-9.
Seo, J. and Lee, K. J. (2004). Post-translational modifications and their biological functions: proteomic analysis and systematic approaches. *J Biochem Mol Biol* **37**, 35-44.
Seo, J. H., Cha, J. H., Park, J. H., Jeong, C. H., Park, Z. Y., Lee, H. S., Oh, S. H., Kang, J. H., Suh, S. W., Kim, K. H. et al. Arrest defective 1 autoacetylation is a critical step in its ability to stimulate cancer cell proliferation. *Cancer Res* **70**, 4422-32.
Setty, S. R., Strochlic, T. I., Tong, A. H., Boone, C. and Burd, C. G. (2004). Golgi targeting of ARF-like GTPase Arl3p requires its Nalpha-acetylation and the integral membrane protein Sys1p. *Nat Cell Biol* **6**, 414-9.
Shen, Q., Zheng, X., McNutt, M. A., Guang, L., Sun, Y., Wang, J., Gong, Y., Hou, L. and Zhang, B. (2009). NAT10, a nucleolar protein, localizes to the midbody and regulates cytokinesis and acetylation of microtubules. *Exp Cell Res* **315**, 1653-67.
Sherman, F., Stewart, J. W. and Tsunasawa, S. (1985). Methionine or not methionine at the beginning of a protein. *Bioessays* **3**, 27-31.
Sigrist, C. J., Cerutti, L., de Castro, E., Langendijk-Genevaux, P. S., Bulliard, V., Bairoch, A. and Hulo, N. PROSITE, a protein domain database for functional characterization and annotation. *Nucleic Acids Res* **38**, D161-6.
Singer, J. M. and Shaw, J. M. (2003). Mdm20 protein functions with Nat3 protein to acetylate Tpm1 protein and regulate tropomyosin-actin interactions in budding yeast. *Proc Natl Acad Sci U S A* **100**, 7644-9.
Smith, J. S., Tachibana, I., Pohl, U., Lee, H. K., Thanarajasingam, U., Portier, B. P., Ueki, K., Ramaswamy, S., Billings, S. J., Mohrenweiser, H. W. et al. (2000). A transcript map of the chromosome 19q-arm glioma tumor suppressor region. *Genomics* **64**, 44-50.
Somers, W. G. and Saint, R. (2003). A RhoGEF and Rho family GTPase-activating protein complex links the contractile ring to cortical microtubules at the onset of cytokinesis. *Dev Cell* **4**, 29-39.
Somma, M. P., Fasulo, B., Cenci, G., Cundari, E. and Gatti, M. (2002). Molecular dissection of cytokinesis by RNA interference in Drosophila cultured cells. *Mol Biol Cell* **13**, 2448-60.
Song, O. K., Wang, X., Waterborg, J. H. and Sternglanz, R. (2003). An Nalpha-acetyltransferase responsible for acetylation of the N-terminal residues of histones H4 and H2A. *J Biol Chem* **278**, 38109-12.

Song, Y. H. (2005). Drosophila melanogaster: a model for the study of DNA damage checkpoint response. *Mol Cells* **19**, 167-79.
Sonnichsen, B., Koski, L. B., Walsh, A., Marschall, P., Neumann, B., Brehm, M., Alleaume, A. M., Artelt, J., Bettencourt, P., Cassin, E. et al. (2005). Full-genome RNAi profiling of early embryogenesis in Caenorhabditis elegans. *Nature* **434**, 462-9.
Sousa-Nunes, R., Chia, W. and Somers, W. G. (2009). Protein phosphatase 4 mediates localization of the Miranda complex during Drosophila neuroblast asymmetric divisions. *Genes Dev* **23**, 359-72.
Spiro, R. G. (2002). Protein glycosylation: nature, distribution, enzymatic formation, and disease implications of glycopeptide bonds. *Glycobiology* **12**, 43R-56R.
Starheim, K. K., Arnesen, T., Gromyko, D., Ryningen, A., Varhaug, J. E. and Lillehaug, J. R. (2008). Identification of the human N(alpha)-acetyltransferase complex B (hNatB): a complex important for cell-cycle progression. *Biochem J* **415**, 325-31.
Starheim, K. K., Gromyko, D., Evjenth, R., Ryningen, A., Varhaug, J. E., Lillehaug, J. R. and Arnesen, T. (2009a). Knockdown of human N alpha-terminal acetyltransferase complex C leads to p53-dependent apoptosis and aberrant human Arl8b localization. *Mol Cell Biol* **29**, 3569-81.
Starheim, K. K., Gromyko, D., Velde, R., Varhaug, J. E. and Arnesen, T. (2009b). Composition and biological significance of the human Nalpha-terminal acetyltransferases. *BMC Proc* **3 Suppl 6**, S3.
Steffensen, S., Coelho, P. A., Cobbe, N., Vass, S., Costa, M., Hassan, B., Prokopenko, S. N., Bellen, H., Heck, M. M. and Sunkel, C. E. (2001). A role for Drosophila SMC4 in the resolution of sister chromatids in mitosis. *Curr Biol* **11**, 295-307.
Stone, E. M., Swanson, M. J., Romeo, A. M., Hicks, J. B. and Sternglanz, R. (1991). The SIR1 gene of Saccharomyces cerevisiae and its role as an extragenic suppressor of several mating-defective mutants. *Mol Cell Biol* **11**, 2253-62.
Strunnikov, A. V., Hogan, E. and Koshland, D. (1995). SMC2, a Saccharomyces cerevisiae gene essential for chromosome segregation and condensation, defines a subgroup within the SMC family. *Genes Dev* **9**, 587-99.
Sugiura, N., Adams, S. M. and Corriveau, R. A. (2003). An evolutionarily conserved N-terminal acetyltransferase complex associated with neuronal development. *J Biol Chem* **278**, 40113-20.
Sugiura, N., Patel, R. G. and Corriveau, R. A. (2001). N-methyl-D-aspartate receptors regulate a group of transiently expressed genes in the developing brain. *J Biol Chem* **276**, 14257-63.
Sullivan, M. and Morgan, D. O. (2007). Finishing mitosis, one step at a time. *Nat Rev Mol Cell Biol* **8**, 894-903.

Sullivan, W. and Theurkauf, W. E. (1995). The cytoskeleton and morphogenesis of the early Drosophila embryo. *Curr Opin Cell Biol* **7**, 18-22.

Sumara, I., Vorlaufer, E., Gieffers, C., Peters, B. H. and Peters, J. M. (2000). Characterization of vertebrate cohesin complexes and their regulation in prophase. *J Cell Biol* **151**, 749-62.

Sumara, I., Vorlaufer, E., Stukenberg, P. T., Kelm, O., Redemann, N., Nigg, E. A. and Peters, J. M. (2002). The dissociation of cohesin from chromosomes in prophase is regulated by Polo-like kinase. *Mol Cell* **9**, 515-25.

Takahashi, T. S., Yiu, P., Chou, M. F., Gygi, S. and Walter, J. C. (2004). Recruitment of Xenopus Scc2 and cohesin to chromatin requires the pre-replication complex. *Nat Cell Biol* **6**, 991-6.

Tamura, K., Dudley, J., Nei, M. and Kumar, S. (2007). MEGA4: Molecular Evolutionary Genetics Analysis (MEGA) software version 4.0. *Mol Biol Evol* **24**, 1596-9.

Tanaka, K., Hao, Z., Kai, M. and Okayama, H. (2001). Establishment and maintenance of sister chromatid cohesion in fission yeast by a unique mechanism. *EMBO J* **20**, 5779-90.

Tang, Z., Shu, H., Qi, W., Mahmood, N. A., Mumby, M. C. and Yu, H. (2006). PP2A is required for centromeric localization of Sgo1 and proper chromosome segregation. *Dev Cell* **10**, 575-85.

Tang, Z., Sun, Y., Harley, S. E., Zou, H. and Yu, H. (2004). Human Bub1 protects centromeric sister-chromatid cohesion through Shugoshin during mitosis. *Proc Natl Acad Sci U S A* **101**, 18012-7.

Tatsumoto, T., Xie, X., Blumenthal, R., Okamoto, I. and Miki, T. (1999). Human ECT2 is an exchange factor for Rho GTPases, phosphorylated in G2/M phases, and involved in cytokinesis. *J Cell Biol* **147**, 921-8.

Tercero, J. C., Dinman, J. D. and Wickner, R. B. (1993). Yeast MAK3 N-acetyltransferase recognizes the N-terminal four amino acids of the major coat protein (gag) of the L-A double-stranded RNA virus. *J Bacteriol* **175**, 3192-4.

Tomonaga, T., Nagao, K., Kawasaki, Y., Furuya, K., Murakami, A., Morishita, J., Yuasa, T., Sutani, T., Kearsey, S. E., Uhlmann, F. et al. (2000). Characterization of fission yeast cohesin: essential anaphase proteolysis of Rad21 phosphorylated in the S phase. *Genes Dev* **14**, 2757-70.

Uemura, T., Ohkura, H., Adachi, Y., Morino, K., Shiozaki, K. and Yanagida, M. (1987). DNA topoisomerase II is required for condensation and separation of mitotic chromosomes in S. pombe. *Cell* **50**, 917-25.

Uhlmann, F. (2001). Secured cutting: controlling separase at the metaphase to anaphase transition. *EMBO Rep* **2**, 487-92.

Uhlmann, F., Lottspeich, F. and Nasmyth, K. (1999). Sister-chromatid separation at anaphase onset is promoted by cleavage of the cohesin subunit Scc1. *Nature* **400**, 37-42.

Unal, E., Heidinger-Pauli, J. M., Kim, W., Guacci, V., Onn, I., Gygi, S. P. and Koshland, D. E. (2008). A molecular determinant for the establishment of sister chromatid cohesion. *Science* **321**, 566-9.

Unal, E., Heidinger-Pauli, J. M. and Koshland, D. (2007). DNA double-strand breaks trigger genome-wide sister-chromatid cohesion through Eco1 (Ctf7). *Science* **317**, 245-8.

Vagnarelli, P., Hudson, D. F., Ribeiro, S. A., Trinkle-Mulcahy, L., Spence, J. M., Lai, F., Farr, C. J., Lamond, A. I. and Earnshaw, W. C. (2006). Condensin and Repo-Man-PP1 co-operate in the regulation of chromosome architecture during mitosis. *Nat Cell Biol* **8**, 1133-42.

Van Damme, P., K. Hole, A. Pimenta-Marques, K. Helsens, J. Vandekerckhove, R.G. Martinho, K. Gevaert, T. Arnesen. (2011). NatF contributes to an evolutionary shift in protein N-terminal acetylation and is important for normal chromosome segregation *PLoS Genet*.

Van Damme, P., Van Damme, J., Demol, H., Staes, A., Vandekerckhove, J. and Gevaert, K. (2009). A review of COFRADIC techniques targeting protein N-terminal acetylation. *BMC Proc* **3 Suppl 6**, S6.

Vass, S., Cotterill, S., Valdeolmillos, A. M., Barbero, J. L., Lin, E., Warren, W. D. and Heck, M. M. (2003). Depletion of Drad21/Scc1 in Drosophila cells leads to instability of the cohesin complex and disruption of mitotic progression. *Curr Biol* **13**, 208-18.

Verni, F., Gandhi, R., Goldberg, M. L. and Gatti, M. (2000). Genetic and molecular analysis of wings apart-like (wapl), a gene controlling heterochromatin organization in Drosophila melanogaster. *Genetics* **154**, 1693-710.

Vetting, M. W., LP, S. d. C., Yu, M., Hegde, S. S., Magnet, S., Roderick, S. L. and Blanchard, J. S. (2005). Structure and functions of the GNAT superfamily of acetyltransferases. *Arch Biochem Biophys* **433**, 212-26.

Virshup, D. M. and Shenolikar, S. (2009). From promiscuity to precision: protein phosphatases get a makeover. *Mol Cell* **33**, 537-45.

Visintin, R., Craig, K., Hwang, E. S., Prinz, S., Tyers, M. and Amon, A. (1998). The phosphatase Cdc14 triggers mitotic exit by reversal of Cdk-dependent phosphorylation. *Mol Cell* **2**, 709-18.

Wall, D. S., Gendron, R. L., Good, W. V., Miskiewicz, E., Woodland, M., Leblanc, K. and Paradis, H. (2004). Conditional knockdown of tubedown-1 in endothelial cells leads to neovascular retinopathy. *Invest Ophthalmol Vis Sci* **45**, 3704-12.

Walsh, C. T., Garneau-Tsodikova, S. and Gatto, G. J., Jr. (2005). Protein posttranslational modifications: the chemistry of proteome diversifications. *Angew Chem Int Ed Engl* **44**, 7342-72.

Walsh, J. B. (1995). How often do duplicated genes evolve new functions? *Genetics* **139**, 421-8.
Wang, J. C. (2002). Cellular roles of DNA topoisomerases: a molecular perspective. *Nat Rev Mol Cell Biol* **3**, 430-40.
Wang, Y., Mijares, M., Gall, M. D., Turan, T., Javier, A., Bornemann, D. J., Manage, K. and Warrior, R. Drosophila variable nurse cells encodes arrest defective 1 (ARD1), the catalytic subunit of the major N-terminal acetyltransferase complex. *Dev Dyn*.
Watanabe, Y. and Kitajima, T. S. (2005). Shugoshin protects cohesin complexes at centromeres. *Philos Trans R Soc Lond B Biol Sci* **360**, 515-21, discussion 521.
Watrin, E., Schleiffer, A., Tanaka, K., Eisenhaber, F., Nasmyth, K. and Peters, J. M. (2006). Human Scc4 is required for cohesin binding to chromatin, sister-chromatid cohesion, and mitotic progression. *Curr Biol* **16**, 863-74.
Weissman, A. M. (2001). Themes and variations on ubiquitylation. *Nat Rev Mol Cell Biol* **2**, 169-78.
Wenzlau, J. M., Garl, P. J., Simpson, P., Stenmark, K. R., West, J., Artinger, K. B., Nemenoff, R. A. and Weiser-Evans, M. C. (2006). Embryonic growth-associated protein is one subunit of a novel N-terminal acetyltransferase complex essential for embryonic vascular development. *Circ Res* **98**, 846-55.
Wickner, R. B. and Toh-e, A. (1982). [HOK], a new yeast non-Mendelian trait, enables a replication-defective killer plasmid to be maintained. *Genetics* **100**, 159-74.
Wignall, S. M., Deehan, R., Maresca, T. J. and Heald, R. (2003). The condensin complex is required for proper spindle assembly and chromosome segregation in Xenopus egg extracts. *J Cell Biol* **161**, 1041-51.
Williams, B. C., Garrett-Engele, C. M., Li, Z., Williams, E. V., Rosenman, E. D. and Goldberg, M. L. (2003). Two putative acetyltransferases, san and deco, are required for establishing sister chromatid cohesion in Drosophila. *Curr Biol* **13**, 2025-36.
Willis, D. M., Loewy, A. P., Charlton-Kachigian, N., Shao, J. S., Ornitz, D. M. and Towler, D. A. (2002). Regulation of osteocalcin gene expression by a novel Ku antigen transcription factor complex. *J Biol Chem* **277**, 37280-91.
Wullschleger, S., Loewith, R. and Hall, M. N. (2006). TOR signaling in growth and metabolism. *Cell* **124**, 471-84.
Xiong, B. and Gerton, J. L. Regulators of the cohesin network. *Annu Rev Biochem* **79**, 131-53.
Yanagida, M. (2009). Clearing the way for mitosis: is cohesin a target? *Nat Rev Mol Cell Biol* **10**, 489-96.
Yang, X. J. (2004). Lysine acetylation and the bromodomain: a new partnership for signaling. *Bioessays* **26**, 1076-87.

Yu, H. (2002). Regulation of APC-Cdc20 by the spindle checkpoint. *Curr Opin Cell Biol* **14**, 706-14.

Yu, M., Gong, J., Ma, M., Yang, H., Lai, J., Wu, H., Li, L. and Tan, D. (2009). Immunohistochemical analysis of human arrest-defective-1 expressed in cancers in vivo. *Oncol Rep* **21**, 909-15.

Zachariae, W., Schwab, M., Nasmyth, K. and Seufert, W. (1998). Control of cyclin ubiquitination by CDK-regulated binding of Hct1 to the anaphase promoting complex. *Science* **282**, 1721-4.

Zhang, J., Shi, X., Li, Y., Kim, B. J., Jia, J., Huang, Z., Yang, T., Fu, X., Jung, S. Y., Wang, Y. et al. (2008). Acetylation of Smc3 by Eco1 is required for S phase sister chromatid cohesion in both human and yeast. *Mol Cell* **31**, 143-51.

APPENDIX

OPEN ACCESS Freely available online

PLoS GENETICS

NatF Contributes to an Evolutionary Shift in Protein N-Terminal Acetylation and Is Important for Normal Chromosome Segregation

Petra Van Damme[1,2☯], Kristine Hole[3,4☯], Ana Pimenta-Marques[5☯], Kenny Helsens[1,2], Joël Vandekerckhove[1,2], Rui G. Martinho[5], Kris Gevaert[1,2], Thomas Arnesen[3,6*]

1 Department of Medical Protein Research, Ghent University, Ghent, Belgium, **2** Department of Biochemistry, Ghent University, Ghent, Belgium, **3** Department of Molecular Biology, University of Bergen, Bergen, Norway, **4** Department of Surgical Sciences, University of Bergen, Bergen, Norway, **5** Instituto Gulbenkian de Ciência, Oeiras, Portugal, **6** Department of Surgery, Haukeland University Hospital, Bergen, Norway

Abstract

N-terminal acetylation (N-Ac) is a highly abundant eukaryotic protein modification. Proteomics revealed a significant increase in the occurrence of N-Ac from lower to higher eukaryotes, but evidence explaining the underlying molecular mechanism(s) is currently lacking. We first analysed protein N-termini and their acetylation degrees, suggesting that evolution of substrates is not a major cause for the evolutionary shift in N-Ac. Further, we investigated the presence of putative N-terminal acetyltransferases (NATs) in higher eukaryotes. The purified recombinant human and *Drosophila* homologues of a novel NAT candidate was subjected to *in vitro* peptide library acetylation assays. This provided evidence for its NAT activity targeting Met-Lys- and other Met-starting protein N-termini, and the enzyme was termed Naa60p and its activity NatF. Its *in vivo* activity was investigated by ectopically expressing human Naa60p in yeast followed by N-terminal COFRADIC analyses. hNaa60p acetylated distinct Met-starting yeast protein N-termini and increased general acetylation levels, thereby altering yeast *in vivo* acetylation patterns towards those of higher eukaryotes. Further, its activity in human cells was verified by overexpression and knockdown of hNAA60 followed by N-terminal COFRADIC. NatF's cellular impact was demonstrated in *Drosophila* cells where NAA60 knockdown induced chromosomal segregation defects. In summary, our study revealed a novel major protein modifier contributing to the evolution of N-Ac, redundancy among NATs, and an essential regulator of normal chromosome segregation. With the characterization of NatF, the co-translational N-Ac machinery appears complete since all the major substrate groups in eukaryotes are accounted for.

Citation: Van Damme P, Hole K, Pimenta-Marques A, Helsens K, Vandekerckhove J, et al. (2011) NatF Contributes to an Evolutionary Shift in Protein N-Terminal Acetylation and Is Important for Normal Chromosome Segregation. PLoS Genet 7(7): e1002169. doi:10.1371/journal.pgen.1002169

Editor: Michael Snyder, Stanford University School of Medicine, United States of America

Received January 17, 2011; **Accepted** May 20, 2011; **Published** July 7, 2011

Funding: The authors acknowledge support of research grants from the Fund for Scientific Research - Flanders (Belgium) (project numbers G.0042.07 and G.0440.10), the Concerted Research Actions (project BOF07/GOA/012) from the Ghent University, the Inter University Attraction Poles (IUAP06), the Norwegian Research Council (Grant 197136) and the Norwegian Cancer Society, Fundacao para Ciencia e Tecnologia [PPCDT/DG/BIA/82013/2006 and PTDC/BIA-BCM/69256/2006], and Association for International Cancer Research [AICR 10-0553]. P Van Damme and K Helsens are Postdoctoral Fellows of the Research Foundation - Flanders (FWO-Vlaanderen). A Pimenta-Marques has a fellowship from Fundacao para a Ciencia e Tecnologia [SFRH/BD/28767/2006]. The funders had no role in study design, data collection and analysis, decision to publish, or preparation of the manuscript.

Competing Interests: The authors have declared that no competing interests exist.

* E-mail: Thomas.Arnesen@mbi.uib.no

☯ These authors contributed equally to this work.

Introduction

N-terminal acetylation (N-Ac) is a common modification of proteins, but its general role has remained rather enigmatic. For specific proteins, N-Ac is recognized as an important regulator of function and localization [1–4]. Recently, it was suggested that it may act as a general destabilization signal for some yeast proteins, [5] while other reports imply that it might serve as a stabilizer, for instance by blocking N-terminal ubiquitination mediated degradation [6]. N-Ac in eukaryotes mainly occurs co-translationally when 25–50 amino acids protrude from the ribosome, by the action of ribosome associated N-terminal acetyltransferases (NATs) [7–12]. N-Ac may occur on the initiator Met (iMet) or on the first residue after iMet excision by methionine aminopeptidases (MAPs) [13,14]. Three major NAT complexes conserved from yeast to humans are thought to be responsible for the majority of N-terminal acetylation events: NatA, NatB and NatC [15]. Each complex is composed of specific catalytic and auxiliary subunits. NatA, the first NAT defined by Sternglanz and co-workers [16], potentially acetylates Ser-, Ala-, Thr-, Val-, Gly-, and Cys- N-termini after iMet-cleavage [17–19]. NatB and NatC potentially acetylate Met- N-termini when the second residue is either acidic or hydrophobic respectively [19–21]. In yeast, NatD was described to acetylate the Ser- N-termini of histones 2A and 4 *in vitro* and *in vivo* [22], while no such activity has yet been presented for higher eukaryotes. NatE is another NAT of which the *in vitro* activity was described for the human hNaa50p towards some Met-Leu-N-termini [23], but direct evidence of *in vivo* activity is still lacking. Thus, each hitherto *in vivo* characterized NAT appears to acetylate a distinct subset of substrates defined by the very first N-terminal amino acids. Phenotypes induced by loss or

Author Summary

Small chemical groups are commonly attached to proteins in order to control their activity, localization, and stability. An abundant protein modification is N-terminal acetylation, in which an N-terminal acetyltransferase (NAT) catalyzes the transfer of an acetyl group to the very N-terminal amino acid of the protein. When going from lower to higher eukaryotes there is a significant increase in the occurrence of N-terminal acetylation. We demonstrate here that this is partly because higher eukaryotes uniquely express NatF, an enzyme capable of acetylating a large group of protein N-termini including those previously found to display an increased N-acetylation potential in higher eukaryotes. Thus, the current study has possibly identified the last major component of the eukaryotic machinery responsible for co-translational N-acetylation of proteins. All eukaryotic proteins start with methionine, which is co-translationally cleaved when the second amino acid is small. Thereafter, NatA may acetylate these newly exposed N-termini. Interestingly, NatF also has the potential to act on these types of N-termini where the methionine was not cleaved. At the cellular level, we further found that NatF is essential for normal chromosome segregation during cell division.

reduction of NATs suggest that these enzymes, and thus probably N-Ac, are implicated in a number of cellular processes. In higher eukaryotes, depletion of NatA, NatB or NatC is associated with cell cycle arrest or apoptosis [20,21,24–28] while sister chromatid cohesion defects are observed upon NatE depletion [29–31].

N-Ac occurs on more than 50% and 80% of cytosolic yeast and human proteins, respectively [18]. The reason for the major difference in occurrence of N-Ac between yeast and humans to date is not known. Furthermore, the fact that specific subsets of protein N-termini, like those initiated by Met-Lys-, are often acetylated in humans and fruit fly while rarely being acetylated in yeast, is also an unsolved issue [18,32]. Further, such substrates do not match the predicted substrate specificity of any of the known NATs. Potential explanations for this evolutionary shift from lower to higher eukaryotes include: i) evolution towards more acetylation-prone N-termini in higher eukaryotes, ii) a shift in the substrate specificity between species-specific NATs, iii) the presence of novel, yet uncharacterized NATs in higher eukaryotes, and iv) the presence of species-specific co-factors or chaperones such as HYPK [33]. However, so far, no evidence for any of these hypotheses was presented.

In the current investigation, we sought to elucidate the mechanistic explanations for the evolutionary shift in N-terminal acetylation from lower to higher eukaryotes. To this end we investigated the potential evolution of acetylation prone N-termini, but found this to be a trivial contributing factor. We further explored the presence of novel NATs in higher eukaryotes as a possible explanation. *In silico* analysis revealed the existence of an uncharacterized human protein with a significant sequence similarity to known catalytic NAT subunits. Indeed, multiple lines of *in vitro* and *in vivo* evidence clearly demonstrate that this candidate protein conserved among animals is a major NAT displaying distinct substrate specificity, denoted Naa60p (NatF). Our data collectively suggest that Naa60p contributes to the increased occurrence of N-terminal acetylation in higher versus lower eukaryotes, and additionally revealed a novel regulator of chromosome segregation.

Results

Analyses of yeast and human N-termini reveal deviations of the residue contact order but provide no evidence for a significant evolution to more acetylation-prone N-termini in higher eukaryotes

We first investigated whether an evolution towards more acetylation-prone N-termini in higher eukaryotes could help explain the higher acetylation levels observed. Upon comparing the yeast, fruit fly and human proteomes, it is evident that the general distribution of N-termini is largely unaltered between the different classes, 'NatA', 'NatB', 'NatC' and 'Other' (Figure 1A). However, when considering all different subgroups based on the first two N-terminal amino acids, some significant alterations ($p<0.01$) appeared. Besides the general difference of the amino acid usage in yeast versus human N-termini in agreement with recent observations [34], the occurrence of (Met-)Ala- N-termini increased from 8% in yeast to 23% in humans, while Met-Glu- N-termini increased from 5% to 10%. On the other hand, (Met-)Ser-N-termini have decreased in occurrence from 23% in yeast to 11% in humans (Figure 1B). Interestingly, for these major trends, the occurrences in fruit-fly are intermediate between yeast and humans, indicating that these might be characteristic of the evolution to multicellular and more complex organisms. The next question is thus whether these changes in N-terminal sequences are causing a shift in N-Ac. In the current work, we performed COFRADIC-based N-terminal acetylation analyses of yeast and HeLa proteomes and present datasets covering 868 and 1,497 unique yeast and human N-termini, respectively (Tables S1 and S2). An overview of the occurrence of N-Ac of the different classes of assigned N-termini in the yeast ($n = 648$) and human ($n = 1345$) control samples is presented in Table 1. When relating the occurrence of N-Ac in yeast to the distribution of human N-termini and *vice versa* (based on the first two amino acids of the identified N-termini), we found no overall significant changes in N-Ac levels (Table S3). Thus, alteration in usage of the first two N-terminal amino acids, which are the major determinants for N-Ac, is not a significant cause for the observed shift from lower to higher eukaryotes.

Since it was shown that amino acid usage at protein N-termini differs significantly from what is expected [34], and differences in dipeptide composition have been used to predict protein expression levels [35], thermostability [36] and subcellular localization [37], we further characterized the residue contact order at protein N-terminal parts by studying dipeptide frequencies in the theoretical proteomes of *Homo sapiens*, *Drosophila melanogaster* and *Saccharomyces cerevisiae* (UniProt/SwissProt entries (version 2011-05)). Therefore, the occurrence of the 400 possible dipeptides from the 20 amino acids in all proteins was estimated for randomly selected human dipeptides and N-terminal (amino acids 2–11) dipeptides by Monte-Carlo sampling. Further, a z-score was applied to correct for differences in database size. Contacting residues in a random, non-N-terminal set correlate well with the expected theoretical contact order (data not shown). In sharp contrast, the overall dipeptide composition deviates significantly for database-annotated N-termini. A heatmap visualization centered and scaled by species mean and standard deviation for *Homo sapiens*, *Drosophila melanogaster* and *Saccharomyces cerevisiae* is shown for the ten dipeptides with the highest and lowest z-scores (union of $n = 49$) (Figure 1C). Overall, these data strengthen the observation that N-terminal sequences not only display altered patterns of amino acid frequencies but deviate extensively in their residue contact order in a species-specific

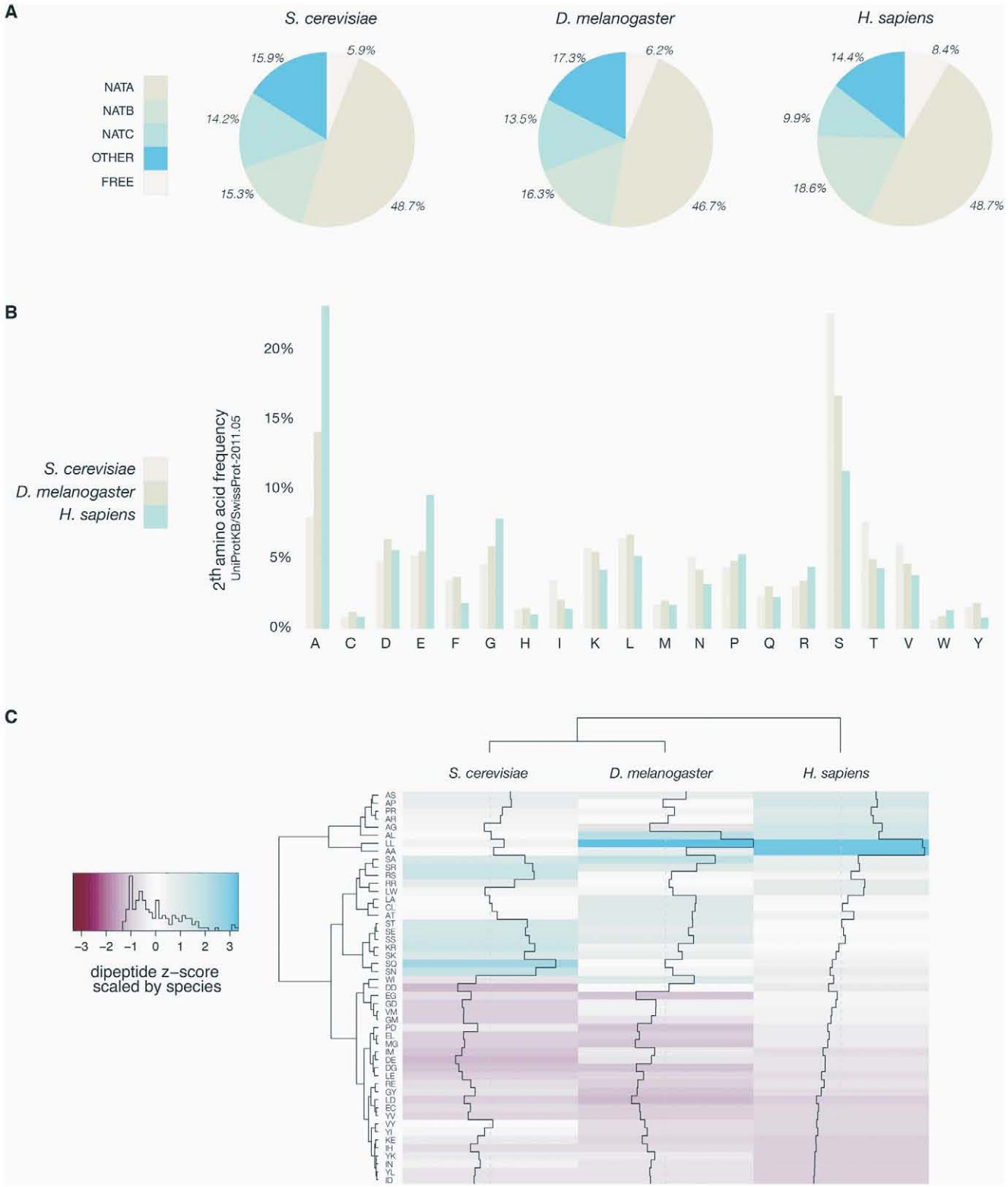

Figure 1. Overview of yeast, fruit fly, and human N-termini in NAT-classes and amino acid prevalence. A. Comparative analyses of the distribution of all methionine-starting yeast (6561), fruit fly (3120) and human SwissProt entries (20238) (SwissProt version 2011-05) according to their Nat-type. For simplicity, methionine processing was assumed to occur for (M)A-, (M)S-, (M)T-, (M)V-, (M)C-, (M)G- and (M)P- starting N-termini, while the X-P- rule was used to assign unacetylated database entries [32]. B. Bar charts of the amino acid occurrence at position 2 of yeast, fruit fly and human SwissProt protein entries. C. Heatmap of the ten highest and lowest ranking dipeptide z-scores across *H. sapiens*, *D. melanogaster* and *S. cerevisiae*. Z-scores are scaled by species, with the highest and lowest ranking z-score colored with the same intensity in blue and red respectively. The species (X-axis) and the dipeptides (Y-axis) were grouped by hierarchical clustering using the euclidian distance matrix of the z-scores.
doi:10.1371/journal.pgen.1002169.g001

Table 1. Overview of N-terminal acetylation of yeast and human proteins.*

	hNat			yNat		
	No.	completely, %	completely and partially, %	No.	completely, %	completely and partially, %
NatA substrates						
Ala-	495	91.6	95.3	52	25.0	48.1
Cys-	4	75.0	75.0	2	0.0	0.0
Gly-	10	0.0	0.0	12	0.0	8.3
Ser-	188	95.4	98.0	186	89.2	97.3
Thr-	39	75.9	89.7	36	19.4	55.6
Val-	39	3.2	19.3	31	0.0	9.7
NatB substrates						
Met-Asp-	93	95.7	98.9	59	93.2	100.0
Met-Glu-	165	97.6	100.0	35	94.3	100.0
Met-Asn-	32	100.0	100.0	46	89.1	100.0
NatC substrates						
Met-Ile	10	30.0	50.0	14	26.7	33.3
Met-Leu-	32	56.3	75.0	30	26.7	33.3
Met-Phe-	18	83.3	83.3	10	60.0	60.0
Other						
Asp-	1	100.0	100.0			
Ile-	1	0.0	0.0	1	0.0	0.0
Glu-	1	100.0	100.0			
Pro-	68	0.0	0.0	25	0.0	0.0
Met-Ala	14	64.3	92.9	1	0.0	100.0
Met-Cys-	1	100.0	100.0			
Met-Gly-	3	33.3	100.0	3	0.0	100.0
Met-Lys-	46	13.0	47.8	46	4.3	13.0
Met-Met-	12	83.3	100.0	6	16.7	83.3
Met-Pro-	6	0.0	0.0			
Met-Gln-	16	81.3	93.8	13	30.8	84.6
Met-Ser-	9	88.9	88.9	14	7.1	64.3
Met-Thr-	18	83.3	94.4	7	0.0	28.6
Met-Val-	20	50.0	85.0	11	0.0	45.5
Met-Tyr-	4	75.0	100.0	8	25.0	62.5
Total	**1345**	**79.1**	**85.2**	**648**	**52.5**	**67.9**

Quantitative COFRADIC-based analysis of N-terminal acetylation in yeast (*S. cerevisiae*) and HeLa proteomes determined the acetylation status of 648 and 1345 unique N-termini in the two species, respectively. Overall, 67.9% and 85.2% of the yeast and HeLa proteomes, respectively, are N-terminally acetylated (fully or partially). The analysed proteins are categorized based on their N-terminal sequences (substrate classes).

*Only N-termini of which the degree of N-Ac could be univocally calculated/determined in the control yeast (648) and control human (1345) setups were used for the overall calculation of N-Ac.

doi:10.1371/journal.pgen.1002169.t001

manner, which might additionally impose yet undetected constraints in determining N-Ac.

When considering each type of N-terminus, it is evident that several of these are more acetylated in humans while some are mainly unchanged, but none are less N-Ac. The major groups of protein N-termini with an increase in N-Ac in humans as compared to yeast include (Met-)Ala-, (Met-)Val-, and Met-Lys-N-termini and thus represent major contributors to the overall evolutionary shift (Table 1 and Table S3).

Another potential cause for the evolution towards the higher level of N-Ac is a shift in the substrate specificity between species-specific NATs. For NatA, which is responsible for N-Ac of two of the important N-terminal types mentioned above, (Met-)Ala- and (Met-)Val- this seemed not to be the case as both human NatA and yeast NatA acetylated the very same subset of N-termini in yeast [18]. For the final group, Met-Lys- N-termini, no information is available since such N-termini have not been linked to any of the NAT classes previously characterized.

Naa60p is a novel NAT displaying a unique substrate specificity *in vitro*

In search of novel human NATs, we used the sequences of known human NATs in NCBI BLAST queries (search set: Swiss-Prot database restricted to human proteins). We identified one

protein with a significant similarity to several of the known NATs, namely NAT15/Q9H7X0/Naa60p (Figure 2). NAT15/Naa60p is highly conserved among animals (Figure 2B) and homologues are also potentially present in plants (for instance At5g16800). In order to assess whether NAT15 was an N-terminal acetyltransferase, the *NAT15* ORF was recombinantly expressed and purified from *Escherichia coli* and applied to a newly developed *in vitro* proteome-derived peptide library N-terminal acetylation assay [38]. In brief, natural proteomes are used to generate N^{α}-free peptide substrate pools (libraries) by enrichment with strong cation exchange (SCX). When such a peptide library is incubated with a NAT enzyme, the newly N^{α}-acetylated peptides are enriched by a second SCX fractionation step, resulting in a positive selection of NAT-specific peptide substrates. Subsequently, the NAT-oligopeptide substrates are identified by LC-MS/MS, and the *in vitro* substrate specificity profile of the NAT in question is analyzed using IceLogo [39], an analytical tool that uses probability theory to visualize significant conserved sequence patterns in multiple peptide sequence alignments by comparing against a chosen background (reference) sequence set. Using this proteome-derived peptide assay, NAT15 N^{α}-acetylated numerous peptides *in vitro* and displayed a distinct substrate specificity profile (Figure 3A). Thus, according to the revised NAT-nomenclature system [15], we named this protein Naa60p and its activity NatF. Remarkably, the preferred N-termini included Met-Lys-, Met-Ala-, Met-Val-, and Met-Met-, categories for which there are currently no known N-terminal acetyltransferase(s). Of particular interest, recent data revealed that several Met-Lys- N-termini were acetylated in humans and fruit fly while no such N-Ac events of Met-Lys- N-termini were found in yeast, pointing to the presence of (a) NAT(s) specific for higher eukaryotes or an altered specificity profile of (a) higher eukaryotic NAT(s) as compared to yeast NAT(s) [18,32]. To expand these observations to higher eukaryotes in general, we purified the predicted fruit fly homologue dNaa60p (CG18177) and confirmed this protein to be a NAT with a nearly indistinguishable specificity profile as compared to hNaa60p (Figure 3B). As deduced from the *in vitro* specificity profile, besides Met-; Leu- was also preferred at the first position, which, as we described previously [38], is expected since both Met and Leu share similar physiochemical characteristics [40,41]. However, for co-translational N^{α}-acetylation, Leu at the first position appears physiologically irrelevant as it is not expected as the first amino acid, since when it follows the initiator methionine, its size precludes the removal of this initiator methionine by MAPs [14]. When only including Met residues at the first position, the specificity profile remains largely unchanged (Figure 3C, 3D and Figure S1). Given its *in vitro* specificity, we considered Naa60p a qualified candidate for the Met-Lys- acetylation activities observed in higher eukaryotes.

Naa60p is a NAT *in vivo*, and ectopic expression in yeast shifts the global N-Ac patterns

In order to assess whether hNaa60p represents a NAT *in vivo* and to address its potential role in the evolutionary N-Ac shift, we generated a yeast strain expressing hNaa60p. We were not able to observe any differences in growth rates or plating efficiencies between yeast control strains and yeast strains expressing hNaa60p (data not shown). Since yeast does not have an obvious homolog of hNaa60p, ectopic expression was expected to reveal whether hNaa60p endows yeast with a greater acetylating potential. Indeed, when comparing N-terminal acetylation in the proteome of control yeast (yeast control) to the yeast expressing hNaa60p (yeast+NatF), significant alterations in the N^{α}-acetylome were observed (Figure 4). For example the Smr domain-containing protein YPL199C and uncharacterized protein YGR130C, with respectively Met-Lys- and Met-Leu- N-termini, were unacetylated in control yeast while 82% and 48% acetylated in the strain expressing hNaa60p/NatF (Figure 5). In total, for 464 of the 544 (or 85%) unique N-termini identified in both proteomes, the N-acetylation status could univocally be determined. Of these, 72 N-termini were more acetylated in the hNaa60p expressing strain, while none were less acetylated, indicating that at least 16% of the identified yeast proteome was acetylated by hNaa60p (Figure 4 and Table S4). 44 of the 72 hNaa60p acetylated N-termini were completely unacetylated in control yeast, while 28 were partially acetylated. For the latter group, hNaa60p increased the degree of acetylation with at least 10%. It should be noted that this may represent an underestimation of hNaa60p's capacity since fully acetylated N-termini (53%) in the control strain may also represent targets, which would be masked by redundancy with the yeast NAT-machinery. The hNaa60p yeast substrates identified *in vivo* were in agreement with the *in vitro* determined substrate specificities. The most common *in vivo* substrate classes were Met-Lys- (n = 14), Met-Ser- (n = 9), Met-Val- (n = 8), Met-Leu- (n = 8), Met-Gln- (n = 6), Met-Ile- (n = 5), Met-Tyr- (n = 5), and Met-Thr- (n = 5) (Table 2).

Among those acetylated by hNaa60p were proteins with Met-Lys- starting N-termini, which are of particular interest because these are acetylated in humans by an unknown NAT, while only rarely acetylated in yeast [18]. When considering the yeast control dataset, only 13% of the Met-Lys- N-termini are fully or partially acetylated, while the corresponding number for the yeast+NatF strain increases to 48%. In striking resemblance, 40% to 70% of Met-Lys- N-termini are N-terminally acetylated in human cell lines as respectively demonstrated previously [18] and in the current dataset (Table 1). Met-Leu-, Met-Ile-, and Met-Phe-starting N-termini, a class of N-termini considered NatC substrates, are other types of N-termini frequently found to be acetylated by hNaa60p. Finally, many substrate N-termini without a proper NAT-classification (including initiator Met-retaining N-termini of which the iMet is only partially removed) were acetylated: Met-Ser-, Met-Val-, Met-Thr- and Met-Met-, and Met-Gln-. Thus, hNaa60p acetylates both N-free besides partially acetylated protein N-termini in yeast, some without any known corresponding yeast NAT, as well as N-termini for which there is a putative NAT (NatC). This indicates that Naa60p may mediate a significant part of the shift in N-terminal acetylation from lower to higher eukaryotes. Furthermore, in contrast to the current opinion, this also strongly suggests redundancy in the N^{α}-acetylation system, meaning that different NATs may have (partially) overlapping substrates. The effect of hNaa60p on overall N-terminal acetylation in yeast is shown in Figure 5C. Overall, the expression of hNaa60p increased the fraction of N^{α}-acetylated yeast proteins from 68% to 78%, in particular affecting the groups 'yNatC' and 'Other' (Figure 4 and Figure 5).

Overexpression or knockdown of h*NAA60* affects N-terminal acetylation in HeLa cells

Overexpression or knockdown of h*NAA60* in HeLa cells was found to increase or decrease, respectively, the N-terminal acetylation of proteins matching the above defined *in vitro* and *in vivo* substrate specificity of hNaa60p (Table S5). Examples include the proteins STIP1 homology and U-box containing protein1 (^{1}MKGKEEKEGGAR^{12}) and mediator of RNA polymerase II transcription subunit 25 (^{1}MVPGSEGPAR^{10}) where the N^{α}-acetylation status is shifted as a consequence of h*NAA60* overexpression (from 18% to 32% acetylation) or knockdown (from 26% to 17% acetylation), respectively (Figure 6). These data

A

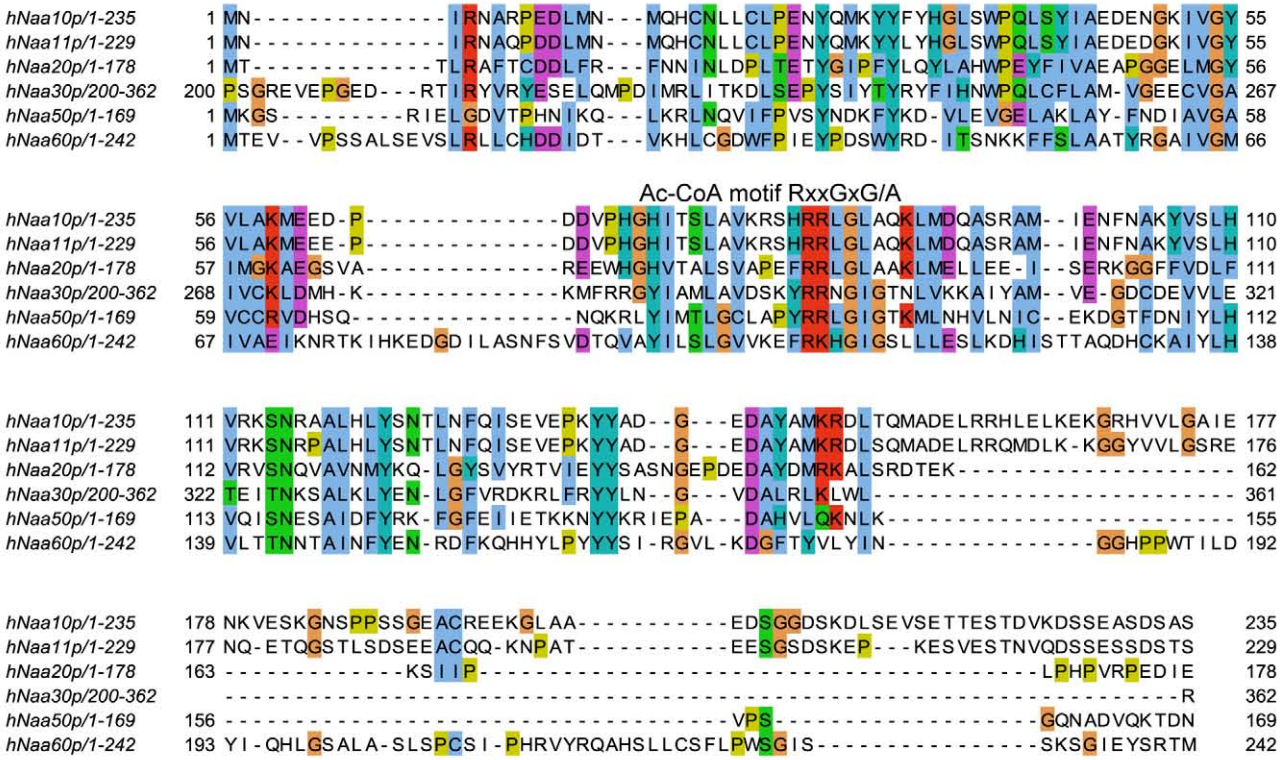
Ac-CoA motif RxxGxG/A
hNaa10p/1-235
hNaa11p/1-229
hNaa20p/1-178
hNaa30p/200-362
hNaa50p/1-169
hNaa60p/1-242

B

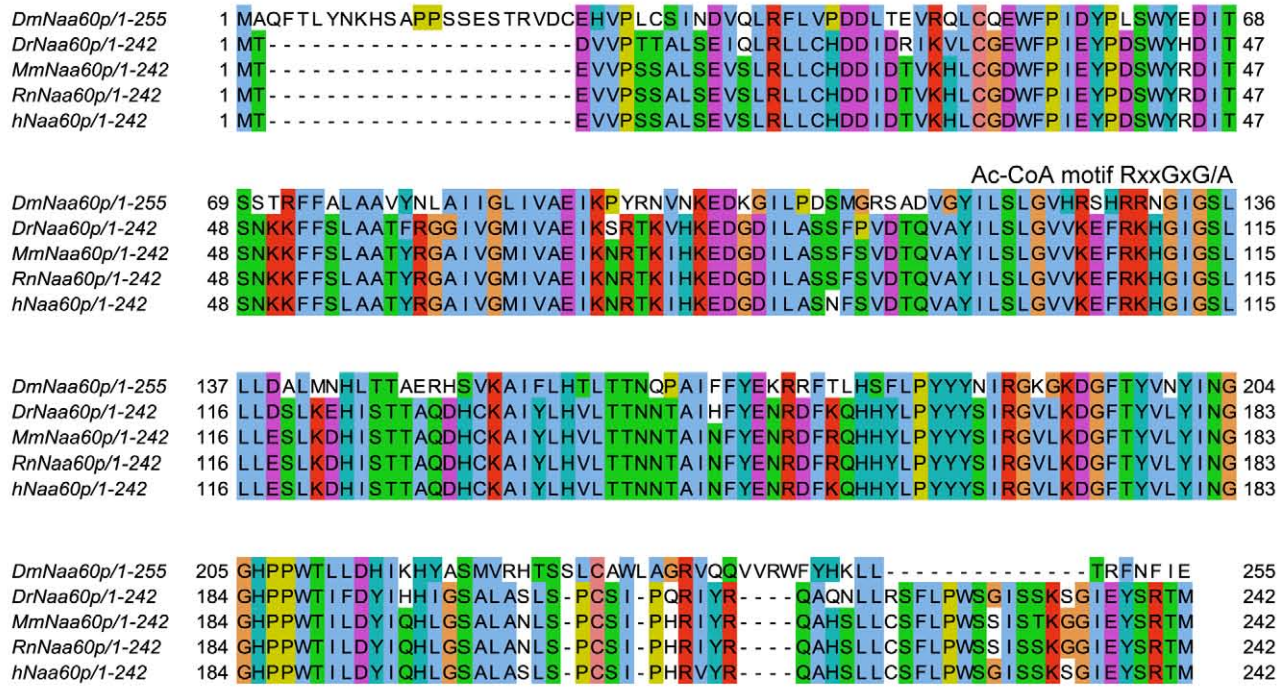
Ac-CoA motif RxxGxG/A
DmNaa60p/1-255
DrNaa60p/1-242
MmNaa60p/1-242
RnNaa60p/1-242
hNaa60p/1-242

Figure 2. Amino acid sequence alignments of hNaa60p and other NATs. A. Amino acid sequence alignment of NAT15/hNaa60p and known human NATs. Only amino acid 200–362 of hNaa30p was included in the alignment. The consensus Acetyl Coenzyme A (AcCoA) binding motif RxxGxG/A, where x can be any amino acid, is indicated. T-Coffee (http://www.ebi.ac.uk/Tools/t-coffee/index.html) was used to make the alignment. Purple background indicates acidic residues, red indicates basic residues, orange indicates glycine, yellow indicates proline, blue indicates hydrophobic residues, green indicates polar residues, and turquoise indicates histidine and tyrosine. B. Amino acid sequence alignment of Naa60p from *Drosophila melanogaster* (Dm), *Danio rerio* (Dr), *Mus musculus* (Mm), *Rattus norvegicus* (Rn) and *Homo sapiens* (Hs). The consensus Acetyl Coenzyme A (AcCoA) binding motif RxxGxG/A, where x can be any amino acid, is indicated. Colour codes are used as in A.
doi:10.1371/journal.pgen.1002169.g002

strongly point to the fact that hNaa60p in human cells can act on the classes of N-termini deduced from the *in vitro* and *in vivo* yeast analyses described above (Table 2). Obviously, overexpression analysis will be limited by the redundancy among NATs and by the fact that naturally hNaa60p-acetylated N-termini may be fully acetylated and as such do not appear as substrates for the overexpressed hNaa60p. Furthermore and in line with previous knockdown analyses of NatA in HeLa cells, the semi-effective nature of siRNA-mediated knockdown as well as the long time period needed for a clear effect on N-terminal acetylations to occur, make such analyses indicative rather that providing the full picture of acetylation events mediated via a specific NAT and as shown previously, primarily affects the least efficiently acetylated N-termini [18]. Thus, the real number of Naa60p substrates in human cells is likely to be significantly higher as compared to the substrates identified in these particular analyses.

Finally, two of the acetylated N-termini of the predicted NatF class picked up from the HeLa dataset (Table S2) were tested by a direct *in vitro* approach. Synthetic peptides derived from the Met-Lys- and Met-Ala- N-termini of Septin 9 and Protein phosphatase 6, respectively, were subjected to an *in vitro* acetylation assay with purified hNaa60p followed by an HPLC-based analysis of acetylated and unacetylated peptides. In agreement with the human and yeast *in vivo* data and *in vitro* substrate profiles obtained above, hNaa60p acetylated both these peptides, as well as representatives of NatC and NatE class substrates (Figure 7). Thus, we confirmed the N-terminal acetylation of human substrates as well as the potential redundancy with NatC and NatE enzyme classes (Table 2).

dNaa60p is required for chromosome segregation during anaphase

In order to assess the cellular function of dNaa60p, its expression was knocked down in *Drosophila* Dmel2 cells by RNAi. Similarly to d*NAA50*-depleted cells [30,31] (data not shown), d*NAA60*-depleted cells showed chromosomal segregation defects

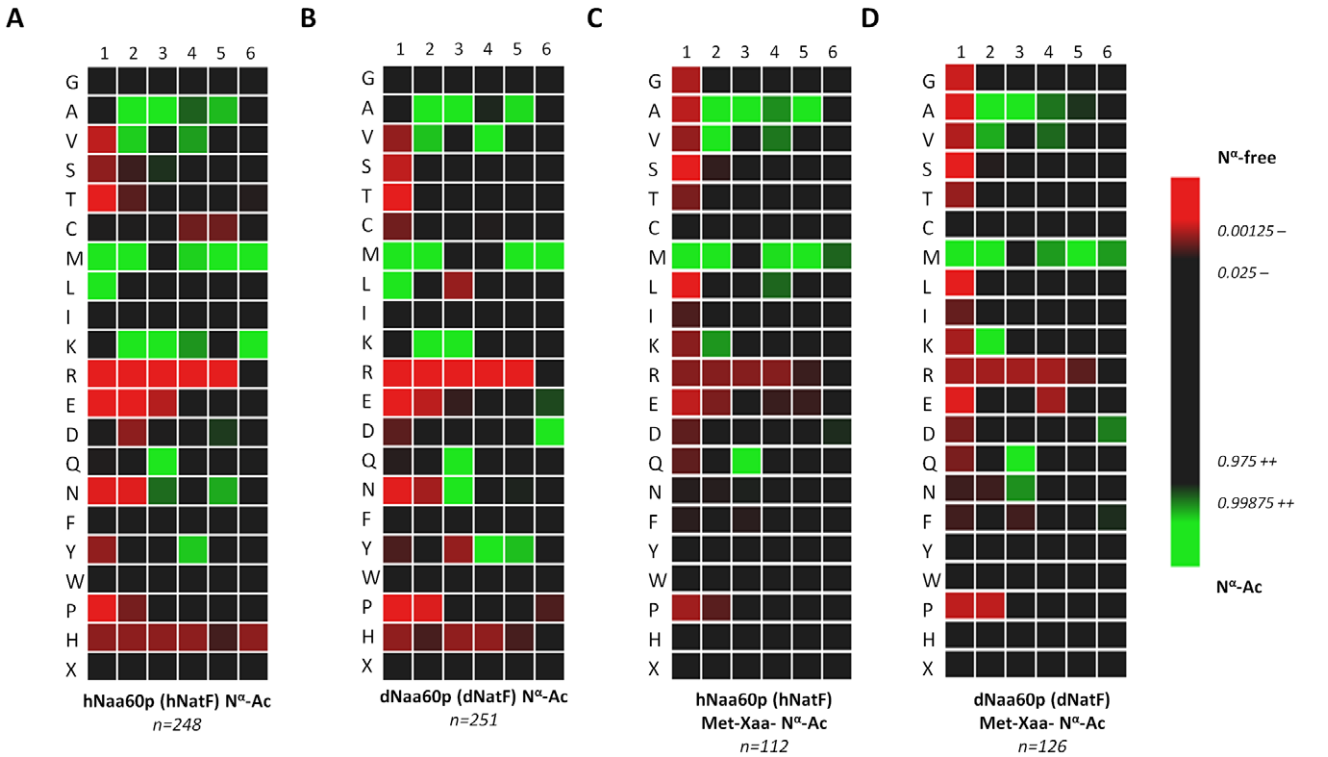

Figure 3. Heatmap visualization reflecting the *in vitro* substrate specificity of hNaa60p and dNaa60p. A. Heatmap of the 248 unique hNaa60p-specific oligopeptide substrates (353 substrate peptides in total). B. Heatmap of the 251 unique dNaa60p-specific oligopeptide substrates (345 substrate peptides in total). C. Heatmap of the subset of 112 unique hNaa60p-specific methionine-starting oligopeptide substrates. D. Heatmap of the subset of 126 unique dNaa60p-specific methionine-starting oligopeptide substrates. Data was normalized against the natural positional amino acid composition of SwissProt (version 57.8) [iterative rounds (n = 100) of randomly selected sequences (n = 100) were taken as to correct for the statistical variations (SD = standard deviation) intrinsically present at each position in the experimental datasets ranging from amino acid 1 to 6]. The significance threshold was set at 0.01. Red color shades are negatively correlated with the occurrence in Naa60p peptide-substrates as compared to random sequences in SwissProt, while green shades are positively correlated.
doi:10.1371/journal.pgen.1002169.g003

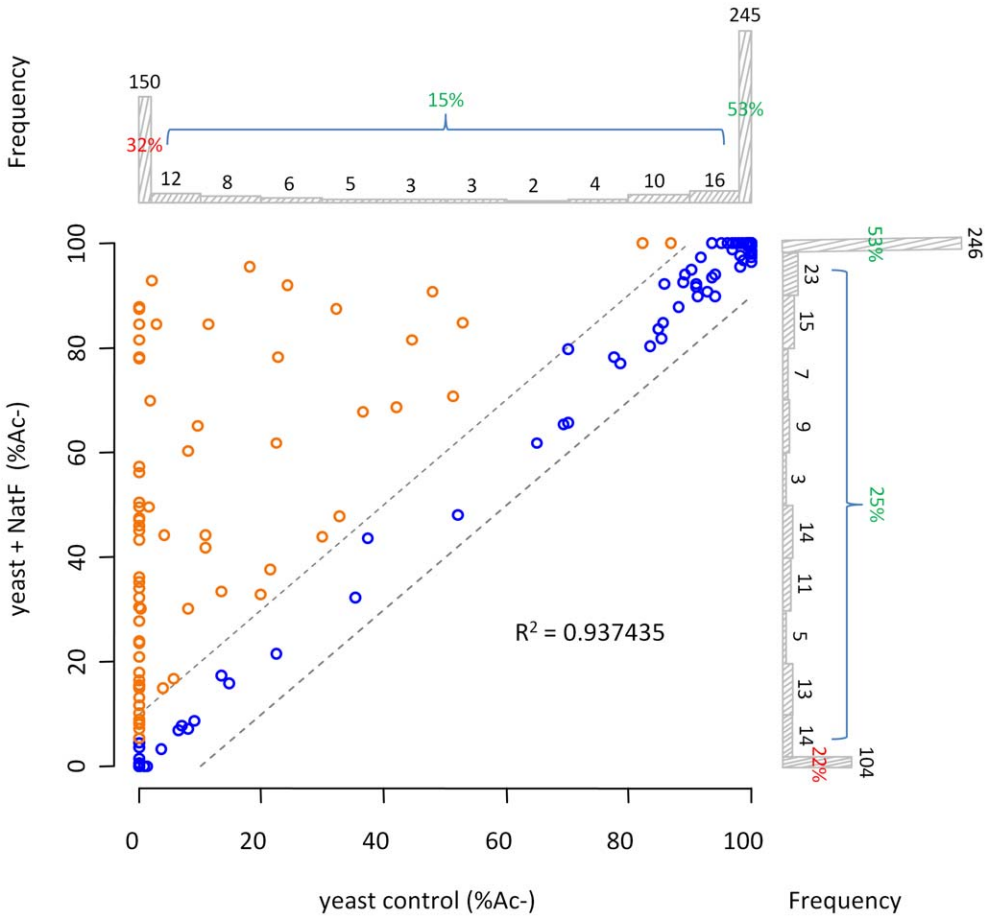

Figure 4. NatF N-terminally acetylates yeast substrates *in vivo*. Scatterplot displaying the correlation of the degrees of N^{α}-acetylation when comparing a control (X-axis) and a human NatF (hNaa60p)-expressing (Y-axis) yeast N-terminome dataset. The correlation was calculated with the R statistical package to be $R^2 = 0.937$. The N-termini displaying a significant variation in the degree of N^{α}-acetylation (see Materials and Methods) are highlighted in orange. The frequency histograms of the number of matching data points are also shown.
doi:10.1371/journal.pgen.1002169.g004

during anaphase (Figure 8A–C, 8F, 8G, 8J, 8K). However, while d*NAA50*-depleted cells exhibit abnormal metaphases with an obvious mitotic arrest, control and d*NAA60*-depleted cells exhibited normal metaphases, with all chromosomes perfectly aligned within the spindle equator and without any mitotic arrest (Figure 8D, 8E, 8H, 8I and Figure S2). In contrast, during anaphase we consistently observed chromosome segregation defects in d*NAA60*-depleted cells, which included lagging chromosomes (Figure 8K, highlighted by asterisk) and chromosomal bridges (Figure 8B, 8G, highlighted by asterisk; quantification of abnormal anaphases is shown in Figure 8C). Chromosome lagging and bridging in d*NAA60*-depleted cells may be explained by kinetochore abnormalities; however we failed to detect any obvious defect in the localization of the Centromere identifier protein (Cid) during metaphase or anaphase (Figure 8D–G). We also failed to detect any obvious cohesion defect since the distance between kinetochores during metaphase was normal according to Cid localization (Figure 8D, 8E). Chromosome lagging could also be explained by centrosome/mitotic spindle defects. Yet, we did not detect any obvious defect in the localization of Centrosomin (Cnn), and the mitotic spindle was bipolar and correctly attached to chromosomes and centrosomes (Figure 8D–G). Furthermore, d*NAA60*-depleted cells showed no obvious defects in the actin and microtubule cytoskeleton in both mitotic and interphase cells (Figure 8H–M). Since d*NAA60*-depleted cells were otherwise normal, our data suggest that dNaa60p is required for chromosome segregation during anaphase. Naa60p-dependent N-terminal acetylation of one or more substrates is therefore likely to be required for chromosome segregation *in vivo*.

Discussion

The basic co-translational machinery performing N-Ac in eukaryotes was believed to be fully identified and mostly characterized, with five NATs, NatA-NatE, each of which composed of specific subunits and acetylating its own subset of substrates [15]. However, the significant shift in occurrence of N-Ac from lower to higher eukaryotes, clearly points to the fact that species-specific factors are major determinants for N-Ac. Indeed, in the current study we revealed that higher eukaryotes express NatF/Naa60p, a unique NAT responsible for N-Ac of a large subset of eukaryotic proteins. These N-termini include Met-Lys-, Met-Met-, Met-Val- and Met-Ser- to which so far no NAT has been assigned. Also N-termini like Met-Leu- and Met-Ile-, previously believed to be solely NatC substrates, may be acetylated by NatF. Thus, the previous clear-cut classification between Nat substrate classes based on the N-terminal sequences should be re-evaluated when *in vivo* datasets are considered. The current

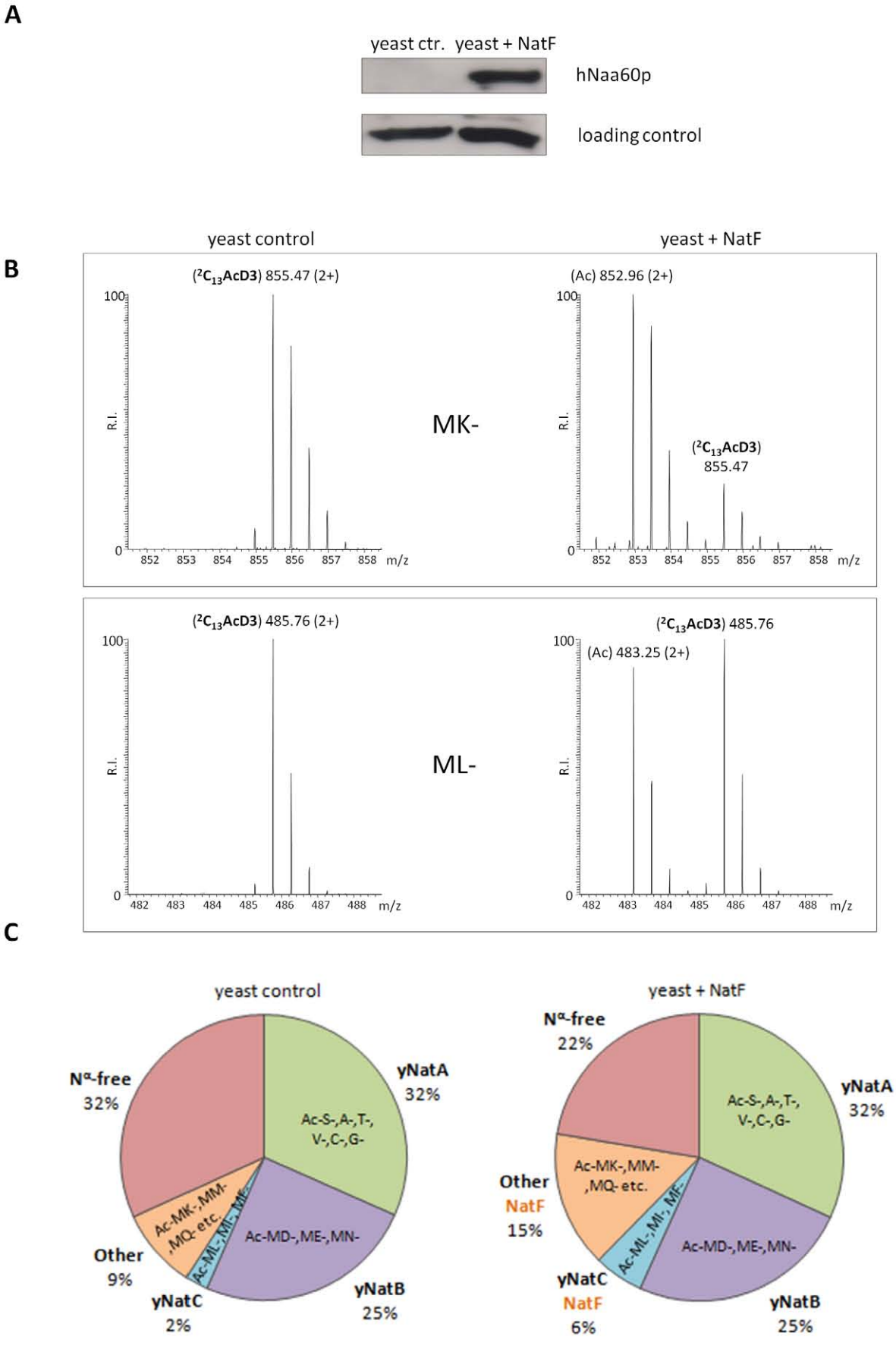
A
yeast ctr.
yeast + NatF
hNaa60p
loading control
B
yeast control
yeast + NatF
(2C13AcD3) 855.47 (2+)
(Ac) 852.96 (2+)
MK-
(2C13AcD3) 855.47
(2C13AcD3) 485.76 (2+)
(2C13AcD3) 485.76
(Ac) 483.25 (2+)
ML-
R.I.
m/z
C
yeast control
yeast + NatF
Nα-free 32%
yNatA 32%
Ac-S-,A-,T-, V-,C-,G-
Ac-MK-,MM-,MQ- etc.
Ac-ML-,MI-,MF-
Ac-MD-,ME-,MN-
Other 9%
yNatC 2%
yNatB 25%
Nα-free 22%
Other NatF 15%
yNatC NatF 6%

Figure 5. NatF expression shifts the overall status of the yeast N-terminal acetylome. A. A yeast strain expressing hNaa60p/NatF 'Yeast+NatF' was generated (see Materials and Methods), and processed by SDS-PAGE and Western blotting along with the control strain 'Yeast ctr.' containing an empty control plasmid. Anti-hNaa60p verified expression of hNaa60p in the Yeast+NatF strain (an unspecific band served as loading control). B. MS-spectra from the MK- starting N-terminal peptide (doubly charged precursor) of the Smr domain-containing protein YPL199C (^{1}MKGTGGVVVGTQNPVR^{16}) reveals two distinguishable isotopic envelopes in the hNaa60p expressing yeast strain [i.e. the acetylated (Ac) and $^{2}C_{13}$ and trideutero-acetylated forms ($^{2}C_{13}$AcD3), right upper panel] indicative for the fact that this N-terminus is 82% *in vivo* N^{α}-acetylated while being N^{α}-free in the control sample (left upper panel). The lower panels show MS-spectra of the ML-starting N-terminal peptide (doubly charged precursor) of the uncharacterized protein YGR130C (^{1}MLFNINR^{7}) in the control sample (0% N^{α}-acetylated, left lower panel) or hNAA60 sample (48% acetylated, right lower panel). C. Nat-category specific distribution of experimentally identified yeast N-termini in the yeast control or hNaa60p-expressing yeast strain. Only those N-termini of which the N-Ac status could univocally be assigned (n = 464) were considered.
doi:10.1371/journal.pgen.1002169.g005

knowledge on the NATs of higher eukaryotes and their corresponding substrates is presented in Figure 9.

In contrast to the N-termini acetylated by NatF, for the increased N-Ac of the processed (Met-)Ala- and (Met-)Val- N-termini there is presently no explanation. The intrinsic enzymatic properties of human and yeast NatA appeared to be very similar when expressed in yeast [18]. Co-determining factors that should be elaborated upon concerning the NatA substrates are interaction partners specific for NatA of higher eukaryotes, like HYPK which was demonstrated to modulate N-terminal acetylation [33]. Notwithstanding the generally lower expression levels, the existence of higher eukaryotic paralogues of Naa15p and Naa10p, being Naa16p and Naa11p respectively [42,43], might additionally account for modulators of the observed N^{α}-acetylome. However, information regarding their potential proteome-wide contribution to N-Ac is currently lacking.

We found that evolution of N-Ac prone N-termini most likely contributes only to a very small degree to the overall evolutionary shift in the occurrence of N-Ac. Furthermore, there might be a shift in the substrate specificity between species-specific NATs, for instance for the NatB, NatC and NatE activities, requiring further experimental validation. However viewing their strict evolutionary conservation, this may be rather unlikely.

The current data are more comprehensive as compared to previous analyses [18], and overall the 648 unique yeast and 1345 unique human N-termini identified were analysed for their acetylation status (Table 1, Tables S1 and S2). 68% of the yeast N-termini and 85% of the human N-termini are partially or fully N-terminally acetylated. Previously, we determined that 57% of yeast proteins and 84% of human proteins were N-terminally acetylated, thus implicating some shift in the N-Ac of the yeast N-termini between experiments. We believe the current dataset likely holds a more representative picture since more N-termini were sampled and since yeast was grown under slightly different deprivating (SILAC) conditions in the previous setup. Nevertheless, still a significant difference between yeast (68%) and humans (85%) can be observed and as demonstrated, this difference is significantly diminished in yeast expressing NatF (78%) (Figure 4 and Figure 5).

The current study provides to the best of our knowledge, the first evidence shedding light on the molecular basis of the evolutionary shift in the N^{α}-acetylome from lower to higher eukaryotes. With the presence of NatF, higher eukaryotes are

Table 2. Types of N-termini acetylated by NatF using different methods.

In vitro peptide library assay specificity of recombinant hNaa60p (Figure 3 and Figure S1)	*In vivo* yeast substrates of ectopically expressed hNaa60p# (Figure 4, Figure 5, and Table S4)	HeLa substrates affected by knockdown or overexpression of hNaa60p# (Figure 6 and Table S5)	*In vitro* assay using synthetic peptides to verify selected substrates of recombinant hNaa60p (Figure 7)
Met-Lys-	Met-Lys-	Met-Lys-	positive
Met-Ala-	Met-Ala-	Met-Ala-	positive
Met-Val-	Met-Val-	Met-Val-	n.d.
Met-Met-	Met-Met-	Met-Met-	n.d.
	Met-Ser-	Met-Ser-	n.d.
	Met-Leu-	Met-Leu-	positive
	Met-Gln-	Met-Gln-	n.d.
	Met-Ile-		n.d.
	Met-Tyr-		n.d.
	Met-Thr-		n.d.
	Met-Phe-		n.d.
	Met-Gly-		n.d.
	Ser-(Glu-)		negative
	Ala-(Gly-)	Ala-(Ala-)	n.d.
		Thr-(Asp-)	n.d.

NatF/hNaa60p was shown to acetylate several types of N-terminal sequences by the different *in vitro* and *in vivo* methods applied in this study. This overview displays which N-termini are acetylated by NatF using the different methods. Met-Lys-, Met-Ala-, Met-Val- and Met-Met- are among the N-terminal sequences that appear to represent the preferred NatF substrates.
Underlined N-termini were most commonly represented (n>4).
#Underlined N-termini have at least two independent hits. N.d., not determined.
doi:10.1371/journal.pgen.1002169.t002

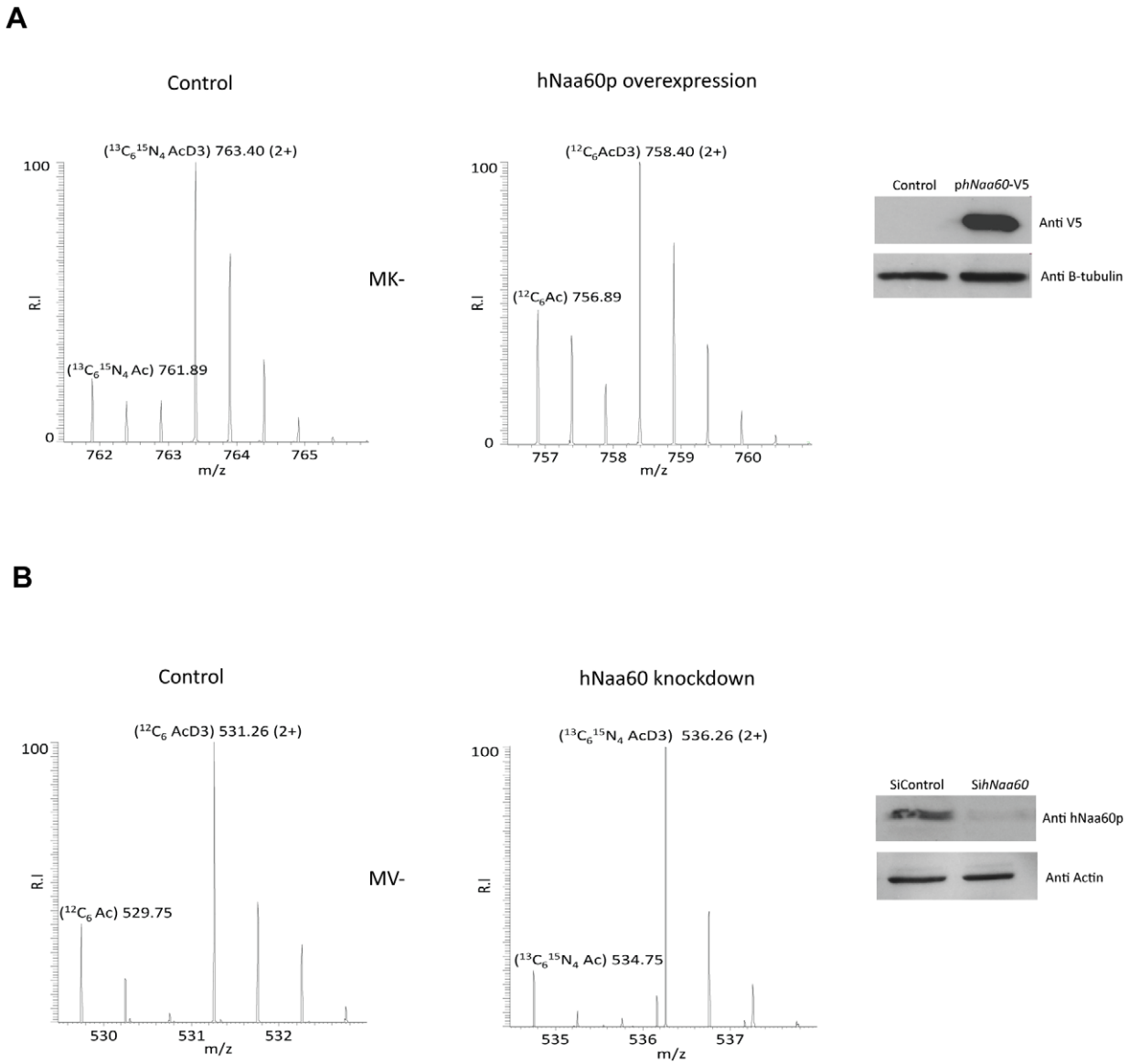

Figure 6. Knockdown and overexpression of hNaa60p affects N-terminal acetylation in HeLa cells. A. HeLa cells cultivated in $^{13}C_6{}^{15}N_4$ L-arginine were transfected with control vector and cells cultivated in $^{12}C_6$ L-arginine were transfected with ph*NAA60*-V5. After 48 hours of transfection the cells were harvested, lysed and subjected to COFRADIC and MS and MS/MS- analysis. MS spectra of the peptide ^{1}MKGKEEKEGGAR^{12}, originating from the STIP1 homology and U-box containing protein1 is shown. The protein is more acetylated when hNaa60p is overexpressed (32% N^{α}-acetylated) as compared to the control (18% N^{α}-acetylated). Aliquots were processed by SDS-PAGE and Western blotting using anti-V5 and anti-β-tubulin antibodies. B. Control cells cultivated in $^{12}C_6$ L-arginine were transfected with 50 nM siNon-targeting control, and cells cultivated in $^{13}C_6{}^{15}N_4$ L-arginine were transfected with 50 nM si*hNAA60* pool. After 84 hours of transfection the cells were harvested and subjected to COFRADIC and MS analysis. MS spectra of the peptide ^{1}MVPGSEGPAR^{10}, originating from the protein Mediator of RNA polymerase II transcription subunit 25 is shown. The peptide was partially acetylated in both control (26% N^{α}-acetylated) and knockdown setup (17% N^{α}-acetylated), however the peptide was less N^{α}-acetylated when the levels of hNaa60p was reduced. Aliquots were processed for SDS-PAGE and Western blotting using anti-hNaa60p and anti-actin antibodies.
doi:10.1371/journal.pgen.1002169.g006

enforced in their capacity to acetylate Met-Lys-, Met-Leu- and other Met- starting N-termini, thus explaining in part the increased occurrence of N-Ac. This additional NAT may have evolved to meet the increased demands of more complex proteomes with a higher level of regulation. In light of the recent suggestion that N-Ac generates degrons and thus acts as a destabilizer [5], these issues will be of particular importance. Our results suggested that dNaa60 activity is likely to be specifically required for chromosome segregation during anaphase, as cells depleted for dNaa60 showed normal alignment of chromosomes during metaphase plates and progressed normally through mitosis, without any obvious cell cycle arrest (Figure 8 and Figure S2). With an increasing support for N-Ac in controlling protein stability, function and subcellular localization, it is very likely that Naa60p will emerge as a key regulator for several proteins. Future investigations will aim at elucidating these specific Naa60p substrates.

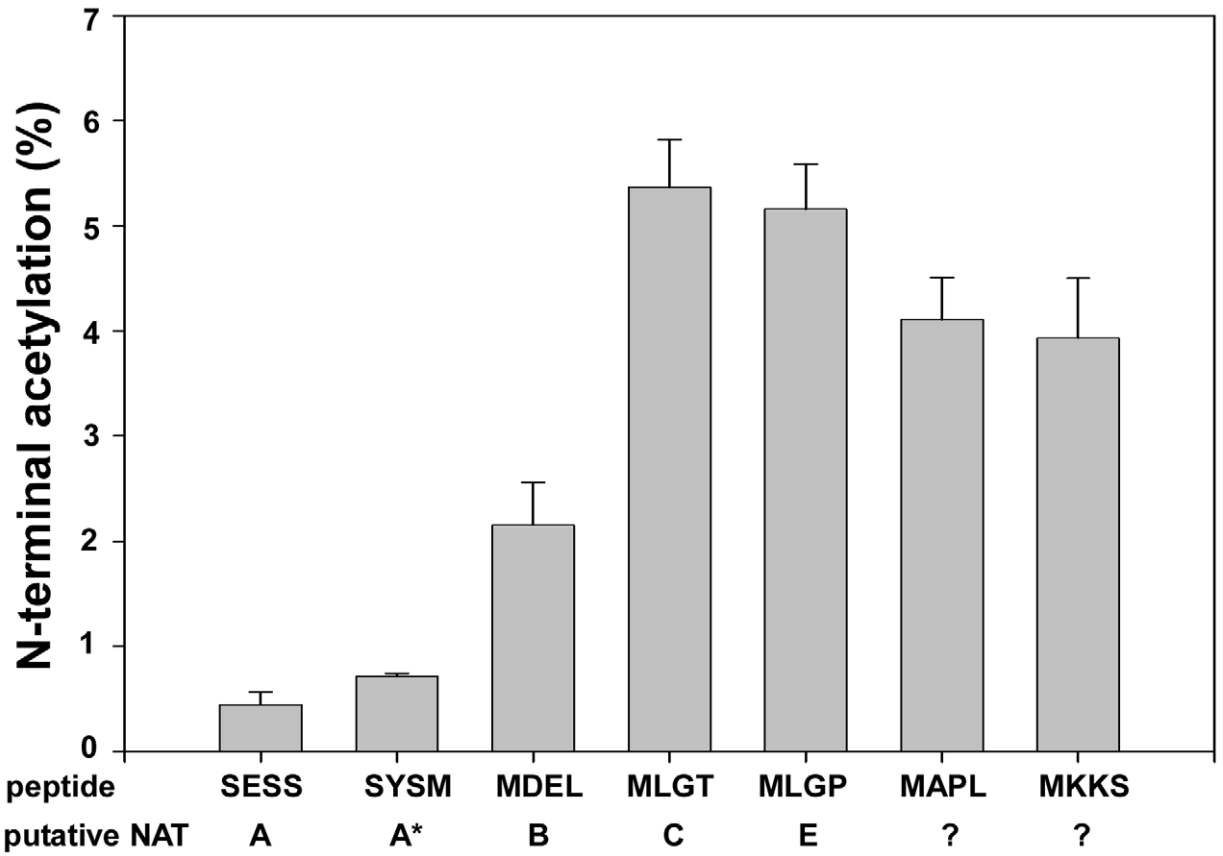

Figure 7. NAT-activity of recombinant hNaa60p towards synthetic N-terminal oligopeptides. MBP-hNaa60p was incubated with the indicated oligopeptide substrates (200 μM) and acetyl-Coenzyme A (300 μM) in acetylation buffer for 35 minutes at 37°C. Peptide acetylation was determined by RP-HPLC peptide separation. The NATs responsible for acetylating the different peptides are shown. Question marks indicate that no NAT has yet been identified to acetylate these peptides. *SYSM represents the ACTH N-terminus which is an artificial *in vitro* substrate of NatA. The four first amino acids in the oligopeptides are indicated, for further details see Materials and Methods.
doi:10.1371/journal.pgen.1002169.g007

Materials and Methods

N-terminal dipeptide frequency analysis for *H. sapiens*, *D. melanogaster*, and *S. cerevisiae*

The random dipeptide frequencies (n = 400) were estimated by Monte Carlo sampling of one randomly selected decapeptide per protein in the databases of; *Homo sapiens*, *Drosophila melanogaster* and *Saccharomyces cerevisiae* (UniProt/SwissProt entries (version 2011-05)). After 100 sampling rounds, the mean and standard deviation for each dipeptide were estimated. Thereafter, the N-terminal dipeptide frequency of all decapeptides from position 2 to 11 were calculated, and the obtained frequencies compared with the random frequencies. The corresponding species-specific z-score, reflecting the amino acid dipetide frequency differences between the protein N-terminal and overall protein sequence were calculated as follows:

$$\frac{\text{AA freq (N-term)-AA freq (random)}}{\text{AA stdev (random)}} = \text{AA z-score}$$

Searching for novel human NATs

Sequences of the known human catalytic NAT units/subunits, hNaa10p (P41227), hNaa11p (Q9BSU3), hNaa20p (P61599), hNaa30p (Q147X3) and hNaa50p (Q9GZZ1), were used in the search of novel human NATs by making use of NCBI BLAST (blastp) queries (search set: 'Swiss-Prot protein sequences' restricted to organism: 'Homo sapiens' and otherwise the predefined parameters). Besides the known human NATs, there was in particular one significant hit, the uncharacterized NAT15 (Q9H7X0), which held sequence similarity to all query NATs with E-values between 3×10^{-6} and 0.24. NAT15 is an automatically annotated name due to the presence of a N-acetyltransferase domain (pfam00583) in the protein sequence. When using hNaa30p and hNaa50p as query sequences, NAT15 scored even better than some of the known human NATs (hNaa20p and hNaa10p/hNaa11p/hNaa20p, respectively). When using hNaa30p as query sequence, some other human proteins scored equally well as NAT15: NAT8 (Q9UHE5), NAT8B (Q9UHF3), NAT8L (Q8N9F0) and ATAC2/CRP2BP (Q9H8E8) with E-values ranging from 7×10^{-5} to 0.034. However, all these candidates were biochemically characterized as members of the GNAT family (pfam00583) with functions distinct from protein N-terminal acetylation. NAT8 is a cysteinyl-*S*-conjugate N-acetyltransferase catalyzing the last step of mercapturic acid formation while NAT8B is a likely pseudogene of NAT8 [44]. NAT8L catalyses the synthesis of N-acetylaspartate [45] and ATAC2 catalyses lysine acetylation on histone H4 [46]. Thus, NAT15 was the only uncharacterized protein with a significant similarity to the known human NATs (Figure 2) and was therefore further pursued.

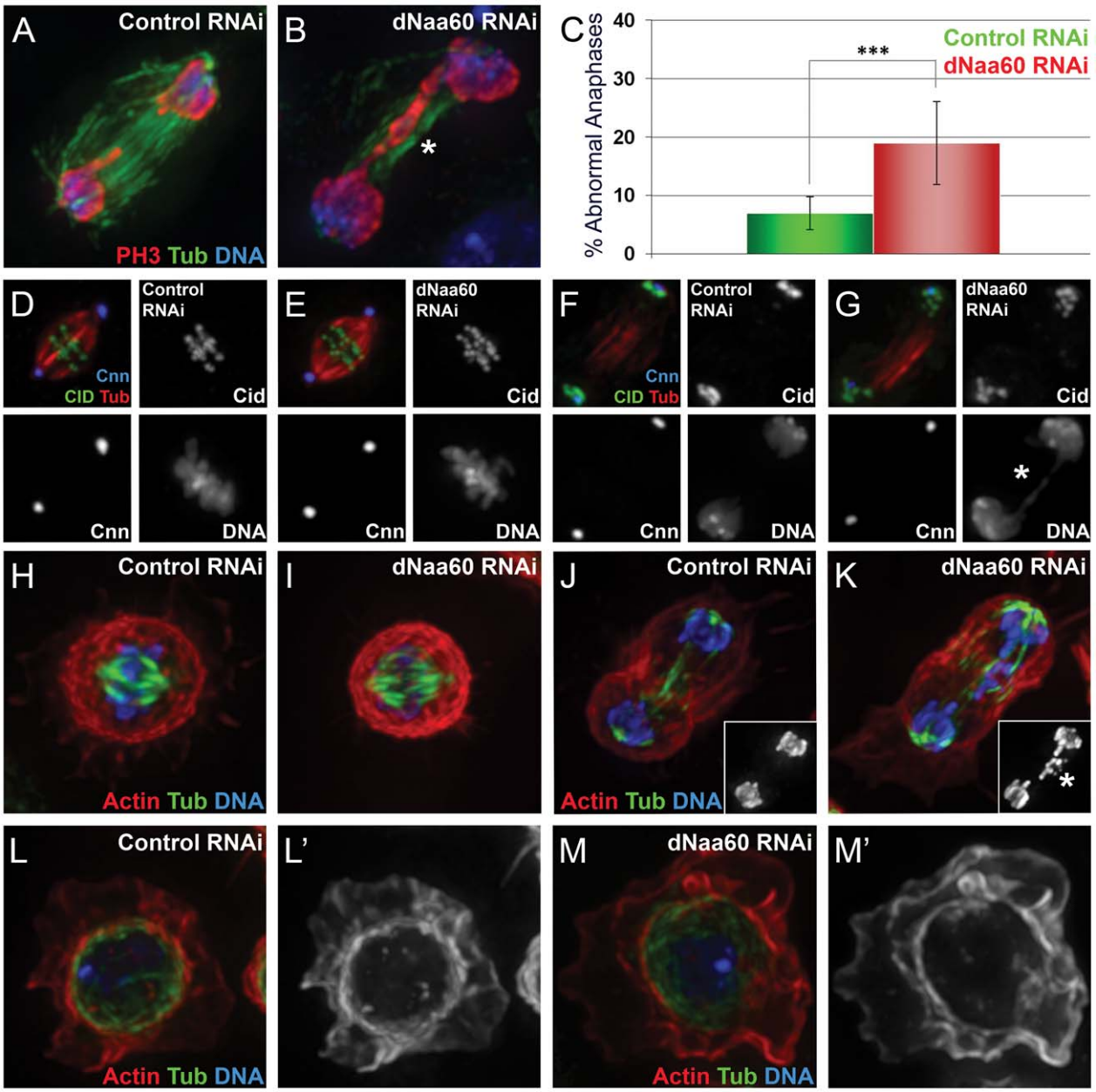

Figure 8. dNaa60p is required for chromosome segregation during anaphase. Control dsRNA treated cells (A,D,F,H,J and L). d*NAA60* dsRNA treated cells (B,E,G,I,K and M). d*NAA60*-depleted cells exhibited chromosome segregation defects during anaphase (A–C). These defects included lagging chromosomes (K, highlighted by asterisk) and chromosome bridges (B and G, highlighted by asterisk). Quantification of chromosome segregation defects in d*NAA60*-depleted cells (n = 278) and control cells (n = 179) (***p<0,001 Student's test) (C). Histone 3 phosphorylated on Serine 10 (red), α-tubulin (green) and DNA (blue). d*NAA60*-depleted cells showed no significant defects in the localization of both Cnn and Cid proteins (D–G). Both control and d*NAA60*-depleted cells exhibited bypolar spindles with correct alignment of chromosomes at the metaphase plate (D,E). Anaphase cells with chromosome segregation defects in d*NAA60*-depleted cells showed no obvious defects in Cnn and Cid localization (F,G). α-tubulin (red), Cid (green) and Cnn (blue). Control and d*NAA60*-depleted cells exhibit proper chromosome alignment during metaphase with no detectable defects in the actin and microtubule cytoskeleton (H,I). d*NAA60*-depleted cells undergoing anaphase with chromosome segregation defects also showed a normal actin and microtubule cytoskeleton (J,K; details show histone 3 phosphorylated on serine 10 staining). d*NAA60*-depleted cells in interphase show no detectable defects regarding the actin and microtuble cytoskeleton (L–M). Actin (red), α-Tubulin (green) and Histone 3 phosphorylated on Serine 10 (blue).
doi:10.1371/journal.pgen.1002169.g008

Construction of plasmids

Plasmid encoding V5-tagged NAT15/hNaa60p (Gene ID: 79903) used for mammalian expression was constructed from human HEK293 cDNA by use of Transcriptor Reverse Transcriptase (Roche). The PCR product containing the CDS plus four 5′ nucleotides (gaga) was inserted into the TOPO TA vector pcDNA 3.1/V5-His TOPO Invitrogen) according to the instruction manual. An *E. coli* expression vector encoding MBP-His-tagged hNaa60p was constructed by subcloning h*NAA60* from ph*NAA60*-V5 to the pETM-41 vector using the *Acc65I* and *NcoI*

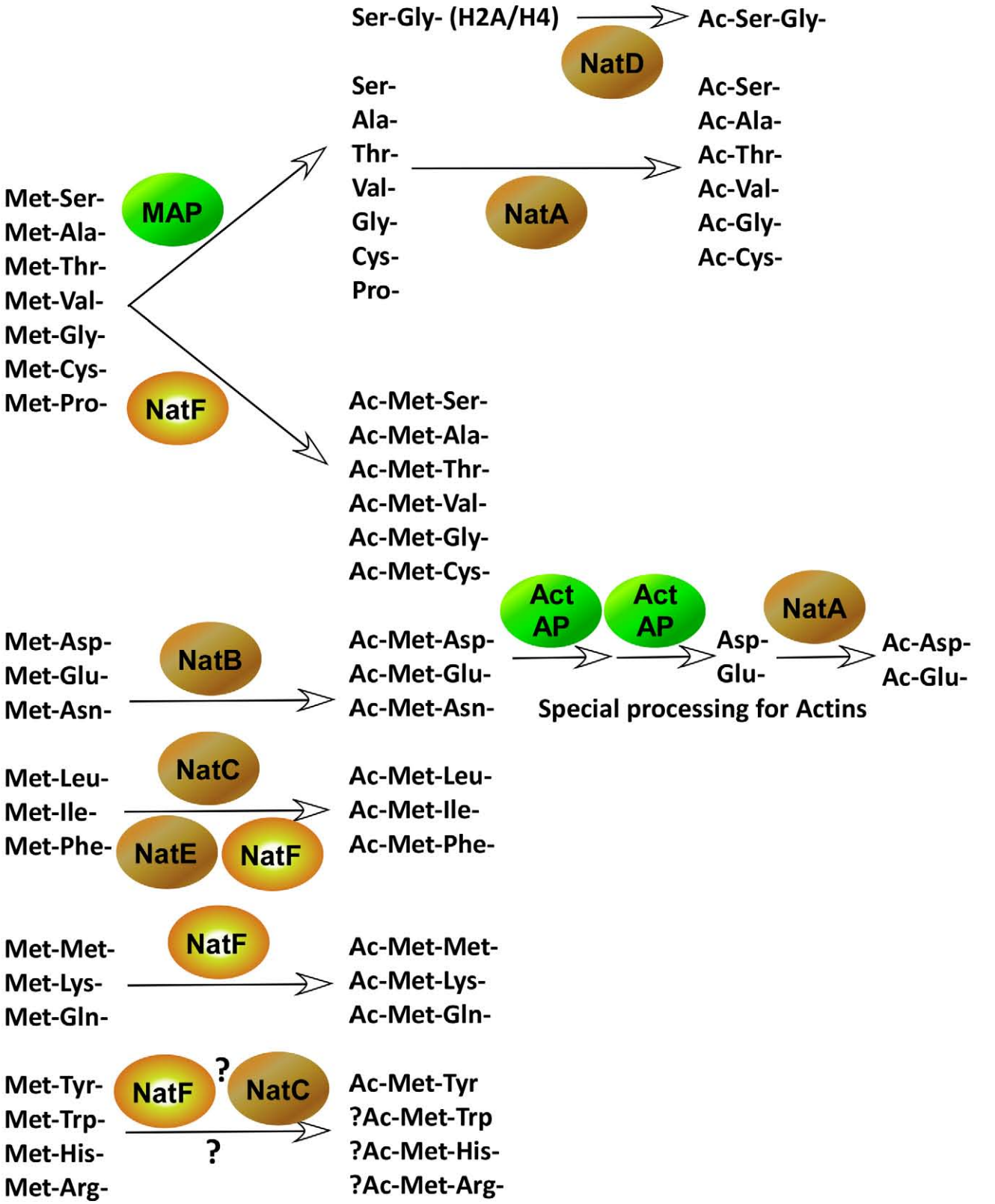

Figure 9. The major pathways of protein N-terminal processing in higher eukaryotes. N-termini of which the iMet is followed by one of the small amino acids, Ser-, Ala-, Thr-, Val-, Gly-, Cys-, and Pro- often undergo iMet cleavage performed by a methionine aminopeptidase (MAP). These N-termini, with the exception of Pro-, are often further acetylated by NatA, or in the case of Histone H2A and H4, by NatD (Hole K. *et al.*, unpublished). However, this group of N-termini may also be acetylated by NatF. Met-Asp-, Met-Glu- and Met-Asn- are acetylated by NatB. Actins are further processed in one or more steps by unidentified Actin aminopeptidases (Act AP). The acidic actin N-termini are then acetylated by at NAT, presumably NatA [38]. Hydrophobic Met-Leu-, Met-Ile- and Met-Phe- are acetylated by NatC, but also by NatF as well as by NatE *in vitro*, suggesting potential

redundancy between these NATs. Met-Met-, Met-Lys- and Met-Gln- are acetylated by NatF and potentially other NATs. Information about Met-His-, Met-Arg-, Met-Trp- and Met-Tyr- is limited, but it is likely that some of these N-termini are acetylated as well, by NatF and perhaps NatC.
doi:10.1371/journal.pgen.1002169.g009

sites. pETM-41-d*NAA60*, encoding the predicted fruit fly Naa60p was made by subcloning the CG18177 CDS from pOT2-CG18177 (clone LD27619 from the Drosophila Genomics Resource Centre, Indiana University) to pETM-41. pETM-41 was generously provided by G. Stier, EMBL, Heidelberg. A yeast expression vector, pBEVY-U-h*NAA60* encoding untagged hNaa60p was constructed by subcloning h*NAA60* from ph*NAA60*-V5 to the pBEVY-U vector [47] using the *BamHI* and *SalI* sites.

E. coli protein expression and purification

The plasmid pETM-41-h*NAA60* or pETM-41-d*NAA60* was transformed into *E. coli* BL21 Star^{TM} (DE3) cells (Invitrogen) by heat shock. A 200 ml cell culture was grown in LB (Luria Bertani) medium to an OD_{600} nm of 0.6 at 37°C and subsequently transferred to 20°C. After 30 min of incubation, protein expression was induced by IPTG (1 mM). After 17 h of incubation, the cultures were harvested by centrifugation and the pellets stored at −20°C. *E. coli* pellets containing recombinant proteins were thawed at 4°C and the cells lysed by sonication in lysis buffer (1 mM DTT, 50 mM Tris-HCl (pH 7.5 or 8.3 for MBP-dNAA60p and MBP-hNAA60p, respectively), 300 mM NaCl, 1 tablet EDTA-free protease Inhibitor cocktail per 50 ml (Roche)). Following centrifugation, the cell extracts were applied on a metal affinity FPLC column (HisTrap HP, GE Healthcare, Uppsala, Sweden). MBP-hNaa60p and MBP-dNaa60p were eluted with 300 mM Imidazole in 50 mM Tris (pH 7.5 or 8.3 for MBP-dNAA60 or MBP-hNAA60, respectively), 300 mM NaCl and 1 mM DTT. Fractions containing recombinant protein were pooled and further purified using size exclusion chromatography (Superdex^{TM} 75, GE Healthcare) until apparent purity as analysed by Coomassie stained SDS-PAGE gels. The protein concentrations were determined by OD_{280} nm measurements.

In vitro peptide library-based NAT assay using hNaa60p and dNaa60p

Preparation of proteome derived peptide libraries. Proteome-derived peptide libraries were generated from human K-562 cells. Cells were repeatedly (3×) washed in D-PBS and then re-suspended at 7×10^6 cells per ml in lysis buffer (50 mM sodium phosphate buffer pH 7.5, 100 mM NaCl, 1% CHAPS and 0.5 mM EDTA) in the presence of protease inhibitors (Complete protease inhibitor cocktail tablet (Roche Diagnostics, Mannheim, Germany)). After lysis for 10 min on ice, the lysate was cleared by centrifugation for 10 min at 16,000× g and solid guanidinum hydrochloride was added to the supernatant to a final concentration of 4 M. The protein samples were reduced and *S*-alkylated, followed by tri-deuteroacetylation of primary amines and digestion with trypsin as described previously [48,49]. The resulting peptide mixtures were vacuum dried. The dried peptides were re-dissolved in 500 µl 50% acetonitrile. The sample was acidified to pH 3.0 using a stock solution of 1% TFA in 50% acetonitrile and further diluted with 10 mM sodium phosphate in 50% acetonitrile to a final volume of 1 ml. This peptide mixture was then loaded onto an AccuBONDII SCX SPE cartridge (Agilent Technologies, Waldbronn, Germany) and SCX separation (SCX fractionation 1) of N^{α}-blocked N-terminal peptides (and C-terminal peptides) from N^{α}-free peptides was performed as described previously [48,50]. The flow-through containing the N^{α}-blocked N-terminal peptides and C-terminal peptides was discarded and the SCX-bound fraction (containing the N^{α}-free peptides) was collected by elution with 4 ml of 400 mM NaCl and 10 mM sodium phosphate in 40% of acetonitrile (pH 3.0). Eluted peptides were vacuum dried and re-dissolved in 1 ml of HPLC solvent A (10 mM ammonium acetate in 2% acetonitrile, pH 5.5). C18 solid-phase extraction (SPE desalting step) of the N^{α}-free peptides was performed by loading the peptide mixture onto a AccuBONDII ODS-C18 SPE cartridge (1 ml tube, 100 mg, Agilent Technologies). This cartridge has a binding capacity of 1 mg of peptides and thus for each mg of material, a separate cartridge was used. Prior to sample loading, the cartridges were washed with 2 ml of 50% acetonitrile and then washed with 5 ml of HPLC solvent A. Sample loading was followed by washing the C18 cartridge with 5 ml of 2% acetonitrile. Peptides were eluted with 3 ml of 70% acetonitrile and subsequently vacuum dried.

In vitro peptide library-based NAT assay. 100 nmol of the desalted N^{α}-free peptide pool was reconstituted in acetylation buffer (50 mM Tris-HCl (pH 8.5), 1 mM DTT, 800 µM EDTA, 10% glycerol) together with equimolar amounts of a stable isotope encoded variant of acetyl-CoA, $^{13}C_2$-acetyl CoA, (99% $^{13}C_2$-acetyl CoA, ISOTEC-Sigma (lithium salt)) and 1 nmol of enzyme (i.e. recombinant hNaa60p or dNaa60p) was added to a final reaction volume of 1 ml. The reaction was allowed to proceed for 1 h at 37°C and stopped by addition of acetic acid to a 5% final concentration. SPE was then performed as described above.

NAT oligopeptide-substrate recovery and RP-HPLC based separation. Peptides starting with pyroglutamate were unblocked prior to the second SCX fractionation step. Here, 25 µl of pGAPase (25 U/ml) (TAGZyme kit, Qiagen, Hilden, Germany) was activated for 10 min at 37°C by addition of 1 µl of 50 mM EDTA (pH 8.0), 1 µl of 800 mM NaCl, and 11 µl of freshly prepared 50 mM cysteamine-HCl. 25 µl of Qcyclase (50 U/ml, TAGZyme) was then added to the pGAPase solution. The dried peptides were re-dissolved in 212 µl of buffer containing 16 mM NaCl, 0.5 mM EDTA, 3 mM cysteamine, and 50 µM aprotinin. The activated pGAPase and Q-cyclase mixture was added to the peptide sample and the mixture (275 µl total volume) was incubated for 60 min at 37°C. 275 µl acetonitrile was then added and the sample was acidified to pH 3 using a 1% TFA stock solution in 50% acetonitrile. The sample was further diluted with 10 mM sodium phosphate in 50% acetonitrile to a final volume of 1 ml. SCX enrichment of N^{α}-blocked N-terminal peptides was performed as described [48] (SCX fractionation 2). The SCX fraction containing the newly blocked N-terminal peptides was vacuum dried and re-dissolved in 100 µl of HPLC solvent A. To prevent oxidation of methionine between the primary and secondary RP-HPLC separations (and thus unwanted segregation of methionyl peptides [51], methionines were uniformly oxidized to sulfoxides prior to the primary RP-HPLC run by adding 2 µl of 30% (w/v) H_2O_2 (final concentration of 0.06%) for 30 min at 30°C. This peptide mixture was injected onto a RP-column (Zorbax 300SB-C18 Narrowbore, 2.1 mm (internal diameter)×150 mm length, 5 µm particles, Agilent Technologies) and the RP-HPLC separation was performed as described previously [48]. Fractions of 30 s wide were collected from 20 to 80 min after sample injection (120 fractions). To reduce LC-MS/MS analysis time, fractions eluting 12 min apart were pooled, vacuum dried and re-dissolved in 40 µl of 2% acetonitrile. In total, 24 pooled

fractions per setup were subjected to LC-MS/MS analysis (see below).

LC-MS/MS analysis. LC-MS/MS analysis was performed using an Ultimate 3000 HPLC system (Dionex, Amsterdam, The Netherlands) in-line connected to a LTQ Orbitrap XL mass spectrometer (Thermo Electron, Bremen, Germany) and, per LC-MS/MS analysis, 2 µl of sample was consumed. LC-MS/MS analysis and generation of MS/MS peak lists were performed as described [52]. These MS/MS peak lists were then searched with Mascot using the Mascot Daemon interface (version 2.2.0, Matrix Science). The Mascot search parameters were set as follows. Searches were performed in the Swiss-Prot database with taxonomy set to human (UniProtKB/SwissProt database version 2010_05 containing 20,286 human protein sequences). Trideutero-acetylation at lysines, carbamidomethylation of cysteine and methionine oxidation to methionine-sulfoxide were set as fixed modifications. Variable modifications were trideutero-acetylation, acetylation and $^{13}C_2$-acetylation of protein N-termini and pyroglutamate formation of N-terminal glutamine. Endoproteinase Arg-C/P (Arg-C specificity with arginine-proline cleavage allowed) was set as enzyme allowing no missed cleavages. The mass tolerance on the precursor ion was set to 10 ppm and on fragment ions to 0.5 Da. The estimated false discovery rate by searching decoy databases was typically found to lie between 2 and 4% on the spectrum level [48]. Quantification of the degree of N-Ac was done as previously explained [18].

In vitro N-terminal acetylation assay using purified MBP-hNaa60p and synthetic peptides

Purified MBP-hNaa60p (500 nM) was mixed with selected oligopeptide substrates (200 µM) and 300 µM of acetyl-CoA in a total volume of 50 µl acetylation buffer (50 mM Tris (pH 8.5), 800 µM EDTA, 10% glycerol, 1 mM DTT) and incubated at 37°C for 35 min. The enzyme activities were quenched by the addition of 5 µl of 10% TFA. Peptide acetylation was quantified using RP-HPLC as described previously [23].

Synthetic peptide sequences

Peptides were custom-made (Biogenes) to a purity of 80–95%. All peptides contain 7 unique amino acids at their N-terminus, as these are the major determinants influencing N-terminal acetylation. The next 17 amino acids are essentially identical to the ACTH peptide sequence (RWGRPVGRRRRPVRVYP) however; lysines were replaced by arginines to minimize any potential interference by N^{ε}-acetylation. Oligopeptide sequences:

SYSM-RRR (ACTH (aa138–161, P01189): [H] SYSMDHF*RWGRPVGRRRRPVRVYP* [OH]; MDEL-RRR (NF-kκB p65, Q04206): [H] MDELFPL*RWGRPVGRRRRPVRVYP* [OH]; MLGT-RRR (hnRNP H, P31943): [H] MLGTEGG*RWGRPVGRRRRPVRVYP* [OH]; MAPL-RRR (Prot phosphatase 6, O00743): [H] MAPLDLD*RWGRPVGRRRRPVRVYP* [OH]; MLGP-RRR (hnRNP F, P52597): [H] MLGPEGG*RWGRPVGRRRRPVRVYP* [OH]; SESS-RRR (High mob. gr. prot A1, P17096): [H] SESSSKS*RWGRPVGRRRRPVRVYP* [OH]; MKKS-RRR (Septin 9, Q9UHD8): [H] MKKSYSG*RWGRPVGRRRRPVRVYP* [OH].

Yeast strain generation and cultivation for *in vivo* N-terminal acetylation analysis

The *S. cerevisiae* MATalpha strain BY4742 (Euroscarf) was transformed with pBEVY-U or pBEVY-U-h*NAA60* and transformants were selected on plates lacking uracil. The two strains generated, BY4742-pBEVY-U (yeast normal) and BY4742-pBEVY-U-h*NAA60* (yeast+NatF), were cultivated in 300 ml synthetic medium lacking uracil (Sigma) to an OD600nm of ~3. After harvesting, cells were washed twice in lysis buffer (50 mM Tris, 12 mM EDTA, 250 mM NaCl, 140 mM Na_2HPO_4 (pH 7.6) supplemented with a complete protease inhibitor mixture tablet (1 tablet per 100 mL) (Roche Diagnostics) and glass beads were added before several rounds of vortex/ice (10×). One milliliter of lysis buffer was used for a pellet resulting from 300 mL of yeast culture. The lysates were centrifuged at 5000× *g* for 10 min and the retained supernatants were analyzed by COFRADIC analyses. Aliquots were analysed by SDS-PAGE and Western blotting using anti-hNaa60p. Solid guanidinium hydrochloride was added to a final concentration of 4 M in order to inactivate proteases and denature all proteins. Subsequently, proteins were reduced and alkylated simultaneously, using TCEP.HCl (1 mM final concentration (f.c.)) and IAA (2 mM f.c.) respectively, for 1 h at 30°C. Subsequent steps of the N-terminal COFRADIC protocol were performed as described previously [48]. Aliquots were analysed by SDS-PAGE and Western blotting using anti-hNaa60p.

Human cell culture and transfection

HeLa cells (epithelial cervix adenocarcinoma, ATCC CCL-2) were cultured in Glutamax-containing DMEM medium supplemented with 10% dialyzed foetal bovine serum (Invitrogen, Carlsbad, CA, USA), 100 units/ml penicillin (Invitrogen) and 100 µg/ml streptomycin (Invitrogen). Cells were grown in media containing either natural ($^{12}C_6$) or $^{13}C_6{}^{15}N_4$ L-arginine (Cambridge Isotope Labs, Andover, MA, USA) [53] at a concentration of 80 µM (i.e. 20% of the suggested concentration present in DMEM at which L-arginine to proline conversion was not detectable for HeLa cells). Cells were cultured for at least six population doublings to ensure complete incorporation of the labeled arginine. Human K-562 cells (ATCC CCL-243) were grown in Glutamax-containing RPMI-1640 medium supplemented with 10% foetal calf serum, 100 units/ml penicillin and 100 µg/ml streptomycin. Cells were cultured at 37°C and in 5% CO_2.

Plasmid transfections were performed using Fugene6 (Roche) according to the instruction manual. siRNA transfections were performed using Dharmafect 1 (Dharmacon). In the overexpression experiment, 10×10 cm dishes of cells cultivated in $^{13}C_6{}^{15}N_4$ L-arginine were transfected with control vector and cells cultivated in $^{12}C_6$ L-arginine were transfected with ph*NAA60*-V5. Cells were harvested 48 hours post-transfection. Aliquots were analysed by SDS-PAGE and Western blotting using anti-V5 (Invitrogen) to confirm efficient overexpression (See Figure 6A). In the knockdown experiment, 10×10 cm dishes of control control cells cultivated in $^{12}C_6$ L-arginine were transfected with 50 nM si-non-targeting control (D-001810, Dharmacon) and cells cultivated in $^{13}C_6{}^{15}N_4$ L-arginine were transfected with 50 nM sih*NAA60* pool (D-014479, Dharmacon). After 48 hours of transfection, the medium was replaced by new SILAC medium containing 5 µM zVAD-fmk. After 84 hours, cells were harvested, lysed and subjected to COFRADIC analysis as described previously [18]. Aliquots were analysed by SDS-PAGE and Western blotting using anti-hNaa60p (Custom made affinity purified rabbit antibody targeting a peptide corresponding to aa 69–82 of hNaa60p, Biogenes) to confirm efficient knockdown (See Figure 6B). Each sample of the knockdown- and overexpression experiments resulted from 10×10 cm dishes of cells and was processed further for N-terminal COFRADIC analyses as described previously [18].

Quantification of the degree of N^{α}-acetylation

The ratios of N^{α}-acetylation for all N-termini were quantified using MASCOT Distiller. The extent of N^{α}-acetylation was calculated after extracting the corresponding peak intensities (extracted from the resulting rov-files). The modified peptide sequences were used to calculate the theoretical isotope peak distribution using the MS-isotope pattern calculator (http://prospector.ucsf.edu). For both variants (i.e., in vivo N^{α}-acetylated (peak at m/z) and *in vitro* $^{13}C_2D_3$-N^{α}-acetylated (peak at m/z+5 Da)), the predicted intensity of the 5th contributing isotope was subtracted from the measured intensity of the corresponding monoisotopic peak of the other overlapping isotopic envelopes in order to correct for overlapping isotopic envelopes. Only the corresponding highest scoring MS/MS-spectra were withheld and inspected to evaluate the calculated N^{α}-acetylation degree (in case of inconsistencies, whenever possible the second, third or next highest scoring MS/MS-spectra were inspected to evaluate the calculated N^{α}-acetylation degree, if inconclusive the status was set as "N.D."). When unclear MS-spectra were observed, the N-Ac status was also documented as "N.D.". When no clear isotopic envelope was present for one of the possible variants, the status was set at 0% and 100% or 100% and 0% respectively. Further, if the N^{α}-acetylation calculated was $\leq$2% of $\geq$98%, the overall N-Ac status was accounted for as being free or fully N-Ac respectively.

When comparing the degrees of N^{α}-acetylation from two independent control experiments (with the degrees of N^{α}-acetylation of more than 1,000 unique N-termini calculated) and taking into account a [x−10%, x+10%] interval around the calculated x-value (the x-value being the degree (%) of N^{α}-acetylation for the calculated data point in one dataset), the p-value was calculated to be $p<0.01$, indicating that upon setting these limits, less than 1% of all measured N-Ac values differed more than 10%. Therefore, a significant variation in the degree of N^{α}-acetylation was set to 10% or more. In the case of free N-termini identified in a control setup however, significance was set to 5% since in this case two isotopic envelopes could clearly be distinguished.

RNA interference and immunofluorescence microscopy of *Drosophila* Dmel2 cells

Dmel2 cells were cultured at 25°C and RNAi was performed according to standard procedures. To deplete dNaa60 (CG18177), Dmel2 cells were separately transfected with two different double-stranded RNAs (dsRNA) corresponding to fragments of dNaa60 defined by the set of primers (Forward-1) CAACAAACA-CAGTGCGCC and (Reverse-1) CACATTTCGATAGGGTTT-GATTTC or (Forward-2) GACTCGATGGGTCGTTCCGC and (Reverse-2) GTGGATGGCCGCCGTTAAT. GFP-targeting dsRNA was used as control. Each primer incorporates a T7 RNA polymerase binding site. All PCR products were used as template to synthesize dsRNA by use of the T7 RiboMAX Express kit (Promega). *Drosophila* Dmel2 cells were grown in SFM Medium (GIBCO) supplemented with 1× glutamine and 1× PenStrep (GIBCO). Cells were counted and diluted to 2×10^6 cells/ml in SFM medium supplemented with glutamine. Cells were incubated during 1 h with 40 µg for each dsRNA at a concentration of 1 µg/µl. After 1 h incubation with dsRNA, 3 ml of SFM media supplemented with glutamine and PenStrep (GIBCO) was added back. After 93 h dsRNA treatment, 2×10^6 cells were added to coverslips by 1 h incubation at 25°C. Cells were fixed with 4% formaldehyde, 0.03 M PIPES, 0.11 M HEPES, 0.01 M EGTA and 4 mM $MgSO_4$ for 10 min, followed by two washes in 1× PBS. Permeabilization and blocking was performed for 1 h with PBS-TB (PBS, 0.1% Triton X-100, 1% fetal bovine serum). Primary antibody incubations were done in blocking solution for 2 h at room temperature or overnight at 4°C, followed by three 5 min washes in PBS-TB. Secondary antibody incubations were performed as described for the primary antibodies, including three 5 min washes. Primary antibodies included mouse anti-α-tubulin DM1A (1:500; Sigma), rabbit anti-pSer10-Histone H3 (1:500; Upstate Biotechnology), chicken anti-Cid (1:500; kindly provided by David Glover's laboratory) and rabbit anti-Cnn (1:500; kindly provided by Jordan Raff). F-actin was stained with rhodamine-conjugated phalloidin (Sigma) and DNA was stained with DAPI at 1:1000 (stock concentration 1 mg/ml), with the addition of 5 µg/ml RNAse A. Visualization of fixed cells was performed using a Delta Vision Core System (Applied Precision) using a 100× UplanSApo objective and a cascade2 EMCCD camera (Photometrics). Images were acquired as a series of z-sections separated by 0.2-µm intervals. Deconvolution was performed using the conservative ratio method in softWoRx software. Phenotypic quantification was performed using a regular Epifluorescent microscope Leica DMRA2.

Supporting Information

Figure S1 Amino acid frequencies at position 2 of hNaa60p and dNaa60p substrates. Bar charts of the amino acid frequencies at the 2nd position in the Met- (black bars) and Leu-starting (red bars) oligopeptide substrates identified in proteome-derived peptide library screens of hNaa60p (upper panel) and dNaa60p (lower panel).
(TIF)

Figure S2 d*NAA50* but not d*NAA60* dsRNAi treated cells arrest in mitosis. Graph showing mitotic index in control, *dNAA60* and *dNAA50* dsRNA treated Dmel2 cells. Mitotic index is the percentage of cells positive for phospho-Histone H3 (pSer10).
(TIF)

Table S1 List of 868 unique N-terminal peptides (start position 1 or 2) identified in the proteome of the control yeast strain and/or the yeast strain expressing hNaa60p.
(DOC)

Table S2 List of 1,497 human N-terminal peptides (start position 1 or 2) identified in the hNaa60p overexpression or knockdown experiments in HeLa cells.
(DOC)

Table S3 Relating the occurrence of N-Ac and different N-termini in yeast and humans. An unbiased estimation of N-Ac for all methionine-starting yeast (6613) and human SwissProt entries (20102) (SwissProt version 57.8) was performed based on the nature of the N-terminal amino acids and the N-terminal acetylation status uncovered in this study.
(DOC)

Table S4 List of the 72 unique *in vivo* hNaa60p substrate N-termini identified in yeast. S4A. hNaa60p yeast substrate N-termini (44) which were completely unacetylated in the control setup analyzed. S4B. hNaa60p yeast substrate N-termini (28) which were partially N-Ac in the control setup analyzed.
(DOC)

Table S5 List of N-termini affected in their N-Ac status by knockdown or overexpression of hNaa60p in HeLa cells.
(DOC)

Acknowledgments

Nina Glomnes is thanked for valuable technical assistance.

Author Contributions

Conceived and designed the experiments: P Van Damme, RG Martinho, K Gevaert, T Arnesen. Performed the experiments: P Van Damme, K Hole, A Pimenta-Marques, K Helsens, T Arnesen. Analyzed the data: P Van Damme, K Hole, A Pimenta-Marques, J Vandekerckhove, RG Martinho, K Gevaert, T Arnesen. Wrote the paper: P Van Damme, K Gevaert, T Arnesen.

References

1. Behnia R, Panic B, Whyte JR, Munro S (2004) Targeting of the Arf-like GTPase Arl3p to the Golgi requires N-terminal acetylation and the membrane protein Sys1p. Nat Cell Biol 6: 405–413.
2. Caesar R, Blomberg A (2004) The stress-induced Tfs1p requires NatB-mediated acetylation to inhibit carboxypeptidase Y and to regulate the protein kinase A pathway. J Biol Chem 279: 38532–38543.
3. Coulton AT, East DA, Galinska-Rakoczy A, Lehman W, Mulvihill DP (2010) The recruitment of acetylated and unacetylated tropomyosin to distinct actin polymers permits the discrete regulation of specific myosins in fission yeast. J Cell Sci 123: 3235–3243.
4. Setty SR, Strochlic TI, Tong AH, Boone C, Burd CG (2004) Golgi targeting of ARF-like GTPase Arl3p requires its Nalpha-acetylation and the integral membrane protein Sys1p. Nat Cell Biol 6: 414–419.
5. Hwang CS, Shemorry A, Varshavsky A (2010) N-terminal acetylation of cellular proteins creates specific degradation signals. Science 327: 973–977.
6. Ciechanover A, Ben Saadon R (2004) N-terminal ubiquitination: more protein substrates join in. Trends Cell Biol 14: 103–106.
7. Gautschi M, Just S, Mun A, Ross S, Rücknagel P, et al. (2003) The yeast N(alpha)-acetyltransferase NatA is quantitatively anchored to the ribosome and interacts with nascent polypeptides. Mol Cell Biol 23: 7403–7414.
8. Giglione C, Fieulaine S, Meinnel T (2009) Cotranslational processing mechanisms: towards a dynamic 3D model. Trends Biochem Sci 34: 417–426.
9. Pestana A, Pitot HC (1975) Acetylation of nascent polypeptide chains on rat liver polyribosomes in vivo and in vitro. Biochemistry 14: 1404–1412.
10. Polevoda B, Brown S, Cardillo TS, Rigby S, Sherman F (2008) Yeast N(alpha)-terminal acetyltransferases are associated with ribosomes. J Cell Biochem 103: 492–508.
11. Strous GJ, van Westreenen H, Bloemendal H (1973) Synthesis of lens protein in vitro. N-terminal acetylation of alpha-crystallin. Eur J Biochem 38: 79–85.
12. Strous GJ, Berns AJ, Bloemendal H (1974) N-terminal acetylation of the nascent chains of alpha-crystallin. Biochem Biophys Res Commun 58: 876–884.
13. Bradshaw RA, Brickey WW, Walker KW (1998) N-terminal processing: the methionine aminopeptidase and N alpha-acetyl transferase families. Trends Biochem Sci 23: 263–267.
14. Tsunasawa S, Stewart JW, Sherman F (1985) Amino-terminal processing of mutant forms of yeast iso-1-cytochrome c. The specificities of methionine aminopeptidase and acetyltransferase. J Biol Chem 260: 5382–5391.
15. Polevoda B, Arnesen T, Sherman F (2009) A synopsis of eukaryotic Nalpha-terminal acetyltransferases: nomenclature, subunits and substrates. BMC Proc 3 Suppl 6: S2.
16. Mullen JR, Kayne PS, Moerschell RP, Tsunasawa S, Gribskov M, et al. (1989) Identification and characterization of genes and mutants for an N-terminal acetyltransferase from yeast. EMBO J 8: 2067–2075.
17. Arnesen T, Anderson D, Baldersheim C, Lanotte M, Varhaug JE, et al. (2005) Identification and characterization of the human ARD1-NATH protein acetyltransferase complex. Biochem J 386: 433–443.
18. Arnesen T, Van Damme P, Polevoda B, Helsens K, Evjenth R, et al. (2009) Proteomics analyses reveal the evolutionary conservation and divergence of N-terminal acetyltransferases from yeast and humans. Proc Natl Acad Sci U S A 106: 8157–8162.
19. Polevoda B, Norbeck J, Takakura H, Blomberg A, Sherman F (1999) Identification and specificities of N-terminal acetyltransferases from Saccharomyces cerevisiae. EMBO J 18: 6155–6168.
20. Starheim KK, Arnesen T, Gromyko D, Ryningen A, Varhaug JE, et al. (2008) Identification of the human N(alpha)-acetyltransferase complex B (hNatB): a complex important for cell-cycle progression. Biochem J 415: 325–331.
21. Starheim KK, Gromyko D, Evjenth R, Ryningen A, Varhaug JE, et al. (2009) Knockdown of human N alpha-terminal acetyltransferase complex C leads to p53-dependent apoptosis and aberrant human Arl8b localization. Mol Cell Biol 29: 3569–3581.
22. Song OK, Wang X, Waterborg JH, Sternglanz R (2003) An Nalpha-acetyltransferase responsible for acetylation of the N-terminal residues of histones H4 and H2A. J Biol Chem 278: 38109–38112.
23. Evjenth R, Hole K, Karlsen OA, Ziegler M, Arnesen T, et al. (2009) Human Naa50p (Nat5/San) displays both protein N alpha- and N epsilon-acetyltransferase activity. J Biol Chem 284: 31122–31129.
24. Ametzazurra A, Larrea E, Civeira MP, Prieto J, Aldabe R (2008) Implication of human N-alpha-acetyltransferase 5 in cellular proliferation and carcinogenesis. Oncogene 27: 7296–7306.
25. Arnesen T, Gromyko D, Pendino F, Ryningen A, Varhaug JE, et al. (2006) Induction of apoptosis in human cells by RNAi-mediated knockdown of hARD1 and NATH, components of the protein N-alpha-acetyltransferase complex. Oncogene 25: 4350–4360.
26. Fisher TS, Etages SD, Hayes L, Crimin K, Li B (2005) Analysis of ARD1 function in hypoxia response using retroviral RNA interference. J Biol Chem 280: 17749–17757.
27. Gromyko D, Arnesen T, Ryningen A, Varhaug JE, Lillehaug JR (2010) Depletion of the human N(alpha)-terminal acetyltransferase A (hNatA) induces p53-dependent apoptosis and p53-independent growth inhibition. Int J Cancer.
28. Lim JH, Park JW, Chun YS (2006) Human arrest defective 1 acetylates and activates beta-catenin, promoting lung cancer cell proliferation. Cancer Res 66: 10677–10682.
29. Hou F, Chu CW, Kong X, Yokomori K, Zou H (2007) The acetyltransferase activity of San stabilizes the mitotic cohesin at the centromeres in a shugoshin-independent manner. J Cell Biol 177: 587–597.
30. Pimenta-Marques A, Tostões R, Marty T, Barbosa V, Lehmann R, et al. (2008) Differential requirements of a mitotic acetyltransferase in somatic and germ line cells. Dev Biol 323: 197–206.
31. Williams BC, Garrett-Engele CM, Li Z, Williams EV, Rosenman ED, et al. (2003) Two putative acetyltransferases, san and deco, are required for establishing sister chromatid cohesion in Drosophila. Curr Biol 13: 2025–2036.
32. Goetze S, Qeli E, Mosimann C, Staes A, Gerrits B, et al. (2009) Identification and functional characterization of N-terminally acetylated proteins in Drosophila melanogaster. PLoS Biol 7: e1000236. doi:10.1371/journal.pbio.1000236.
33. Arnesen T, Starheim KK, Van Damme P, Evjenth R, Dinh H, et al. (2010) The chaperone-like protein HYPK acts together with NatA in cotranslational N-terminal acetylation and prevention of Huntingtin aggregation. Mol Cell Biol 30: 1898–1909.
34. Helbig AO, Gauci S, Raijmakers R, van Breukelen B, Slijper M, et al. (2010) Profiling of N-acetylated protein termini provides in-depth insights into the N-terminal nature of the proteome. Mol Cell Proteomics 9: 928–939.
35. Raghava GP, Han JH (2005) Correlation and prediction of gene expression level from amino acid and dipeptide composition of its protein. BMC Bioinformatics 6: 59.
36. Ding Y, Cai Y, Zhang G, Xu W (2004) The influence of dipeptide composition on protein thermostability. FEBS Lett 569: 284–288.
37. Bhasin M, Raghava GP (2004) ESLpred: SVM-based method for subcellular localization of eukaryotic proteins using dipeptide composition and PSI-BLAST. Nucleic Acids Res 32: W414–W419.
38. Van Damme P, Evjenth R, Foyn H, Demeyer K, De Bock PJ, et al. (2011) Proteome-derived peptide libraries allow detailed analysis of the substrate specificities of N{alpha}-acetyltransferases and point to hNaa10p as the posttranslational actin N{alpha}-acetyltransferase. Mol Cell Proteomics.
39. Colaert N, Helsens K, Martens L, Vandekerckhove J, Gevaert K (2009) Improved visualization of protein consensus sequences by iceLogo. Nat Methods 6: 786–787.
40. Finney JL, Gellatly BJ, Golton IC, Goodfellow J (1980) Solvent effects and polar interactions in the structural stability and dynamics of globular proteins. Biophys J 32: 17–33.
41. Guy HR (1985) Amino acid side-chain partition energies and distribution of residues in soluble proteins. Biophys J 47: 61–70.
42. Arnesen T, Betts MJ, Pendino F, Liberles DA, Anderson D, et al. (2006) Characterization of hARD2, a processed hARD1 gene duplicate, encoding a human protein N-alpha-acetyltransferase. BMC Biochem 7: 13.
43. Arnesen T, Gromyko D, Kagabo D, Betts MJ, Starheim KK, et al. (2009) A novel human NatA Nalpha-terminal acetyltransferase complex: hNaa16p-hNaa10p (hNat2-hArd1). BMC Biochem 10: 15.
44. Veiga-da-Cunha M, Tyteca D, Stroobant V, Courtoy PJ, Opperdoes FR, et al. (2010) Molecular identification of NAT8 as the enzyme that acetylates cysteine S-conjugates to mercapturic acids. J Biol Chem 285: 18888–18898.
45. Wiame E, Tyteca D, Pierrot N, Collard F, Amyere M, et al. (2010) Molecular identification of aspartate N-acetyltransferase and its mutation in hypoacetylaspartia. Biochem J 425: 127–136.
46. Guelman S, Kozuka K, Mao Y, Pham V, Solloway MJ, et al. (2009) The double-histone-acetyltransferase complex ATAC is essential for mammalian development. Mol Cell Biol 29: 1176–1188.
47. Miller CA, III, Martinat MA, Hyman LE (1998) Assessment of aryl hydrocarbon receptor complex interactions using pBEVY plasmids: expressionvectors with bi-directional promoters for use in Saccharomyces cerevisiae. Nucleic Acids Res 26: 3577–3583.
48. Staes A, Van Damme P, Helsens K, Demol H, Vandekerckhove J, et al. (2008) Improved recovery of proteome-informative, protein N-terminal peptides by combined fractional diagonal chromatography (COFRADIC). Proteomics 8: 1362–1370.
49. Van Damme P, Martens L, Van Damme J, Hugelier K, Staes A, et al. (2005) Caspase-specific and nonspecific in vivo protein processing during Fas-induced apoptosis. Nat Methods 2: 771–777.

50. Van Damme P, Staes A, Bronsoms S, Helsens K, Colaert N, et al. (2010) Complementary positional proteomics for screening substrates of endo- and exoproteases. Nat Methods 7: 512–515.
51. Gevaert K, Van Damme J, Goethals M, Thomas GR, Hoorelbeke B, et al. (2002) Chromatographic isolation of methionine-containing peptides for gel-free proteome analysis: identification of more than 800 Escherichia coli proteins. Mol Cell Proteomics 1: 896–903.
52. Ghesquiere B, Colaert N, Helsens K, Dejager L, Vanhaute C, et al. (2009) In vitro and in vivo protein-bound tyrosine nitration characterized by diagonal chromatography. Mol Cell Proteomics 8: 2642–2652.
53. Ong SE, Blagoev B, Kratchmarova I, Kristensen DB, Steen H, et al. (2002) Stable isotope labeling by amino acids in cell culture, SILAC, as a simple and accurate approach to expression proteomics. Mol Cell Proteomics 1: 376–386.